University of Alberta

Characterization of the DEAD box protein DDX1

by

©

Stacey Bléoo

A thesis submitted to the Faculty of Graduate Studies and Research in partial fulfillment of the requirements for the degree of

Doctor of Philosophy

In

Medical Sciences – Oncology

Edmonton, Alberta

Spring 2003

National Library
of Canada

Acquisitions and
Bibliographic Services

395 Wellington Street
Ottawa ON K1A 0N4
Canada

Bibliothèque nationale
du Canada

Acquisisitons et
services bibliographiques

395, rue Wellington
Ottawa ON K1A 0N4
Canada

Your file Votre référence
ISBN: 0-612-82083-1
Our file Notre référence
ISBN: 0-612-82083-1

The author has granted a non-exclusive licence allowing the National Library of Canada to reproduce, loan, distribute or sell copies of this thesis in microform, paper or electronic formats.

The author retains ownership of the copyright in this thesis. Neither the thesis nor substantial extracts from it may be printed or otherwise reproduced without the author's permission.

L'auteur a accordé une licence non exclusive permettant à la Bibliothèque nationale du Canada de reproduire, prêter, distribuer ou vendre des copies de cette thèse sous la forme de microfiche/film, de reproduction sur papier ou sur format électronique.

L'auteur conserve la propriété du droit d'auteur qui protège cette thèse. Ni la thèse ni des extraits substantiels de celle-ci ne doivent être imprimés ou aturement reproduits sans son autorisation.

Canada

University of Alberta

Library Release Form

Name of Author: Stacey Bléoo

Title of Thesis: Characterization of the DEAD box protein DDX1.

Degree: Doctor of Philosophy

Year this Degree Granted: 2003

Permission is hereby granted to the University of Alberta Library to reproduce single copies of this thesis and to lend or sell such copies for private, scholarly or scientific research purposes only.

The author reserves all other publication and other rights in association with the copyright in the thesis, and except as herein before provided, neither the thesis nor any substantial portion thereof may be printed or otherwise reproduced in any material form whatever without the author's prior written permission.

S. Bléoo

18923-98 Ave.
Edmonton, Alberta
T5T 5K3

January 22, 2003

University of Alberta

Faculty of Graduate Studies and Research

The undersigned certify that they have read, and recommend to the Faculty of Graduate Studies and Research for acceptance, a thesis entitled *Characterization of the DEAD box protein DDX1* submitted by Stacey Lynn Bléoo in partial fulfillment of the requirements for the degree of Doctor of Philosophy in Medical Sciences – Oncology.

Roseline Godbout
Dr. Roseline Godbout

Dr. George Owttrim

Dr. Joan Turner

Charlotte Spencer
Dr. Charlotte Spencer

Walt Dixon
Dr. Walter Dixon

Dr. David Bazett-Jones

Friday October 18, 2002

Dedication

This thesis is dedicated to my daughter Kayla. You can accomplish anything you set your mind to and remember “Mommy loves you”.

Abstract

DDX1, a member of the DEAD box protein family, is amplified and over-expressed in a subset of retinoblastoma and neuroblastoma cell lines and tumours. DEAD box proteins are putative RNA helicases that have been found to function in all aspects of cellular RNA metabolism. To define the biological role for DDX1 we constructed a *DDX1* targeting vector that was used to successfully generate *DDX1+/-* mouse embryonic stem cells. These stem cells are being injected into host blastocyst cells with the aim of producing a germline chimeric mouse. To determine the biochemical role for DDX1 we have defined the cellular localization of DDX1 protein using fluorescent microscopy in combination with anti-DDX1 antibodies. DDX1 is a predominantly nuclear protein with accumulations occurring in ~5 discrete 0.5 μm foci per nucleus. These foci commonly colocalize with nuclear structures called cleavage bodies, which are known to contain general transcription factors and proteins involved in pre-mRNA 3' end processing. Although less frequent, DDX1 foci have also been shown to colocalize with nuclear structures called gems. Gems contain the protein responsible for spinal muscular atrophy, spinal motor neuron (SMN). A portion of DDX1 foci have been found to localize adjacent to Cajal bodies and PML bodies, although the function of these nuclear bodies remains unknown. Co-immunoprecipitation and fluorescence energy transfer (FRET) experiments have shown that DDX1 associates with CstF-64, a protein essential for pre-mRNA 3'-end cleavage. Furthermore, preliminary experiments using an *in vitro*

polyadenylation assay suggest that DDX1 may specifically decrease substrate polyadenylation.

DDX1 has a filamentous pattern in the cytoplasm. We have shown by fluorescence microscopy and FRET that cytoplasmic DDX1 localizes to regions surrounding the mitochondria; however, it is not found within purified mitochondria. Although we have no formal proof that DDX1 undergoes nuclear export, we predict that DDX1 promotes the final step of pre-mRNA 3'-end processing and in the case of nuclear-encoded mitochondrial transcripts, it escorts the transcript out of the nucleus to the vicinity of the mitochondria for translation. We hypothesize that DDX1 foci associate with other nuclear bodies to supply transcriptional complexes for RNA polymerase II transcription and processing.

Acknowledgements

During my Ph.D. I have had the opportunity to meet wonderful people who will remain lifelong friends. It is their support that has enabled me to progress through difficult times and allowed me to celebrate during successful ones. Firstly I would like to thank my friends and collegues who have worked with me in the Godbout lab: Randy Andison, Rhonda Witte, June Bie, Dwayne Bisgrove, Mary Packer, Elizabeth Monckton, Christina Sereda, Sachin Katyal, Jeffrey Coles, and John Rowe. There are also my cherished friends outside of the lab: Elke Aippersbach, Kelly Peloquin, Sandra Rees, Carla Poirier, Sarah Bernard, Kelly Wolf, Renée Baldwin, Maryse Hatchard, Tanya Gillan, Kirk McManus, Paul Boucher, and Gabrielle Zimmerman.

In addition to the support of my friends, I am so grateful to have worked with many talented mentors. First and foremost is my supervisor Roseline Godbout who had strength when I did not and encouraged me when I felt I couldn't make it. Without her belief in me, I would not have made it where I am today. Secondly I am eternally grateful to both Xuejun Sun and Michael Hendzel who guided me through some of my Ph.D. providing me both assistance and stimulating discussions.

Most importantly, I would like to thank my family for their unwavering strength and for their belief in me: my parents, Linda and Bill, (you instilled in me the belief that I could accomplish anything in life that I set my mind to), my sister, Carolyn (you are my best friend), my husband Jean (you are an amazingly unselfish man who has supported both my career and our family), and my

daughter Kayla (you are my life). I love all of you and really, I wish this Ph.D. could be awarded to all of us.

I also want to acknowledge my Mom for sacrificing her time to raise Kayla while I was at work. Mom, this is the greatest gift you could have ever given to me; you truly are Kayla's second Mom.

Table of Contents

CHAPTER 1

Introduction 1

- **1.1 Retinoblastoma** 1
  - 1.1.1 Involvement of pRB in cell cycle progression 1
  - 1.1.2 Mechanisms of pRB-mediated transcriptional repression 4
  - 1.1.3 pRB and cellular differentiation 7
  - 1.1.4 pRB and apoptosis 7
  - 1.1.5 pRB and genome integrity 9
- **1.2 DEAD box proteins** 10
  - 1.2.1 Identification of DDX1 10
  - 1.2.2 DEAD box protein functions 10
  - 1.2.3 DEAD box proteins and cancer 15
  - 1.2.4 *DDX1* 20
- **1.3 Nuclear Architecture** 26
  - 1.3.1 Nucleolus 29
  - 1.3.2 Splicing factor compartments 29
  - 1.3.3 PML bodies 31
  - 1.3.4 Cajal Bodies (CBs) 40
  - 1.3.5 Gems 46
  - 1.3.6 Cleavage Bodies 50
  - 1.3.7 Perinucleolar Structures 52

1.4 3'-end pre-mRNA processing 55

1.5 Thesis Objectives 64

CHAPTER 2

Materials and Methods 66

2.1 Molecular Techniques 66

2.1.1 Library Screening 66

2.1.2 Bacteriophage rescue 68

2.1.3 DNA labeling and nitrocellulose hybridization 71

2.1.4 Southern Blot Analysis 71

2.1.5 Plasmid Purification 72

2.1.6 DNA Insert Purification 72

2.1.7 DNA ligations 72

2.1.8 DNA blunting and dephosphorylation 73

2.1.9 Automated and Manual Sequencing 73

2.2 Embryonic Stem (ES) Cell Manipulations 74

2.2.1 Preparation of Leukemia Inhibitory Factor (LIF) 74

2.2.2 Culturing of ES and SNL cells 76

2.2.3 ES cell electroporations 76

2.2.4 Isolation of drug-resistant ES colonies 77

2.2.5 Preparation of ES cell DNA 78

2.2.6 Analysis of mouse genomic DNA isolated from tails 78

2.3 Cell Culture 79

2.4 Microscopy Techniques 80

2.4.1 Immunofluorescence labeling 80
2.4.2 Antibodies 81
2.4.3 Affinity Purification of anti-DDX1 antibody 82
2.4.4 Light Microscopy 83
2.4.5 Microscopic Fluorescence Resonance Energy Transfer 84
2.4.6 Measuring transcription by RNA polymerase II and III 86
2.4.7 Viral infection by herpes simplex virus type 1 87
2.4.8 Construction of GFP-DDX1 plasmids and DNA transfections 88
2.4.9 Labeling with MitoTracker 88
2.5 Biochemical techniques 88
2.5.1 Immunoprecipitations 88
2.5.2 Cell Synchronization and Flow Cytometric Analysis 89
2.5.3 Cellular fractionation and mitochondria isolation 89
2.5.4 Purification of recombinant DDX1 by HPLC 90
2.5.5 *In vitro* transcription and *in vitro* polyadenylation assay 90

CHAPTER 3

Generation of *DDX1+/-* Mouse Embryonic Stem Cells 93
3.1 Identification and cloning of the genomic mouse DDX1 94
3.2 Restriction mapping of clone 3030 95
3.3 Overall strategy behind the generation of our targeting vector 99
3.4 Generation of the targeting vector 99
3.5 Generation of properly targeted ES cells 100
3.6 Chimeras generated using *DDX1* +/- R1 ES cells 103

3.7 Summary: Our *DDX1+/-* ES cells have thus far been unable to contribute to the germline 106

CHAPTER 4

* A portion of this chapter has been published: Bléoo *et al.*, 2001

Localization of DDX1 to Nuclear Foci that Correspond to Correspond to Cleavage Bodies 111

4.1 Subcellular localization of DDX1 112

4.2 DDX1 foci are adjacent to PML and Cajal bodies 116

4.3 DDX1 foci associate with cleavage bodies 122

4.4 Immunoprecipitation of DDX1 and CstF-64 125

4.5 Close proximity of DDX1 and CstF-64 as determined by fluorescence resonance energy transfer 128

4.6 DDX1 foci do not accumulate nascent RNA 135

4.7 DDX1 during the cell cycle 139

4.8 DDX1 foci localize to the periphery of viral compartments 145

4.9 DDX1 levels correlate with HeLa transcriptional activity 146

4.10 Purified recombinant DDX1 decreases pre-mRNA polyadenylation 149

4.11 Summary: DDX1 frequently colocalizes with CstF-64 in nuclear cleavage bodies and DDX1 may play a role in 3'-end pre-mRNA processing 154

CHAPTER 5

Colocalization of DDX1 foci with Gems 165

5.1 Colocalization of DDX1 foci with gems 166

5.2 Immunoprecipitation of DDX1 and SMN 170

5.3 The relationship between gems and cleavage bodies 174

5.4 Gems, CBs, cleavage bodies and DDX1 foci: the dynamic nature of nuclear structures 178

5.5 Relationship between DDX1 foci, cleavage bodies and gems in HeLaPV 185

5.6 Summary: Gems appear to be dynamic structures with the capacity to colocalize with CBs, DDX1 foci or cleavage bodies 187

CHAPTER 6

Localizing cytoplasmic DDX1 192

6.1 Frequent colocalization of DDX1 with microtubules 195

6.2. Localization of DDX1 to mitochondria 195

6.3 GFP-DDX1 expression coincides with mitochondria 198

6.4 DDX1 localizes to the vicinity of the mitochondria 201

6.5 Comparing the cytoplasmic signal of DDX1 with the location of polyribosomes 206

6.6 Summary: DDX1 appears to localize to mitochondrial areas 207

CHAPTER 7

Discussion 213

7.1 A germline heterozygous mouse has yet to be achieved for DDX1 213

7.2 Nuclear bodies – storage or function? 215

7.3 Individual nuclear bodies are spatially heterogeneous 215

7.4 The cellular function for DDX1 218

7.5 DDX1 and SMN 223

7.6 DDX1 and hnRNP K 224

7.7 DDX1 and cancer 226

REFERENCES 229

List of Tables

Table	Title	Page
3.1	A chronological list of blastocyst injections done by Dr. Peter Dickey.	107
4.1	Nuclear localization of PML, Cajal, and Cleavage Bodies with respect to DDX1 foci	120
4.2	Localization of Cajal bodies (CBs), cleavage bodies (CstF-64), and DDX1 foci in three cell lines: HeLa, SKN, and COS-7.	126
4.3	Quantitative FRET calculations.	134
5.1	Nuclear localization of DDX1 foci with respect to SMN-containing gems in HeLa cells.	167
5.2	Nuclear localization of CstF-64 containing cleavage Bodies with respect to SMN-containing gems in HeLa cells.	177
5.3	Configurations of DDX1 foci, cleavage bodies (ClvgBds) and gems in triple-labeled HeLa cells.	180
5.4	Configurations of cleavage bodies (ClvgBds), gems, and Cajal bodies (CBs) in triple-labeled HeLa cells.	182
5.5	Nuclear localization of SMN-containing gems with respect to DDX1 foci and CstF-64 containing cleavage bodies in HeLaPV.	186

List of Figures

Figure	Title	Page
1.1	The retinoblastoma protein (pRB) regulates the G1-S cell cycle transition by binding to the transcription factor complex E2F/DP.	2
1.2	Conserved sequence motifs of two members of the RNA helicase family.	11
1.3	Nuclear domains commonly found in the eukaryotic cell nucleus.	27
3.1	Positioning of *DDX1* genomic clones in relation to the 5' end of *DDX1*.	96
3.2	Restriction map of clone 3030 and *DDX1* targeting strategy.	97
3.3	Selection of undifferentiated ES colonies.	102
3.4	Southern blot analysis of *DDX1*+/- ES cells as well as *DDX1*+/+ cells.	104
3.5	Western blot analysis of DDX1.	105
4.1	Immunofluorescent labeling of DDX1.	113
4.2	The subnuclear localization of DDX1 with respect to other nuclear bodies.	117
4.3	DDX1 foci colocalize with cleavage bodies in non-transformed GM38 cells.	124
4.4	Co-immunoprecipitation of DDX1 and CstF-64.	127
4.5	The three filter sets used to measure FRET and the fluorescence spectra for Cy3 and Alexa 488.	130
4.6	DDX1 and CstF-64 undergo FRET in HeLa cells.	131
4.7	DDX1 foci do not accumulate nascent RNA.	137
4.8	Disappearance of DDX1 and CstF-64 foci during mitosis.	140
4.9	Cell cycle analysis of DDX1 protein levels.	143

4.10 DDX1 foci localize to the periphery of viral compartments. 147
4.11 DDX1 nuclear signal correlates with transcriptional activity in HeLa cells. 150
4.12 Purified recombinant DDX1 decreases pre-mRNA polyadenylation. 152
5.1 Colocalization of DDX1 foci and SMN-containing gems. 168
5.2 Relationship between gems and CBs in HeLa cells. 169
5.3 The location of DDX1 foci with respect to SMN-containing gems. 171
5.4 Co-immunoprecipitation of DDX1 and SMN. 173
5.5 The nuclear configurations of CstF-64-containing cleavage bodies with respect to SMN-containing gems. 175
5.6 Triple labeling of DDX1 foci, cleavage bodies, and gems in HeLa cells. 181
5.7 Triple labeling of cleavage bodies, gems, and CBs in HeLa cells. 183
6.1 Localization of DDX1 in relation to cytoskeletal components. 196
6.2 Localization of DDX1 to mitochondrial regions. 197
6.3 Filamentous pattern of GFP-DDX1. 199
6.4 Localization of GFP-DDX1 to mitochondrial regions. 200
6.5 DDX1 is not found within purified mitochondria. 202
6.6 DDX1 and cytochrome *c* oxidase subunit 1 undergo FRET in HeLa cells. 204
6.7 Localization of DDX1 to areas that contain ribosomes. 208
7.1 Putative biochemical function for DDX1. 219

List of Abbreviations

A	adenine
adj	adjacent
ALDH	aldehyde dehygrogenase
ALT	alternative lengthening of telomeres
APC	anaphase-promoting complex
APL	acute promyelocytic leukemia
ATP	adenosine triphosphate
ATPase	adenosine triphosphatase
avg	average
bp	base pair
BrdU	bromodeoxyuridine
BrUTP	bromouridine triphosphate
BSA	bovine serum albumin
CARD	caspase recruitment domain
CB	Cajal body
CCD	cooled charge-coupled device
cdk	cyclin-dependent kinase
cDNA	copy deoxyribonucleic acid
$CFII_m$	cleavage factor II mammalian
CFI_m	cleavage factor I mammalian
CFP	cyan fluorescent protein
chDDX1	chicken DEAD box protein 1

CNS	central nervous system
coloc	colocalization
conc	concentration
CPSF	cleavage and polyadenylation specificity factor
CstF	cleavage stimulation factor
CTD	carboxy-terminal domain
CTP	cytosine triphosphate
DAPI	4',6,-diamidino-2-phenylindole
dCTP	deoxycytosine triphosphate
DDX1	DEAD box protein 1
DIC	digital interference contrast
DmDdx1	*Drosophila melanogaster* DEAD box protein 1
DMSO	dimethylsulfoxide
DNA	deoxyribonucleic acid
DNase I	deoxyribonuclease I
DNMT1	DNA methyltransferase I
DTT	dithiothreitol
EDTA	ethylenediaminetetraacetic acid
eIF	eukaryotic initiation factor
e-published	electronically published
ES	embryonic stem
ESI	electron spectroscopic imaging
FBS	fetal bovine serum

Fig	figure
FLIM	fluorescence lifetime imaging microscopy
FLIP	fluorescence loss in photobleaching
FRAP	fluorescence recovery after photobleaching
FRET	fluorescence resonance energy transfer
FU	5’-fluorouridine
FWHM	full width at half maximum
GFP	green fluorescent protein
GR	glucocorticoid receptor
GST	glutathathione-S-transferase
GTP	guanosine triphosphate
HDAC	histone deacetylase
HeNe	helium-neon
hnRNP K	heterogeneous ribonucleoprotein K
hnRNP U	heterogeneous ribonucleoprotein U
HPLC	high performance liquid chromatography
hr	hour
HRP	horseradish peroxidase
HSV-1	Herpes simplex virus type 1
IGC	interchromatin granule cluster
IgM	immunoglobulin M
IMAC	immobilized metal affinity chromatography
IP	immunoprecipitation

kb	kilobases
kDa	kilodaltons
KRSP	KH-type splicing regulatory protein
LIF	leukemia inhibitory factor
LSM	laser scanning microscope
M	molar
MDPK	myotonin dystrophy protein kinase
mg	milligram
MHC	major histocompatibility complex
min	minute
ml	milliliter
mm	millimeter
mM	millimolar
mRNA	messenger ribonucleic acid
mRNP	messenger ribonucleoprotein
NBs	nuclear bodies
ND10	nuclear domain 10
neo	neomycin
ng	nanogram
nm	nanometer
nM	nanomolar
NTP	nucleoside triphosphate
OD	optical density

p	probability
PAB II	poly(A) binding protein II
PAP	poly(A) polymerase
PARN	poly(A) ribonuclease
PBS	phosphate-buffered saline
PFU	plaque-forming units
PGK	phophoglycerate kinase
PML	promyelocytic leukemia
PNC	perinucleolar compartment
PNS	peripheral nervous system
POD	PML oncogenic domain
pol I	RNA polymerase I
pol II	RNA polymerase II
pol III	RNA polymerase III
PolIO	hyperphosphorylated RNA polymerase II
poly(A)	polyadenosine triphosphate
ps	picosecond
PTB	polypyrimidine tract binding protein
RARα	α-retinoic acid receptor
RB	retinoblastoma
rDNA	ribosomal deoxyribonucleic acid
RHA	RNA helicase A
RNA	ribonucleic acid

RNase	ribonuclease
RNPase	ribonucleoproteinase
rRNA	ribosomal ribonucleic acid
RXR	retinoid X receptor
S	supernatant
S.D.	standard deviation
SDS	sodium dodecyl sulfate
sec	second
SFC	splicing factor compartment
SFII	superfamily II
SMN	spinal motor neuron
SNB	Sam68 nuclear body
snoRNA	small nucleolar ribonucleic acid
snoRNP	small nucleolar ribonucleoprotein
snRNA	small nuclear ribonucleic acid
snRNP	small nuclear ribonucleoprotein
SPRY	domain discovered in splA kinase of *Dictyostelium* and in rabbit ryanodine receptor
SR	splicing regulatory
t-AML	therapy related acute myeloid leukemia
TBS	tris-buffered saline
TFIIE	transcription factor IIE
TFIIF	transcription factor IIF
TFIIH	transcription factor IIH

TK	thymidine kinase
t-MDS	therapy-related myelodysplastic syndrome
TMG	trimethylguanosine
tRNA	transfer ribonucleic acid
TSA	Trichostatin A
U	units
UTP	uridine triphosphate
UV	ultraviolet
V	volts
W	watts
YFP	yellow fluorescent protein
μF	microFaraday
μg	microgram
μl	microliter
μm	micrometer

Chapter 1. Introduction

1.1 Retinoblastoma

Retinoblastoma is a malignant tumour of the retina that occurs primarily in young children at an incidence of 1/ 20,000. Studies of both the inherited form (~40% of patients) and the noninherited form of retinoblastoma led Knudson in 1971 to predict the 2-hit hypothesis (Knudson, 1971). This hypothesis postulated that two mutational events would cause malignant transformation of a developing retinoblast; patients with the inherited form would acquire one mutation through the germinal cells and the second mutation from somatic cells, and patients with the nonhereditary form would have both mutations in somatic cells. Confirmation of this hypothesis came with the identification of the retinoblastoma tumour suppressor gene (*RB*) on chromosome 13q14 (Friend *et al.*, 1986). Both copies of the *RB* gene were shown to be inactivated in retinoblastoma as well as in many other types of cancers (Horowitz *et al.*, 1990).

1.1.1 Involvement of pRB in cell cycle progression

The *RB* gene product, pRB, has been shown to both positively and negatively regulate gene expression thereby influencing cellular events such as cell-cycle progression, apoptosis, and differentiation (reviewed in Kaelin, 1999; Zheng and Lee, 2001). Central to pRB's role in regulating cell cycle progression and apoptosis, is its ability to bind to members of the E2F transcription factor family (Fig. 1.1). The E2F proteins function to activate the transcription of gene

Fig. 1.1 The retinoblastoma protein (pRB) regulates the G1-S cell cycle transition by binding to the transcription factor complex E2F/DP.

In G0 (not shown) and G1, pRB is hypophosphorylated and can bind to the E2F/DP transcription factor complex. When the cellular conditions are favourable phosphorylation is initiated on pRB by the D-type cyclins in conjunction with either cyclin-dependent kinase (cdk) 4 or 6. Further phosphorylation of pRB occurs by the cyclinE-cdk2 complex. These events result in the release of E2F/DP from pRB and consequently the cell proceeds past the restriction point (R), into S phase. The E2F/DP family members mediate the transcription of genes whose products are involved in cell cycle progression. Phosphorylation of pRB in S phase is maintained by the cyclin A-cdk2 complex.

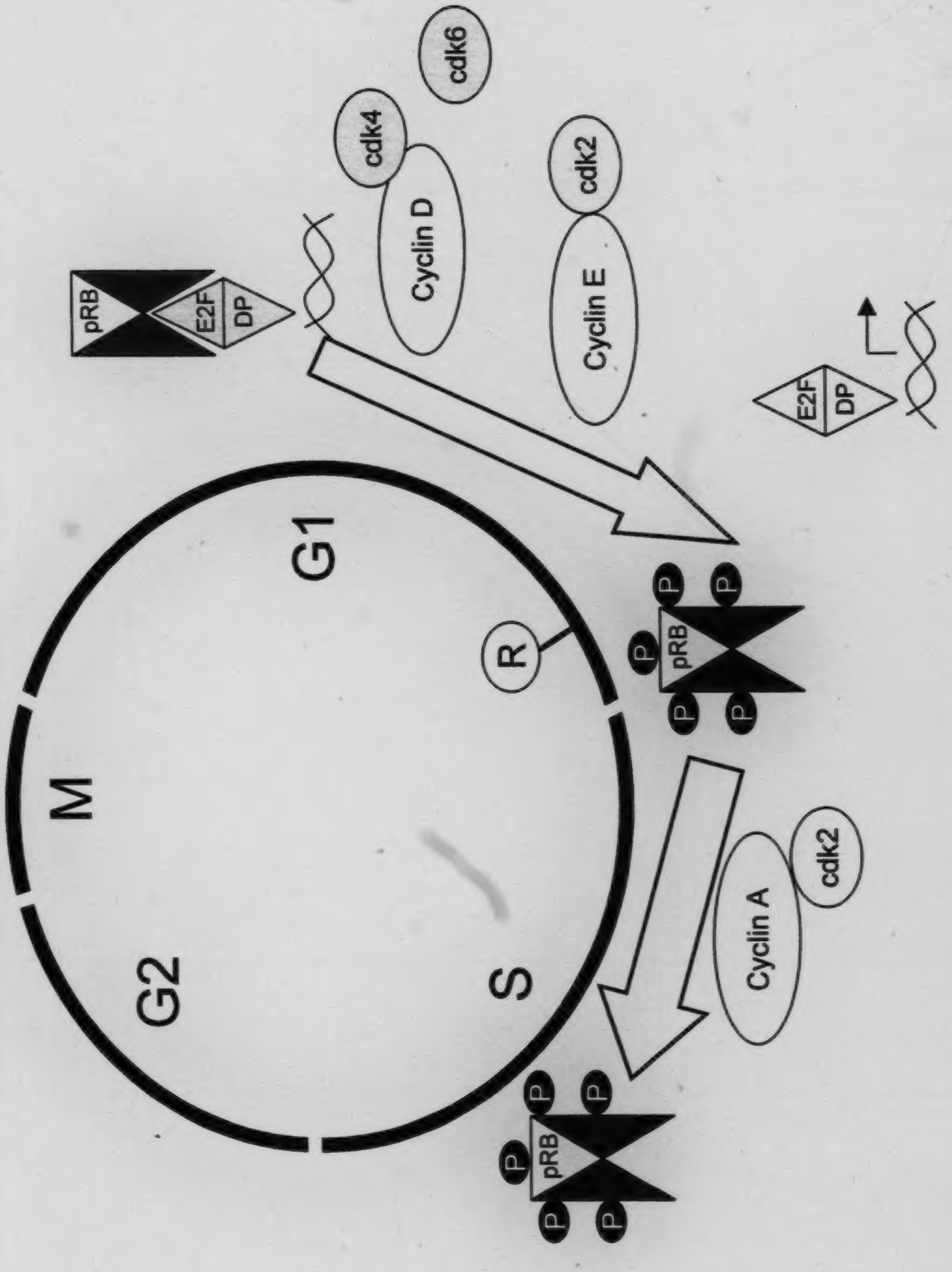
pRB
E2F
DP
Cyclin D
cdk4
cdk6
Cyclin E
cdk2
E2F
DP
G1
R
M
G2
S
P
pRB
Cyclin A
cdk2
P
pRB

products involved in the cell cycle transition from G1 to S phase (Harbour and Dean, 2000). Deregulated expression of E2F triggers cell cycle entry into S phase and can led to transformation (Johnson *et al.*, 1993; Johnson *et al.*, 1994; Singh *et al.*, 1994). The binding of hypophosphorylated pRB to E2F in G1 phase of the cell cycle is now known to inhibit E2F mediated gene transactivation through several mechanisms as discussed below.

1.1.2 Mechanisms of pRB-mediated transcriptional repression

Initially, pRB was thought to inhibit E2F activation by binding to its activation domain thereby effectively blocking interaction with components of the transcriptional machinery (Flemington *et al.*, 1993; Helin *et al.*, 1993). However, removal of E2F sites from some E2F-responsive promoters lead to an increase in transcriptional activity in G1 phase rather than the expected decrease in transcription at S phase, suggesting that in addition to simple neutralization of E2F, pRB might be actively repressing transcription. This hypothesis was further supported by observations that insertion of E2F binding sites into synthetic promoters repressed transcription and that pRB, when tethered to a heterologous DNA-binding domain, actively repressed transcription (reviewed in Dyson, 1998). Evidence for pRB playing an active role in transcriptional repression emerged as pRB was shown to bind histone deacetylases (HDACs) 1, 2 and 3 (Brehm *et al.*, 1998; Luo *et al.*, 1998; Magnaghi-Jaulin *et al.*, 1998; Lai *et al.*, 1999). Because pRB binds HDACs at a separate site from E2F, pRB can function to repress E2F-mediated transcription by recruiting HDACs; the HDACs then cause the histones to become deacetylated which then presumably promotes chromosome condensation and transcriptional inhibition (Luo *et al.*, 1998). In addition, inhibiting HDAC activity using Trichostatin A (TSA) prevents pRB-mediated repression of some genes important for G1/S progression suggesting that HDAC-mediated repression is important for regulation of the G1 restriction point by pRB (Luo *et al.*, 1998).

In addition to HDAC-mediated repression, pRB also binds and mediates transcriptional regulation through BRG1 and hBRM (Dunaief *et al.*, 1994; Strober *et al.*, 1996). BRG1 and hBRM are two components of an ATP-dependent nucleosome remodelling complex. These proteins are orthologs of yeast SW12/SNF2 that function in the SWI/SNF nucleosome remodelling complex. Nucleosome remodelling complexes use energy from ATP to convert nucleosome structure to either opened or closed conformations; the conversion is thought to be due to its ability to alter nucleosome positioning or spacing along the DNA or possibly an ability to directly influence higher-order chromatin structure (reviewed in Havas *et al.*, 2001). Ectopic expression of either BRG1 or hBRM in a human carcinoma cell line SW13, caused tumour suppression mediated in part by pRB (Dunaief *et al.*, 1994; Strober *et al.*, 1996). In addition, the pRB/hBRM complex has been found to bind to E2F thereby suppressing E2F-mediated gene transcription (Trouche *et al.*, 1997). Recently, complexes consisting of HDAC-pRB-hSWI/SNF and pRB-hSWI/SNF have been found to regulate the order of cyclin and cdk expression during the cell cycle. This differential regulation of the cyclins and cdks modulates cell cycle exit from both G1 and S phase (Zhang *et al.*, 2000).

pRB may also modify chromatin structure through its interaction with DNA methyltransferase I (DNMT1). Robertson *et al.* (2000) demonstrated that DNMT1 and pRB can form a complex with E2F and this complex mediates transcriptional repression at E2F promoters. Although transcriptional repression by DNMT1 is usually presumed to be due to methylation (methylation recruits a methyl binding protein – HDAC complex), the repression was shown to not rely on DNA methylation. A separate observation by Fuks *et al.* (2000) established that DNMT1 has the ability to bind to HDAC1, suggesting a more direct role for DNMT1 in transcriptional repression. This finding may explain the methylation-independent repression observed by Robertson *et al.* (2000). On a slightly different note, Pradhan and Kim (2002) have recently identified pRB as an negative regulator of DNMT1 activity. The loss of pRB in many tumours may explain the hypermethylation seen at many gene promoters. Therefore, pRB appears to mediate both transcriptional repression at E2F promoters and maintenance methylation on hemimethylated DNA.

Chromatin structure regulation, however, is not the only mechanism for pRB-mediated transcriptional repression. pRB can inhibit E2F-dependent transcription by blocking formation of the transcriptional preinitiation complex (Ross *et al.*, 1999). pRB also confers repression by binding to other corepressors such as RBP1 and CtIP, although these repressors have been implicated in the recruitment of chromatin remodelling activity (reviewed in Zheng and Lee, 2001).

1.1.3 pRB and cellular differentiation

In addition to regulating cell cycle progression through genes such as E2F, pRB also affects cellular differentiation. *Rb* knockout mice die by embryonic day 15 and display defects in neurogenesis and erythropoiesis; loss of pRb appears to result in abnormal proliferation and differentiation in both of these areas (Clarke *et al.*, 1992; Jacks *et al.*, 1992; Lee *et al.*, 1992). pRb has been found to positively regulate adipocyte differentiation by enhancing the DNA binding ability of C/EBPβ (and possibly other C/EBPs) (Chen *et al.*, 1996). In addition to positive regulation, pRB also negatively promotes differentiation by binding to inhibitors such as Id2 (Iavarone *et al.*, 1994). Id2, which is known to modulate the timing of differentiation in many tissues, inhibits differentiation by sequestering basic helix-loop-helix transcription factors (Yokota, 2001). Uncontrolled Id2 may underlie the differentiation defects seen in *Rb -/-* mice as a null mutation at the *Id2* allele in *Rb -/-* mice rescues differentiation defects and permits survival of the mice until birth (Lasorella *et al.*, 2000).

1.1.4 pRB and apoptosis

Rb-deficient embryos display increased apoptosis in the central nervous system (CNS), peripheral nervous system (PNS), and within the ocular lens (Morgenbesser *et al.*, 1994; Macleod *et al.*, 1996). *p53* and *Rb* double mutant mice establish that this cell death is p53-dependent in the CNS and lens, but occurs through a p53-independent pathway in the PNS (Morgenbesser *et al.*, 1994; Macleod *et al.*, 1996). Likewise, mice lacking both pRb and E2F-1 display very little apoptosis in the CNS and ocular lens suggesting that the p53-dependent apoptotic pathway is mediated through the transcription factor E2F-1 (Tsai *et al.*, 1998). The apoptosis within the PNS is only partially relieved by the concomitant inactivation of *E2F-1*, therefore pRb must also regulate an alternative apoptotic pathway (Tsai *et al.*, 1998). The pRb apoptotic pathway mediated through E2F has been thought to be due to ARF (alternative reading frame protein encoded by the *INK4A* locus) activation. Although ARF is a likely candidate as it inhibits MDM2-mediated turnover of p53 (Pomerantz *et al.*, 1998; Zhang *et al.*, 1998), mice deficient in *Rb* and *ARF* do not show a substantial decrease in apoptosis in the ocular lens or in the CNS (Tsai *et al.*, 2002). An alternative p53-dependent pathway has not yet been found.

Studies with *E2F* constructs lacking a transactivation domain (but containing the DNA-binding domain) have revealed that p53-independent apoptosis does not require gene activation by E2F (Hsieh *et al.*, 1997; Phillips *et al.*, 1997). Subsequently, Phillips *et al.* (1999) demonstrated that these *E2F* mutants induced apoptosis through the death receptor pathway. They also showed that E2F functions to downregulate TRAF2 protein which, in turn prevents cell survival signals from NF-κB and JNK/SAPK. Therefore, the induction of the p53-independent apoptotic pathway by E2F is thought to occur due to the inhibition of the NF-κB and JNK/SAPK pathways, both of which provide protection from death receptor-induced apoptosis.

1.1.5 pRB and genome integrity

The inactivation of pRB precedes multiple genetic abnormalities that likely contribute to tumour progression in retinoblastoma (Squire *et al.* 1985). Recently, a role for pRB in chromosome segregation has been discovered which may help to explain the genetic abnormalities. pRB has been found to associate with Hec1, a protein involved in chromosome segregation; introduction of pRB reduced chromosome segregation errors fivefold in yeast cells with a temperature-sensitive mutation of Hec1 (Zheng *et al.*, 2000). pRB also plays a role in G2/M phase cell cycle progression, not only through the regulation of cyclin expression with chromatin remodelling complexes, but through its association with H-nuc, a component of the anaphase-promoting complex (APC) (Chen *et al.*, 1995). APC is responsible for the degradation of mitotic cyclins, and it controls the onset of sister chromatid separation (Page and Hieter, 1999). pRB has also been implicated in the inhibition of DNA synthesis prior to the completion of chromosome segregation and cytokinesis (Di Leonardo *et al.*, 1997; Khan and Wahl, 1998).

The discovery of the *RB* gene has had a profound impact on our understanding of hereditary cancers and tumour suppressor genes. Although pRB has many more functions than those listed above, these examples highlight the fact that pRB inactivation has substantial cellular effects due to its involvement in a wide range of biochemical processes.

1.2 DEAD box proteins

1.2.1 Identification of DDX1

To identify genes whose expression might be altered as a result of pRB inactivation, a subtracted library was constructed by hybridizing single-stranded cDNA from two retinoblastoma cell lines to poly(A^+) RNA isolated from an unrelated pRB positive tumour cell line, CaCo-2, and human fetal tissue (Godbout and Squire, 1993). The library was then differentially screened using cDNA from two retinoblastoma cell lines and cDNA from the CaCo-2 cell line and fetal tissue. Upon examination of the plaques that selectively hybridized to the retinoblastoma cDNA probes, 21 of the 26 clones were found to represent a novel member of the DEAD box protein family, called DEAD box 1 (*DDX1*) (Godbout and Squire, 1993).

1.2.2 DEAD box protein functions

DEAD box proteins are ATP-dependent RNA unwinding/destabilizing proteins that belong to the superfamily II of NTP helicases (SFII) according to the classification of Gorbalenya and Koonon (1993). Families of RNA helicase proteins are classified based on the presence of 8 conserved motifs, including the signature motif - Asp-Glu-Ala-Asp or DEAD (Fig. 1.2). Other related members of SFII include DEAH and DExH box RNA helicases (where x can be

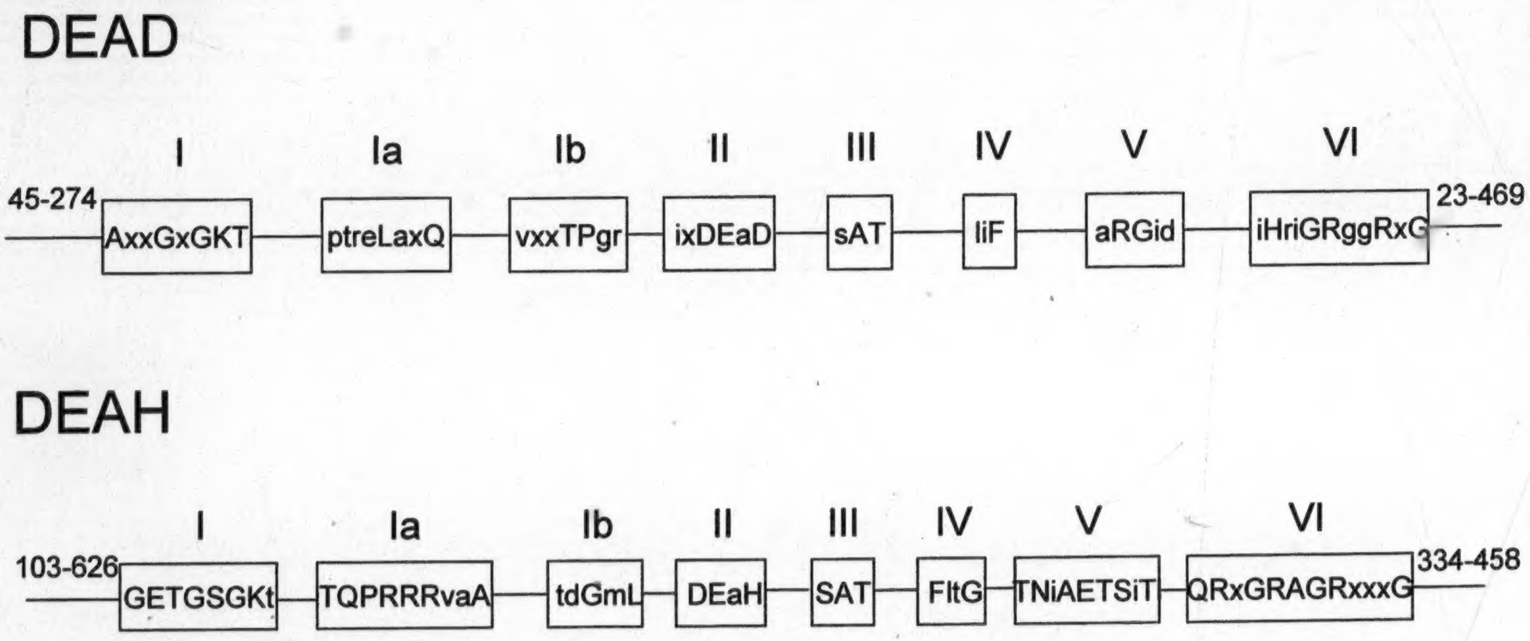
DEAD
I
Ia
Ib
II
III
IV
V
VI
45-274
AxxGxGKT
ptreLaxQ
vxxTPgr
ixDEaD
sAT
liF
aRGid
iHriGRggRxG
23-469
DEAH
I
Ia
Ib
II
III
IV
V
VI
103-626
GETGSGKt
TQPRRRvaA
tdGmL
DEaH
SAT
FltG
TNiAETSiT
QRxGRAGRxxxG
334-458

Fig. 1.2 Conserved sequence motifs of two members of the RNA helicase family.

The conserved sequence motifs of the DEAD (top) and DEAH (bottom) box protein family. Capital letters indicate identical amino acids, and lower case letters indicate highly conserved amino acids (>50% occurrence). The letter x represents any amino acid. The average number of amino acids in the N- and C- terminal extensions are indicated.

This figure is adapted from de la Cruz *et al.*, 1999.

any amino acid). DExD/H helicases have been found in all organisms from bacteria and viruses to humans, and most have demonstrated ATPase activity that is stimulated by RNA. RNA helicase activity has not been demonstrated for all members of the family, presumably due to substrate specificity or the lack of required cofactors. Furthermore, unlike DNA helicases, which are processive enzymes, DExD/H proteins have traditionally been thought to only modify local RNA structure, as has been shown for DEAD box protein eIF-4A (Rogers *et al.*, 1999). This hypothesis has come into question since the discovery that vaccinia virus DExD/H protein, NPH-II, is a highly processive RNA helicase (Jankowsky *et al.*, 2000). One other DEAD box helicase, DbpA from *E. coli*, has subsequently been shown to possess similar processive activity (Henn *et al.*, 2001).

In addition to RNA unwinding activity, Jankowsky *et al.* (2001) have shown that the vaccinia virus DExD/H protein, NPH-II, is able to disrupt *in vitro* RNA – protein interactions. *In vivo* confirmation of such a function for RNA helicases comes from two groups who demonstrated that mutation of some RNA helicases in yeast could be tolerated if mutations were simultaneously introduced into either an snRNP complex or a protein that binds to mRNA (Chen *et al.*, 2001; Kistler and Guthrie, 2001). These secondary mutations destabilized the binding of the snRNP complex or the RNA binding protein to the pre-mRNA such that splicing could proceed without the RNA helicase. These experiments have led to the suggestion that some RNA helicases function as 'RNPases' (Linder *et al.*, 2001; Schwer, 2001; Will and Lührmann, 2001). Therefore biochemically, DExD/H box proteins function to modify RNA structure, in either a step-wise or processive manner, and additionally or alternatively they may also regulate RNA – protein interactions.

Mutational analysis of the human DEAD box protein, eIF-4A, has defined specific functions for four of the eight conserved motifs. Motif I (Fig. 1.2) is responsible for ATP binding, whereas mutations to motif II affect ATPase activity. Mutations to both motifs I and II affect RNA helicase activity, demonstrating that ATP hydrolysis is required for RNA unwinding (Rozen *et al.*, 1989; Pause and Sonenberg, 1992). Mutations to motif III affect RNA unwinding activity, but not ATP binding or hydrolysis (Pause and Sonenberg, 1992). Motif VI is involved in both ATPase activity and RNA-binding (Pause and Sonenberg, 1992; Pause *et al.*, 1993). Similar analyses using vaccinia virus DExH box protein, NPH-II, have shown that mutations in motif Ia abolish ATP hydrolysis and consequently RNA helicase activity (Gross and Shuman, 1998); whether motif Ia in DEAD box proteins performs the same function remains to be determined. Although mutational analysis of motif V has yet to be done, elucidation of eIF-4A crystal structure led to the hypothesis that this domain is responsible for the coupling of ATP binding and hydrolysis to conformational changes in eIF-4A that permit RNA binding (Caruthers *et al.*, 2000).

DExD/H box proteins are involved in all aspects of RNA metabolism including: translation initiation, ribosome biogenesis, pre-mRNA splicing, RNA export, RNA degradation, mitochondrial RNA processing, *Drosophila* dosage compensation, the biosynthesis of distinct RNA species (ie: tRNA, rRNA, snRNA, snoRNA), and recently, transcriptional activation and translational silencing (http://www.expasy.ch/linder/RNA_helicases.html;http://www.helicase.net/dexhd/about-p.htm; de la Cruz *et al.*, 1999; Endoh, *et al.*, 1999; Aratani *et al.*, 2001; Minshall *et al.*, 2001; Nakamura *et al.*, 2001; Tanner and Linder, 2001; Westermarck *et al.*, 2002). The archetypal DEAD box protein is human eIF-4A. eIF-4A functions to unwind RNA secondary structure in the 5' untranslated region so as to permit binding of the ribosome for translation initiation (reviewed in Pestova and Hellen, 2000). Originally eIF-4A was thought to require eIF-4B for helicase function, however it has now been shown that eIF-4A can function by itself on RNA duplexes of limited stablity (Rogers *et al.*, 1999). When characterized alone, eIF-4A is a non-processive helicase (approximately 4 – 5 base pairs unwound per binding event); the addition of eIF-4B causes it to become slightly more processive (Rogers *et al.*, 1999; Rogers *et al.*, 2001). Using a dominant negative mutant of eIF-4A, Svitkin *et al.* (2001) demonstrated that mRNAs with very stable secondary structure were more susceptible to translational inhibition. These results support the view that eIF-4A functions to remove secondary structure at the 5' end of mRNA. In contrast to eIF-4A, the role of most DExD/H proteins in higher eukaryotes remains poorly characterized. However, some functions for these DExD/H proteins have been proposed based on similarity to their yeast orthologs, which have been well characterized (http://www.helicase.net/dexhd/about-p.htm).

1.2.3 DEAD box proteins and cancer

The involvement of DExD/H box proteins in every aspect of RNA metabolism suggests that these proteins are likely to be important in the control of cell growth and proliferation. Indeed, deletion of any of the 32/34 DExD/H proteins in *Saccharomyces cerevisiae* is lethal, and deletion of one other results in a slow-growing phenotype (http://www.expasy.ch/linder/RNA_helicases.html). Within the human DExD/H box family, several have been implicated in tumourigenesis.

The genes encoding three RNA helicases, *DDX26* (*Dice1*) (Wielend *et al.*, 1999), *DDX10* (Arai *et al.*, 1997; Ikeda *et al.*, 1999; Nishiyama *et al.*, 1999; Nakao *et al.*, 2000), and *RCK/p54* (Akao *et al.*, 1991) have been shown to undergo either loss of heterozygosity (LOH) (*DDX26*) or translocations. *DDX26* has been mapped to a region adjacent to *RB* on 13q14 that is frequently lost in non-small cell lung carcinoma, head and neck cancers, and carcinomas of the breast, ovary, and prostate. This gene may account for a critical tumour suppressor in these malignancies as it has been shown that LOH at 13q14 does not affect *RB* expression (Wieland *et al.*, 1999 and references therein). Wieland *et al.* (1999) demonstrated that in human non-small cell lung carcinoma cell lines and primary tumours, *DDX26* expression is down-regulated. The decreased expression in the cell lines is due to promoter hypermethylation and aberrant splicing. Wieland *et al.* (2002) did not investigate whether DDX26 expression was affected by LOH at the *DDX26* allele. These results implicate DDX26 as a tumour suppressor in solid tumours (Wieland *et al.*, 1999).

Another DEAD box gene, *DDX10*, is frequently found fused with the nucleoporin gene *NUP98* in therapy-related acute myeloid leukemia (t-AML) and therapy-related myelodysplastic syndrome (t-MDS), and less frequently in *de novo* AML and MDS (Arai *et al.*, 1997; Ikeda *et al.*, 1999; Nishiyama *et al.*, 1999; Nakao *et al.*, 2000). NUP98 is a component of the nuclear pore complex which functions to transport proteins and RNAs between the nucleus and cytoplasm. DDX10 is similar to the yeast RNA helicases involved in ribosome biogenesis (Savitsky *et al.*, 1996). Therefore, the *NUP98-DDX10* fusion transcript is thought to cause aberrant nucleocytoplasmic transport of proteins or mRNA or alterations in ribosome assembly (Arai *et al.*, 1997).

Translocations involving chromosome 11q23 have been observed in many hematopoietic malignancies including malignant lymphoma, acute promyelocytic leukemia, and infantile leukemia (Trent *et al.*, 1991). Studies of a B-cell lymphoma revealed the *RCK/p54* gene at the site of chromosomal translocation t(11;14)(q23;q32) (Akao *et al.*, 1991). This gene is fused after its first intron to an immunoglobulin heavy chain (*IgH*) gene (Akao *et al.*, 1992) and this is predicted to cause overexpression of RCK/p54 protein (Akao *et al.*, 1998). The protein was later identified as a member of the DEAD box protein family (Akao *et al.*, 1995), and its overexpression has been documented in colorectal adenomas and carcinomas (Nakagawa *et al.*, 1999; Hashimoto *et al.*, 2001). The overexpression of *RCK/p54* in colorectal adenomas is frequently seen in conjunction with *MYCC* overexpression, and the co-overexpression occurs more often in high grade dysplasias (ie. carcinoma *in situ*) than in low grade dysplasias

(Hashimoto *et al.*, 2001). Contradicting this finding is the observation that transfection of *RCK/p54* into tumourigenic guinea pig cells reduced cell growth and inhibited colony formation in soft agar (Akao *et al.*, 1998). As overexpression of RCK/p54 protein in cultured cells increased MYCC protein (but not mRNA), a role for RCK/p54 in translation was suggested (Hashimoto *et al.*, 2001). Recently the *Xenopus* ortholog of RCK/p54, Xp54, was found to repress translation when tethered to a nonadenylated reporter mRNA (Minshall *et al.*, 2001). The Xp54 protein is thought to participate in the translational activation of mRNAs that have been stored until completion of meiosis in early *Xenopus* development. Further studies will be needed to determine whether human RCK/p54 functions similarly to repress translation.

Two DExD/H proteins, other than RCK/p54, have been linked to the *MYC* proto-oncogene pathway. The product of the *MYC* proto-oncogene is a transcription factor that dimerizes with MAX protein to affect transcription of genes involved in proliferation, differentiation and apoptosis. Deregulated *MYC* expression, therefore, leads to aberrant expression of many genes and consequently cellular transformation. The regulation of genes by MYC has recently been attributed to its ability to recruit chromatin remodelling factors (reviewed in Lusher, 2001). One gene that the MYC-MAX heterodimer is known to activate is the DEAD box gene *MrDb* (Grandori *et al.*, 1996). The *Drosophila* ortholog of *MrDb*, *pitchoune (pit)*, affects cell growth and proliferation, possibly by playing a role in ribosome biogenesis (Zaffran *et al.*, 1998). Ectopic expression of *d-Myc* in the central nervous system of Drosophila caused ectopic expression of *pit*, suggesting that *pit* is also a target of d-Myc. In addition to regulating the transcription of a DEAD box gene, MYCC has also been found to complex with two human DExH box proteins, TIP48 and TIP49 (Wood *et al.*, 2000). Although the cellular functions of either protein are unknown, TIP49 was found to be essential for cellular transformation by MYCC.

Aberrant or ectopic expression of many DExD/H box proteins has been found in a variety of tumours. p68 is a human DEAD box protein that has been shown to be growth and developmentally regulated (Stevenson *et al.*, 1998; Seufert *et al.*, 2000). Preliminary evidence indicated a role for p68 in pre-mRNA splicing (Neubauer *et al.* 1998; Rossler *et al.*, 2000), and recently Huang and Lui (2002) have reported that they have unpublished data proving that p68 functions as an essential splicing factor. The first report of p68 in tumourigenesis was by Dubey *et al.* (1997) who determined that a somatic mutation of p68 existed in mouse CD8+ T cell clones that were collected from tumours induced by ultraviolet light. Injection of tumours derived from p68 mutant T cell clones into naïve mice triggered an immune response that resulted in tumour regression while injection of tumours derived from a T cell clone with wild-type p68 did not elicit an immune response permitting tumour growth. These experiments suggest that the altered p68 may represent a useful tumour antigen for vaccination, and that p68 may play a role in the tumourigenic process. Supporting a role for p68 in tumourigenesis is the observation by Causevic *et al.* (2001) that p68 protein, but not mRNA, is overexpressed in benign colorectal adenomas as well as in malignant colorectal adenocarcinoma. The increase in p68 protein in these cells correlated with the appearance of a higher molecular weight form of p68. The post-translational modification seen in these tumours was identified as ubiquitylation; as this modification usually targets proteins for degradation by the 26S proteasome, it is not known how poly-ubiquitylation of p68 can coexist with an increase in protein expression.

The remaining DExD/H box genes reported to affect tumourigenesis are less well characterized. DExD/H box gene, *MDA-5*, was found using a subtractive library created from melanoma cells that were induced to differentiate. Ectopic expression of *MDA-5* in human melanoma cells inhibited their colony-forming ability, suggesting that this RNA helicase plays a role in growth inhibition. MDA-5 contains a caspase recruitment domain (CARD) in its N-terminal domain. It is not known how this domain, which is involved in recruiting factors involved in apoptosis, functions in a putative RNA helicase protein. A novel DEAD box helicase, CAGE (cancer-associated gene), was found to be expressed in normal testes as well as in gastric cancer cells (Cho *et al.*, 2002). This gene is frequently demethylated in some cancer cell lines that do not normally express it suggesting a mechanism for gene activation. A non-related gene, HAGE, identified by cDNA subtraction, was shown to be selectively expressed in a human sarcoma cell line (Martelange *et al.*, 2000). This gene is expressed in many tumours at much greater levels than corresponding normal tissue.

1.2.4 *DDX1*

The *DDX1* gene covers approximately 40 kb of genomic DNA and encodes a transcript of 2.7 kb (Kuroda *et al.*, 1996; Godbout *et al.*, 1998). The *DDX1* gene was found to be amplified in a subset of retinoblastoma cell lines as well as in neuroblastoma tumours and cell lines. Neuroblastoma is a childhood malignancy of the peripheral nervous system. Examination of the *DDX1*-amplified retinoblastoma and neuroblastoma cell lines demonstrated a corresponding increase in RNA (Godbout and Squire, 1993), and protein (Godbout *et al.*, 1998), suggesting that overexpression of the protein may provide cellular growth advantage. *DDX1* was mapped to chromosome 2p24, which is the location of the proto-oncogene *MYCN* (Godbout and Squire, 1993). Southern blot analysis of retinoblastoma and neuroblastoma cell lines revealed that those cell lines with amplified *DDX1* also displayed *MYCN* amplification. Subsequent reports demonstrated that *DDX1* was situated 340 kb telomeric to *MYCN* (Amler *et al.*, 1996; Kuroda *et al.*, 1996; Noguchi *et al.*, 1996; Pandita *et al.*, 1997).

It is known that *MYCN* amplification is an important prognostic factor in neuroblastoma (Bown, 2001). *MYCN* amplification occurs in approximately 25% of untreated tumours, and signifies advanced disease stage and poor prognosis (Brodeur *et al.*, 1984; Seeger *et al.*, 1985; Schwab and Amler, 1990). *MYCN* is located on a core amplicon of 130 kb (Reiter and Brodeur, 1996); however the amplicon can extend to over 1Mb in size (Schneider *et al.*, 1992). These amplicons can occur as double minute chromosomes or as homogenously staining regions integrated into the chromosomes (Schwab *et al.*, 1983, 1984).

Within some neuroblastomas, enhanced *MYCN* mRNA expression has been observed without *MYCN* amplification (Gradi-Leopardi *et al.*, 1986; Niesen *et al*, 1988; Slavc *et al.*, 1990). These tumours do not show a worse clinical prognosis than non-amplified tumours, making it likely that additional genes co-amplified with *MYCN* contribute to the aggressive phenotype seen with *MYCN* amplified tumours. The observation that *DDX1* is co-amplified with *MYCN* in neuroblastoma led Squire *et al.* (1995) to investigate its role in this tumour. Examination of 32 neuroblastoma tumours revealed that 13 had *MYCN* amplification and out of these 13, seven also had amplification of *DDX1* (Squire *et al.*, 1995). Although Squire *et al.* (1995) observed a trend towards a worse clinical prognosis when both genes were amplified, the number of tumours was too small to reach statistical significance. Another study by Manohar *et al.* (1995), which included 35 patients with *MYCN* amplification, concluded that no significant difference in patient outcome occurred with both genes amplified compared to just *MYCN* amplification. Yet a third report by George *et al.* (1997) indicated that patients with stage 4 neuroblastomas have a significantly shorter disease-free interval when both genes were amplified.

A second gene *NAG*, neuroblastoma amplified gene, is a novel gene of unknown function that has also been found to reside on the *MYCN* amplicon with *DDX1* and therefore has been predicted to similarly contribute to neuroblastoma tumour progression (Wimmer *et al.*, 1999; Wimmer *et al.*, 2001). Recently, De Preter *et al.* (2002) analysed 128 neuroblastoma tumours for *MYCN*, *DDX1* and *NAG* amplification; out of the 66 *MYCN* amplified tumours, 24 were amplified for

DDX1 and *NAG* and 11 had only *DDX1* amplification. Neither of the latter two groups displayed decreased survival when compared to *MYCN* amplification alone. However, these authors failed to independently examine survival for all 35 patients with *DDX1* and *MYCN* amplified tumours (ie. the DDX1 tumour group was divided into two groups - NAG positive and NAG negative). Therefore, these studies have not conclusively proven whether the amplification of *DDX1* with *MYCN* negatively affects the prognosis of neuroblastoma patients. This may be partly because patients with *MYCN* amplification fair so poorly that it is difficult to assess whether amplification of a second gene creates a more aggressive tumour (Manohar *et al.*, 1995). All four reports, however, were in agreement that *DDX1* was amplified in 60 – 70% of *MYCN* amplified tumours. The fact that *MYCN* amplification is the mechanism for overexpression (and not another mechanism such as up-regulation of transcription or increased mRNA stability) suggests that other co-amplified genes may provide a selective cellular growth advantage. Furthermore, it has been noted that *DDX1* is consistently amplified as an intact gene, and the amplification is always accompanied by an increase in protein (Squire *et al.*, 1995; Godbout *et al.*, 1998). Considering the large size of this gene (~40 kb) and the fact that it is not a part of the core *MYCN* amplicon, it is unlikely that it would exist as an intact unit through all duplication events unless there was pressure to produce a functional protein.

DDX1 and *MYCN* co-amplification has been reported in one other human tumour: alveolar rhabdomyosarcoma (Pandita *et al.*, 1999). This is a childhood soft tissue sarcoma that affects skeletal muscle. Examination of 12 alveolar tumours revealed 6 with *MYCN* amplification, and in all cases, *DDX1* was co-amplified. Furthermore, these patients displayed a shorter disease free period and their mortality rates were higher than for those patients without gene amplification.

Although *MYCN* amplification is usually only seen in tumours of neuronal origin, Karlsson *et al.* (2001), observed that *MYCN* amplification occurred in an estrogen-dependent endometrial adenocarcinoma of the rat. The *MYCN* amplification was coupled with the low-level amplification of several other genes, including *DDX1*. These results suggest that *DDX1* and *MYCN* amplification could be important in other tumours such as those that are hormone-dependent.

A definitive role for DDX1 in neoplastic transformation has been reported in two abstracts (George *et al.*, 1998; Elsden *et al.*, 2001). In the first abstract the authors transfected *DDX1* into NIH 3T3 cells and then injected the cells into nude mice (George *et al.*, 1998). In two separate experiments, all injected mice showed tumour formation that appeared to be high grade sarcomas. Control experiments with c-Ha-*ras* transformed cells similarly injected into nude mice demonstrated a shorter time to tumour formation than *DDX1*-transformed cells; however, *DDX1*-transfected cells produced more invasive tumours. These results suggest that DDX1 can contribute to the malignant process without the presence of MYCN. The second abstract, by the same group, reports that NIH 3T3 cells stably transfected with *DDX1* show increased growth rates and increased growth in soft agar when compared to parental cell lines (Elsden *et al.*, 2001). These investigators also demonstrate that cells transfected with a mutationally active *c-Ha-ras* gene have increased DDX1 expression. This suggests that DDX1 may contribute to ras-induced cellular alterations.

Sequencing of *DDX1* cDNA uncovered not only the eight conserved DEAD box helicase motifs, but also a region with homology to heterogeneous nuclear ribonucleoprotein U (hnRNP U) (Godbout *et al.*, 1994). This region is located between motifs Ia and Ib (Fig. 1.2) and encompasses 128 amino acids that are 37% identical and 53% similar to the hnRNP U region. This feature is unique to DDX1; most DEAD box proteins have an average of 22-42 amino acids separating motifs Ia and Ib (Luking *et al.*, 1998) in contrast to DDX1, which has 240 amino acids. HnRNP U or SAF-A (scaffold attachment factor A), a protein located in the nuclear matrix, has recently been shown to function as a repressor of RNA polymerase II elongation by inhibiting TFIIH-mediated carboxy-terminal domain (CTD) phosphorylation (Kim and Nikodem, 1999). Interestingly, the domain common to both hnRNP U and DDX1 was found to mediate binding of TFIIH to the RNA polymerase II holoenzyme. This hnRNP U-like region within DDX1 was later identified as a SPRY domain (Godbout *et al.*, 2002). SPRY domains, first identified in splA kinase of *Dictyostelium* and in rabbit ryanodine receptor, have since been found in many ryanodine receptors as well as in RanBPM, RING finger proteins, and hnRNP U (Ponting *et al.*, 1997). The function of this domain remains unknown but has been hypothesized to be involved in protein-RNA interactions.

Expression analysis of *DDX1* revealed that the RNA is preferentially found in tissues of neuroectodermal origin including the retina, brain and spinal cord

(Godbout and Squire, 1993). Using the chick as a model system, Godbout *et al.* (2002), examined the tissue specific developmental expression of chDDX1. Similar to human tissues, expression was seen in all tissues examined (retina, brain, heart, liver, kidney). In general, transcript levels were higher at earlier stages of development. Western blot analysis performed on the same tissues using antibodies generated to the N-terminal end of recombinant DDX1 (amino acids 1-186) displayed a similar expression pattern, with a decrease in protein levels observed in the differentiating heart, liver and kidney. DDX1 protein remained elevated in the retina and brain. Concordantly, *in situ* hybridization analysis of the chick retina and brain demonstrated higher levels of *DDX1* transcripts in proliferating cells. Based on these data, we propose that DDX1 has an important role in actively dividing cells of neuroectodermal origin.

A *Drosophila* DDX1 ortholog has been cloned, and similar to human *DDX1*, *DmDdx1* (*Ddx1d)* shows elevated expression in early embryos. The protein is 58.3% identical to human DDX1 (Rafti *et al.*, 1996). Fortuitous creation of a *DmDdx1* mutant resulted in a recessive embryonic lethal phenotype (Zinsmaier *et al.*, 1994).

Western blot analysis has revealed that DDX1 exists in at least three forms with the top band at 89.5 kDa and the bottom band at 83.5 kDa (Godbout *et al.*, 1998). Thus far, it is unknown whether protein truncation or post-translational modifications contribute to the difference in protein size. Subcellular fractionation has shown that DDX1 is present predominantly in the nucleus of non-amplified cells with some protein appearing in the cytoplasm (Godbout *et al.*, 1998). In *DDX1*-amplified cells, the protein is located in approximately equal amounts in the cytoplasm and nucleus. Confocal microscopy analysis (Bléoo *et al.*, 2001) demonstrated that DDX1 is distributed in the nucleoplasm and as well, within discrete nuclear foci. Cytoplasmic DDX1 appears to follow a slightly filamentous pattern (unpublished observations). As both the nucleus and cytoplasm contain defined structures, localizing DDX1 to a specific region may help define a cellular function.

1.3 Nuclear Architecture

The nucleus is a membrane-bound organelle that is comprised of many distinct domains (Fig. 1.3). Although the specific function of many subnuclear domains has only been hypothesized, they are all thought to be temporally and spatially organized so as to promote efficient gene expression. Most of these domains are proving to be dynamic structures; not only do proteins flux between the nucleoplasm and the domain, but the domains themselves often disassemble during mitosis and reassemble in newly formed daughter cells (Mistelli, 2001). Moreover, some nuclear domains frequently reside adjacent to other domains. The reason behind this pairing is unknown; however, it is thought that the domains might each be contributing to a similar nuclear process. With this assumption, knowledge of the function of one domain may impart information as to the role of an adjacent domain. Pertinent to this thesis, cleavage bodies frequently reside adjacent to Cajal bodies (CBs) and PML bodies. Therefore an extended description of these particular bodies is included below.

Fig. 1.3 Nuclear domains commonly found in the eukaryotic cell nucleus.

The most well-characterized nuclear domains are illustrated in a eukaryotic cell nucleus. The nucleus is enclosed by a double-membrane, which is fused together in areas by nuclear pores (brown cylinders). Nuclear pores function to shuttle materials between the nucleus and the cytoplasm. The nucleolus is commonly found in association with perinucleolar compartments (PNC) and Sam68 nuclear bodies (SNB) in transformed cells. Splicing factor compartments (SFC) occur throughout the nucleus and are frequently observed to localize adjacent to sites of transcription. Cajal bodies (CB) may be found adjacent to the nucleolus, PML bodies, cleavage bodies, or gems. Chromosomes arrange into chromosome territories with active genes present on the surface.

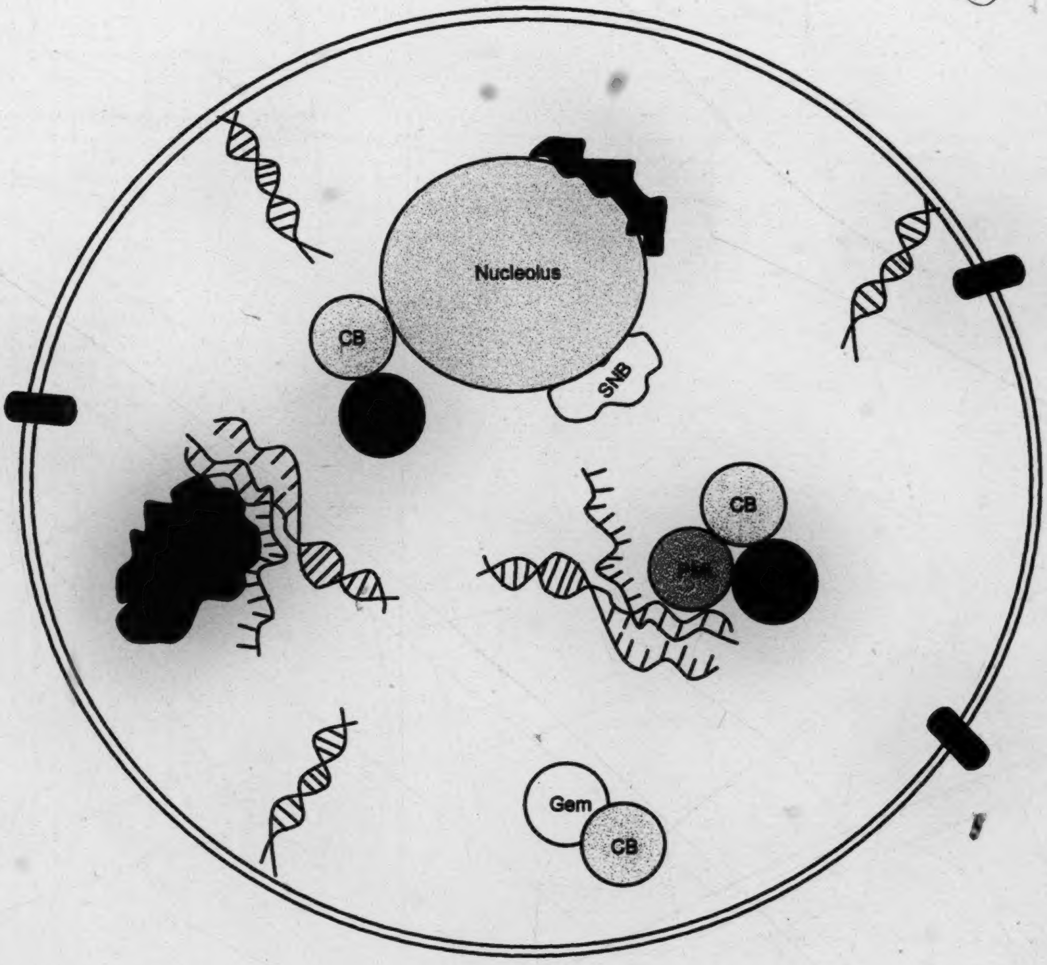
Nucleolus
CB
SNB
CB
Gem
CB

1.3.1 Nucleolus

The list of subnuclear domains is continually growing; however, the best studied domains include the nucleolus, splicing factor compartments (SFCs), PML bodies, CBs, gems, cleavage bodies, the perinucleolar compartment, and Sam68 nuclear bodies (SNBs) (Spector, 2001). The nucleolus is subdivided into three discrete compartments where the different aspects of ribosome biogenesis are thought to take place (Leary and Huang, 2001). The fibrillar centers contain the rDNA and transcription to rRNA is thought to take place on the borders of the fibrillar center, within the dense fibrillar component. rRNA undergoes multiple cleavages and modifications to become mature rRNA. This processing occurs within the granular component. The role of the nucleolus in ribosome biogenesis has been well established, however the nucleolus has been suggested to play a role in additional nuclear functions such as the ribonucleoprotein assembly of telomerase RNA and processing or export of RNA species including specific mRNAs, tRNA, U6 RNA, and signal recognition particle RNA (Pederson, 1998).

1.3.2 Splicing factor compartments

Splicing factor compartments (SFCs), or interchromatin granule clusters (IGCs) as they are known by electron microscopy, are 0.8-1.8 μm in diameter and number 10-50 per nucleus (Schul *et al.*, 1998a; Spector, 2001). SFCs are known to contain splicing factors (Fu and Maniatis, 1990; Spector *et al.*, 1991), hyperphosphoylated RNA polymerase II (Bregman *et al.*, 1995), and poly(A) binding protein II (PAB II) (Krause *et al.*, 1994). Recently, Mintz *et al.* (1999)

have isolated SFCs and using mass spectrometry have found other proteins such as lamins, histones, ribosomal proteins and hnRNPs associated with SFCs. Whether the latter are true constituents of SFCs or whether they are merely contaminating proteins remains to be determined.

The function of SFCs has not been conclusively proven; however, substantial evidence indicates that SFCs supply splicing factors to sites of transcription (Jiménez-Garcia and Spector, 1993; Huang and Spector, 1996; Misteli *et al.*, 1997; Smith *et al.*, 1999). Transcription likely does not occur in the center of SFCs as they contain little newly synthesized RNA as measured by [^{3}H]uridine or BrUTP incorporation (Fakan and Bernhard, 1971; 1973; Fakan and Nobis, 1978; Fakan *et al.*, 1976; Jackson *et al.*, 1993; Wansink *et al.*, 1993; Cmarko *et al.*, 1999). It was previously established that the periphery of SFCs often contains active genes (Huang and Spector, 1991; Xing *et al.*, 1993; 1995; Smith *et al.*, 1999); however, active genes may also be found elsewhere in the nucleoplasm (Zhang *et al.*, 1994; Dirks *et al.*, 1997; Smith *et al.*, 1999). Recently Smith *et al.* (1999) have hypothesized that SFCs nucleate at genomic sites undergoing high transcription and pre-mRNA processing. Other genes that are active will have an affinity for the components of SFCs and tend to cluster in the region. Following SFC formation, expressed genes that reside in distant chromosome territories will associate with SFC domains at a frequency similar to inactive genes. This theory explains both the almost 100% colocalzation of the highly expressed β-cardiac myosin heavy chain gene with SFCs as well as the virtual exclusion of the active lamin B1 gene from SFCs in cultured myotubes (Smith *et al.*, 1999).

By electron microscopy, IGCs are composed of smaller granules, 20-25 nm in diameter, and these are connected by 9-10 nm fibrils (Monneron and Bernhard, 1969). These fibrils are labeled with [^{3}H]uridine suggesting that they represent sites of transcription (Bachellerie *et al.*, 1975; Fakan *et al.*, 1976; Fakan, 1994). Corroborating these observations, Mintz and Spector (2000) have used immunofluorescence microscopy to reveal that SFCs are composed of smaller 'subspeckles' that loop out to form string-like structures in actively transcribing cells. These subspeckles are located near sites of transcription, and contain splicing factors as well as PAB II. Therefore, the recent results of Mintz and Spector as well as those by Smith *et al.*, support the view that SFCs likely exist to supply pre-mRNA processing factors to areas undergoing gene transcription.

1.3.3 PML bodies

A nuclear domain that often exists in close proximity to the nucleolus is the PML body, also known as nuclear domain 10 (ND10), or PML oncogenic domain (POD). There are 5-20 PML bodies per nucleus and they range in size from 0.1-1.0 μm in diameter (Seeler and Dejean, 1999). The PML body contains the PML protein, whose gene is found fused to the α-retinoic acid receptor (RARα) gene in acute promyelocytic leukemia (APL) patients with a t(15,17) translocation. This fusion protein results in the disruption of PML bodies; however, treatment with retinoic acid results in caspase cleavage of the fusion protein, release of RARα (Nervi *et al.*, 1998), and reformation of PML nuclear bodies (Dyck *et al.*, 1994; Koken *et al.*, 1994; Weis *et al.*, 1994). The role of PML and PML bodies in APL remains controversial. Observations that RARα can be fused to other proteins such as PLZF, NPM, and NuMA suggest that it is RARα and not PML that contributes to the malignant process (Seeler and Dejean, 1999). Contradicting this view are the observations that transgenic expression of PML-RARα in the myeloid promyelocytic cell lineage of mice causes slow onset leukemia reminiscent of APL (Grisolano *et al.*, 1997; He *et al.*, 1997), while crossing these mice with Pml-/- mice greatly increases the incidence of disease and accelerates disease onset (Rego *et al.*, 2001). These findings suggest that PML inactivation is a critical component in APL pathogenesis.

The PML protein exists as several different isoforms due to alternative splicing (Jensen *et al.*, 2001) and all isoforms are covalently modified by a ubiquitin-like protein called SUMO-1 (Sternsdorf *et al.*, 1997; Kamitani *et al.*, 1998). SUMO-1 modification of PML specifically targets PML to PML bodies (Muller *et al.*, 1998), and this PML modification is also essential for the localization of other proteins to PML bodies (Ishov *et al.*, 1999; Fogal *et al.*, 2000; Zhong *et al.*, 2000a). SUMO-1 modification does not target proteins for degradation; rather, this modification makes proteins such as RanGAP1 and IκBα resistant to degradation (Mahajan *et al.*, 1997; Desterro *et al.*, 1998) suggesting that SUMO-1 modification may serve to prevent ubiquitin conjugation and therefore increase protein stability (Ruggero *et al.*, 2000). Interestingly, proteins from other nuclear compartments such as HIPK2 and TEL localize to SFCs and unidentified nuclear foci, respectively, when SUMO-modified (Kim *et al.*, 1999; Chakrabarti *et al.*, 2000). This may imply a role for SUMO modification in protein targeting to specific nuclear compartments.

The function of PML bodies is currently speculative. It is known that PML bodies do not contain RNA and therefore do not represent sites of active transcription (Boisvert *et al.*, 2000). In addition to the PML protein, other proteins that localize to PML bodies include DAXX (Ishov *et al.*, 1999; Torii *et al.*, 1999), pRB (Alcalay *et al.*, 1998), Sp100 (Maul *et al.*, 1995), CBP (LaMorte *et al.*, 1998), p53 (Ferbeyre *et al.*, 2000; Fogal *et al.*, 2000; Guo *et al.*, 2000; Pearson *et al.*, 2000), TRF1 and TRF2 (Yeager *et al.*, 1999), SIRT1 (Langley *et al.*, 2002) and several other proteins some of which have unknown functions (Seeler and Dejean, 1999; Negorev and Maul, 2001). Both PML and the number of PML bodies are upregulated by type I and type II interferons (Lavau *et al.*, 1995; Stadler *et al.*, 1995; Grotzinger *et al.*, 1996), and both appear upregulated in inflammatory tissues (Terris *et al.*, 1995). These observations coupled with the fact that PML bodies are destroyed upon viral infection (Maul *et al.*, 1993; Kelly *et al.*, 1995; Puvion-Dutilleul *et al.*, 1995) have led to the hypothesis that PML bodies are involved in viral defense mechanisms.

PML bodies have also been associated with transcriptional regulation. The PML protein does not bind DNA itself; however, when tethered to the promoter of a Gal4 DNA-binding domain, PML imparts transcriptional repression (Vallian *et al.*, 1997). Overexpression of PML also leads to transcriptional repression of MDR and EGF-receptor promoters (Mu *et al.*, 1994). This activity is attributed to PML's ablility to bind the Sp1 transcription factor thereby preventing DNA binding (Vallian *et al.*, 1998). PML has also been found to bind non-phosphorylated pRB, consequently eliminating pRB-mediated transactivation of the glucocorticoid receptor (Alcalay *et al.*, 1998). PML has likewise been found to enhance pRB-mediated transcriptional repression of a luciferase reporter construct (Khan *et al.*, 2001a). PML may confer its repressive activity indirectly by binding to pRB-HDAC or through direct binding to HDAC-1 (Khan *et al.*, 2001b; Wu *et al.*, 2001) or other corepressors such as c-Ski, N-CoR, and mSin3A (Khan *et al.*, 2001b). The binding of PML to corepressors has been shown to be required for MAD-dependent transcriptional repression (Khan *et al.*, 2001b). Although these studies clearly implicate PML in transcriptional repression, it is not known if PML bodies are the sites where this activity occurs.

In contrast to its role in transcriptional repression, PML and PML bodies have also been implicated in transcriptional activation or inhibition of transcriptional repression. Viral genes localize to the periphery of PML bodies suggesting that they provide a permissive environment for viral transcription (Ishov *et al.*, 1997). Additional observations that nascent RNA accumulates on the periphery of PML bodies, and highly acetylated chromatin can be found within PML bodies suggest that transcriptional events occur in close proximity to PML bodies (Boisvert *et al.*, 2000). PML bodies also contain the histone acetyltransferase protein, CBP (LaMorte *et al.*, 1998; Zhong *et al.*, 2000a). CBP is a transcriptional coactivator for a variety of transcription factors including the glucocorticoid receptor (GR) and the retinoid X receptor (RXR) (Chakravarti *et al.*, 1996; Kamei *et al.*, 1996). PML was found to bind CBP *in vitro*, and PML expression was found to potentiate transactivation by RXR and GR (Doucas *et al.*, 1999; Zhong *et al.*, 1999). This transactivation is likely due to the ability of PML to recruit CBP to PML bodies (Doucas *et al.*, 1999), and suggests that PML bodies may function to stabilize transcriptional activator complexes. PML may also reverse transcriptional repression as Li *et al.* (2000) have observed that overexpression of PML eliminates transcriptional repression by DAXX. This activity once again correlated with the localization of DAXX to PML bodies. Likewise, PML also suppresses transcription inhibition by HTLV-1 Tax protein by sequestering it to PML bodies (Doucas and Evans, 1999). Taken together, these observations suggest that PML bodies may modulate the function of transcriptional activators or repressors through interaction with PML and/or sequestration into specific nuclear domains.

Several observations point to a role for PML in apoptosis. Studies on *Pml-/-* splenocytes suggest that Pml is involved in apoptosis induced by Fas, TNFα, ceramide, and type I/II interferons (Wang *et al.*, 1998). This induction is through the caspase 1 and 3 pathways. A role for PML in caspase-independent cell death was reported by Quignon *et al.* (1998) who observed that overexpression of PML did not trigger caspases yet it induced cell death in HeLa and CHO cells. DAXX was first identified by its ability to bind Fas, an apoptosis-inducing protein belonging to the tumor necrosis factor receptor family (Yang *et al.*, 1997). Although DAXX has recently been shown to not bind Fas, it does enhance Fas-induced apoptosis and this activity is dependent on its localization to PML bodies (Torii *et al.*, 1999). The Fas signaling cascade induced by DAXX is mediated by caspases rather than the other caspase-independent pathway that Fas can also trigger. The fragment of DAXX that is responsible for Fas activation and for proper localization to PML bodies was found to mediate transcriptional repression when bound to a heterologous DNA-binding domain. A more recent report provides evidence that PML and DAXX physically interact, and that PML protein is required for DAXX activated apoptosis (Zhong *et al.*, 2000b). Therefore, the activation of apoptosis by DAXX could be linked to the transcriptional modulator activity of PML bodies. Although these observations support a role for DAXX in promoting apoptosis, the fact that *Daxx-/-* mice show increased apoptosis leaves the exact function of DAXX in apoptosis unresolved (Michaelson *et al.*, 1999)

PML may also be involved in p53-dependent apoptosis (Fogal *et al.*, 2000; Guo *et al.*, 2000). DNA-damage induced apoptosis is impaired in *Pml-/-* cells, and this correlates with decreased p53 activity, and decreased p53-DNA binding (Guo *et al.*, 2000). Transfection of *Pml* into the *Pml-/-* cells was found to enhance p53 transactivation of a Bax-luciferase reporter construct; however this only occurred when Pml was able to localize within PML bodies. An explanation for the activation of p53 by PML came from observations by Pearson *et al.* (2000) that activated Ras could induce the relocalization of p53 and CBP acetyltransferase into PML bodies, as well as stimulate complex formation between PML, CBP and p53. Ras activation also induced p53 acetylation thereby implicating PML bodies as critical sites for p53 activation. Interestingly, Fogal *et al.* (2000) have observed that only a specific isoform of PML, PML3, could interact, transactivate, and localize p53. This activation required that PML3 localize within PML bodies. In addition to acetylation, p53 may also be activated by phosphorylation. Recently, upon UV irradiation, homeodomain-interacting protein kinase-2 (HIPK2) phosphorylated and activated p53 (D'Orazi *et al.*, 2002; Hofmann *et al.*, 2002). This presumably took place in PML bodies as p53 was seen to colocalize there with HIPK2 and PML3. The phosphorylation on Ser46 of p53 resulted in its acetylation by CBP, which also colocalized to PML bodies (Hofmann *et al.*, 2002). Therefore the activation of p53 by phosphorylation and acetylation is linked to its localization to PML bodies, further enforcing the hypothesis that PML bodies function to activate p53.

Yet another function for PML involves cellular senescence. Cellular senescence is responsible for the definitive lifespan that occurs in primary cells, and is characterized by cellular growth arrest without apoptosis (reviewed in Mathon and Lloyd, 2001). Senescence is naturally triggered in most human cell types by telomere shortening that occurs with each round of DNA synthesis. Senescence can also be triggered prematurely by serial passaging of cells, exposure to some DNA damaging agents, or Ras overexpression. Studies of premature senescence in Ras-activated fibroblasts demonstrated that PML was upregulated, and this upregulation activated both the p53 and pRB pathways – both of which are required to maintain senescence (Ferbeyre *et al.*, 2000; Pearson *et al.*, 2000). The activation of PML corresponded with the acetylation of p53 and this was likely due to the tricomplex formed by p53, CBP acetyltransferase and PML within PML bodies (Pearson *et al.*, 2000). It was noted that a fraction of pRB was also recruited into PML bodies (Ferbeyre *et al.*, 2000). A regulator of cellular senescence, SIRT1, was also found to localize within PML bodies following Ras overexpression (Langley *et al.*, 2002). SIRT1 is a histone deacetylase, which was observed to bind both PML and p53 thereby triggering p53 deacetylation. SIRT1 overexpression interfered with p53-mediated transactivation, and abrogated PML-induced cellular senescence.

In apparent contradiction to PML's role in cellular senescence, PML has also been reported to be involved in telomere lengthening. Whereas most tumour cells activate the enzyme telomerase to prevent telomere shortening, a small portion of tumours and cell lines instead use a mechanism termed alternative lengthening of telomeres (ALT) to retain or increase telomere length (reviewed in Henson *et al.*, 2002). Cell lines that use ALT have altered PML bodies which contain the ALT proteins, telomere repeat binding factors 1 and 2 (TRF1 and TRF2), extrachomosomal telomeric DNA, and proteins involved in DNA recombination and repair (Yeager *et al.*, 1999). It has been suggested that ALT occurs through a mechanism involving DNA recombination explaining both the presence of the recombination and repair proteins found in PML bodies, and the heterogeneous nature of their telomeres (Colgin and Reddel, 1999). The presence of ALT-associated PML bodies and heterogeneous telomere length is not affected by telomerase expression in ALT cells (Cerone *et al.*, 2001; Perrum *et al.*, 2001; Grobelny *et al.*, 2001); however, hybridization of these cells with telomerase-positive cell lines causes stability of telomere length concordant with PML body disappearance suggesting that telomerase-positive cells contain a factor that represses ALT (Perrem *et al.*, 2001). Whether the ALT-associated PML bodies are the sites of ALT activity remains to be determined.

The aforementioned data clearly describe PML bodies as functional domains. Indeed, Shiels *et al.* (2001) have recently reported that PML bodies specifically associate with the major histocompatibility complex (MHC) gene cluster on chromosome 6 at all stages of the cell cycle regardless of MHC transcriptional activity. This organization is predicted to reflect a functional requirement for PML bodies. A role for PML bodies in apoptosis and cellular senescence can be rationalized by its abililty to modulate transcription. Likewise, the association with the MHC gene cluster could allow PML bodies to both activate and suppress transcription (Shiels *et al.*, 2001). There is, however, a body of evidence that supports a role for PML bodies as nonessential, regulatory storage depots (reviewed by Negorev and Maul, 2001). Several proteins, such as Int6, BRCA-1, and influenza NP1, only localize to PML bodies upon ectopic or overexpression suggesting that PML bodies function as storage facilities for 'unwanted' proteins (Desbois *et al.*, 1996; Maul *et al.*, 1998; Anton *et al.*, 1999). The discovery of RNA polymerase II at PML bodies (von Mikecz *et al.*, 2000) but not RNA (Boisvert *et al.*, 2000) indicates that PML bodies are not actively functioning in transcription but instead may be regulating the release of the RNA polymerase II enzyme (Negorev and Maul, 2001). This hypothesis can also be applied to the numerous transcription modulators found in PML bodies. The involvement of PML and DAXX in apoptosis can be interpreted as a function delegated by default; the cell receives an external stimulus and this causes release of PML body proteins, some of which mediate apoptosis (Negorev and Maul, 2001). Although these two views of PML body function seem contradictory, they are both compatible with the idea that PML bodies are involved in transcription. The contentious issue is the location of transcription with respect to PML body distribution.

1.3.4 Cajal Bodies (CBs)

CBs were first discovered in 1903 by Professor Santiago Ramón y Cajal using silver staining in conjunction with light microscopy. Although Cajal first named them accessory bodies because they were often close to or touching the nucleolus, Monneron and Bernhard (1969) later termed them coiled bodies due to their appearance as electron dense threads in the electron microscope. They were later renamed Cajal bodies to honour their original founder (Gall, 1999).

CBs range in size from 0.1 to 1.5 µm in diameter and number on average between 1-10 foci per nucleus (reviewed in Lamond and Earnshaw, 1998). They are more prevalent in rapidly growing cells (Brasch and Ochs, 1992; Spector *et al.*, 1992) and these structures disassemble during prophase and reform in early G1 after the resumption of transcription (Andrade *et al.*, 1993; Ferreira *et al.*, 1994). Examination of PML bodies and CBs has revealed that these structures often display non-random pairing (Grande *et al.*, 1996). The significance of this relationship is thus far unresolved.

The mechanism by which CBs assemble is unknown. In addition to their frequent association with the nucleolus, CBs have been observed to exist free in the nucleoplasm as well as adjacent to histone, snRNA, and snoRNA gene loci (Gall *et al.*, 1981; Callan *et al.*, 1991; Frey and Matera, 1995; Smith *et al.*, 1995; Gao *et al.*, 1997; Frey *et al.*, 1999; Jacobs *et al.*, 1999; Schul *et al.*, 1999a). However, unlike the nucleolus, which assembles in nucleolar organizing regions around ribosomal DNA, CBs do not appear to require specific DNA sequences for their formation as they will assemble in *Xenopus* egg extracts containing only prokaryotic DNA (Bell *et al.*, 1992). No single protein has been discovered to be responsible for CB formation, and the process does not seem to require active transcription or translation (Handwerger *et al.*, 2002). One current hypothesis is that CBs initiate due to the accumulation and interaction of its constituents within the nucleoplasm (Handwerger *et al.*, 2002).

The function of CBs also remains speculative. CBs do not contain DNA (Thiry, 1994) and they do not accumulate nascent RNA making them unlikely sites of transcription (Fakan and Bernhard, 1971; Jordan *et al.*, 1997; Schul *et al.*, 1998b). Examination of CB protein content has revealed only one common theme: CBs contain proteins and ribonucleoproteins involved in the transcription and processing of RNAs from RNA polymerase I, II and III. Blocking transcription leads to the disappearance of splicing factors from CBs suggesting that CBs are not simply storage facilities (Carmo-Fonseca *et al.*, 1992). Taken together, observations support the hypothesis that CBs function to assemble complexes involved in transcription (Gall, 2000).

The first components identified in CBs were the Sm proteins detected using autoimmune sera from patients with systemic lupus erythematosus (Eliceiri and Ryerse, 1984; Fakan *et al.*, 1984, Raška *et al.*, 1991). Sm proteins associate with snRNAs in the cytoplasm to create snRNPs. Assembled snRNPs, which contain a trimethylguanosine (TMG) cap structure, are recruited back to the nucleus where they function as essential cofactors in the pre-mRNA splicing process. Later, it was established that capped snRNAs themselves are present in CBs suggesting that CBs might play a role in the final assembly of snRNPs following their nuclear import (Raska *et al.*, 1991; Carmo-Fonseca *et al.*, 1991, 1992; Huang and Spector, 1992; Matera and Ward, 1993). GFP-targeting experiments have given further credibility to this theory as tagged Sm proteins have been shown to first localize within CBs in the nucleus after which they migrate to splicing factor compartments (Sleeman and Lamond, 1999). The discovery of the spinal motor neuron (SMN) protein within CBs further suggested a role in snRNP biogenesis as SMN and its cofactors are crucial for cytoplasmic snRNP assembly (Fischer *et al.*, 1997; Matera and Frey, 1998; Carvalho *et al.*, 1999; Meister *et al.*, 2001).

In addition to containing essential splicing factors, *Xenopus* oocyte CBs also contain phosphorylated RNA polymerase II (Gall and Murphy, 1998; Morgan *et al.*, 2000). Tagging of the two small subunits of RNA polymerase II revealed that it initially resides within CBs for a few hours prior to its distribution to the nucleoplasm (Morgan *et al.*, 2000). Interestingly, other components of CBs include some of the subunits of general transcription factor TFIIH including p62, cyclin-dependent kinase 7, cyclin H and MATI all of which co-ordinate to phosphorylate the CTD *in vitro* (Grande *et al.*, 1997; Jordan *et al.*, 1997). The significance of phosphorylated RNA polymerase II within oocyte CBs is unknown as phosphorylation of the CTD of RNA polymerase II is thought to occur after the enzyme initiates transcription, just prior to elongation (Dahmus, 1996). In contrast to the results in *Xenopus*, human cells were found to contain hypophosphorylated RNA polymerase II that partially overlapped CBs (Schul *et al.*, 1998b). Other factors involved in transcription and processing of pre-mRNA also localize to either human or *Xenopus* oocyte CBs including: cleavage factor CstF 77, cleavage and polyadenylation specificity factor (CPSF100), transcription factors IIF and IIS (TFIIF and TFIIS), TATA-box binding protein (Schul *et al.*, 1998b; Gall *et al.*, 1999, 2000), and TATA-binding protein associated factor II70 (TAFII70) (Bucci *et al.*, 2001). In some cells, cleavage and polyadenylation factors are located adjacent to CBs in a structure termed cleavage bodies (discussed later). Therefore, many components of RNA polymerase II transcription and pre-mRNA processing are found within or adjacent to CBs.

Although CBs have been implicated in the assembly of the transcription and processing complex, the observation that CBs frequently lie adjacent to histone gene clusters is intriguing as histone transcripts do not get processed in a similar manner to other pre-mRNA transcripts (reviewed in Dominski and Marzluff, 1999). Instead of acquiring a poly(A) tail, histone transcripts end with a 26-nucleotide sequence that contains a stem-loop structure. Correct processing of histone mRNA requires a 3'-end cleavage step that is dependent on several proteins including stem-loop binding protein, and a small nuclear RNP, U7 snRNP. Both of these proteins have been shown to localize within CBs. Although histone gene transcripts have not been observed to localize within CBs (reviewed in Gall, 2000), the arrangement of histone genes in a cluster implies the presence of histone pre-mRNA processing centers (Dominski and Marzluff, 1999). CBs may localize near such centers to supply components required for histone transcript 3'end processing. Supporting a role in histone gene transcription, Ma *et al.* (2000) have observed that a protein called p220^{NPAT} localizes within CBs where it is phosphorylated by cyclinE/Cdk2 at late G1 or S phase. The timing of this phosphorylation co-ordinates with the onset of histone gene transcription, and mutation of the Cdk2 phosphorylation site abrogates histone H2B transcription. Corroborating evidence was provided by Zhao *et al.* (2000) who observed that p220^{NPAT} expression in U2OS osteosarcoma cells activated histone gene transcription, and that process is enhanced by cyclinE/Cdk2 co-transfection.

The number of proteins that are shared by both the CB and the nucleolus epitomizes the tight association of CBs with the nucleolus. These shared proteins, which are often required for rRNA transcription and processing, include: fibrillarin (Raška *et al.*, 1990,1991), NAP57, Nopp140 (Meier and Blobel, 1994), ribosomal protein S6 (Jiménez-García *et al.*, 1994), Brix (Kaser *et al.*, 2001), and DNA topoisomerase I (Raška *et al.*, 1991). Processing of rRNA involves small nucleolar ribonucleoproteins (snoRNPs), which are comprised of proteins bound to snoRNA (reviewed in Lafontaine and Tollervey, 1998). The snoRNAs, specifically U3 and U8, have been observed to localize to CBs (Bauer *et al.*, 1994; Jiménez-García *et al.*, 1994) and, recently, injection of fluorescent U3 and U8 snoRNA into *Xenopus* oocytes demonstrated that U3 and U8 travel through CBs on their way to nucleoli (Narayanan *et al.*, 1999; Speckman *et al.*, 1999). Within *Xenopus* oocytes, Gall *et al.* (1999) have also observed the two largest subunits of RNA polymerase I, RPA194 and RPA127. Taken together, the localization of nucleolar proteins to CBs suggest that CBs assist the nucleolus in rRNA transcription and processing.

The finding of RNA polymerase I and II within CBs prompted Gall *et al.* (1999) to examine RNA polymerase III localization in *Xenopus* oocytes. Immunofluorescent staining of two RNA polymerase III subunits revealed strong CB labelling. As RNA polymerase III is responsible for transcribing 5S rRNA in addition to tRNA, Gall *et al.* (1999) examined TFIIIA location because it has been shown to be a specific transcription factor for the 5S rRNA gene. TFIIIA likewise strongly stained CBs, suggesting that CBs are also involved in RNA polymerase III transcription.

The hypothesis that CBs are involved in 'transcriptosome' assembly for all three polymerases is an attractive one; however, it does not account for the observation that cells in which CBs have been disrupted continue to survive without apparent effects (Almeida *et al.*, 1998). Additionally, cells from some human tissues do not have CBs (Young *et al.*, 2000). Regardless, until a new hypothesis surfaces which encompasses all observations, the CB as a 'transcriptosome' assembly unit will remain.

1.3.5 Gems

Gems, first identified by Liu and Dreyfuss (1996), are a nuclear structure that exists adjacent to CBs. After this initial report, gems became immediately notorious because one of its constituents was discovered to be the SMN protein (Liu and Dreyfuss, 1996). This protein is frequently mutated or displays a low level of expression in patients with spinal muscular atrophy, a potentially lethal neurodegenerative disease (reviewed in Talbot, 1999; Jablonka *et al.*, 2000). Subsequent to the initial observation that SMN localizes to gems, others examined several cell lines and primary cells for SMN only to discover that it usually is found within CBs (Matera and Frey, 1998; Carvalho *et al.*, 1999; La Bella *et al.*, 2000; Young *et al.*, 2000). The cell line used by Liu and Dreyfuss, HeLa PV, appeared to be the exception; however, a recent report by Young *et al.* (2001) has demonstrated that in fetal tissues, gems and CBs are distinct structures which merge in adult tissues. The concept of alterations in nuclear structure during development is intriguing and will need further investigation.

Despite the controversy over SMN localization, examination of SMN-binding proteins has given some insight as to a potential function. Not surprising, some proteins that have been found to interact with SMN are components of CBs (reviewed in Terns and Terns, 2001). One function for SMN is related to its cytoplasmic localization where it binds to SMN-interacting protein 1 (SIP1) (Liu *et al.*, 1997). Together these proteins form a complex with spliceosomal snRNP proteins. The SMN-SIP1 complex likely functions in snRNP biogenesis as injection of anti-SIP1 antibodies into *Xenopus* oocytes inhibited snRNP assembly and nuclear import (Fischer *et al.*, 1997). Other proteins reported to exist in an SMN complex also bind to Sm proteins and therefore may function in snRNP biogenesis. These include a DEAD box protein, DP103 (Gemin3) (Charroux *et al.*, 1999; Campbell *et al.*, 2000), Gemin4 (Charroux *et al.*, 2000), Gemin5 (Gubitz *et al.*, 2002), and Gemin6 (Pellizzoni *et al.*, 2002).

With respect to its nuclear localization, SMN is reported to affect pre-mRNA splicing as antibodies against SMN inhibit *in vitro* splicing (Pellizzoni *et al.*, 1998; Meister *et al.*, 2000; Gangwani *et al.*, 2001). Interactions with three hnRNP Q proteins and hnRNP R (Mourelatos *et al.*, 2001; Rossoll *et al.*, 2002) provide further evidence for SMN's role in splicing as one of these proteins, hnRNP Q3, has been identified by nanoelectrospray mass spectrometry as a constituent of the spliceosome (Neubauer *et al.*, 1998). Furthermore, immunodepletion of HeLa nuclear extracts using an antibody that recognizes hnRNP Q1-3 and hnRNP R impairs *in vitro* splicing of two pre-mRNA substrates and splicing efficiency is restored only upon addition of all four proteins (Mourelatos *et al.*, 2001). Another protein of unknown function, ZPR1, was reported to colocalize with SMN and similarily, immunodepletion of ZPR1 inhibited *in vitro* splicing of a pre-mRNA substrate (Gangwani *et al.*, 2001). Interestingly, antisense oligonucleotide depletion of ZPR1 in HeLa cells conferred SMN mislocalization, suggesting that ZPR1 is critical for proper SMN targeting to CBs/gems (Gangwani *et al.*, 2001). These studies, together with the discovery that a conditional knockout of the *Schizosaccharomyces pombe* gene, *Yab8p*, which is structurally related to SMN, causes nuclear accumulation of poly(A) mRNA and inhibition of splicing (Hannus *et al.*, 2000), advocate a role for SMN in the splicing process.

In addition to splicing, SMN has been reported to interact with nucleolar proteins involved in ribosome biogenesis including fibrillarin (Lui and Dreyfuss, 1996; Jones *et al.*, 2001; Pellizoni *et al.*, 2001a), and GAR1 (Pellizoni *et al.*, 2001a). Expression of a dominant-negative mutant of SMN causes inhibition of RNA polymerase I transcription (Pellizzoni *et al.*, 2001b) and accumulation of snoRNPs in CBs. It has been speculated that this reorganization of snoRNPs into CBs is responsible for the cessation of transcription in the nucleolus (Pellizzoni *et al.*, 2001a). These observations suggest that in addition to a role in snRNP biogenesis (occurring within the cytoplasm), SMN is involved with snoRNP assembly, which occurs exclusively within the nucleus (Pellizzoni *et al.*, 2001a).

Several reports have linked SMN and its complex to a role in transcription. SMN has been shown to bind RNA helicase A (RHA), a DEAD box RNA helicase that binds to RNA polymerase II (Pellizzoni *et al.*, 2001b). Immunoprecipitation of RHA pulled down the SMN-gemin complex as well as both hyper- and hypophosphorylated RNA polymerase II. RHA likely mediates the association of the SMN complex with the CTD of RNA polymerase II as *in vitro* binding assays display largely enhanced binding of SMN to GST-CTD when RHA is present. Similar to its effects on RNA polymerase I, expression of the dominant-negative SMN mutant caused inhibition of RNA polymerase II transcription correlating with the hypophosphorylated form accumulating in CBs (Pellizzoni *et al.*, 2001b). The interaction with both forms of RNA polymerase II, yet accumulation of only the hypophosphorylated form within CBs hints at a possible involvement of the SMN complex with RNA polymerase II regeneration prior to subsequent rounds of transcription (ie. dephosphorylation) (Pellizzoni *et al.*, 2001b).

SMN has also been reported to interact with two other transcriptional regulators including bovine papillomavirus (BPV) E2 (Strasswimmer *et al.*, 1999) and the FUSE (far-upstream element) binding protein (FBP) (Williams *et al.*, 2000). Binding of SMN to BPV E2 was demonstrated by a yeast two-hybrid screen and confirmed using GST pull-down assays and immunoprecipitations (Strasswimmer *et al.*, 1999). Cells transfected with an E2-binding site reporter construct, E2, and SMN displayed enhanced activation of gene expression compared to transfection with reporter and E2 alone. These results suggest that SMN can enhance transcriptional activation mediated by a transcriptional activator. Whether this activation is due to enhanced snRNP biogenesis is unknown. Similar to BPV E2, FBP activates transcription, specifically of *c-myc* (Duncan *et al.*, 1994). FBP also stabilizes *GAP-43* mRNA, a protein which affects axonal growth and formation of neuronal connections (Benowitz *et al.*, 1997; Irwin *et al.*, 1997). Therefore, SMN has many connections to RNA polymerase II transcription leading to the hypothesis that SMN plays a central role in transcriptosome assembly within CBs (Pellizzoni *et al.*, 2001b).

Although not well characterized, a few reports have implicated SMN in apoptosis. SMN binds to human Bcl-2 (but not chicken Bcl-2) and enhances its anti-apoptotic effect on Bax- or Fas-induced apoptosis (Iwahashi *et al.*, 1997;

Sato *et al.*, 2000). Further supporting this interaction is the observation that in rat spinal cord cells SMN is located in close proximity to the outer mitochondrial membrane, where Bcl-2 also localizes (Pagliardini *et al.*, 2000). Contradicting this observation, La Bella *et al.* (2000) report no association of SMN with the mitochrondria in rat spinal cord cells. SMN has also been reported to bind p53 (Young *et al.*, 2002). Therefore, although an active role for SMN in motoneuron maintenance is appealing, further evidence is required before assigning such a function to SMN.

1.3.6 Cleavage Bodies

Cleavage bodies are yet another type of nuclear body which frequently resides adjacent to CBs. These structures were first described by Schul *et al.* (1996) who were investigating the localization of two RNA 3' cleavage factors in T24 bladder carcinoma cells: cleavage stimulation factor-64 (CstF-64) and cleavage and polyadenylation specificity factor (CPSF). CstF-64 is part of a heterotrimeric complex, CstF, which functions not only in pre-mRNA 3' cleavage, but also in transcription termination (Wahle and Rüegsegger, 1999; Calvo and Manley, 2001). CPSF, an essential factor for the cleavage and polyadenylation process, binds to both RNA polymerase II (Dantonel *et al.*, 1997) and the polyadenylation signal sequence AAUAAA, effectively linking transcriptional termination with 3' pre-mRNA processing (reviewed in Proudfoot *et al.*, 2002). Co-labelling of these proteins revealed that they localized to nuclear structures 0.3 – 1 μm in diameter. Within T24 cells, anti-CstF-64 antibody labelled 1-4 structures, and co-labelling with anti-p80-coilin, which recognizes CBs, revealed perfect colocalization with 42% of CstF-64 foci, and adjacent localization with 18% of CstF-64 foci. The 18% of distinct CstF-64 foci located adjacent to CBs was later found to represent the population of cells in S phase (Schul *et al.*, 1999b). In G1 phase, the cleavage bodies and CBs were found to be completely overlapping, whereas in late S and G2 phase, the cleavage bodies disintegrated. As snRNA and histone genes were known to associate with CBs, Schul *et al.* (1999b) examined whether cleavage bodies were preferentially localized to these gene loci. Approximately 37% of T24 nuclei displayed partial or complete overlap between the histone gene cluster on chromosome 6 and cleavage bodies. This overlap was specific for S phase cells. Because they had previously observed some BrUTP incorporation into cleavage bodies (Schul *et al.*, 1996), the authors hypothesized that cleavage bodies function adjacent to CBs to promote histone gene transcription. These findings, although intriguing, were unexpected as histone gene transcripts do not undergo typical pre-mRNA 3' end processing (reviewed in Dominski and Marzluff, 1999).

Cleavage bodies have also been reported to contain general transcription factors. Labelling of human cells with antibodies that recognize the p62 subunit of TFIIH and with antibodies directed against the RAP74 subunit of TFIIF revealed foci that overlapped, yet extended beyond CBs (Schul *et al.*, 1998). Co-labelling with anti-CstF-64 demonstrated that these extensions represent cleavage bodies. Unpublished results in a review by Gall (2000) verified the localization of TFIIF to cleavage bodies in HeLa cells. Furthermore Gall (2000) reported an additional transcription factor, TFIIE, similarly localized to cleavage bodies. The localization of general transcription factors to cleavage bodies may explain the specific association with histone gene clusters. Overall, the concentration of factors involved in 3' end pre-mRNA processing and transcription factors to a domain adjacent or overlapping with CBs suggests that they collaborate to supply components of the transcription complex.

1.3.7 Perinucleolar Structures

The perinucleolar compartment (PNC) is an irregularly shaped domain located at the periphery of the nucleolus (reviewed in Huang, 2000). The structure ranges in size from 0.25 to 1 μm in diameter, and like other nuclear domains it disassembles during mitosis. The PNC is primarily found in transformed cells and rarely in primary cultured cells (Huang *et al.*, 1997).

The first constituents identified in the PNC were the polypyrimidine tract binding protein (PTB), also known as hnRNP I, as well as small RNA polymerase III transcripts (Ghetti *et al.*, 1992; Matera *et al.*, 1995). PTB is an RNA binding protein involved in pre-mRNA alternative splicing, and translational regulation of some viral transcripts (reviewed in Valcarcel and Gebauer, 1997; Wagner *et al.*, 2001). Two other proteins that have been subsequently localized to PNCs include CUG-binding protein (CUG-BP/hNAb50) (Timchenko *et al.*, 1996) and KH-type splicing regulatory protein (KRSP) (unpublished data mentioned in Huang, 2000). CUG-BP is a protein that binds to CUG triplet repeats in the gene myotonin dystrophy protein kinase (MDPK) (Timchenko *et al.*, 1996). This protein is associated with myotonic dystrophy and has recently been found to affect MDPK protein levels (Takahashi *et al.*, 2001). The KRSP protein is part of a complex that binds to an intronic splicing enhancer of the neuron-specific *c-src* N1 exon and therefore likely functions as a splicing regulator (Min *et al.*, 1997).

The RNA polymerase III transcripts that localize to the PNC include: hY RNA, an RNA of unknown function, RNase P RNA which is involved in tRNA and preribosomal RNA processing, and RNase MRP, an exoribonuclease involved in preribosomal and mitochondrial RNA processing (reviewed in Huang, 2000). Although the function of the PNC is unknown it is suspected to involve RNA transcription as the structure accumulates nascent RNA, is destroyed by RNase treatment, and reorganizes upon treatment with an RNA polymerase II and III inhibitor (Huang *et al.*, 1998). Whether transcription by RNA polymerases II or III occurs in the PNC or whether nascent transcripts rapidly accumulate in the PNC remains to be determined.

Sam68 nuclear bodies (SNBs) are also located at the periphery of nucleoli and similar to PNCs, they are found only in some types of transformed cell lines and not in primary cultures (Chen *et al.*, 1999). Electron spectroscopic imaging (ESI) analysis revealed the presence of nitrogen and phosphorus indicative of protein and nucleic acids; however, the nucleic acid is likely not nascent RNA as these structures were not found to label with BrUTP. SNBs disintegrate during mitosis and when cells are treated with transcriptional inhibitors but not cycloheximide suggesting that their presence relies on the activity of RNA polymerase II or III.

SNBs contain some RNA binding proteins that are characterized by a GSG/STAR (signal transduction and activation of RNA) domain including Sam68, SLM-1, and T-STAR/SLM-2 (Chen *et al.*, 1999). Several functions have been linked to Sam68 including acting as an adaptor protein for src kinases (Richard *et al.*, 1995; Taylor *et al.*, 1995), playing a role in cell cycle progression (Barlat *et al.*, 1997), splicing (Stoss *et al.*, 2001), gene transactivation/ RNA export (Reddy *et al.*, 1999). Recently, stress treatment of cells, such as heat shock, has been found to induce recruitment of hnRNP A1 and splicing factors to SNBs (Denegri *et al.*, 2001). These observations led to the hypothesis that SNBs function to modulate gene expression in cells undergoing stress.

The above-mentioned nuclear domains do not represent a complete list. One obvious domain which was not discussed is chromosome territories which also orient themselves so as to permit efficient gene transcription of active loci (reviewed in Carmo-Fonseca, 2002). Furthermore, there are many additional domains which have been reported in the literature; however, they are relatively uncharacterized, and sometimes localization with formerly characterized domains has not been performed (Pinol-Roma *et al.*, 1989; Pombo *et al.*, 1998; Naylor *et al.*, 2000; Fox *et al.*, 2002). Although the exact function of most nuclear domains is under intensive investigation, the general agreement is that nuclear bodies impart organization to all nuclear processes.

1.4 3'-end pre-mRNA processing

Most eukaryotic pre-mRNAs, transcribed by RNA polymerase II, require further processing including capping, splicing, and 3'-end processing to produce the mature form. Although each of these processes is a separate reaction, emerging evidence indicates mutual associations with each other and with transcription. For example, formation of the 5' cap binding complex facilitates 5' splice site recognition (reviewed in Proudfoot *et al.*, 2002), and in 3' end processing of transcripts, the cap structure stimulates the cleavage reaction and promotes polyadenylation complex stability on the RNA substrate (Flaherty *et al.*, 1997). Splicing of 3'-end introns stimulates 3'-end processing and likewise, 3'-end processing aids splicing factors with terminal exon definition (Niwa *et al.*, 1992). Numerous reports have linked all processes with RNA polymerase II transcription, establishing that processing occurs co-transcriptionally (McCracken *et al.*, 1997). In all three processing events, some components are found associated with the phosphorylated CTD of RNA polymerase II (PolIO). For example, the cleavage and polyadenylation specificity factor, CPSF, associates with TFIID in the preinitiation complex and then transfers to PolIO as elongation commences (Dantonel *et al.*, 1997). Furthermore, the CTD of RNA polymerase II has been shown to be required for 3'-end cleavage and can be regarded as a cofactor in the reaction (Hirose and Manley, 1998).

All protein-encoding mRNAs with the exception of replication-dependent histone genes undergo 3'-end processing to acquire a poly(A) tail. The 3'-end processing of the pre-mRNA is a two-step reaction that involves endonucleolytic cleavage followed by the addition of poly(A) residues (reviewed in Wahle and Rüegsegger, 1999). The reaction can be separated *in vitro* using a chain-terminating ATP analog, but the *in vivo* reaction is tightly coupled such that a 5' intermediate cleavage fragment lacking a poly(A) tail cannot be detected experimentally. This tightly linked reaction is likely due to the protein overlap between the two processing machineries.

The cleavage and polyadenylation steps usually require at least two sequence elements: the AAUAAA hexanucleotide which is located 10-30 bases upstream of the cleavage site, and a GU-rich element located 20 – 40 bases downstream of the cleavage site. The multi-subunit complex responsible for recognizing the AAUAAA sequence is CPSF. This protein consists of four subunits and is central to both the cleavage and polyadenylation reaction. The binding of CPSF to RNA alone is weak; however, when another protein, cleavage stimulation factor (CstF) binds to the downstream GU element, the two factors co-operate to stabilize their binding to the RNA (Gilmartin and Nevins, 1989; Wilusz *et al.*, 1990). In addition to signalling the cleavage and polyadenylation site (Murthy and Manley, 1995), numerous functions have been assigned to CPSF including linking 3'-end processing with transcription (Dantonel *et al.*, 1997; McCracken *et al.*, 1997), cytoplasmic polyadenylation (Bilger *et al.*, 1994; Dickson et al., 2001), limiting the length of the poly(A) tail (Whale, 1995), and interactions with components of the splicing apparatus (Lutz *et al.*, 1996; McCracken *et al.*, 2002).

CstF exists as a heterotrimeric protein with all of its subunits essential for the cleavage process (Takagaki *et al.*, 1990; Takagaki and Manley, 1994). The CstF-77 subunit connects CstF-50 and CstF-64 and it interacts with CPSF (Takagaki and Manley, 1994; Murthy and Manley, 1995). RNA binding is the responsibility of the CstF-64 subunit (Takagaki *et al.*, 1992), and evidence also links CstF-64 with transcription termination in yeast (Birse *et al.*, 1998; Calvo and Manley, 2001). The third subunit, CstF-50, has been shown to link 3'-end processing with transcription and DNA repair through its interactions with the CTD of RNA polymerase II (McCracken *et al.*, 1997) and the BARD1-BRCA1 complex (Kleiman and Manley, 1999, 2001), respectively. Although the CstF complex is dispensable for the polyadenylation process, there is some evidence that CstF binds to an upstream sequence element to stimulate the polyadenylation of some genes (Moreira *et al.*, 1998).

Other components of the 3'-end processing reaction include poly(A) polymerase (PAP), cleavage factors I_m and II_m (CFI_m and $CFII_m$, where m denotes mammalian) and the poly(A) binding protein II (PAB II). PAP is the nucleotidyl transferase that catalyzes the addition of the poly(A) tail, but it is also important for the endonucleolytic cleavage step. CFI_m and $CFII_m$ are required for the cleavage process only (Takagaki *et al.*, 1989). CFI_m binds to the pre-mRNA early in the 3'-end processing reaction thereby stabilizing the CPSF-RNA interaction (Rüegsegger *et al.*, 1998). Recently CFI_m has also been shown to bind PAP (Kim and Lee, 2001). $CFII_m$ has been shown to bind both CFI_m and CPSF (de Vries *et al.*, 2000). PAB II binds to the pre-mRNA after the addition of at least 10 poly(A) nucleotides and serves two purposes: i) to stabilize the processing complex and ii) to act with CPSF in stimulating PAP to elongate the poly(A) tail in a processive rather than distributive manner (Bienroth *et al.*, 1993). It is an intriguing feature of poly(A) addition that the elongation reaction terminates when the tail length is approximately 200-250 residues long. It is known that the processive property of PAP is interrupted at ~250 A nucleotides and the enzyme adds further poly(A) residues in an inefficient distributive manner (Wahle, 1995). The precise mechanism used to achieve proper tail length is currently unknown.

3'-end processing of pre-mRNA serves many purposes including aiding in the splicing of terminal introns (reviewed in Proudfoot *et al.*, 2002), mRNA stability (reviewed in Wilusz *et al.*, 2001), translation initiation (reviewed in Pestova and Hellen, 2000), transcription termination (reviewed in Proudfoot *et al.*, 2002), and nuclear export (reviewed in Reed and Hurt, 2002). Splicing involves the removal of intronic sequences from pre-mRNA by a two step reaction including the nucleophilic attack of the 5' splice site by the 2'OH of the adenosine residue in the 3' branch site, followed by the *trans*-esterification reaction which fuses the two exon sequences (reviewed in Proudfoot *et al.*, 2002). Splicing is facilitated by the spliceosome, which is composed of U1, U2, U4, U5, and U6 snRNPs as well as many other proteins. It is now known that in higher eukaryotes, the determination of exonic sequences is mediated by a process called 'exon definition' (Niwa *et al.*, 1992). In this process, splicing regulatory (SR) proteins bind to specific exon enhancer sequences. These SR proteins interact with the components of the spliceosome to define the exon sequence (reviewed in Smith and Valcarcel, 2000). Terminal exon definition is mediated by the recognition of the poly(A) signal. The basis for this definition has recently been discovered to involve an interaction between the spliceosome component U2AF65 and PAP (Vagner *et al.*, 2000). Interestingly, both the splicing and polyadenylation that occur on either side of the terminal exon are stimulated by each other (Niwa *et al.*, 1992); however, situating the poly(A) site too close to the 5' splice site will actually repress polyadenylation thereby ensuring that poly(A) sequences within an exon are not used (reviewed in Proudfoot, 1996). Further interactions between polyadenylation and splicing have been reported in genes that undergo alternative polyadenylation. For example, the developing B cell expresses a membrane-bound IgM antibody. In the more differentiated B cell, the plasma cell, the IgM gene uses a weak polyadenylation site located in an upstream intron causing polyadenylation to prevail over the splicing reaction (reviewed in Proudfoot *et al.*, 2002). This smaller IgM antibody represents the secreted form. The recognition of the weak polyadenylation site only in plasma cells is due to the presence of increased amounts of the CstF-64 protein (Takagaki *et al.*, 1996; Takagaki and Manley, 1998). Therefore polyadenylation serves not only to aid in terminal exon definition, but can also mediate the expression of protein isoforms.

mRNA decay is regulated by two distinct pathways including deadenylation-dependent decay, and nonsense mediated decay. The former pathway is the main process used to degrade mRNA in yeast and higher eukaryotes and involves the removal of the poly(A) tail, whereas the latter pathway is not dependent on the removal of the poly(A) tail and is responsible for destroying mRNAs containing premature stop codons (reviewed in Wilusz *et al.*, 2001). Briefly, the deadenylation-dependent process involves the initial removal of the poly(A) tail by poly(A) ribonuclease (PARN), followed by elimination of the 5' 7'methylguanosine cap. The RNA is then susceptible to degradation by both 5' and 3' exonucleases. The protection of mRNA from degradation is likely due to the binding of PAB II to the poly(A) tail and to the translation initiation factor eIF-4G, which binds the cap-binding protein eIF-4E. This complex acts to circularize the RNA thereby likely providing protection from deadenylating and decapping enzymes. The overall stability of mRNA is mediated through various proteins that bind to cis-acting sequence elements possibly affecting the binding of PAB II to the poly(A) tail or eIF-4E to the 5' cap.

The poly(A) tail also plays a role in translation initiation. The poly(A) tail aids in the loading of the 43S translation preinitiation complex onto the 5' terminal cap (reviewed in Pestova and Hellen, 2000). This occurs through the binding of PAB II to the translation initiation factor eIF-4G, a factor which binds to the preinitiation complex constituent, eIF-3. Interestingly, PAB II has also been shown to stimulate cap-dependent translation initiation by an unknown process that does not involve interactions with either eIF-4G or the poly(A) tail (Otero *et al.*, 1999).

Little is known about RNA polymerase II transcription termination, a process that releases both the RNA transcript and RNA polymerase II from the site of transcription. Early experiments defined the requirement of 3'-end processing for proper transcription termination (Whitelaw and Proudfoot, 1986; Edwalds-Gilbert *et al.*, 1993; Birse *et al.*, 1998). It is known that RNA polymerase transcribes RNA up to 1.5 kb downstream of the poly(A) signal (Dye and Proudfoot, 1999). Therefore the current model of transcription termination involves the pausing of RNA polymerase II at sites downstream of the polyadenylation signal (Birse *et al.*, 1997; Yonaha and Proudfoot, 1999; reviewed in Proudfoot *et al.*, 2002). This allows for enhanced poly(A) site recognition by cleavage and polyadenylation factors bound to the CTD of RNA polymerase II. The remaining transcribed RNA, which is looped out, then undergoes cotranscriptional cleavage, which removes the 3' end of the RNA from the RNA polymerase II complex (Dye and Proudfoot, 2001). Subsequently, but occurring independently, the pre-mRNA undergoes 3' cleavage. This cleavage reaction releases both the RNA polymerase II from the DNA template and the pre-mRNA transcript. The factors that mediate cotranscriptional cleavage have yet to be identified.

The nuclear export of mRNA has, until recently, been largely uncharacterized. It was assumed that the karyopherins (importins/exportins), which mediate the export of tRNA, rRNA and snRNAs also in some way mediated the export of mRNA. It is now thought that the export receptor for mRNA is most likely the Mex67/Tap protein, as it is known in yeast and metazoans, respectively (reviewed in Reed and Hurt, 2002). This protein was found to interact with mRNA and components of the nuclear pore complex and mutations to this gene result in accumulation of poly(A)$^+$ RNA (Segref *et al.*, 1997). Another protein, YraI/Aly, as it is known in yeast and metazoans, respectively, has been identified as a nuclear export cofactor that binds to Mex67 (Strasser and Hurt, 2000). This protein localizes to SFCs with other splicing factors and is known to couple splicing with nuclear export in metazoans (Zhou *et al.*, 2000). Aly has been further found to interact with the DECD box protein UAP56 (or Sub2 in yeast), a component of the spliceosome (Strasser and Hurt, 2001; Luo *et al.*, 2001). The Yra1-Sub2 complex has recently been found in a larger complex of transcription factors in yeast and this new larger complex has been termed the TREX (transcription/export) complex (Strasser *et al.*, 2002). The identification of such a complex strengthens the evidence that transcription is integrated with downstream processes such as splicing, polyadenylation and nuclear export.

In addition to splicing, nuclear export has also been linked to the polyadenylation process. This association was first noted by Eckner *et al.* (1991) who discovered that genes must undergo 3'-end processing to be exported from the nucleus. Supporting this observation, Brodsky and Silver (2000) visualized a GFP-tagged mRNA binding protein in yeast and discovered that mutations to essential components of 3'-end processing impaired nuclear export of the tagged mRNP; likewise, the absence of a polyadenylation signal resulted in the retention of mRNA transcripts (Long *et al.*, 1995). Although the links to 3'-end processing are well established, there are few leads regarding the 3'-end processing components that might aid in the export process. The yeast protein Hrp1 is an essential component of the cleavage and polyadenylation process, and has also been found to exit from the nucleus to the cytoplasm (Kessler *et al.*, 1997). Nab2p, another yeast protein, controls poly(A) tail length and is required for the nuclear export of mRNA (Hector *et al.*, 2002). Recently in *S. cerevisiae*, the nuclear exosome, which is a complex of exonucleolytic enzymes, has been proposed to regulate the release of transcripts from the transcription site by monitoring for proper 3'-end formation (Hilleren *et al.*, 2001). To date, it is not known whether higher eukaryotes contain a quality control mechanism or how they integrate 3'-end processing with mRNA export.

Emerging evidence suggests that all processes in gene transcription are tightly coupled to one another. 3'-end processing is clearly linked to processes such as RNA polymerase II transcription, pre-mRNA splicing, and mRNA nuclear export; however many of the factors mediating this integration are only currently being identified. As will be discussed in this thesis, it is our hypothesis that DDX1 is a mammalian factor that links 3'-end processing with the nuclear export of mRNAs.

1.5 Thesis Objectives

Background:

DDX1 was isolated from a subtracted retinoblastoma library. The gene was subsequently found to be amplified and its transcript overexpressed in a subset of retinoblastoma and neuroblastoma cell lines and tumours. As DDX1 belongs to the DEAD box family of putative RNA helicase proteins, it is likely that DDX1 functions in some aspect of RNA metabolism.

Overall Objective:

To determine the biological and biochemical function of the DDX1 protein.

Working Hypothesis:

DDX1 will affect some aspect of cellular RNA metabolism. This function will be particularly evident in tissues of neuronal origin, where DDX1 transcript is highest. It is expected that cellular localization of DDX1 will impart knowledge of the potential RNA process and/or substrate; this may in turn aid in the development of an *in vitro* assay for DDX1 biochemical function.

Specific Objectives:

1. To examine the biological function of DDX1. To achieve this objective *DDX1* knockout mice will be generated.

2. To examine DDX1 subcellular distribution. These analyses will involve immunofluorescence microscopy to identify DDX1 and as well any associated cellular structures.
3. To adapt or create an *in vitro* assay to test for DDX1 biochemical function.

Chapter 2. Materials and Methods

2.1 Molecular Techniques

2.1.1 Library Screening

Two genomic libraries were screened for *DDX1*: a mouse embryonic stem (ES) cell library in lambda dash II, obtained from Dr. Derrick Rancourt, University of Calgary, Calgary, Alberta, and a mouse liver library obtained from Dr. Jim Stone, University of Alberta, Edmonton, Alberta. One cDNA library was screened: a mouse day 5 brain cDNA library obtained from Dr. Jim Stone, University of Alberta, Edmonton, Alberta. The titre of each library was obtained by infecting *E. coli* XL1 Blue (ES library), *E. coli* LE 392 (mouse liver library), or *E. coli* BB4 (cDNA library). Briefly, the bacteria were grown overnight at 37°C in 40 ml of NZY broth (5 g/L NaCl, 2 g/L $MgSO_4$, 5 g/L yeast extract, 10 g/L NZ amine) supplemented with 10 mM $MgSO_4$ and 0.1% maltose. The cells were pelleted and resuspended to 2 optical density $(OD)_{600}$ units/ml in 10 mM $MgSO_4$. The bacteria were kept at 4°C and used within 2 weeks of preparation. Infection was achieved by adding phage at 5×10^4 plaque-forming units (PFU)/ml to 600 µl of bacteria. The infection was allowed to proceed at 37°C with constant agitation for 20 min. Top agar (NZY amine plus 0.8% agar) was added to the infection mixture and this was plated on 150 mm agar plates (NZY amine plus 1.5% agar). The bacteria were grown at 37°C for approximately 6 hr (or until cell lysis occurred).

The bacteriophage DNA was transferred to Millipore HA (0.45 µm) nitrocellulose filters. Briefly, nitrocellulose was placed on the plates, and the position marked using a needle dipped in India ink. Filters were allowed to sit on the plate for 1–2 min after which they were removed and soaked in denaturing solution (1.5 M NaCl, 0.5 N NaOH) for 5 min. The filters were then neutralized [1.5 M NaCl, 0.5M Tris·HCl (pH 7.5)] for 5 min and rinsed [2X SSC (20X solution: 3 M NaCl; 0.3 M Na_3 citrate]), 0.2 M Tris·HCl (pH 7.5)]. The filters were air dried and then baked in a vacuum oven at 80°C for 2 hr.

After drying, filters were sealed in a plastic bag with prehybridization solution [50% formamide (Fluka), 5X SSC, 5X Denhardt's, 50 mM NaH_2PO_4 (pH 6.5), 250 μg/ml salmon sperm DNA] and incubated for a minimum of 4 hr in a shaking H_2O bath at 42°C. The probe, either a human or mouse *DDX1* cDNA fragment, was labeled with $\alpha[^{32}P]$-dCTP (800 Ci/mmol) by nick translation and mixed with hybridization solution (see 2.1.3) prior to overnight incubation at 42°C with shaking. Subsequently, the filters were washed in 2X SSC + 0.1% SDS at R.T. (3 X 5 min) and 0.1X SSC + 0.1% SDS (2 X 1 hr) at 60°C. The filters were air-dried and exposed at –80°C overnight to X-ray film (Kodak®) in the presence of intensifying screens.

Following DNA hybridization, positive plaques were lined up according to their India ink marks and cored using a P1000 pipette tip. The agar was placed in 500 μl SM buffer [0.1 M NaCl, 0.01 M $MgSO_4$, 0.05 M Tris·HCl (pH 7.5) and 0.01 % gelatin] plus 35 μl chloroform and allowed to elute overnight at 4°C. This eluate was then used to re-infect the appropriate *E. coli* strain, and a second round of library screeing ensued using 200 μl BB4 and 3 ml 0.8% top agar with 100 mm agar plates. Upon completion of 3 rounds of screening using the same

DNA probe, the positives were selected onto a grid matrix nitrocellulose filter placed on a 100 mm NZY amine agar plate covered in a lawn of the appropriate *E. coli* strain. The filter was hybridized with the same DNA probe and positive clones identified according to their position on the plate. The positive plaques were once again cored for bacteriophage isolation.

2.1.2 Bacteriophage rescue

The bacteriophage from the cDNA library were cloned into lambda ZAP II (Stratagene). Excision into pBluescript plasmids was according to the Stratagene *in vivo* excision protocol. The mouse liver library and ES library bacteriophage were purified using either mini phage preparations or maxi phage preparations. Mini phage preparations were done according to a protocol from Miller (1987). The final plaques were cored and placed in 10 ml LB broth plus 10 mM $MgSO_4$ and 50 µl of freshly grown *E. coli* (2 OD_{600} units/ml). The bacteriophage infected the bacteria over a course of 6-12 hr at 37°C with constant agitation. The infection was considered done when the bacteria started to lyse and the stringy DNA could be seen in the medium. Complete lysis was obtained by adding 100 µl chloroform to the mixture and allowing it to shake at 37°C for another 2 min. The bacterial remnants were spun down and the aqueous bacteriophage layer was transferred to a new tube containing 100 µl of 1 M $MgSO_4$. The bacteriophage were stored at -80°C in 7% DMSO. To isolate DNA, 1 ml of bacteriophage was added to 9 ml of LB broth, 10 ml of TM buffer [50 mM Tris·HCl (pH 7.4), 10 mM $MgSO_4$] and 320 µl of 1 µg/µl DNase I . The mixture was inverted and incubated at R.T. for 15 min. Subsequently, 2 ml of 5 M NaCl and 2.2 g of polyethylene glycol (PEG) molecular weight (M.W.) 6000 (Sigma) were added. The solution was mixed by inversion until all the PEG had dissolved. After a 15 min incubation on ice, the solution was centrifuged at 12,000 X g for 10 min. The supernatants were discarded and the pellet was allowed to dry. The pellet was resuspended in 300 µl TM buffer. For DNA purification, organic extractions were done in the order listed: 2 X chloroform, phenol, chloroform and ether. After the last extraction, the aqueous phase was removed and 30 µl 0.25 M EDTA (pH 7.5) and 30 µl of 5 M NaCl were added. The DNA was precipitated by adding 2 volumes of 100% ethanol and incubating on ice for 10 min. The DNA was centrifuged and washed using 75% ethanol. The pellets were dried and resuspended in 50 µl of TE buffer [10 mM Tris·HCl (pH 7.5) + 1 mM EDTA].

Maxi bacteriophage preparations began with the inoculation of 100 mL of NZCYM (10 g/L NZ amine, 5 g/L NaCl, 5 g/L yeast extract, 1 g/L casamino acids, 2 g/L $MgSO_4 \cdot 7\ H_2O$; pH 7.5) with a single colony of *E. coli*. The bacteria were grown overnight at 37°C. The bacteria were divided into 4 aliquots with 1×10^{10} cells in each (1 $OD_{600} = 8 \times 10^8$ cells). The aliquots were spun at 4000 X g at R.T. for 10 min and the resultant pellets resuspended in 3 ml SM buffer. The bacteriophage, previously prepared by the mini phage technique, were added to the bacteria (approximately 5×10^7–5×10^8 PFU). The bacteria and bacteriophage were incubated at 37°C for 20 min and then 500 ml of NZCYM was added. The infection was allowed to proceed until lysis began (~6-12 hr).

Ten ml of chloroform was added and the lysis was completed by either an overnight incubation at 4°C or 30 min at 37°C. The bacteriophage were allowed to cool to R.T. and then 1 μg/ml of pancreatic DNase I and 1 μg/ml of RNase was added. The flask was left for 30 min at R.T. and then a final concentration of 1 M NaCl was added. The flask was swirled to dissolve the NaCl and then it was left on ice for 1 hr. The contents were spun at 10,000 X g at 4°C and the bacteriophage supernatent was poured into a clean flask. PEG M.W. 6000 was added to a final concentration of 10% (w/v). The contents were then stirred for ~1 hr at R.T. until all the PEG had dissolved. The flasks were spun at 10,000 X g and the supernatents were discarded. The bacteriophage were resuspended in 8 ml SM buffer, and an equal volume of chloroform was added. The bacteriophage were spun and 7.5 g cesium chloride was added to the aqueous phase. The refractive index was measured to ensure that it was at 1.383. The bacteriophage were centrifuged at 111,000 X g rpm for 24 hr at 4°C in a Sorvall ultracentrifuge. The bacteriophage band was collected and dialyzed against 1 L of 10 mM NaCl, 50 mM Tris·HCl (pH 7.5), 10 mM $MgCl_2$ at R.T. for 1 hr in dialysis tubing with a 10,000 nominal molecular weight cut-off. The dialysis was repeated with fresh buffer for a second hr, and then the bacteriophage were removed and resuspended in 0.02 M EDTA pH 7.5, 50 μg/ml proteinase K, and 0.5% sodium dodecyl sulfate (SDS). The mixture was incubated at 65°C for 1 hr. The DNA was then extracted three times using an equal volume of phenol, then phenol:chloroform, and finally chloroform. The DNA was dialyzed overnight at 4°C in 2 L of TE (which was changed 3 times). The DNA was removed from the dialysis tubing and precipitated using 1/10 volume 5 M NaCl and 2 volumes of 100% ethanol. Precipitated DNA was spooled from the ethanol using Pasteur pipettes that had been flamed to generate a hook. The DNA was then washed with 75% ethanol, dried, and resuspended in 500 μl of TE buffer. The DNA was rotated overnight to aid in suspension.

2.1.3 DNA labeling and nitrocellulose hybridization

The nitrocellulose filters were sealed into plastic bags together with prehybridization solution [50% formamide (Fluka), 5X SSC, 5X Denhardt's, 50 mM NaH_2PO_4 (pH 6.5), 250 μg/ml freshly denatured salmon sperm DNA]. The nitrocellulose filters were subjected to prehybridization for 4–16 hr in a shaking 42°C H_2O bath.

The DNA was labeled by nick translation using $\alpha[^{32}P]$-dCTP (800 Ci/mmol). The probe was then denatured and mixed with hybridization solution (50% formamide, 5X SSC, 1X Denhardt's solution, 20 mM NaH_2PO_4, 10% dextran sulfate) prior to incubation with the nitrocellulose filters overnight at 42°C.

2.1.4 Southern Blot Analysis

Loading dye was added to DNA (1 μg) and electrophoresed in 1% agarose gels in 1X Howley [40 mM Tris·HCl, 33 mM NaoAc, 1 mM EDTA; pH 7.2]. The gels were denatured in 0.5 N NaOH + 1.5 M NaCl and neutralized in 0.5 M Tris·HCl (pH 7.5) + 3 M NaCl following which, the DNA was transferred overnight to a nitrocellulose membrane (Amersham Biosciences) by capillary action. The membrane was then baked for 2 hr in an 80°C vacuum oven. After prehybridization, and hybridization (see 2.1.3) the membranes were washed in 2X SSC + 0.1% SDS (3 X 5 min) at R.T. and 0.1X SSC + 0.1% SDS (2 X 1 hr) at 45-60°C depending on the probe size.

2.1.5 Plasmid Purification

To isolate small amounts of plasmid DNA, we used a lysozyme boiling method according to Sambrook *et al.* (1989). Isolation of large amounts of highly purified plasmid DNA was done using an alkali lysis method followed by CsCl purification (Sambrook *et al.*, 1989).

2.1.6 DNA Insert Purification

Subsequent to restriction enzyme digestion, DNA inserts were isolated by electrophoresis in a 5% polyacrylamide gel in 1X TBE at 170 V. The inserts were viewed using ethidium bromide staining and the fragments that were removed were subjected to electroelution in 1X TBE. TE was added to a volume of 2 ml and the DNA was phenol/chloroform extracted. Following precipitation for at least 1 hr in 2 volumes 100% ethanol and 1/10 volume 5 M NaCl, the DNA was dried and resuspended in sterile H_2O. All DNA was stored at -20°C.

2.1.7 DNA ligations

Approximately 200 ng insert DNA (~50 ng/ul) was used for every 200 ng vector in a final volume of 20 μl containing 0.1 μg/μl BSA, 1X ligase buffer [50 mM Tris·HCl (pH 7.8), 10 mM $MgCl_2$, 20 mM DTT (dithiothreitol)], 1 mM ATP and 1 U T_4 DNA ligase. Reactions were incubated at 16°C overnight. If the vector was pBluescript, positive colonies were detected by colour selection upon transformation into competent *E. coli* XL1-Blue bacteria cells. Colonies were screened for the presence of the appropriate insert by plasmid isolation as described in 2.1.5.

2.1.8 DNA blunting and dephosphorylation

DNA was blunt-ended using either Klenow polymerase (Amersham Biosciences) for 5' overhangs or T4 DNA polymerase (Amersham Biosciences) for 3' overhangs according to the manufacturer's specifications. Removal of 3' phosphates was achieved by incubating DNA with 0.1 U of calf alkaline phosphatase (Roche) at 37°C for 1 hr. Following either procedure, the DNA was extracted and precipitated prior to further use.

2.1.9 Automated and Manual Sequencing

Automated sequencing was done according to the manufacturer's directions (Perkin Elmer Applied Biosystems), except that all reactions were halved. Briefly, 200-500 ng of double-stranded DNA template, 4 µl Terminator Ready Reaction Mix (Perkin Elmer), 1.5 µM primer and H_20 to a final volume of 10 µl, were amplified in a thermal cycler (PE Applied Biosystems) under the following conditions: 25 cycles at 96°C for 10 sec, 50°C for 5 sec and 60°C for 4 min, followed by a hold at 4°C. Extension products, precipitated 15 min at R.T.

by adding 25 μl 100% ethanol and 1 μl 3 M NaoAc (pH 5.2), were centrifuged, washed twice in 70% ethanol, and dried in a vacuum centrifuge. Prior to loading into the sequencing machine, the pellets were resuspended in 12.5 μl fresh formamide (Fluka), boiled for 5 min, and immediately cooled on ice. The samples were subsequently loaded into the automated sequencer (ABI PRISM 310 Genetic Analyser).

Manual sequencing was performed according to Sanger *et al.* (1977) using the dideoxynucleotide chain termination method using T7 DNA polymerase as modified for double-stranded DNA templates (Mierendorf and Pfeffer, 1987). Primers for all sequencing reactions were produced on site by Dr. Brian Taylor.

2.2 Embryonic Stem (ES) Cell Manipulations

2.2.1 Preparation of Leukemia Inhibitory Factor (LIF)

The LIF plasmid was obtained from Dr. Andràs Nagy (Samuel Lunenfeld Research Institute, Toronto, Ontario). This plasmid was originally generated in Dr. John Heath's laboratory and contains the LIF cDNA in pGEX-2T. The LIF plasmid was transformed into *E. coli* HB101 and subsequent to large scale plasmid preparations, the presence of the 600 bp insert was verified using a *Bam*HI restriction enzyme digestion. To prepare the bacterially-expressed fusion protein, 50 ml of LB + 50 μg/ml ampicillin was inoculated with a colony of bacteria-containing LIF plasmid and grown at 37°C overnight. The next morning the 50 ml culture was used to inoculate 500 ml of LB + 50 μg/ml ampicillin. This culture was grown for approximately 1.5 hr at 37°C until the OD_{600} = 0.6–1.0.

Protein expression was then induced by adding IPTG to a final concentration of 0.1 mM and allowing the culture to grow for another 3 hr. The culture was then pelleted at 8300 X g for 15 min and the cells resuspended in 5 ml MTPBS (150 mM NaCl, 16 mM Na_2HPO_4, 4 mM NaH_2PO_4; pH 7.3). Subsequent to lysing the cells by French press at 1000 psi, Triton X-100 was added to a 1% final concentration. The cells were vortexed, left on ice for 5 min, and pelleted at 10,500 X g for 15 min. The supernatants were then frozen at -80°C overnight.

The next day, 2 ml of glutathione-Sepharose beads (Roche) in a packed volume of 50% were washed 3X in MTPBS and then resuspended in 2 ml MTPBS prior to the addition of the LIF supernatants. Binding occurred for 2 hr on a rotator and the mixture was then centrifuged over a 20% sucrose cushion in MTPBS at 1400 X g. The supernatant was discarded and the beads washed 1 X in 10 ml wash buffer 1 (1% Triton X-100 in MTPBS), 1 X in 10 ml wash buffer 2 [50 mM Tris·HCl (pH 8.5), 150 mM NaCl], and 1X in 10 ml elution buffer [50 mM Tris·HCl (pH 8.5), 150 mM NaCl, 2.5 mM $CaCl_2$]. The LIF + beads were resuspended in 750 µl of elution buffer to which 20 U of thrombin was added. The digestion proceeded overnight at 4°C on a rotator. The following day the beads were spun down and then washed in 3 X 2 ml elution buffer. The LIF was then frozen at -80°C in aliquots. A Bradford assay (Bradford, 1976) and Western blot analysis revealed that LIF represented approximately ½ of total protein recovered and therefore the concentration was estimated to be 0.1 µg/µl. The activity of purified LIF is approximately 10^6 units/10 µg.

2.2.2 Culturing of ES and SNL cells

The medium for growing ES cells was as follows: high glucose DMEM, 0.1 mM non-essential amino acids, 100 μM β-mercaptoethanol, 15% HyClone fetal bovine serum (Wisent Inc.), 50 μg/ml penicillin + streptomycin, 1000U LIF/ml, 2 mM L-glutamine, and 1 mM sodium pyruvate. The ES cells, which were obtained at passage number 11 from Dr. Andràs Nagy (Samuel Lunenfeld Research Institute, Toronto, Ontario), were grown on irradiated SNL STO primary mouse fibroblasts obtained from Dr. Nancy Dower (University of Alberta, Edmonton, Alberta) prior to electroporation. ES cells were split 1:7 every second day in 100 mm tissue culture plates and the medium was changed every day. All plates used for culturing ES cells were treated with 0.1% gelatin in H_2O for 5 min prior to use.

SNL feeder cells were trypsinized and then irradiated with 6 Gray in a gamma irradiator. A 100 mm confluent plate contained ~10^7 SNL cells. Therefore 1 plate of confluent SNL cells could be used to grow 20 plates of ES cells (5×10^5 cells/100 mm plate). SNL STO cells could also be irradiated and frozen in vials for subsequent use.

2.2.3 ES cell electroporations

The vector was prepared using a Qiagen plasmid kit (Qiagen, Inc.) or purified by 2 X CsCl. The vector was linearized by restriction enzyme digestion with *Pvu*I or *Nde*I, cleaned by phenol/chloroform extractions and precipitated using 2 volumes of 100% ethanol. On the day of electroporations (day 0), the ES cells were trypsinized, counted and resuspended in 4°C PBS at a concentration of 7.5 x 10^6 cells/ml. In a separate tube the cells were mixed (0.8 ml per cuvette) together with linearized DNA (15 µg per cuvette). The cells + DNA (0.8 ml) were then placed in a 0.4 cm path length cuvette (BioRad) and electroporated at 250 V & 500 µF with the capacitance set to Ext. Time constants were generally ~10.0. The cuvettes were left on ice for a 10 min recovery followed by transfer of its contents to 10 ml warm media on a 100 mm gelatinized tissue culture plate.

2.2.4 Isolation of drug-resistant ES colonies

On day 2 after electroporation, geneticin (Gibco BRL) and gancyclovir (Cross Cancer Institute pharmacy) were added to a final concentration of 200 µg/ml and 2.0 µM, respectively. The ES cells received fresh media + drugs daily until ~day 14 when colonies were large enough to be picked. Those colonies that appeared round and had even edges when visualized through the bottom of the plate were circled for later selection. One 96 well flat bottom tissue culture plate was gelatinized and 40 µl of trypsin/well was added to a second plate. The media was removed from the ES plates and replaced with PBS. The circled colonies were aspirated in 20–30 µl of PBS using a Pipetman and placed into one well of the 96 well plate containing trypsin. When the plate was full, the trypsin was stimulated by incubation at 37°C for 5 min. The cells were then transferred to the first 96 well plate, which contained 150 µl of warm media/well. The colonies were aspirated several times to break up cell clumps. The media in the 96 well plate was replaced daily until ~4 days after picking when the cells were split 1:4 into 3 other 96 well plates. This provided 2 plates for freezing and 2 plates for DNA analysis.

The ES colonies were frozen at -80°C when the cells were heavy, but not overgrown. The cells were frozen in 25% HyClone fetal bovine serum, 10% DMSO, and 65% high glucose DMEM directly in their 96 well plates.

2.2.5 Preparation of ES cell DNA

The ES cells, grown to confluence, were washed in PBS and immersed in 50 μl lysis buffer [100 mM Tris·HCl (pH 8.5), 5 mM EDTA, 0.2% SDS, 200 mM NaCl] + proteinase K (150 μg/μl). The 96 well plate was incubated at 37°C for a minimum of 3 hr. The DNA was precipitated by the addition of 120 μl of 100% ethanol to each well. Left undisturbed for a minimum of 2 hr, the plate was then turned upside down on the bench for the supernatant to drain. The DNA was washed in 70% ethanol, dried, and 25 μl of TE was added to each well. The plate was then placed at 4°C overnight to allow the DNA to go into solution. The following day the DNA was digested with *Hin*dIII restriction enzyme in the 96 well plate. The entire well of DNA was subjected to Southern blot analysis following electrophoresis for 6 hr at 36 V in a 0.8% agarose gel.

2.2.6 Analysis of mouse genomic DNA isolated from tails

Mouse tails were processed for DNA as follows: tails were placed into eppendorf tubes containing 500 μl of TEN/SDS buffer [50 mM Tris·HCl (pH 7.5), 100 mM EDTA, 100 mM NaCl, 1% SDS] + 400 μg proteinase K and the tubes were placed at 50°C for 3-4 hr. An additional 400 μg of proteinase K was added and the tubes were left at 37°C overnight. The DNA was then extracted using phenol until the interphase was clear. Final extractions in chloroform, and then ether were done prior to DNA precipitation with 2 volumes of 100% ethanol. Following DNA reconstitution in TE, 386 bp of the neomycin cassette was amplified using primers generated to the 5' (GCTATTCGGCTATGACTGG) and 3' (TGTTTCGCTTGGTGGTCG) ends. The following components, 10 mM dNTPs, 10 μM of each primer, 200 ng DNA, 1X *Taq* polymerase buffer (Amersham Biosciences), 1 U *Taq* polymerase (Amersham Biosciences) + H_2O to 50 μl were heated to 94°C and then subjected to 35 cycles of 1 min each at 94°C, 55°C, and 72°C in a thermal cycler (PE Applied Biosystems). The PCR reaction products were electrophoresed on a 5% polyacrylamide gel.

In addition to amplification of the neomycin cassette, Southern blot analysis was designed to detect properly targeted alleles. Briefly, a 3 kb fragment from outside the region of recombination was cloned and purified. The properly recombined DNA is expected to generate a 15 kb *Hin*dIII fragment whereas the wild-type allele should generate a 20 kb *Hin*dIII fragment when probed with the 3 kb insert.

2.3 Cell Culture

HeLa (human cervical carcinoma cells), GM38 (normal human lung fibroblasts), SKN (human neuroblastoma cells), COS-7 (transformed African green monkey kidney fibroblasts), HISM (human intestinal smooth muscle cells), T24 (human bladder carcinoma cells), MRC-5 (normal human embryo lung fibroblasts), 293 (transformed human kidney cells), C3H 10T1/2 (mouse embryo fibroblasts), NIH 3T3 (mouse embryo fibroblasts), and Indian muntjac fibroblasts were grown on glass coverslips at 37°C in a 6% CO_2 atmosphere in DMEM (Gibco BRL) supplemented with 10% fetal calf serum and antibiotics [100 U/ml penicillin and 100 μg/ml streptomycin (Gibco BRL)]. Human retinoblastoma cells RB778, RB893, RB522A and RB(E)-2 were grown in suspension using the same medium described above. When required for microscopy, retinoblastoma cells were allowed to adhere to poly-L-lysine-coated coverslips for 30 min. All cells were used for microscopy at 40–70% confluence. RNA was labeled by adding 2 mM 5'-fluorouridine (FU) (Sigma) to cells at 37°C for 15 min as previously described (Boisvert *et al.*, 2000).

2.4 Microscopy Techniques

2.4.1 Immunofluorescence labeling

Cells adhering to coverslips were fixed in 1% paraformaldehyde in phosphate-buffered saline (PBS) for 10 min and permeabilized for 5 min in 0.5% Triton X-100/PBS. Alternatively, cells were fixed and permeabilized in –20°C 1:1 methanol/acetone for 10 min. Cells were incubated for 1 hr in blocking buffer (3% bovine serum albumin in PBS) containing the primary antibody, rinsed in PBS, and incubated in blocking buffer containing the secondary antibody. Coverslips were mounted onto slides with glycerol containing 1 mg/ml p-phenylenediamine + 1 μg/ml 4',6-diamidino-2-phenylindole (DAPI). All fluorophores were examined on a single-labeled slide to ensure the dye did not excite and emit energy with other wavelengths and filter sets.

2.4.2 Antibodies

Rabbit polyclonal DDX1 antiserum (batch 2923) was produced using native recombinant DDX1 (amino acids 1-186). To verify antibody specificity, GST-DDX1 was bacterially expressed and purified using glutathione-Sepharose 4B (Godbout *et al.*, 1998). GST was cleaved with thrombin and DDX1 (0 µg or 5 µg) was spotted onto nitrocellulose. The filters were incubated in blocking buffer and subsequently in primary antibody (anti-DDX1 or unrelated rabbit polyclonal anti-aldehyde dehydrogenase) at the dilution used for immunofluorescence labeling (1/400 for 2923 and 1/150 for aldehyde dehydrogenase). After an overnight incubation at 4°C, the unbound antibody was used to stain fixed and permeabilized cells for immunofluorescent detection.

The following primary antibodies were used in this study: rabbit polyclonal p80 coilin at a 1/1200 dilution (Andrade *et al.*, 1993), mouse monoclonal Y12 against the Sm antigens at a 1/6000 dilution (Pettersson *et al.*, 1984), mouse monoclonal CstF-64 at a 1/100 dilution (Takagaki *et al.*, 1990), mouse monoclonal Sam68 at a 1/20 dilution (Santa Cruz Biotechnology Inc.), mouse monoclonal SC-35 at a 1/10 dilution (ATCC hybridoma 2031), mouse monoclonal 5E10 against PML bodies - undiluted (Stuurman *et al.*, 1992), mouse monoclonal bromodeoxyuridine, which recognizes halogenated UTP at a 1/200 dilution (Sigma), mouse monoclonal SMN at a 1/400 dilution (Transduction Laboratories), goat polyclonal SMN at a 1/400 dilution (Santa Cruz Biotechnology), mouse monoclonal vimentin at a 1/300 dilution (Roche), mouse monoclonal pan-cytokeratin at a 1/200 dilution (Roche), mouse monoclonal cytochrome *c* oxidase subunit I at a 1/100 dilution (Molecular Probes), mouse monoclonal ICP4 at a 1/1000 dilution (Goodwin Biotech. Inc.), mouse monoclonal tubulin at a 1/500 dilution (Sigma), and mouse monoclonal ribosome kinase S6 at a 1/100 dilution (Santa Cruz Biotechnology). Secondary antibodies were all used at a 1/200 dilution and included Alexa 488 goat anti-mouse, Alexa 488 donkey anti-goat, Alexa 594 goat anti-rabbit (Cedarlane Laboratories), Cy3 donkey anti-rabbit, Cy3 donkey anti-mouse, Cy5 donkey anti-mouse, and Cy5 donkey anti-rabbit (Jackson Immunoresearch Laboratories).

2.4.3 Affinity Purification of anti-DDX1 antibody

One mg of glutathione-sepharose 4B-purified GST-DDX1 was buffer-exchanged into 1 ml of coupling buffer (0.2 M $NaHCO_3$, 0.5 M NaCl; pH 8.3) using P30 Centricons. The recombinant DDX1 was then applied to a 1 ml HiTrap NHS-activated Sepharose column and incubated for 30 min at R.T. Deactivation and washing of the column was performed with alternate washes of 0.5 M ethanolamine, 0.5 M NaCl; pH 8.3 and 0.1 M acetate, 0.5 M NaCl; pH 4.0. The column was equilibrated with Tris-buffered saline (TBS) and 1 ml of anti-DDX1 antiserum from batch 2923 was diluted 10-fold with TBS and applied to the GST-DDX1 affinity column at a flow rate of 1 ml/min and allowed to recirculate for 18 hr at 4°C. The column was washed with 85% buffer A (10 mM Tris·HCl, 20% glycerol; pH 8.0) and 15% buffer B (buffer A + 1 M NaCl). Non-specifically bound proteins were eluted with 50% buffer A and 50% buffer B. Antibodies were eluted with 100 mM glycine pH 3.0 and fractions neutralized to pH 8.0 with 1 M Tris·HCl, pH 11.0. The anti-DDX1 antibodies were concentrated using P30 Centricons and buffer-exchanged with buffer A in a final volume of 1 ml. Dr. John Rowe performed this procedure.

2.4.4 Light Microscopy

Images of single-labeled cells were collected on a Zeiss-Axioplan II microscope with a cooled charge-coupled device (CCD) camera (Sensi-Cam, Cooke Corp.). All double-labeled cells, and GFP transfected cells were viewed on a Zeiss LSM 510 confocal microscope with a plan apochromat 63X/1.4 oil immersion lens. Argon and helium-neon (HeNe) lasers were sequentially used to scan at wavelengths 488 and 543 nm, respectively. A UV laser was used to excite DAPI stained cells. The image stacks were three-dimensionally reconstructed by maximum likelihood projections using the Zeiss LSM 510 image analysis software. Each picture in the figures represents one 0.2 μm Z section. To measure the 3-D distances between structures, the centers of each foci were marked and the Zeiss LSM 510 software calculated the distance based on pixel dimensions. For colocalization experiments, a minimum of 20 cells were three-dimensionally reconstructed and examined.

Where indicated, images were deconvolved using Softworks 2.5 software (Applied Precision Instruments) to remove out-of-focus information. The required point spread functions were generated as recommended by the manufacturer.

The deconvolution program is based on a constrained iterative algorithm developed in the laboratory of John Sedat (UCSF).

To determine the likelihood of nuclear bodies randomly localizing adjacent to DDX1 foci, we used a method published by Grande *et al.* (1996) which takes into account total cell volume, the size of the foci in question, as well as their abundance. This calculation is based on the following equation: probability = $(4/3)\pi(d)^3 \cdot n \cdot m/v$ where d is the distance between the centers of adjacent structures, n and m are the average number of each structure per nucleus, and v is the volume of the nucleus in μm^3. This equation makes two incorrect assumptions: i) the nucleus is a perfectly round sphere and ii) the nucleus is devoid of other structures permitting unhindered movement of molecules. As such, the equation developed by Grande *et al.* represents only a crude estimate of the probability that nuclear bodies will localize adjacent DDX1 foci.

2.4.5 Microscopic Fluorescence Resonance Energy Transfer (FRET)

HeLa cells were fixed, permeabilized, and labeled for DDX1, CstF-64 and PML as described above, with the exception that the coverslips were mounted in glycerol without p-phenylenediamine. The donors, anti-CstF-64 and anti-PML antibodies, were labeled with Alexa 488 goat anti-mouse secondary antibody. The acceptor, anti-DDX1 antibody, was labeled with Cy3 donkey anti-rabbit secondary antibody. Cells were observed using a Zeiss LSM 510, as described above, except that all images were collected with the pinhole apertures wide open. Alexa 488 was excited with a 488 nm Argon laser and detected using a 505-550 nm band-pass filter. Cy3 was excited with a 543 nm HeNe laser and detected using a 560 nm long-pass filter. The FRET image was collected using the 488 nm Argon laser for excitation and the 560 nm long-pass filter for detection. Photodestruction of the acceptor was done using the 543 nm HeNe laser.

FRET was determined on a pixel-by-pixel basis using the three-filter set as described by Youvan *et al.* (1997). The background noise of every channel in all images was calculated by averaging 4 regions of 20 pixels outside of the cell. Subtracting the background value plus twice the standard deviation produced corrected images. The final FRET image was calculated according to the following equation: final FRET = FRET – (FRET • donor ratio + FRET • acceptor ratio), where the donor and acceptor ratios are the amount of respective fluorophores contributing to the FRET intensity (calculated using single labeled donor and acceptor slides). The Cy3 did not exhibit any excitation by the Argon laser at 488 at the current filter and laser settings. The final FRET images were corrected for background as described above using METAMORPH 4.5 software. All images were rescaled identically in Adobe PHOTOSHOP 6.0 using the CstF-64 image to define the maximum value.

FRET was also measured using fluorescence lifetime imaging microscopy (FLIM). The cells were fixed and mounted as above. The donor, anti-cytochrome *c* oxidase antibody, was labeled with Alexa 488 goat anti-mouse secondary antibody while the acceptor, anti-DDX1 antibody, was labeled with

Cy3 donkey anti-rabbit secondary antibody. The cells were viewed on a Zeiss 510 LSM fitted with a time-correlated single photon counting system. This system uses a fast photodiode (400 ps at FWHM) to detect laser pulses. Arrival of these pulses was used as a synchronization signal for time-correlated photon counting. By correlating the number of photons the detector identified with the timing of the photons, a fluorescence decay curve is constructed for every pixel in the image. Then, using a curve-fitting algorithm (single exponential decay function), the fluorescence lifetime is calculated for every pixel. In these experiments, donor (Alexa 488) was excited by a titanium sapphire laser adjusted to 770 nm. For visualization purposes, Cy3 was excited with a 543 nm HeNe laser and detected using a 560 nm long-pass filter. The occurrence of FRET shifts the decay curve (ie. shortens the lifetime of donor molecules) when compared to the decay curve for a cell solely labeled for the donor.

2.4.6 Measuring transcription by RNA polymerase II and III

HeLa cells were incubated in 2 mM 5'-fluorouridine (FU) (Sigma) at 37°C for 15 min. The cells were then fixed, permeabilized and labeled with anti-DDX1 and anti-BrdU antibodies, and appropriate secondary antibodies. The cells were imaged on a Zeiss-Axioplan II microscope with a cooled charge-coupled device (CCD) camera (Sensi-Cam, Cooke Corp.), keeping the exposure constant between cells. The images were processed using Metamorph Imaging software. Briefly, the corrected image was produced by subtracting the background value plus twice the standard deviation. The FU image was then subjected to a threshold to remove the bright nucleolar signal contributed by RNA polymerase I transcription. This thresholded image was used to create a mask based on the DAPI channel. The thresholding was repeated on the FU image until even the dimmest nucleoli had been removed from the mask. This mask was then used to measure the average gray value of both images, FU and DDX1. Additionally, DDX1 foci were counted and compared to FU intensity. The criterion for a focus was that it must appear in 3 of the 0.2 μm Z planes. All numbers were then subjected to linear regression analysis using a program written by Mr. John Hanson (Cross Cancer Institute, Edmonton, Alberta).

2.4.7 Viral infection by herpes simplex virus type 1

Herpes simplex virus type 1 (HSV-1) (strain KOS1.1) was obtained from Darin McDonald (Dr. Michael Hendzel's laboratory, University of Alberta). The virus had a titer of 2 X 10^8 PFU/ml. HeLa cells were infected at a multiplicity of infection of 10 PFU/cell. Briefly, the virus was added to 250 μl of PBS infection buffer (1X PBS, 0.5 mM $MgCl_2$, 0.9 mM $CaCl_2$, 0.1% glucose, 1% heat inactivated FBS) and incubated with the cells for 1 hr at 37°C. The PBS infection buffer was then replaced with viral medium (DMEM, 2% heat inactivated FBS, 1% penicillin/streptomycin, 1% L-glutamine) and incubated at 37°C for an additional 5 hr. The cells were then fixed in 1% paraformaldehyde, permeabilized in 0.1% Triton X-100 and labeled with antibodies.

2.4.8 Construction of GFP-DDX1 plasmids and DNA transfections

DDX1 cDNA insert was obtained by digesting pGEM-*DDX1* with *Bam*HI and *Xho*I. The pEGFP-C1 plasmid was digested with *Bam*HI and ligated to the *Bam*HI site of *DDX1*. The linear pEGFP-C1-DDX1 DNA was then blunt-ended and re-ligated to produce pGFP-*DDX1*. The plasmid was 2 X CsCl purified and then transfected into HeLa cells using the calcium phosphate method. Western blot analysis was used to confirm GFP-DDX1 expression. All cells were viewed on a Zeiss LSM 510 confocal microscope with a plan apochromat 63X/1.4 oil immersion lens. To destabilize microtubules, nocodazole (Sigma) was added at a 10 μM concentration and cells were imaged at 3 min intervals.

2.4.9 Labeling with MitoTracker

HeLa cells were incubated in 250 nM MitoTracker Red (M-7513, Molecular Probes) for 30 min. For fixed cell analysis, cells were incubated in –20°C 50:50 methanol:acetone for 5 min.

2.5 Biochemical techniques

2.5.1 Immunoprecipitations

For the co-immunoprecipitation experiments, we used rabbit polyclonal antiserum (batch 2910) generated using denatured recombinant DDX1 (amino acids 1-186) (Godbout *et al.*, 1998). The antibody was pre-cleared with protein A agarose beads (Sigma) and incubated for 3 hr with nuclear extracts prepared from HeLa cells (Dignam *et al.*, 1983). Immune complexes were precipitated with protein A agarose beads and run on an SDS polyacrylamide gel. Proteins were transferred to nitrocellulose membrane by electroblotting and Western blot analysis was carried out using anti-DDX1 antibody and either anti-CstF-64 antibody, anti-SMN antibody (Transduction Laboratories), or anti-Sam68 antibody. These immunoprecipitations were performed by Mary Packer.

2.5.2 Cell Synchronization and Flow Cytometric Analysis

RB522A or Y79 cells were synchronized using aphidicolin (Sigma) at 1 μg/ml for 18 hr. Five hr after aphidicolin release, cells were incubated in nocodazole at 0.04 μg/ml for 6 hr. Sample cell populations were harvested and stained with propidium iodide according to a protocol by Vindeløv *et al.* (1983). The samples were then visualized by flow cytometric analysis. Cells were gated to rid aggregates and debris based on their staining intensity (FL2-area) and their size (FL2-width) as described in the FACSort User's Guide. This gated population of cells was then used to detect the overall intensity of propidium iodide within each cell. The number of cells in each peak of the resultant histogram was calculated by the FACSort software with user-defined markers.

2.5.3 Cellular fractionation and mitochondria isolation

Cells were separated into nuclear and cytoplasmic components according to Dignam *et al.* (1983) except that the extracts were not dialyzed in buffer D. Mitochondria, purified by Mary Packer, were isolated as described in Darley-

Usmar *et al.* (1987). The resultant fractions were electrophoresed on a 10% SDS-polyacrylamide gel.

2.5.4 Purification of recombinant DDX1 by HPLC

Approximately 200 μg of recombinant DDX1 was loaded onto a Nickel-IMAC column equilibrated in buffer A (10 mM Tris pH 8.0; 15 mM ammonium sulfate) at 1 ml per minute. UV absorption was monitored at 280 nm. The column was washed with buffer A for 10 min. Bound DDX1 was eluted from the column with a linear gradient from buffer A to 100% buffer B [10 mM Tris·HCl (pH 8.0), 10 mM ammonium sulfate, and 50 mM Imidazole] over 20 min at a flow rate of 1 ml per minute. Fractions 22-24 from 2 separate chromatographies were pooled and concentrated using Centricon P30. The concentrated DDX1 (1 mg per ml) was analysed by western blot and stored at -20°C. Dr. John Rowe performed this procedure.

2.5.5 *In vitro* transcription and *in vitro* polyadenylation assay

The DNA plasmids pSVL-3 (AAUAAA) and pSVL-6 (AAGAAA) were obtained from Dr. Jeffery Wilusz (University of Medicine and Dentistry, Newark, New Jersey). The DNA was linearized with *Dra*I and *in vitro* transcribed at 37°C for 1 hr with the following components: 1X RNA polymerase buffer (Gibco BRL), 12.5 mM DTT, 500 μm ATP, 500 μm CTP, 100 μm GTP, 25 μm UTP, 500 μm 5' 7-methyl guanosine (cap analog) (Promega), 50 μg/ml template DNA, 1 U/μl ribonuclease inhibitor, 5 μl α^{32}P-UTP (3000 Ci/mmol) (Amersham Biosciences), 1 µl SP6 RNA polymerase (Gibco BRL), and H_2O to 20 µl. The DNA was digested with 50 µg/ml DNase I at 37°C for 10 min and the RNA was mixed with RNA loading dye [10 mM Tris·HCl (pH 7.5), 1 mM EDTA, 50% glycerol, 3 mg/ml bromophenol blue]. The RNA, which was electrophoresed on an 8 M urea 8% polyacrylamide gel in 1X TBE at 15 W for 1.5 hr, was subsequently cut out of the gel and eluted overnight at 4°C in 400 µl of elution buffer (0.5 M NH_4oAc, 0.1% SDS, 1 mM EDTA). Phenol:chloroform extractions were done until the interphase was gone and the RNA was precipitated with 1.5 M NH_4oAc, 20 µg yeast tRNA, and 2 volumes of 100% ethanol. The RNA was resuspended in 20 µl of 10 mM Tris·HCl (pH 7.5) and the specific activity was measured in a scintillation counter. The concentration of RNA transcribed was calculated as follows: % incorporation = total cpm obtained / total cpm added; moles of UTP incorporated = % incorporation • moles of limiting NTP (ie. α^{32}P-UTP); moles transcribed = moles UTP incorporated / number of uridine bases in probe; fmol = moles transcribed • 10^{15}; cpm/fmol = total cpm obtained / fmol; fmol/µl = cpm/µl / cpm/fmol.

Nuclear extracts were made according to Dignam *et al.* (1983) with slight modifications: i) after swelling the cells in buffer A, the cells were pelleted and resuspended in 2 packed cell volumes of buffer A prior to homogenization, ii) following the spin after homogenization, the pellets were resuspended in buffer A iii) the nuclear extract was dialyzed for 30 min in buffer D instead of 5 hr.

In vitro polyadenylation required the following components to be incubated at 30°C for 45 min: 3.25 µl 10% polyvinyl alcohol, 1 µl 12.5 mM ATP/

250 mM phosphocreatine, 1 µl ^{32}P-labeled RNA (~200,000 cpm), and 7.25 µl nuclear extract. HSCB buffer [25 mM Tris·HCl (pH 7.5), 400 mM NaCl, 0.1% SDS] was added to a volume of 400 µl and the RNA was extracted with phenol and then phenol:chloroform. The RNA was precipitated with 20 µg yeast tRNA and 2 volumes of 100% ethanol at -80°C. The RNA products were visualized on an 8 M urea 4.5% polyacrylamide gel run at 7 W for 2 hr 45 min.

Chapter 3. Generation of *DDX1+/-* Mouse Embryonic Stem Cells

Targeted gene disruption in mice using homologous recombination is a powerful tool for investigating the function of uncharacterized genes and for discerning phenotypes of genes whose biochemical function may be known. The plethora of targeted gene knockouts is vast with many compiled at http://www.bioscience.org/knockout/knochome.htm. The generation of mutant mouse strains involves the use of cultured embryonic stem cells. These cells are isolated from the inner cell mass of a blastocyst-stage embryo, and are grown on fibroblast feeder cells, or on gelatinized plates with medium supplemented with leukemia inhibitory factor (LIF). The purpose of the feeder cells or the LIF is to prevent differentiation thereby retaining ES totipotency.

DDX1 was a suitable candidate for gene targeting as it did not appear to have any homologs thus minimizing the chances of functional redundancy. As well, the entire human cDNA sequence was cloned permitting easy identification of the mouse ortholog. Furthermore, we have little information regarding its possible biological or biochemical functions; inactivating the gene might reveal possible roles during development. Our specific objectives were therefore to:

a) identify and clone the mouse genomic ortholog of *DDX1*.

b) restriction enzyme map the clone so as to identify a strategy for generating the targeting vector.

c) generate a knockout targeting vector.

d) generate mouse ES cells heterozygous for the *DDX1* gene.

Subsequent to the isolation of properly targeted ES cells, we had arranged to collaborate with Dr. Peter Dickey (University of Alberta, Edmonton, Alberta) for microinjection of the ES cells into normal blastocysts. Any chimeras born would be transferred to the animal care facility at the Cross Cancer Institute for further mating and genomic testing.

3.1 Identification and cloning of the genomic mouse DDX1

A day 5 mouse brain cDNA library cloned in lambda gt11 was obtained from Dr. James Stone (University of Alberta, Edmonton, Alberta). Approximately 150,000 plaques were screened under low stringency using a human 5' *DDX1* cDNA probe (bases 260-842). Mouse cDNA clones were obtained and the 5' ends were sequenced to verify *DDX1* identity. The sequences revealed extensive identity to the human *DDX1* sequence. As we had decided to target the 5' end of the *DDX1* gene, we examined the human *DDX1* cDNA restriction map for an enzyme that would digest within the 5' end to produce a sequence suitable for probing the mouse genomic library. Accordingly, the mouse clone was digested with *Eco*RI to generate a 700 bp 5' *DDX1* cDNA probe. Two mouse genomic libraries were screened: an ES cell library obtained from Dr. Derrick Rancourt (University of Calgary) and a mouse liver library obtained from Dr. James Stone. Both libraries were titered and 400,000 plaques were screened using the 700 bp mouse 5' *DDX1* cDNA probe. One positive clone, 3026, was obtained with the ES library, which was derived using genomic DNA from the mouse strain 129/Sv. Two clones, 3030 and 3031, were obtained with the mouse liver library originating from genomic DNA from the mouse strain 129/J. To identify which clones contained exons 1 and 2, the 700 bp 5' *DDX1* mouse cDNA fragment was further subcloned using *Eco*RV. This digest produced a 100 bp fragment corresponding to exons 1 and 2 and a 600 bp fragment corresponding to exons 3-11. Southern blot analysis of clones 3026, 3030, and 3031 revealed that clone 3026 did not contain exons 1 or 2 (Fig 3.1). Southern blot analysis using the 3' 600 bp probe indicated that 3031 extended further downstream than clone 3030, which contained more 5' sequence (Fig. 3.1). Therefore because we wished to target the upstream exons, clone 3030 was selected for further analysis.

3.2 Restriction mapping of clone 3030

Clone 3030, which was approximately 13 kb long, was subcloned into pBR322. The clone was mapped using several restriction enzymes (Fig. 3.2A) and the region that hybridized to the exon 1 probe was sequenced to reveal its exact position on the map. To verify that the cloned genomic DNA was not rearranged or did not represent a pseudogene, we performed several restriction enzyme digests of mouse genomic DNA and clone 3030. Southern blot analysis using the 100 bp mouse cDNA probe from exons 1 and 2 revealed identical fragments (data not shown). This suggested that there were no gross rearrangements in our clone making it likely that we had identified the active *DDX1* gene.

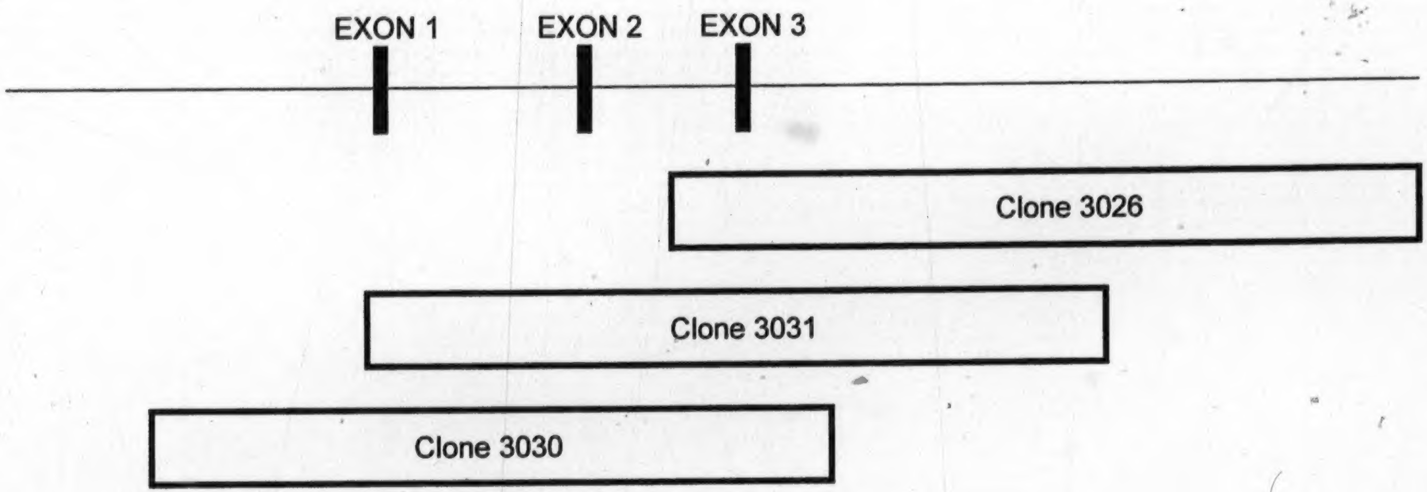
EXON 1
EXON 2
EXON 3
Clone 3026
Clone 3031
Clone 3030

Fig. 3.1 Positioning of *DDX1* genomic clones in relation to the 5' end of *DDX1*.

The 5' end of DDX1 is depicted showing the relative positions of exons 1, 2, and 3. Clone 3026 is 18 kb and does not contain exons 1 or 2. Clone 3031 is 17 kb and extended further 3' than clone 3030. Clone 3030 is 13.6 kb and contains exons 1 and 2 as well as sequence further upstream.

The diagram is not to scale.

Fig. 3.2 Restriction map of clone 3030 and *DDX1* targeting vector.

A. Restriction map of clone 3030. The following enzymes are abbreviated: R1 = *Eco*RI, RV = *Eco*RV, HI = *Bam*HI. The 4.0 kb *Sac*I/*Sac*I fragment was used as the 5' arm in the targeting vector, and the 3.7 kb *Bam*HI/*Pvu*II fragment was used as the 3' arm. The 3.0 *Pvu*II/*Bam*HI probe is indicated. **B.** The targeting vector designed in pBR322 (pBR) contains the 5' and 3' *DDX1* genomic fragments from clone 3030 as well as the neomycin (*neo*) and thymidine kinase (TK) cassettes from pNTK. The newly introduced *Hin*dIII (HIII) fragment adjacent to the *neo* cassette is indicated by the thick black line. **C.** The mutant allele produced by homologous recombination between the wild-type allele and the targeting vector. The *Hin*dIII (HIII) sites are indicated by the thick black lines. The expected *Hin*dIII fragment sizes for both the wild-type allele and the recombinant allele after Southern blot analysis using the 3.0 kb probe are indicated below.

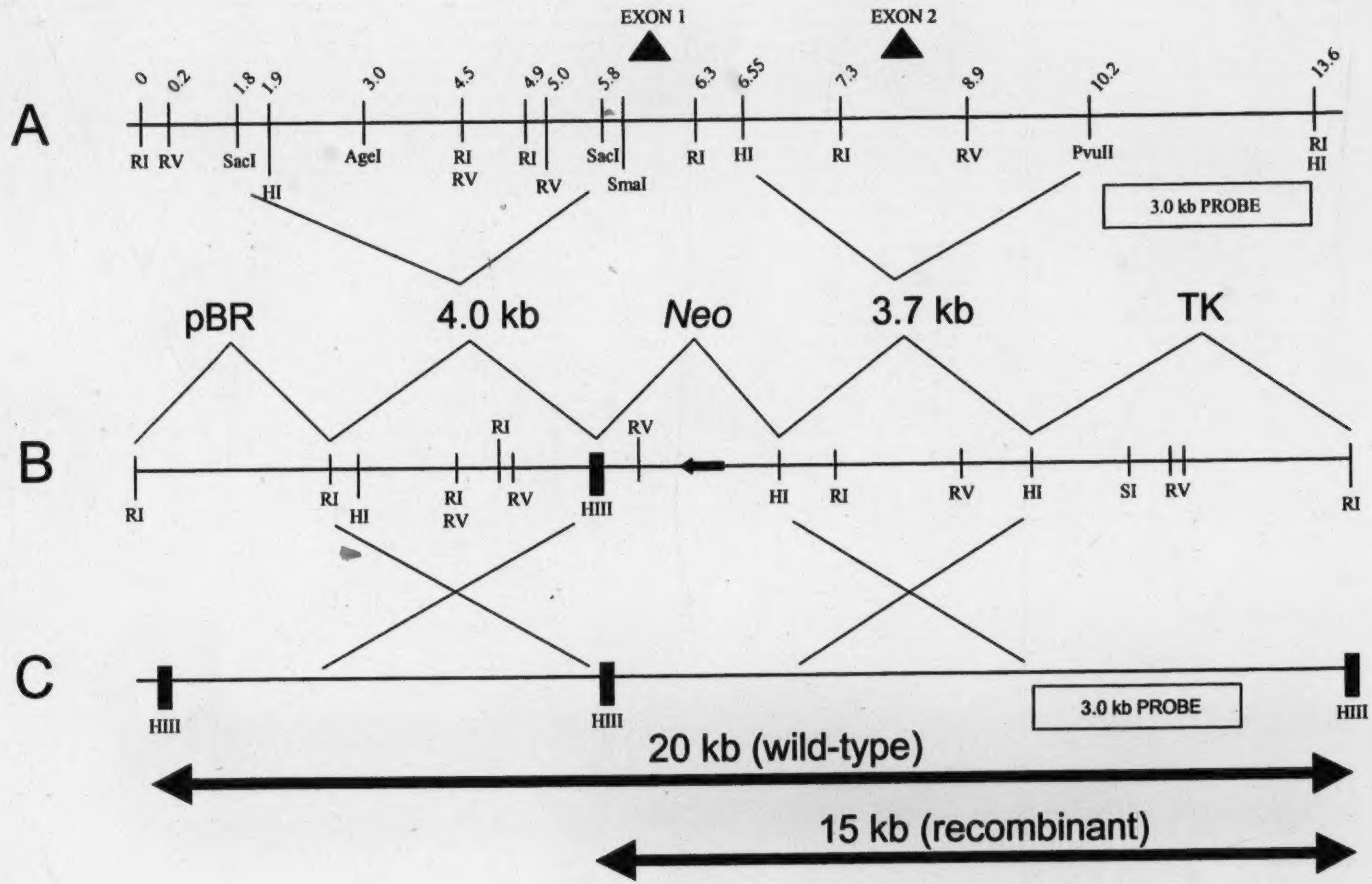
EXON 1
EXON 2
A
0
0.2
1.8
1.9
3.0
4.5
4.9
5.0
5.8
6.3
6.55
7.3
8.9
10.2
13.6
RI
RV
SacI
HI
AgeI
RI
RV
RI
RV
SacI
SmaI
RI
HI
RI
RV
PvuII
RI
HI
3.0 kb PROBE
pBR
4.0 kb
Neo
3.7 kb
TK
B
RI
RI
HI
RI
RV
RI
RV
HIII
RV
HI
RI
RV
HI
SI
RV
RI
C
HIII
HIII
3.0 kb PROBE
HIII
20 kb (wild-type)
15 kb (recombinant)

3.3 Overall strategy behind the generation of our targeting vector

It is known that the length of the homology between the gene of interest and the targeting vector is directly proportional to the frequency of targeting events within ES cells (Hasty and Bradley, 1993). Therefore we sought to use as much of our 13 kb genomic clone as possible in our targeting vector. We also decided to remove exon 1 which contains the ATG start site from the targeting construct. This DNA was replaced with the neomycin (*neo*) cassette to be used for positive selection. Cells that can survive in geneticin (G418) have incorporated the neomycin resistance gene. The expression of *neo* is driven by the phosphoglycerate kinase (PGK) promoter, which is active in ES cells (Mortensen, 1993). The *neo* cassette was inserted 3' to 5' to ensure there was no readthough from the translational machinery. To detect random integration into the genome, we used the negative selection cassette, herpes simplex virus thymidine kinase (TK). If TK becomes incorporated into the genome, cells can activate and incorporate the drug gancyclovir, a thymidine analog, into the genome. Incorporation of gancyclovir results in DNA chain termination and subsequently cell death. Similar to *neo*, TK expression is also driven by the PGK promoter.

3.4 Generation of the targeting vector

Our final strategy involved placing the 3.7 kb *Bam*HI/*Pvu*II *DDX1* fragment (Fig. 3.2A) into pNTK within a *Bam*HI site located between the *neo* cassette and the TK cassette. The entire *neo* - 3.7 kb *DDX1*– TK cassette was removed and inserted into pBR322. The 4.0 kb *SacI/SacI* fragment from clone 3030 (Fig. 3.2A) was removed, blunt-ended and ligated to *Hin*dIII linkers. This permitted cloning of the 4.0 kb fragment into the *Hin*dIII site of pBR322 which already contained the *neo* - 3.7 kb *DDX1*– TK cassette. This completed vector (Fig. 3.2B) generated a new *Hin*dIII site adjacent to the *neo* cassette allowing us to discern a targeted allele by *Hin*dIII restriction enzyme digestion and Southern blot analysis of genomic DNA (Fig. 3.2C). The 3.0 kb *Pvu*II/*Eco*RI fragment located at the 3' end of clone 3030 (Fig. 3.2A) was subcloned and used as a probe on a mouse genomic DNA Southern blot to test for the presence of any repetitive elements. This 3.0 kb probe did not contain any repetitive elements and therefore could be used on Southern blots to screen for correctly targeted alleles.

3.5 Generation of properly targeted ES cells

The R1 cell line of ES cells was obtained from Dr. Andràs Nagy (Samuel Lunenfeld Research Institute, Toronto, Ontario). The R1 cell line was derived from a (129/Sv x 129/Sv-CP) F1 3.5 day blastocyst (Nagy *et al.*, 1993). These cells are of the male sex and will generate progeny with agouti coat colour. We obtained our R1 cells at passage 14, which was previously shown to be totipotent (Nagy *et al.*, 1993).

In order to grow the ES cells we needed LIF, an agent that suppresses differentiation (Smith *et al.*, 1988; Williams *et al.*, 1988). The LIF plasmid was obtained from Dr. Nagy on behalf of Dr. John Heath. The LIF protein was expressed as a GST-fusion protein in *E.coli* HB101, and purified using glutathione-sepharose beads. The protein was cleaved from GST using thrombin and was checked for relative purity by Dr. John Rowe using HPLC (data not shown). Additionally, we obtained mouse SNL STO cells from Dr. Nancy Dower (University of Alberta, Edmonton, Alberta) for use as fibroblast feeders. These feeders function similarly to LIF to suppress differentiation, and have the advantage over other fibroblasts in that they are resistant to geneticin. The STO cell line was established by Dr. A. Bernstein (Mount Sinai Hospital, Toronto) from SIM mouse fibroblasts and the SNL STO subline was generated later by A. Bradley (Wurst and Joyner, 1993). To prevent growth, the SNL STO cultures were expanded and then irradiated with 6 Gray using a gamma irradiator.

The *DDX1* targeting vector was prepared for electroporation by linearization using either *Pvu*I or *Nde*I. Following electroporation, the ES cells were grown without drugs for 2 days. Then both geneticin and gancyclovir were added to the medium and the ES cells were cultured for an additional 12 days. On day 14 the drug resistant colonies were large enough to pick. The colonies that had not differentiated were identifiable without the aid of a microscope as they were round, dark, compact clusters. The colonies that had differentiated had uneven, opaque edges, due to the formation of endodermal cells on the perimeter of the colony (Hogan *et al.*, 1994). Therefore, only the undifferentiated colonies were selected (Fig. 3.3) and cultured in 96-well plates. The colonies

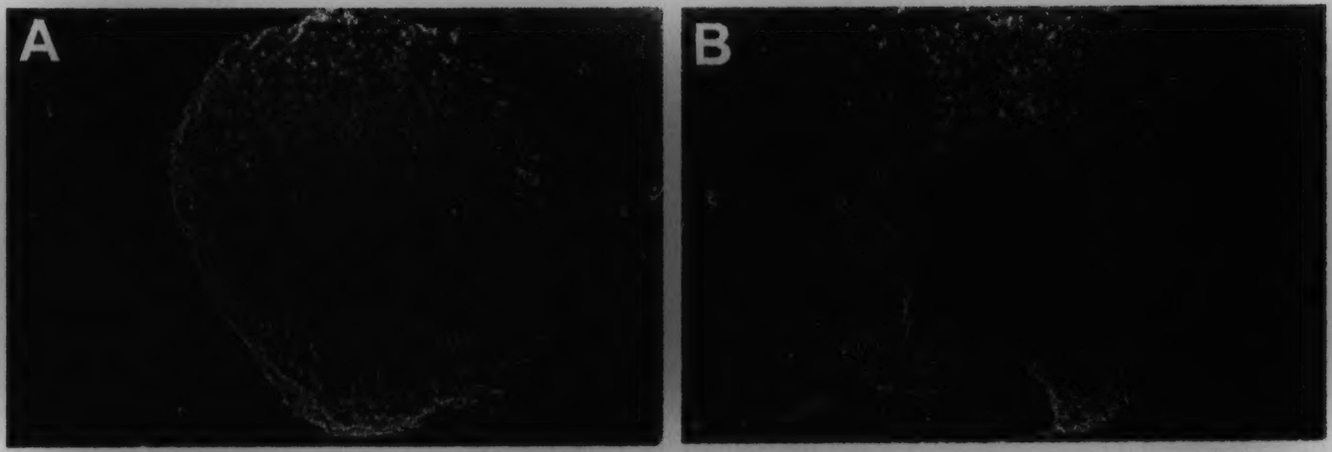

Fig. 3.3 Selection of undifferentiated ES colonies.

A. An undifferentiated ES colony identified by its tight compact edges. **B.** An ES colony that has extensive differentiation at its periphery. The latter colony is unsuitable for gene targeting analysis.

were expanded into four duplicate 96-well plates and 2 plates were frozen at −80°C in 10% DMSO, while the other 2 were used for DNA analysis.

A total of 220 resistant colonies were picked for DNA analysis. Mapping of the *Hin*dIII sites in the genomic mouse DNA using the 3.0 kb probe revealed a 20 kb fragment which would be reduced to 15 kb upon homologous recombination (Fig 3.2C). Southern blot analysis of all 220 colonies identified 5 clones that contained a targeted allele. A Southern blot demonstrating all 5 heterozygous colonies as well as some non-targeted homozygous colonies is shown in Fig. 3.4. To verify that these alleles were correctly targeted we probed the blots with a neomycin probe. All 5 clones contained the neomycin gene within the 15 kb *Hin*dIII fragment (data not shown). This is in contrast to the clones with random integration, which usually had several *neo* fragments (data not shown). We also performed Western blot analysis on cell lysates prepared from various cell types and on wild-type and targeted ES cells (Fig 3.5). The R1 ES cells contained similar amounts of DDX1 as a non-amplified RB cell line RB(E)-3, but less than primary human tonsil cells. The targeted cell lines displayed an approximately 2-fold decrease in DDX1 protein levels when compared to wild-type ES cells. Therefore, approximately 2.3% of our geneticin/gancyclovir resistant clones were properly targeted.

3.6 Chimeras generated using *DDX1* +/- R1 ES cells

Of the 5 heterozygous clones, only 4 survived the freezing process. Dr. Peter Dickey has made numerous attempts to inject all 4 of these clones into

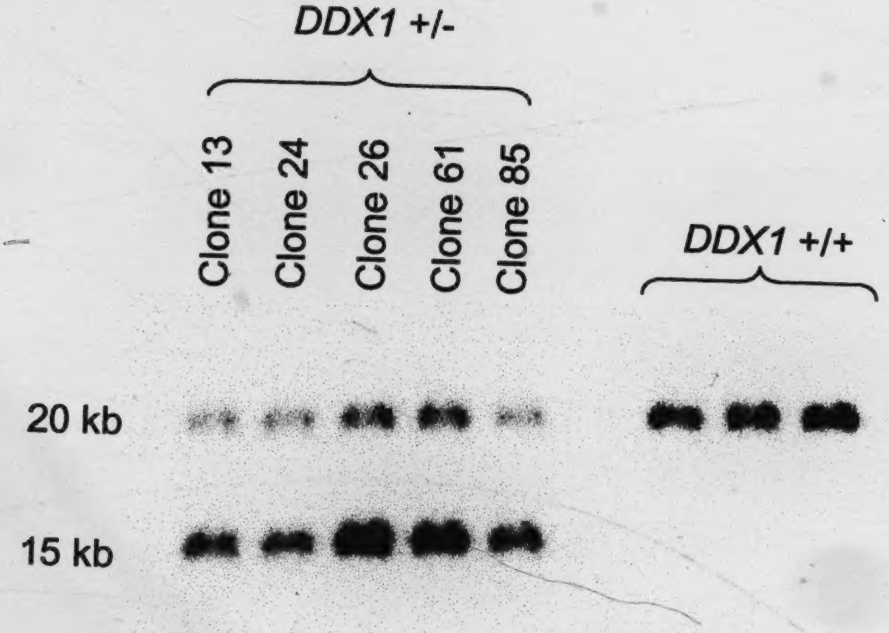
DDX1 +/-
Clone 13
Clone 24
Clone 26
Clone 61
Clone 85
DDX1 +/+
20 kb
15 kb

Fig. 3.4 Southern blot analysis of *DDX1+/-* ES cells as well as *DDX1+/+* cells.

The probe was a 3.0 kb fragment located downstream of the recombined region. Digestion with *Hin*dIII generated a 20 kb fragment representing the wild type allele and a 15 kb fragment representing the targeted allele.

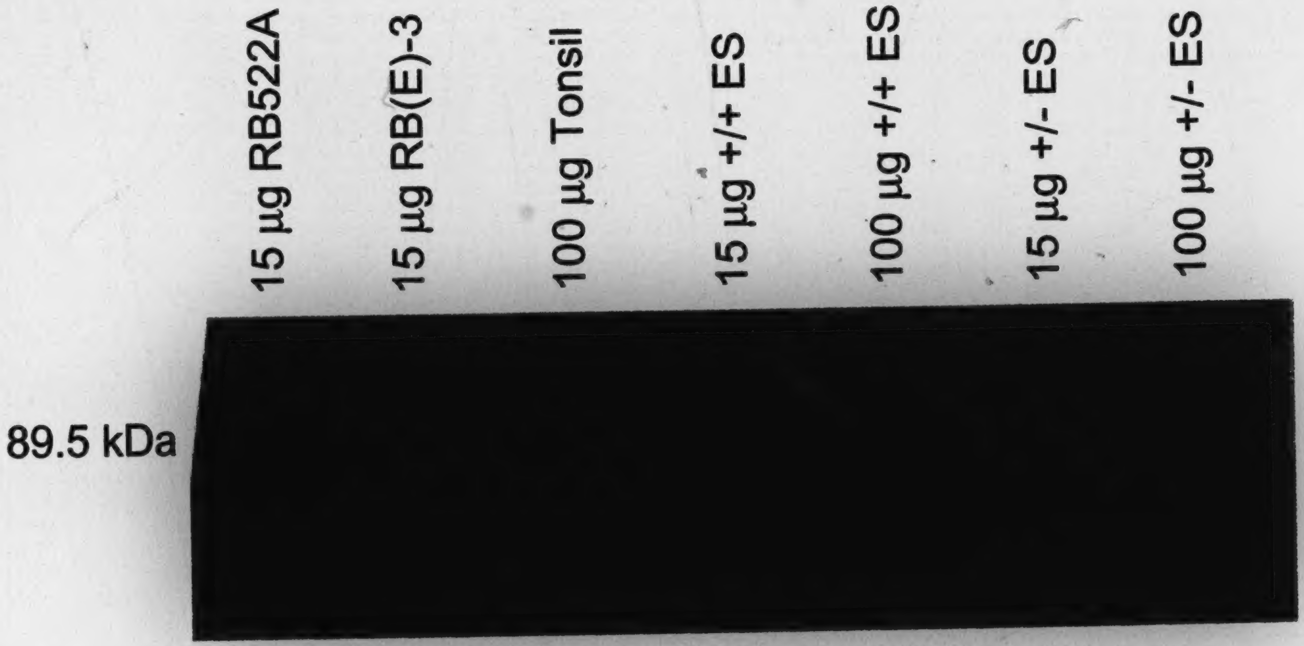
15 µg RB522A
15 µg RB(E)-3
100 µg Tonsil
15 µg +/+ ES
100 µg +/+ ES
15 µg +/- ES
100 µg +/- ES
89.5 kDa

Fig. 3.5 Western blot analysis of DDX1.

Whole cell lysates were prepared from two retinoblastoma cell lines, RB522A (*DDX1*-amplified) and RB(E)-3 (not *DDX1*-amplified), primary human tonsil cells, *DDX1*+/+ ES cells, and *DDX1*+/- ES cells. The lysates (15 µg or 100 µg) were subjected to SDS-PAGE on a 10% gel. The blot was probed with anti-DDX1 antibody, 2910.

blastocysts obtained from superovulated C57BL/6 mice. A total of 12 chimeras have been born, 8 of which were female (Table 3.1). One mouse was a sterile XX←→XY chimera. We have attempted to mate each of the 3 males with C57BL/6 mice. Of the first 2 male chimeras, 1 had to be terminated due to illness before he was able to mate. The 1 male that did mate produced 2 litters with no heterozygotes, and he was subsequently removed from the cage with female mice. When this mouse was reintroduced to females, he refused to mate. The third chimeric male has just been born, and will be mated upon sexual maturity. Any resultant progeny that contain the agouti coat colour will be tested for heterozygosity by performing Southern blot analysis using the 3.0 kb probe from above, and by doing PCR amplification of the *neo* cassette using conditions established using the targeted ES cells. Confirmed heterozygotes will be mated to produce *DDX1-/-* homozygotes.

3.7 Summary: Our *DDX1+/-* ES cells have thus far been unable to contribute to the germline

To date, our *DDX1+/-* targeted ES cells have not contributed to the germline. One potential reason for this is that our cells are no longer pluripotent. A number of tests could be performed on these cells to determine their status including: a karyotype analysis to ensure they contain the correct number of chromosomes with no obvious abnormalities, determination of alkaline phosphatase activity, and production of mice by tetraploid aggregation. The culturing of ES cells requires stringent culture conditions. Any slight deviations

Table 3.1 A chronological list of blastocyst injections done by Dr. Peter Dickey.

Date	Clone #	# Blasts injected[a]	Births	Chimeras[b]
10/1/00	24	30	5	1F
3/3/00	24		7	0
03/16/2000	24		5	0
03/28/2000	24		0	0
06/16/2000	61	30	5	1 XX ⟷ XY[c],1F
06/27/2000	61	20	0	0
07/27/2000	24	20	1	1F
8/8/00	24	16	1	1F
9/10/00	13	24	1	0
10/13/2000	26	22	2	0
10/25/2000	26	30	3	2F
11/1/01	24	23	0	0
01/29/2001	24	20	0	0
12/3/01	61			2M
04/X/2002	24	65	9	2F, 1M

[a] All four targeted ES cells were injected (13, 24, 26, 61).

[b] M= Male, F= Female

[c] indicates an XX ⟷ XY chimera.

such as the cells achieving too high a density can cause selection of variants with chromosomal abnormalities (Hogan *et al.*, 1994). These variants acquire the capacity for increased proliferation and simultaneously, a decreased ability to differentiate. Therefore if at any time during our ES culturing we unknowingly altered the growth conditions, we may have selected for a population with an abnormal chromosome content. Another test for stem cells is alkaline phosphatase activity (Pease *et al.*, 1990). Alkaline phosphatase is expressed in stem cells and then is lost as the cells differentiate. Measuring alkaline phosphatase activity involves fixing the cells and then soaking them in a solution containing α-naphthyl phosphate and Fast-Red (Hogan *et al.*, 1994). The method of tetraploid aggregation was developed by Nagy *et al.* (1990) and is based on the aggregation of ES cells with tetraploid embryos to create a chimeric mouse. The tetraploid embryos are developmentally compromised such that they will only contribute to extraembryonic membranes forcing the ES cells to develop into the entire embryo. The R1 cells have been shown to be totipotent at passage 14 by tetraploid aggregation (Nagy *et al.*, 1993); however, it would be interesting to test our targeted cell lines which are at a higher passage number. In addition to confirming totipotency, this method could be another means of generating our *DDX1* knockout mouse. Another reason for not seeing contribution to the germline is that not enough chimeras have been produced. Only 3 male chimeras have been generated to date with 2 litters produced from one of them. This number is too low to make any definite conclusions about pluripotency. Theoretically, it would be advantageous to produce more chimeras to fully test our 4 targeted R1 ES clones.

Although we have not yet been successful in generating our knockout mouse, our cloning strategy proved highly successful. Our recombination frequency of 1:44 is about average, although it is difficult to compare with other reported recombination frequencies, as there is great variation from ≥ 1:1000 to 1:3 (Mortensen,1993; Yamasaki *et al.*, 1996). Furthermore, the fact that we do observe a reduction in DDX1 protein implies that we have generated a null allele, although a lack of decrease in protein levels in our heterozygote would not necessarily indicate an improperly targeted allele. No smaller versions of DDX1 protein were observed using the anti-DDX1 2910 antibody suggesting that we did not generate a truncated protein.

The completion of this project will await the mating of our newest chimeric male mouse and then possible further blastocyst injections with our R1 *DDX1+/-* cells. If these cells do not prove competent to form the germline it may be necessary to retarget the *DDX1* allele in a different ES cell line, such as the NX1 cell line isolated from 129/J mice (Dower *et al.*, 2000). It is also possible to generate ES cells homozygous for the mutant *DDX1* allele, by culturing the heterozygous clones in increasing amounts of geneticin. However, we would have to replace our *neo* cassette, as the PGK promoter is strong enough to permit cell survival with a single copy of neo at the highest geneticin concentrations obtainable. There are versions of the *neo* cassette that contain point mutations in the promoter region, which decreases *neo* expression

(Mortensen, 1993). Therefore, substitution of our *neo* cassette with a mutant *neo* cassette should allow us to generate a *DDX1-/-* cell. These cells could be tested for their ability to differentiate along various lineages, and they could be used in biochemical assays (such as the cleavage and polyadenyation assay to be discussed in Chapter 4).

Chapter 4. Localization of DDX1 to Nuclear Foci that Correspond to Cleavage Bodies

Defining a biochemical function for DDX1 has proven to be difficult. To date, we have not found any cells that lack DDX1 expression. Additionally, experiments attempting to overexpress DDX1 in eukaryotic cell lines have been largely unsuccessful. Therefore, to begin characterizing DDX1, we decided to examine its subcellular distribution in a variety of cell lines, both normal and transformed. As both the cytoplasm and nucleus contain well-defined compartments, we reasoned that precisely localizing DDX1 to any given compartment could provide insight as to its biochemical function.

Our specific objectives at the start of this project were to:

a) define whether DDX1 existed mainly in the cytoplasm or the nucleus in a variety of cell types. These experiments involved fluorescence microscopy.

b) examine for any specific subcellular patterns that DDX1 may have and attempt to define these in relation to known subcellular structures. These experiments used a variety of fluorescence microscopy techniques.

c) determine if DDX1 localizes with nascent RNA. These experiments involved cell labeling with 5'-flurouridine (FU) in combination with confocal fluorescence microscopy.

d) examine DDX1 protein throughout the cell cycle to determine whether DDX1 levels fluctuate. These experiments involved both fluorescence microscopy and flow cytometric analysis in combination with Western blot analysis.

e) investigate the possibility that DDX1 affects transcription or pre-mRNA processing. These experiments were done using cells labeled for FU and as well cells infected with herpes simplex virus type 1 in combination with confocal fluorescence microscopy.

f) adapt or create an *in vitro* biochemical assay for DDX1 based on results obtained in objectives a and b.

4.1 Subcellular localization of DDX1

The subcellular distribution of DDX1 in HeLa cells was examined by indirect immunofluorescence using anti-DDX1 antiserum (2923). We observed predominant staining in the nucleus, although there was some signal in the cytoplasm as well (Fig. 4.1A). These results are in agreement with previous cellular fractionation experiments (Godbout *et al.*, 1998). In the nucleus, DDX1 was present in a granular/punctate pattern throughout most of the nucleoplasm, as well as in a few brightly-labeled discrete foci. DDX1 was generally depleted in the nucleolus. Simultaneous staining with DAPI precluded a general association with chromatin. Approximately 90% of HeLa cells contained at least one DDX1 focus and 70% of these foci were visible by digital interference contrast (DIC) (Fig. 4.1B). The number of foci in each cell varied from 0 – 15, with an average of 4.7, each ~0.5 μm in diameter. To ensure that DDX1 foci were not due to an artifact caused by cell fixation in paraformaldehyde, we also fixed cells using

Fig 4.1 Immunofluorescent labeling of DDX1.

HeLa cells were labeled using anti-DDX1 polyclonal antibody (2923). **A.** The general staining pattern of DDX1 and its distribution relative to chromatin (DAPI). DDX1 is widely expressed in the nucleus, where it is found in both foci and nucleoplasm. The DDX1 signal has a punctate appearance in both the nucleoplasm and cytoplasm. Nuclear foci are shown in red in the merged (DDX1 + DAPI) image. The cells were observed using a Zeiss Axioplan II microscope coupled to a CCD camera; the image collected was deconvolved using Softworks 2.5 software. **B.** DDX1 foci are often visible by DIC (indicated by the arrowhead). The image was collected using a Zeiss LSM 510 confocal laser scanning microscope. **C.** Anti-DDX1 antibody is specifically competed by purified DDX1. Either anti-DDX1 polyclonal antibody (2923) or anti-ALDH polyclonal antibody was incubated overnight with either 0 µg or 5 µg of nitrocellulose-bound purifed DDX1 protein. The unbound fraction was then used to indirectly label HeLa cells. The image was collected using a Zeiss Axioplan II microscope. The DDX1 signal is greatly reduced after antibody adsorption to 5 µg of DDX1 protein whereas the ALDH signal is unaffected. The bar represents 5 µm.

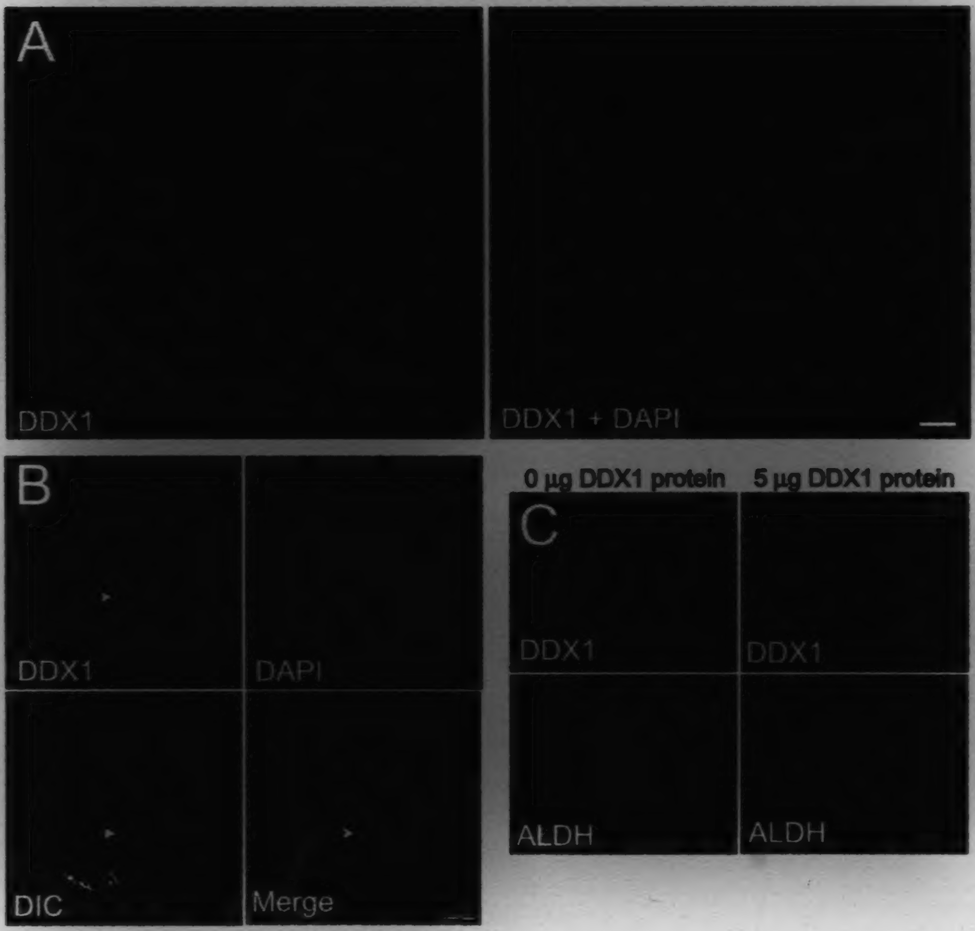
A
DDX1
DDX1 + DAPI
B
DDX1
DAPI
DIC
Merge
0 µg DDX1 protein
5 µg DDX1 protein
C
DDX1
DDX1
ALDH
ALDH

methanol/acetone. DDX1 foci were observed regardless of the fixative used. Labeling with pre-immune serum generated a very slight non-specific signal, and did not label discrete nuclear foci (data not shown).

To verify that anti-DDX1 antiserum specifically recognized DDX1, we carried out competition experiments with bacterially-expressed DDX1 protein as described in Materials and Methods. This method is similar to one used by Almeida *et al.* (1998). As shown in Fig. 4.1C, the DDX1 signal was specifically reduced with 5 μg of DDX1 protein. No alteration in signal intensity was obtained with anti-aldehyde dehydrogenase (ALDH) antibody in the presence of DDX1 protein. Antibody specificity was further documented using anti-DDX1 antibody that had been affinity-purified using a DDX1-sepharose column. Western blot analysis demonstrated that the affinity-purified antibody recognized a predominant band at 90 kDa representing the main form of DDX1 (data not shown). Immunofluorescent staining with purified anti-DDX1 antibody gave a pattern indistinguishable from that of the non-purified antiserum.

We examined 15 cell lines or cultures, including normal and transformed cells from different species, to determine the prevalence of nuclear DDX1 foci. Ten cell lines contained discrete nuclear DDX1 foci, including HeLa, GM38, 293, T24, NIH 3T3, RB778, MRC5, SKN, COS-7 and RB522A (which overexpresses DDX1 as the result of having amplified copies of the gene). Five cell lines contained DDX1 protein but no discrete foci, including Indian muntjac fibroblasts, C3H 10T1/2, HISM, RB(E)-2 and RB893. The presence of DDX1 foci in the normal lung fibroblast culture GM38 indicates that these foci are not restricted to transformed cells. These results suggest that DDX1 foci are nuclear bodies commonly found in a wide variety of cells.

4.2 DDX1 foci are adjacent to PML and Cajal bodies

A number of nuclear bodies have been identified to date. Among the best defined are the splicing factor compartment (SFC), the PML oncogenic domain, and the Cajal body (CB). Within the eukaryotic nucleus, the SC-35 antibody recognizes about 20 – 50 speckles that contain splicing factors, hyperphosphorylated RNA polymerase II, and several polyadenylation factors (Fu and Maniatis, 1990; Schul *et al.*, 1998a). Double labeling with SC-35 and DDX1 antibodies demonstrated that DDX1 foci are not components of splicing factor compartments (Fig. 4.2A).

PML bodies are spherical structures 0.2 to 1.0 μm in diameter that are present in about 10 – 30 copies per cell (Ruggero *et al.*, 2000). Based on the growing list of proteins that localize to PML bodies, a variety of roles have been proposed for these structures, including gene regulation, viral defense, apoptosis, cellular senescence, telomere maintenance, and storage depots (see introduction). CBs are spherical structures of ~0.5 μm in diameter which are often located next to PML bodies (Lamond and Carmo-Fonseca, 1993). The number of CBs, although quite variable, is usually 1-5 per cell (Lamond and Carmo-Fonseca, 1993). Visualization of CBs by immunofluorescence is achieved using one of two antibodies: anti-Sm or anti-p80 coilin. The Sm antibody recognizes snRNPs, which localize to splicing factor compartments and

Fig. 4.2. The subnuclear localization of DDX1 with respect to other nuclear bodies.

HeLa cells were labeled using anti-DDX1 antibody (2923) and either **A** anti-SC-35, **B** anti-PML, **C** anti-Sm, **D** anti-Sam68, or **E** anti-CstF-64 antibodies. Adjacent localization of a DDX1 focus and PML body is indicated by the arrowhead in **B** - merged image. Adjacent localization of DDX1 foci and Cajal bodies are indicated by the arrowheads in **C** - merged image. All three DDX1 foci colocalize with cleavage bodies in **E** - merged image. The images were collected using a Zeiss LSM 510 confocal laser scanning microscope. The bar represents 5 μm.

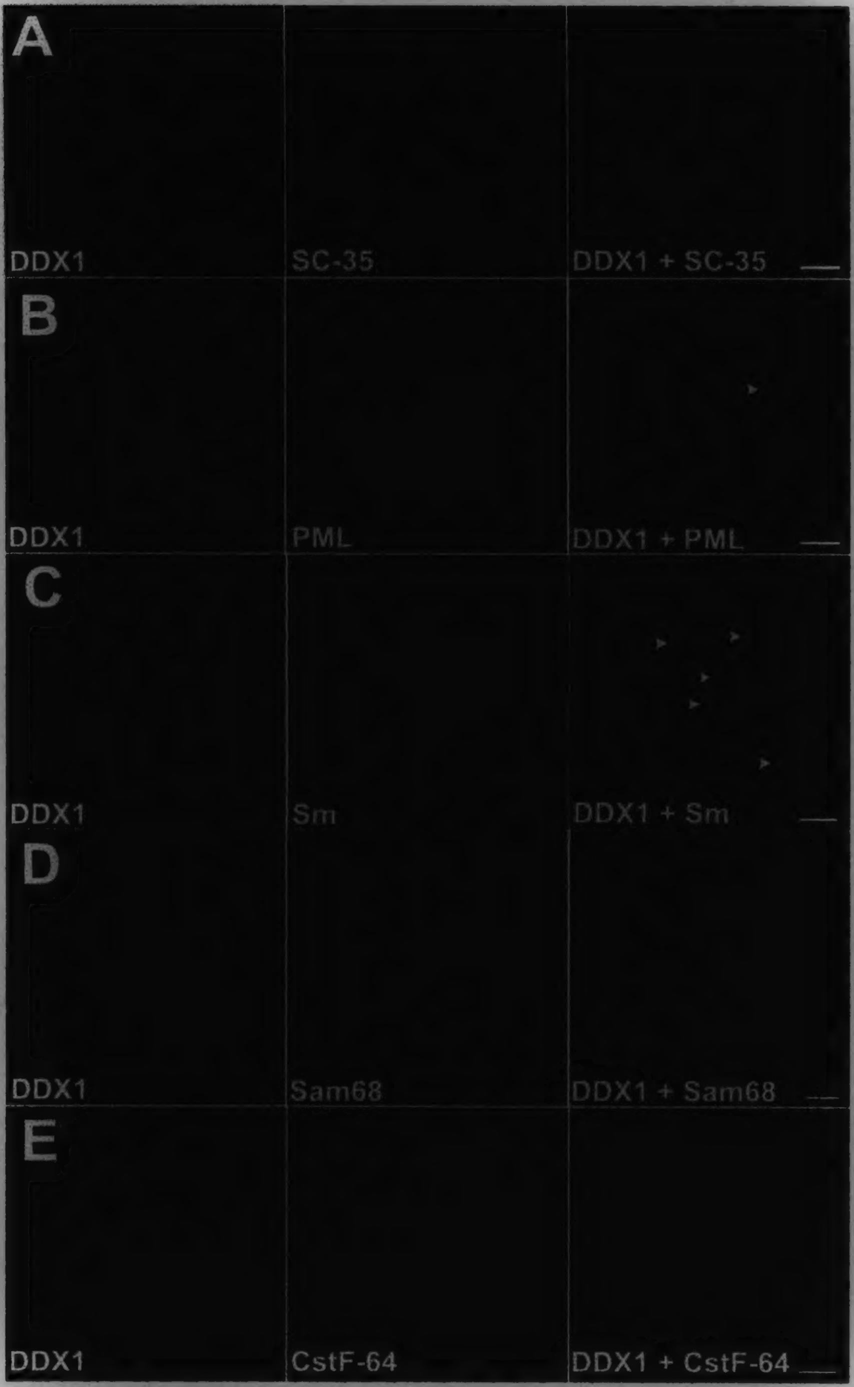
A
DDX1
SC-35
DDX1 + SC-35
B
DDX1
PML
DDX1 + PML
C
DDX1
Sm
DDX1 + Sm
D
DDX1
Sam68
DDX1 + Sam68
E
DDX1
CstF-64
DDX1 + CstF-64

to CBs (Lerner *et al.*, 1981). p80 coilin is a protein first identified using sera from patients with autoimmune diseases (Andrade *et al.*, 1991). Anti-p80 coilin antibodies strongly stain CBs, although they also show a weak diffuse nucleoplasmic signal. The function of p80 coilin is largely unknown; however, recent reports indicate that this protein is essential for both snRNP and SMN recruitment to CBs (Hebert *et al.*, 2001). In addition to p80 coilin and snRNPs, CBs contain many components required for the transcription and processing of pol I, pol II, and pol III RNAs and have been hypothesized to function as transcriptosome assembly sites (Gall, 2000).

We investigated whether there was a relationship between DDX1 foci and PML bodies. HeLa cells were co-stained with a mouse monoclonal antibody to the PML protein and anti-DDX1 antibody. Nuclear foci were observed with both these antibodies with an average of 12.8 PML bodies and 4.8 DDX1 foci per cell (Fig. 4.2B; Table 4.1). The image stacks were three-dimensionally reconstructed to reveal the subnuclear distribution of the two foci. As shown in Fig. 4.2B, DDX1 foci do not colocalize with PML bodies; however, 18% of foci were found next to PML bodies (Table 4.1). The three-dimensional distance between the DDX1 foci and PML bodies located adjacent to each other ranged from 0.35 to 0.6 μm.

Using a method published by Grande *et al.* (1996) (described in the Materials and Methods), we determined the likelihood that nuclear bodies would randomly colocalize with DDX1 foci. This calculation makes two gross assumptions: that the nucleus is an essentially devoid space that will allow free mobility of nuclear bodies, and that the nucleus is a perfect sphere. Therefore,

Table 4.1 Nuclear localization of PML, Cajal, and Cleavage Bodies with respect to DDX1 foci

Nuclear Body (NB)	avg # of NBs per cell[a]	avg # of DDX1 foci per cell	% of DDX1 foci coloc with NBs [b]	% of DDX1 foci partially coloc with NBs[c]	% of DDX1 foci adjacent to NBs [d]
PML	12.8 (30)	4.8	0.0 (0.0)	0.0 (0.0)	18.0 (6.7)
Cajal bodies	3.0 (65)	4.4	1.1 (1.6)	4.6 (6.8)	27.9 (41.0)
Cleavage bodies	4.6 (50)	4.9	65.0 (70.0)	0.0 (0.0)	1.2 (1.3)

[a] Parenthesis indicates number of cells analyzed.

[b] Parenthesis indicates percentage of NBs colocalizing with DDX1 foci.

[c] Parenthesis indicates percentage of NBs partially colocalizing with DDX1 foci.

[d] Parenthesis indicates percentage of NBs adjacent to DDX1 foci.

the equation derived by Grande produces only a crude estimate of the probability that protein structures pair. Regardless, based on our calculations, the probability of a randomly positioned PML body pairing with a randomly positioned DDX1 focus is 1 event in 40 nuclei. We observed pairing in 15 out of 30 nuclei, indicating that even as a crude estimate there is likely a relationship between a fraction of DDX1 foci and PML bodies.

Next, we studied the subnuclear distribution of DDX1 foci in relation to CBs. HeLa cells were double-labeled with anti-DDX1 antibody and mouse monoclonal anti-Sm. In these experiments, there was an average of 3.0 CBs and 4.4 DDX1 foci per cell. Although only 1% of DDX1 foci colocalized with CBs, 4.6% of DDX1 foci partially overlapped with CBs and 28% of DDX1 foci were adjacent to them (Fig. 4.2C; Table 4.1). Three-dimensional distances ranged from 0.2 μm for partially overlapping structures to 0.4 μm for structures that appeared adjacent. If the distribution of these two nuclear bodies is random, we would expect adjacent localization in 1 in 500 nuclei. The observed adjacent localization in 40 out of 64 nuclei indicates a nonrandom relationship between DDX1 foci and CBs.

There was significant variation in the number of nuclear bodies observed from cell-to-cell. We therefore tested whether there was an overall correlation between the number of DDX1 foci and the number of either PML bodies or CBs in any one cell. Linear regression analysis indicated positive correlation between the number of DDX1 foci and the number of PML bodies ($p=0.012$) and CBs ($p=0.027$). Previous studies have shown that fluctuations in PML body number occur during the cell cycle, with the highest number of PML bodies present during the G1-S phase transition (Koken *et al.*, 1995; Terris *et al.*, 1995). The general correlation between the number of DDX1 foci, PML bodies and CBs may therefore reflect similar cell cycle variations.

4.3 DDX1 foci associate with cleavage bodies

Other structures that have been found to localize adjacent to CBs include SNBs and cleavage bodies. SNBs contain Sam68, an RNA-binding protein (Wong *et al.*, 1992), as well as SLM-1 and SLM-2, both of which are nuclear proteins that heterodimerize with Sam68 (Chen *et al.*, 1999; Di Fruscio *et al.*, 1999). Cleavage bodies contain the proteins CstF-64 and CPSF 100 kDa, both of which are involved in mRNA 3' cleavage and polyadenylation (Schul *et al.*, 1996), as well as the transcription factors TFIIH, TFIIE and TFIIF (Schul *et al.*, 1998; Gall, 2000).

We co-stained HeLa cells with purified anti-DDX1 antibody and mouse monoclonal antibody to either Sam68 or CstF-64. DDX1 foci were never found to colocalize with SNBs (Fig. 4.2D). Although HeLa cells were previously reported to contain elevated areas of CstF-64 staining rather than distinct cleavage bodies (Schul *et al.*, 1996), we found that 90% of our HeLa cells had distinct cleavage bodies. When 50 cells, double-labeled with anti-CstF-64 and anti-DDX1 antibodies, were examined, 65% of DDX1 foci colocalized with cleavage bodies and 1.2% showed adjacent localization (Fig. 4.2E). There was an average of 4.6 cleavage bodies and 4.9 DDX1 foci per cell (Table 4.1). Overall, 89% of cells that contained distinct DDX1 and CstF-64 foci appeared to have some foci that colocalized. These measurements only take into account distinct CstF-64 foci that colocalize with DDX1 foci. In cells with no distinct cleavage bodies, most DDX1 foci appeared to contain some CstF-64 protein. The distance between the three-dimensional CstF-64 and DDX1 foci was calculated to be 0.0 μm, strongly suggesting that DDX1 is found in the same structure as CstF-64. The localization of DDX1 to cleavage bodies was confirmed in a non-transformed cell line GM38 suggesting that this phenomenon is not restricted to transformed cells (Fig. 4.3). The colocalization of DDX1 foci and cleavage bodies was also confirmed in a number of other cell lines including 293 (transformed human kidney cells), T24 bladder carcinoma cells, HISM (human intestinal smooth muscle) cells, SKN cells and COS-7 cells (data not shown).

Cleavage bodies have been reported to associate with CBs in a cell cycle-dependent manner in the T24 bladder carcinoma cell line; colocalization with CBs was predominantly observed in G1-phase cells whereas cells in S phase displayed mostly adjacent localization (Schul *et al.*, 1999b). In the colon carcinoma line CaCo, cleavage bodies were found to colocalize with a CB in only 1-5% of nuclei (Schul *et al.*, 1996). In agreement with the latter, we observed 1 HeLa cell out of 20 that showed colocalization of CstF-64 with CBs (this cell had 3 colocalizing foci). However, these 3 CBs were weakly labeled compared to other CBs in the same cell. Overall, 45.0% of CstF-64 cleavage bodies were found adjacent to CBs, implying some spatial and/or functional relationship

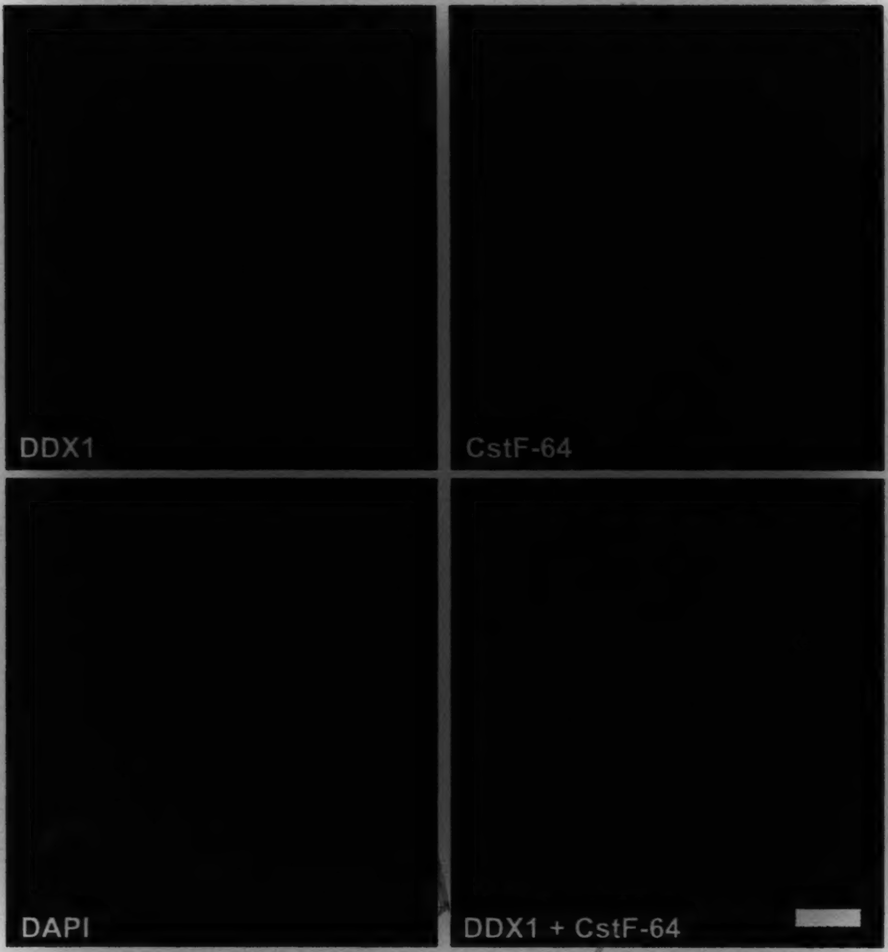

Fig. 4.3 DDX1 foci colocalize with cleavage bodies in non-transformed GM38 cells.

GM38 cells were fixed, permeablized and indirectly labeled with anti-CstF-64 and anti-DDX1 antibodies. Cells were visualized using a Zeiss 510 confocal microscope. The bar represents 5 µm.

(Table 4.2). Based on our results in HeLa cells, cleavage bodies appear to represent a subnuclear domain distinct from CBs.

To further analyze the relationship between cleavage bodies, DDX1 foci and CBs, 10 cells from two additional cell lines were analyzed, SKN and COS-7. The results in Table 4.2 summarize our observations. In SKN cells, labeling with anti-CstF-64 antibody reveals that 64.3% of foci colocalize with CBs and 41.0% of foci colocalize with DDX1. This suggests that CstF-64 shuttles between CBs and DDX1 foci. Examination of COS-7 cells reveals that 19.0% of CstF-64 foci colocalize with CBs, while 55.0% colocalize with DDX1 foci. Therefore, unlike the observations in SKN cells, CstF-64 foci do exist independent of DDX1 foci and CBs in COS-7 cells. Compared to HeLa cells, both COS-7 and SKN cells appear to have a lower percentage of CstF-64 foci that colocalize with DDX1 foci; however, it will be necessary to examine more cells to conclusively prove such a difference exists between these cell lines. Regardless preliminary evidence suggests that although DDX1 frequently resides within CstF-64 labeled cleavage bodies, the proteins can localize to distinct structures.

4.4 Immunoprecipitation of DDX1 and CstF-64

Co-immunoprecipitations were carried out to determine whether DDX1 and CstF-64 are located within the same complex. Using anti-DDX1 antibody (2910), we were able to immunoprecipitate approximately 5-8% of input DDX1 from both HeLa cells and RB522A cells (Fig. 4.4 - top panel, compare IP and S in the last four lanes). Considerably lower levels of DDX1 were immunoprecipitated

Table 4.2 Localization of Cajal bodies (CBs), cleavage bodies (CstF-64), and DDX1 foci in three cell lines: HeLa, SKN, and COS-7.

HeLa cells

	CBs 3.5[c]	CstF-64 4.4[c]	DDX1 4.6[c]
CBs	100[a]	3.9	1.1
CstF-64	2.8	100	65
DDX1 foci	1.6	70	100
CBs	100[b]	45	27.9
CstF-64	33	100	1.2
DDX1 foci	41	1.3	100

SKN cells

	CBs 1.5[c]	CstF-64 1.3[c]	DDX1 1.9[c]
CBs	100[a]	64.3	2.3
CstF-64	64.3	100	23
DDX1 foci	3.8	41	100
CBs	100[b]	0	11.6
CstF-64	0	100	5.7
DDX1 foci	18	10.3	100

COS-7 cells

	CBs 2.3[c]	CstF-64 2.6[c]	DDX1 3.7[c]
CBs	100[a]	19	3.7
CstF-64	25	100	27
DDX1 foci	8.3	55	100
CBs	100[b]	0	7.4
CstF-64	0	100	0
DDX1 foci	16.6	0	100

[a] The percentage of nuclear bodies indicated in the top row that colocalize with the nuclear body on the side column.

[b] The percentage of nuclear bodies indicated in the top row that is adjacent to the nuclear body on the side column.

[c] The average number of nuclear bodies per cell.

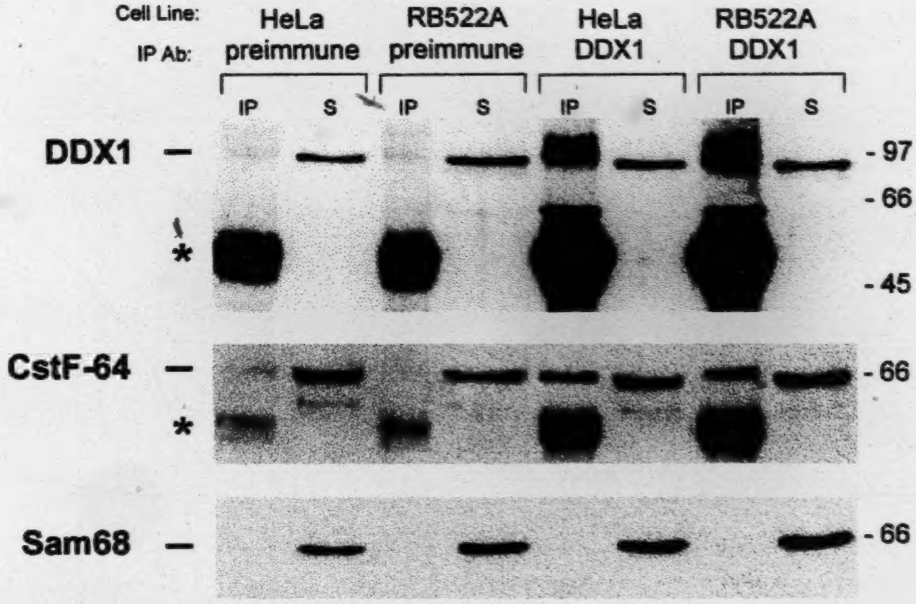
Cell Line:
IP Ab:
HeLa preimmune
RB522A preimmune
HeLa DDX1
RB522A DDX1
IP
S
IP
S
IP
S
IP
S
DDX1
*
CstF-64
*
Sam68
- 97
- 66
- 45
- 66
- 66

Fig. 4.4 Co-immunoprecipitation of DDX1 and CstF-64.

Nuclear extracts from HeLa cells and RB522A cells (100 µg) were pre-cleared and incubated with 3 µl of either pre-immune serum or anti-DDX1 antibody (2910). Complexes were precipitated with protein A-agarose beads and electrophoresed on an 8% SDS-polyacrylamide gel. Proteins were transferred to nitrocellulose and detected using anti-DDX1 antibody (top panel), anti-CstF-64 antibody (middle panel), and anti-Sam68 antibody (bottom panel). For comparison, we have loaded 2.5% of the supernatent (S) from each immunoprecipitation reaction next to the immunoprecipitation (IP) lanes. IgG molecules are indicated by the asterisks. Size markers (in kDa) are indicated on the right.

with pre-immune serum (lanes 1-4). A similar pattern was observed using anti-CstF-64 antibody, with >10-fold more CstF-64 co-immunoprecipitated with anti-DDX1 antibody than with pre-immune serum (Fig. 4.4, middle, compare lanes 1 and 3 with 5 and 7). The portion of CstF-64 that co-immunoprecipitated with DDX1 was relatively small, suggesting either a weak interaction between the two proteins or an association limited to a subset of DDX1 and CstF-64 proteins. To ensure that co-immunoprecipitation of CstF-64 with DDX1 was the result of a specific interaction, the filter was immunostained with an antibody to the RNA binding protein, Sam68. As previously shown (Fig. 4.2D), Sam68-containing nuclear bodies were never found to colocalize with DDX1 foci. Although Sam68 was abundant in both HeLa and RB522A nuclear extracts, there was no detectable Sam68 in any of the immunoprecipitation lanes (Fig. 4.4 bottom).

4.5 Close proximity of DDX1 and CstF-64 as determined by fluorescence resonance energy transfer

Fluorescence resonance energy transfer (FRET) is a technique that detects the radiationless transfer of energy from a fluorescent donor to an acceptor fluorophore. In order for energy transfer to occur, the two fluorophores must exist within the Förster radius (in practice this is <10 nm) and their dipoles aligned in a specific orientation. Additionally, the donor and acceptor fluorophores must have overlapping emission and excitation spectra, respectively, yet the emission spectrum from each must be reasonably separated to allow for their measurement. The FRET technique achieves a resolution that is approximately 25 times greater than that obtained by confocal imaging alone. To determine if the CstF-64 and DDX1 proteins reside in close proximity within cleavage bodies, we analysed the transfer of energy from CstF-64 labeled with Alexa 488 to DDX1 labeled with Cy3 using the three-filter set technique (Fig 4.5) (Youvan *et al.*, 1997; Schmid *et al.*, 2001). In Fig. 4.6, column 1 depicts donor fluorescence collected using a 505-550 nm filter. Column 2 represents acceptor fluorophore emission at 560 nm (except for Fig. 4.6D which contains both the acceptor and donor images). The final FRET image, displayed in column 3, is calculated from the FRET emission at 560 nm minus the contributions from both the donor and acceptor fluorophores (see Materials and Methods). In Fig. 4.6A, the FRET signal is detected in cleavage bodies and to some extent in the nucleoplasm. The photodestruction of Cy3 acceptor molecules efficiently quenches the FRET signal (Fig. 4.6B). To ensure that FRET was indeed occurring within cleavage bodies, a cell was found which contained a DDX1 focus that was not paired with a cleavage body. In this instance, we observed no FRET at the focus site (see arrowhead in Fig. 4.6C). Therefore, CstF-64 may be entirely excluded from some DDX1 foci.

As a negative control for FRET, we replaced the donor anti-CstF-64 antibody with anti-PML antibody. As indicated previously, 18% of DDX1 foci are found adjacent to PML bodies. There was little FRET between DDX1 and PML (2-3 pixels), implying that most of the labeled PML protein is situated at a distance greater than 10 nm from labeled DDX1 (Fig. 4.6D). To further validate the FRET technique, we labeled cells with anti-p80 coilin and anti-Sm antibodies.

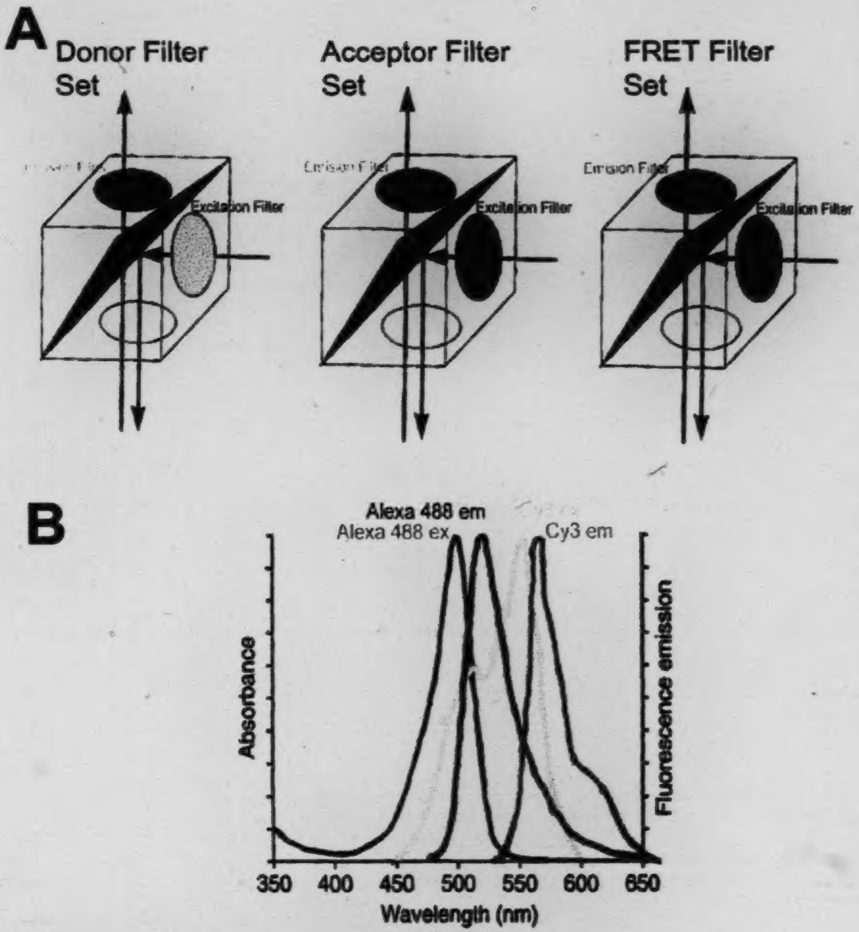
A
Donor Filter Set
Emission Filter
Excitation Filter
Acceptor Filter Set
Emission Filter
Excitation Filter
FRET Filter Set
Emission Filter
Excitation Filter
B
Alexa 488 em
Alexa 488 ex
Cy3 em
Absorbance
Fluorescence emission
350
400
450
500
550
600
650
Wavelength (nm)

Fig. 4.5 The three filter sets used to measure FRET and the fluorescence spectra for Cy3 and Alexa 488.

A. The FRET technique employed uses a three-filter set method as described in Material and Methods. The three filters are arranged as shown in the diagram. **B.** The excitation and emission spectrum for Cy3 and Alexa 488 fluorophores. The emission spectrum of Cy3 sufficiently overlaps the Alexa 488 excitiation spectrum such that FRET may occur between the two dye pairs. Additionally, the emission spectrum of each fluorophore is distinct enough to permit measurement.

Fig. 4.6 DDX1 and CstF-64 undergo FRET in HeLa cells.

HeLa cells were indirectly labeled with anti-DDX1 antibody (2923) and either anti-CstF-64 (**A** – **C**) or anti-PML (**D**) antibody. The images were collected using the three-filter set method as described in Materials and Methods. The first column represents the image obtained with the donor filters. The image in the second column was collected using the acceptor filters (except **D**, which represents the combined acceptor and donor signals). The third column represents the final FRET image processed to remove non-FRET components (as described in Materials and Methods). **A.** FRET was observed between CstF-64 and DDX1 in both the nucleoplasm and cleavage bodies. **B.** After photodestruction of the acceptor molecule, FRET no longer occurred (boxed region). **C.** Areas lacking CstF-64 foci (arrowhead) often did not demonstrate FRET. **D.** Another subnuclear body, PML, demonstrated little FRET with DDX1. The arrow indicates the location of adjacent PML and DDX1 foci. **E.** FRET was observed between two components of Cajal bodies, p80 coilin and Sm proteins. The bar represents 5 μm.

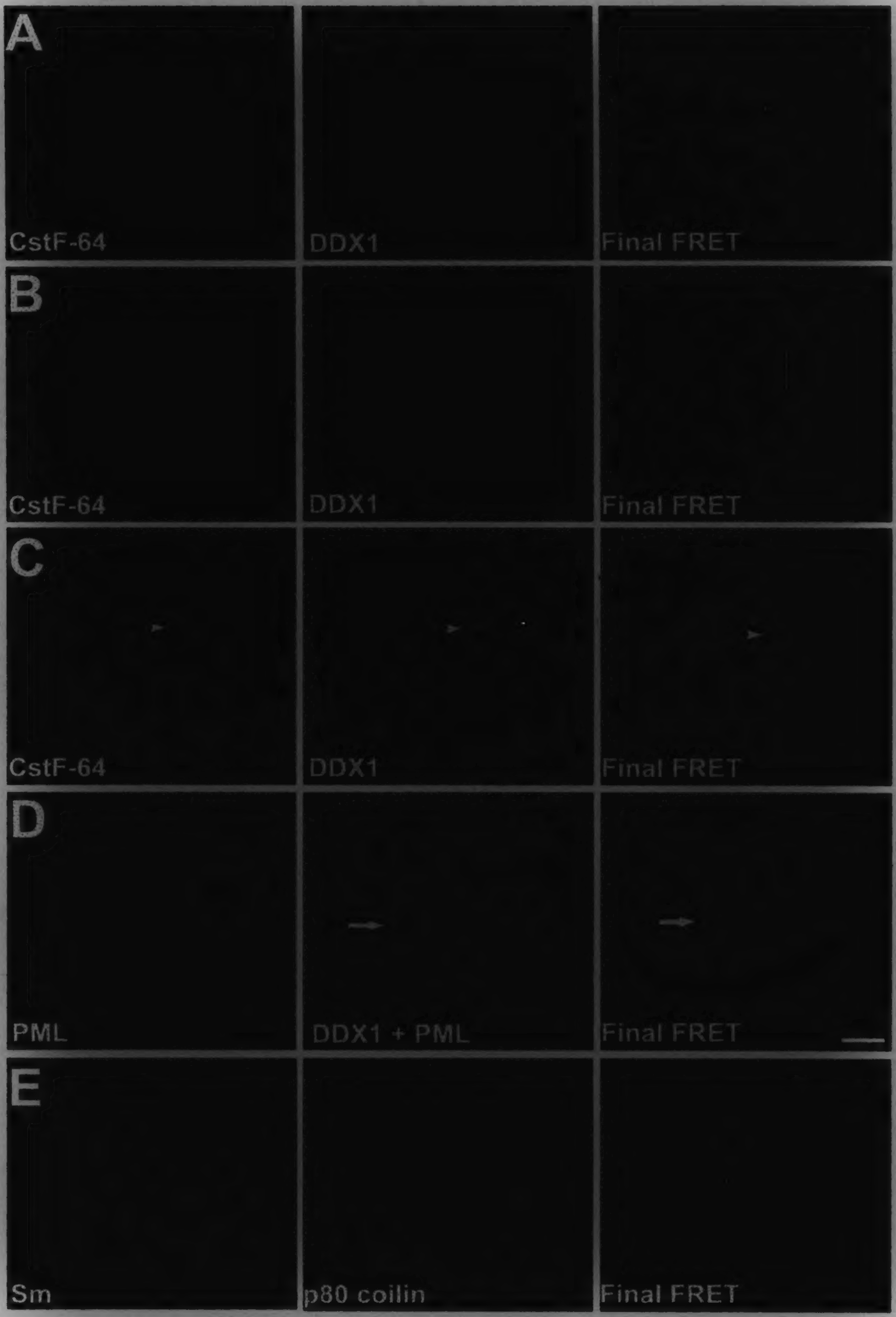
A
CstF-64
DDX1
Final FRET
B
CstF-64
DDX1
Final FRET
C
CstF-64
DDX1
Final FRET
D
PML
DDX1 + PML
Final FRET
E
Sm
p80 coilin
Final FRET

These antibodies recognize proteins that both localize within CBs. As shown in Fig. 4.6E, FRET was observed between labeled p80-coilin and Sm proteins.

It is important to note that because we did our analysis with cells labeled with both primary and secondary antibodies, the distance between the structures may be greater than the (Förster) 10 nm distance. Nevertheless, these experiments represent a considerable improvement over traditional confocal microscopy resolution and suggest that DDX1 resides in close proximity to CstF-64 within cleavage bodies and within the nucleoplasm.

To enhance our qualitative depiction of FRET between labeled CstF-64 and labeled DDX1, we attempted to quantitatively determine FRET using a method published by Gordon *et al*. (1998). This method quantitates corrected FRET, F^C, by subtracting donor and acceptor contributions from the measured FRET intensity. Subsequently, FRET can be 'normalized' by adjusting for the concentrations of the donor and the acceptor ($F^CN = F^C$ / donor conc. • acceptor conc.). The results of the quantitative FRET calculations are presented in Table 4.3. Examination of the F^C number indicates that we have substantial FRET occurring within the CstF-64 and DDX1 labeled cells, but little FRET within the cells labeled with antibodies to DDX1 and PML. Calculating normalized FRET (F^CN) generated numbers that were highly variable and depended entirely on the area chosen for analysis. For example, if we chose an area consisting of 15 pixels (about the same size as the foci), the numbers were 7.98×10^{-5} for CstF-64/DDX1 and 3.04×10^{-5} for PML/DDX1 (Table 4.3). However, selecting a larger area, 30 pixels, resulted in a F^CN for CstF-64/DDX1 of 3.34×10^{-5} and a F^CN for

Table 4.3 Quantitative FRET calculations.

interacting proteins [c]	F^C	F^CN [a]	F^CN [b]
avg.	33.8	5.78E-04	
S.D.	14.1	2.62E-04	
noninteracting proteins [c]			
avg.	2.2	6.39E-05	
S.D.	1.67	3.90E-05	
CstF-64 & DDX1			
avg.	274.6	7.98E-05	3.34E-05
S.D.	84	1.85E-05	1.68E-05
PML & DDX1			
avg.	16.8	3.04E-05	4.09E-05
S.D.	11	2.77E-05	2.99E-05

[a] The CstF-64 & DDX1 and PML & DDX1 data sets are intensity measurements from an area of 15 pixels.

[b] The CstF-64 & DDX1 and PML & DDX1 data sets are intensity measurements from an area of 30 pixels.

[c] These data were obtained from calculations reported by Gordon *et al*., 1998.

S.D., standard deviation

PML/DDX1 of 4.09 X 10^{-5}. Thus, labeled PML/DDX1 cells appear to have more FRET than cells labeled for CstF-64/DDX1. The reason for this is that selecting a larger area for the CstF-64/DDX1 calculation results in a large decrease in FRET intensity, yet only a moderate decrease occurs in the fluorophore intensity (concentration) as both antigens are present in substantial amounts outside of the foci. Selection of a larger area for the PML/DDX1 labeled cells results in virtually no change to the FRET intensity (there was little to begin with); however, the concentration of the fluorophore on the PML antigen decreases greatly because PML is not abundant within the nucleoplasm. Therefore, the PML/DDX1 $F^{C}N$ number artificially increases while the CstF-64/DDX1 number decreases giving the appearance of greater FRET occurring between PML and DDX1. Thus, the quantitative method can produce erroneous results depending on the area chosen for examination. The qualitative method used above is a more reliable indicator of FRET as it employs a pixel-by-pixel analysis.

4.6 DDX1 foci do not accumulate nascent RNA

Previous studies in T24 bladder carcinoma cells have shown that approximately 20% of cleavage bodies contain newly synthesized RNA. In addition, it is known that 18% of cleavage bodies do not colocalize with CBs in these cells (Schul *et al.*, 1996). Since CBs do not contain nascent RNA (Moreno Diaz de la Espina *et al.*, 1982; Raska, 1995; Schul *et al.*, 1996), Schul *et al.* (1996) have postulated that all cleavage bodies not associated with CBs contain newly synthesized RNA. To determine whether cleavage bodies containing

DDX1 have newly synthesized RNA, we examined DDX1 foci for the presence of nascent RNA by 5'-fluorouridine (FU) incorporation into HeLa cells. Cells were exposed to FU for 15 min prior to fixation and analysed by double-labeling with anti-DDX1 antibody and anti-bromodeoxyuridine (BrdU) antibody which recognizes FU (Boisvert *et al.*, 2000). The nuclear distribution of DDX1 and FU is shown in Fig. 4.7A. Although both FU and DDX1 are abundant throughout the nucleus, there does not appear to be any FU within DDX1 foci (see arrowhead in Fig. 4.7A). To quantitate the intensity of the FU within the focus, an axis was drawn through a DDX1 focus (indicated by the arrow in Fig. 4.7A) and the signal intensities were plotted (shown in Fig. 4.7B). There is an inverse relationship between intensity of the DDX1 signal and intensity of the FU signal, indicating that DDX1 foci do not accumulate nascent RNA. Three-dimensional analyses of 25 HeLa nuclei clearly demonstrate that DDX1 foci are not sites of active RNA transcription.

It is possible that DDX1 foci can accumulate various RNA species (ie. snRNA) or RNA at various stages of maturation. Therefore, we embedded cells labeled with anti-DDX1 antibody for examination by electron spectroscopic imaging. This is an electron microscopy technique, which can map the distribution of elements within a structure. For example the detection of nitrogen within a structure would indicate the presence of protein while the detection of phosphorus would indicate the presence of nucleic acid. The embedded cells are currently being investigated in collaboration with Dr. Michael Hendzel (University of Alberta, Edmonton, Alberta).

Fig. 4.7 DDX1 foci do not accumulate nascent RNA.

A. HeLa cells were incubated with FU for 15 min and stained with anti-DDX1 antibody (2923) and anti-bromodeoxyuridine antibody (FU). The arrowhead indicates a DDX1 focus. **B.** The staining intensities of the region through a DDX1 foci (highlighted by the arrow in the bottom left panel) were profiled using the Zeiss LSM 510 image software. The green line represents FU intensity while the red line represents DDX1 intensity. The bar represents 5 μm.

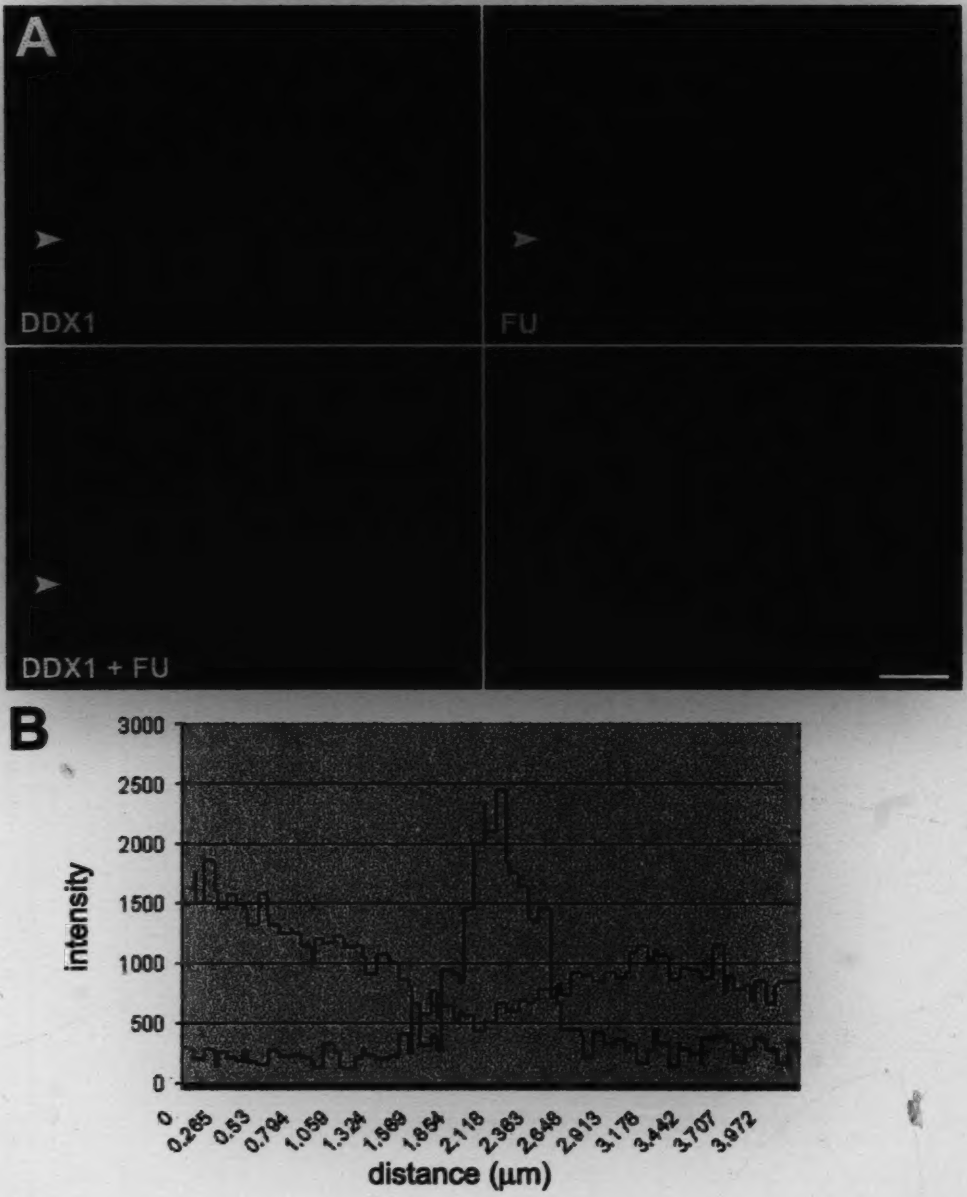
A
DDX1
FU
DDX1 + FU
B
3000
2500
2000
1500
1000
500
0
intensity
0
0.265
0.53
0.794
1.059
1.324
1.589
1.854
2.118
2.383
2.648
2.913
3.178
3.442
3.707
3.972
distance (µm)

4.7 DDX1 during the cell cycle

Previous publications indicate that cleavage bodies do not persist during mitosis in the T24 bladder carcinoma cell line (Schul *et al.*, 1996; Schul *et al.*, 1999b). To investigate whether DDX1 foci follow the same pattern as cleavage bodies, HeLa cells were immunostained with anti-DDX1 antibody and the chromatin stained with DAPI. Stage of the cell cycle was determined by chromatin and cellular morphology. The majority of cells in prophase contained distinct DDX1 foci; however, the foci disappeared at metaphase (Fig. 4.8A-C). Cleavage bodies, as stained by anti-CstF-64, disappeared in late prophase, slightly earlier than DDX1 foci (Fig. 4.8A and B). DDX1 foci reappeared during telophase/early G1, concomitant with cytokinesis (data not shown). Cells in the G1 phase of the cell cycle (as detected by the presence of a midbody) usually contained at least one DDX1 focus, whereas cleavage bodies were not observed (Fig. 4.8D). In contrast to DDX1 levels, which remained constant throughout mitosis, the overall CstF-64 signal was reduced during metaphase and anaphase (Fig. 4.8C – compare the fluorescent intensities of the mitotic cell with the intensities of the surrounding cells).

Further verification that DDX1 levels remained constant during the cell cycle was achieved by synchronizing two retinoblastoma suspension cell lines, RB522A and Y79 with aphidicolin and nocodazole. After various time points, samples of the synchronized cells were stained with propidium iodide and checked by flow cytometric analysis to determine DNA content. The remaining cells were frozen for cell fractionation and Western blot analysis. The results of

Fig. 4.8 Disappearance of DDX1 and CstF-64 foci during mitosis.

HeLa cells were labeled with anti-DDX1 antibody (2923) and anti-CstF-64 antibody. The cells were mounted with DAPI to visualize the chromatin morphology. **A.** Both DDX1 and CstF-64 foci are present during early prophase (indicated by the arrowheads). **B.** Only DDX1 foci are present by late prophase (arrowheads). **C.** Neither DDX1 nor CstF-64 foci can be detected during metaphase. **D.** DDX1 foci reappear during G1 (arrowheads); however, CstF-64 foci are not observed. While the overall DDX1 signal remains constant throughout mitosis, there is a decrease in CstF-64 signal. For example, compare the metaphase cell with adjacent cells in **C**. The bar represents 5 μm.

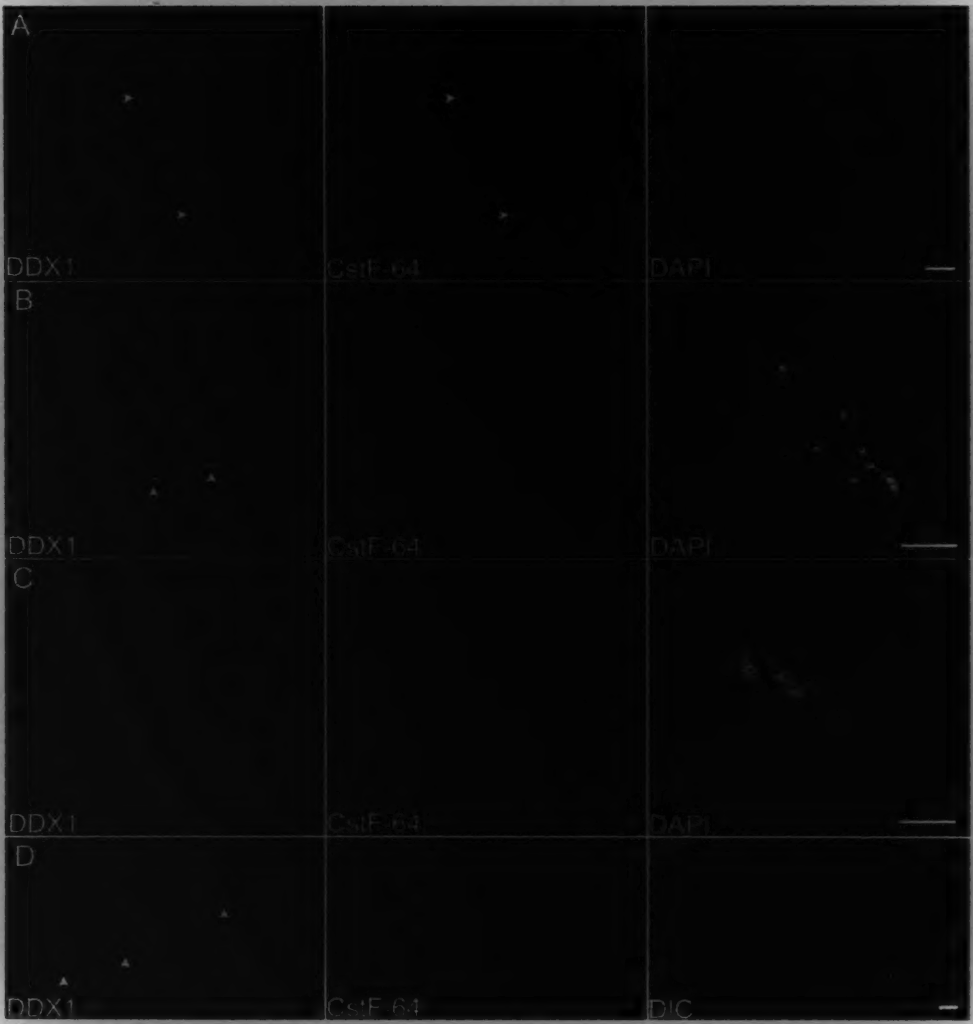
A
DDX1
CstF-64
DAPI
B
DDX1
CstF-64
DAPI
C
DDX1
CstF-64
DAPI
D
DDX1
CstF-64
DIC

the flow cytometric analysis of RB522A at the various time points is shown in Fig. 4.9. In each analysis the population of cells was gated to remove cellular debris and to remove cells which had >2n DNA (such as cellular aggregates) (Fig. 4.9A); the portion of cells included in each analysis represented ~75% of the total signal detected. Prior to synchronization (Fig. 4.9B), ~64% of the cells were in G1 phase, 22% were in S phase, and 14% were in G2/M phase of the cell cycle. Following aphidicolin treatment, 74% of the cells were in G1 phase (Fig. 4.9C). Samples taken 3 hours after aphidicolin release had 50% of cells in S phase (Fig. 4.9D). Five hours after aphidicolin release, cells were incubated in nocodazole. Flow cytometric analysis of cells at this 5 hour time point revealed that 26% of cells were in G2/M phase and 44% still remained in S phase indicating that we had appropriately timed our nocodazole treatment (Fig. 4.9E). Subsequent to a 6 hour incubation in nocodazole, flow cytometric analysis revealed that the G2/M portion of cells had reached 54% (Fig 4.9F).

Cells enriched at each phase of the cell cycle were fractionated according to the Dignam protocol (Dignam *et al.*, 1983). Cytoplasmic and nuclear fractions were run on a 12% SDS-polyacrylamide gel and transferred to nitrocellulose. The Western blot was probed with anti-DDX1 antibody 2910 followed by a secondary antibody coupled to HRP. Staining by enhanced chemiluminescence revealed that DDX1 protein remained constant during all stages of the cell cycle (Fig 4.9G). The drop in nuclear DDX1 levels at G2/M phase of the cell cycle likely represents the dissolution of the nuclear membrane, as nocodazole does not prevent the breakdown of the nuclear envelope (Beaudouin *et al.*, 2002).

Fig. 4.9 DDX1 protein distribution during the cell cycle.

RB522A cells were synchronized using two agents: aphidicolin and nocodazole. Samples of the cells were taken and stained with propidium iodide at various time points to monitor the cell cycle status. The results of the flow cytometric analyses are shown in **A** – **F**. **A.** The entire population of RB522A cells prior to synchronization. The cells in G1, S or G2/M were selected (gated), as indicated by the box, for further analysis. **B.** The DNA content of the gated cells prior to synchronization. The number of cells in each stage of the cell cycle is indicated above the peaks. **C.** The DNA content of the gated cells after 18 hours in aphidicolin. **D**. The DNA content of the gated cells 3 hours after aphidicolin release. **E.** The DNA content of the gated cells 5 hours after aphidicolin release, just prior to the addition of nocodazole. **F.** The DNA content of the gated cells 6 hours after nocodazole treatment. **G.** The cells from the above analyses were collected and fractionated into cytoplasmic and nuclear extracts. 12 μg of each extract were electrophoresed on a 12% SDS-polyacrylamide gel. DDX1 was visualized using an antibody to the amino-terminus of DDX1 (2910).

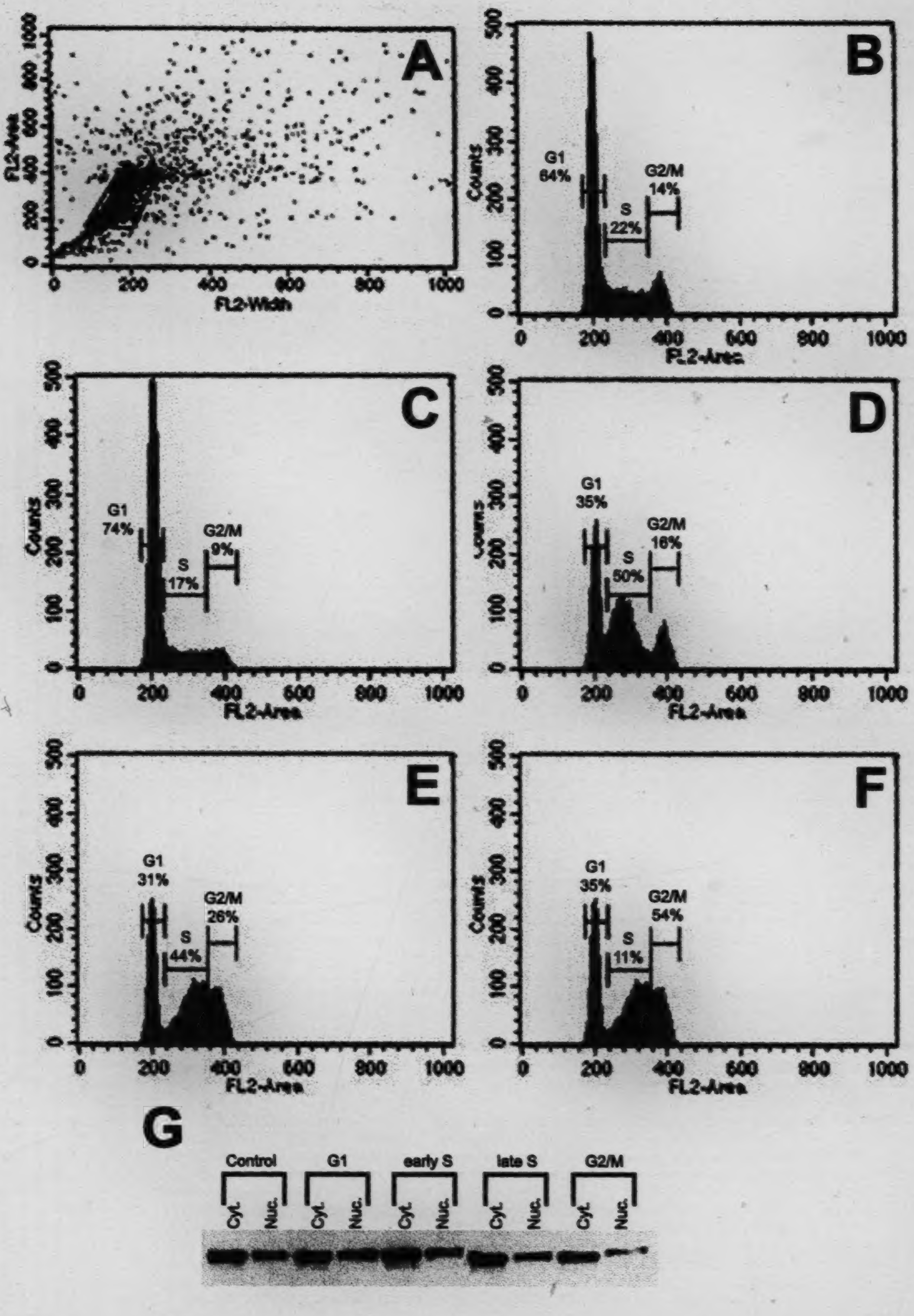
A
FL2-Area
FL2-Width
B
Counts
FL2-Area
G1 64%
S 22%
G2/M 14%
C
G1 74%
S 17%
G2/M 9%
D
G1 35%
S 50%
G2/M 16%
E
G1 31%
S 44%
G2/M 26%
F
G1 35%
S 11%
G2/M 54%
G
Control
G1
early S
late S
G2/M
Cyt.
Nuc.

DDX1 levels also remained steady throughout the cell cycle in the Y79 cell line (data not shown). It is important to note that the Dignam nuclear preparation is a hypertonic extraction; therefore, only soluble protein will be recovered. The fact that DDX1 levels are not altered in the nuclear compartment throughout the cell cycle (with the exception of G2/M phase) suggests that DDX1 does not alter forms (ie. the amount bound to the nuclear matrix vs. the amount of soluble DDX1 does not change during the cell cycle). Therefore, analysis of three different cell lines, one by confocal microscopy, and the other two by Western blot analysis establish that DDX1 protein levels remain stable throughout the cell cycle.

4.8 DDX1 foci localize to the periphery of viral compartments

Herpes simplex virus type 1 (HSV-1), a virus with a double-stranded DNA genome, replicates within the nucleus of its host cell. The replication of the HSV-1 genome requires the virus to seize and use the host cell's transcriptional and processing machinery. Therefore, infection of cells by HSV-1 can relay important information regarding a protein's role in the transcription process: if it is required for HSV-1 gene transcription it accumulates within the viral compartments, otherwise it is excluded or degraded. To discern whether DDX1 is involved in the transcription process, we infected HeLa cells with HSV-1. After a 6 hour infection, the cells were fixed in paraformaldehyde, permeablized with Triton X-100, and labeled with antibodies to DDX1 and viral immediate early protein, ICP4. ICP4 is a transcriptional activator required for the expression of

HSV-1 early and late genes. After a 6 hour infection, various stages of HSV-1 infection could be seen based on the size of the viral compartments. DDX1 appeared to accumulate very slightly within the viral compartments of some cells (Fig 4.10A); however, most cells displayed neither exclusion nor accumulation of DDX1 (Fig. 4.10B). HSV-1 infected cells exhibited a decrease in the number of DDX1 foci with many cells containing no DDX1 foci when compared to mock infected cells. Within the population of infected cells that did contain DDX1 foci, it was observed that many of the foci resided on the periphery of viral compartments (Fig. 4.10A, B). This is particularly intriguing as it suggests that DDX1 foci could be supplying proteins required for viral gene transcription.

4.9 DDX1 levels correlate with HeLa transcriptional activity

To determine whether either number of DDX1 foci or overall nuclear DDX1 level in a cell correlates with transcriptional activity, we exposed HeLa cells to FU for 15 min. Subsequent to fixation and staining with anti-DDX1 and anti-BrdU antibodies, cells were visualized using a Zeiss-Axioplan II microscope with a cooled charge-coupled device (CCD) camera. This camera allows us to control the exposure setting thereby ensuring each image is exposed to the same extent. The resultant pictures were analyzed using Metamorph image analysis software. Briefly, following subtraction of background values and nucleolar signals from a single plane from the center of the cell, the average gray value for each channel was assessed using the DAPI channel as a mask. These values were then subjected to linear regression analysis. Although DDX1 foci numbers

Fig. 4.10 DDX1 foci localize to the periphery of viral compartments.

HeLa cells were infected with Herpes Simplex Virus-1 for 6 hours. The cells were then fixed and stained with anti-DDX1 and anti-ICP4 antibodies. Some infected cells displayed a slight accumulation of DDX1 protein in viral compartments demarcated by ICP4 protein (**A**) whereas viral compartmens of other infected cells displayed neither inclusion nor exclusion of DDX1 protein (**B**). Although there were fewer DDX1 foci within infected HeLa cells, many of the DDX1 foci localized to the periphery of viral compartmens (A & B). The bar represents 5 μm.

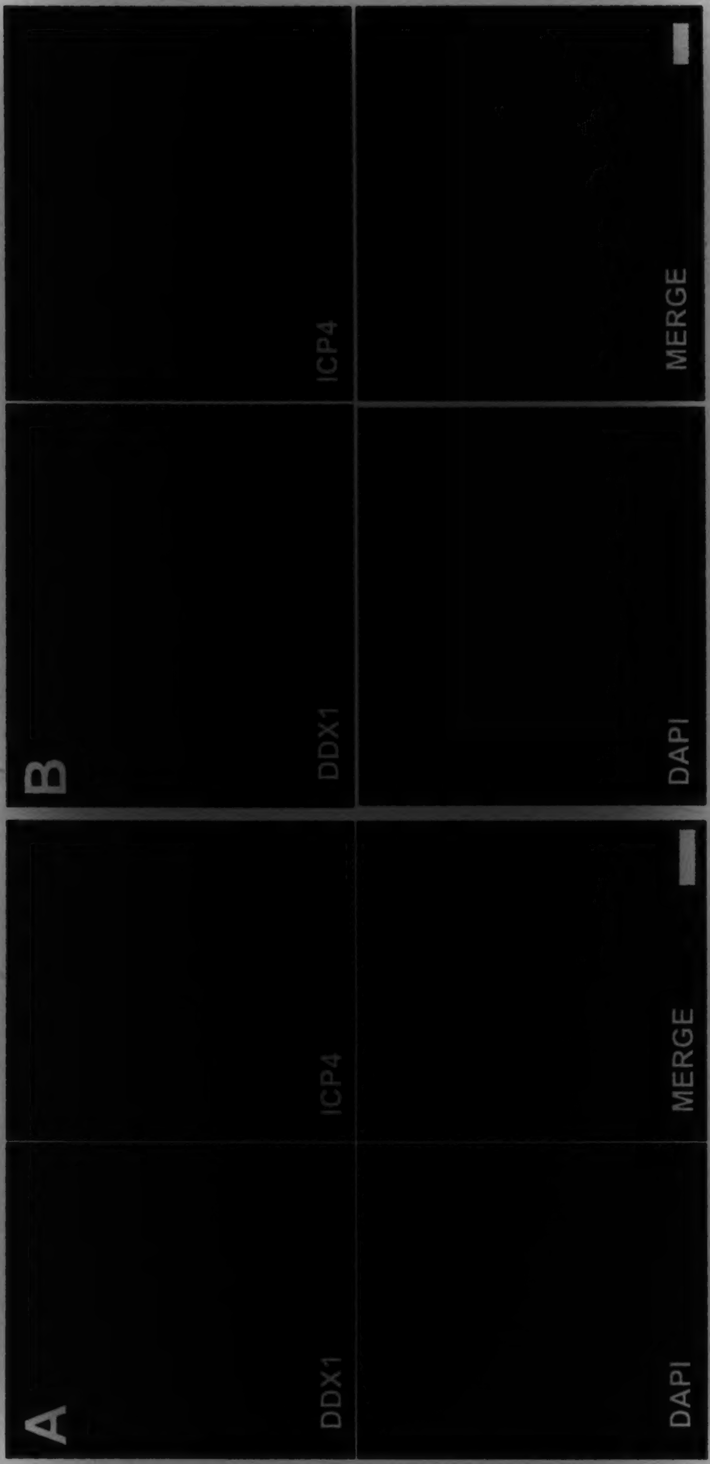
A
DDX1
ICP4
DAPI
MERGE
B
DDX1
ICP4
DAPI
MERGE

did not correlate with transcription (p=0.095), there was a general trend towards increased number of foci with increased transcription. It was noted that in many cells with higher transcription, the overall size of DDX1 foci was also substantially larger than in cells with little transcription. Although the number of DDX1 foci did not statistically correlate with transcription levels, examination of overall nuclear DDX1 levels vs. transcriptional activity by linear regression revealed a positive correlation (p=0.002) (Fig. 4.11). Attempts to confirm this observation using 50 μg/ml α-amanitin, which eliminates transcription by both RNA polymerase II and III, were unsuccessful (p=0.303). However, it is entirely likely that the short incubation time (30 min) was not enough to obtain a DDX1 turnover and therefore the remaining DDX1 protein was still reflective of past transcriptional activity.

4.10 Purified recombinant DDX1 decreases pre-mRNA polyadenylation

The interaction of DDX1 with CstF-64 prompted us to investigate whether DDX1 was involved in 3'-end pre-mRNA cleavage and polyadenylation. To do so, we obtained two plasmids from Dr. Jeffery Wilusz (University of Medicine and Dentistry, Newark, New Jersey) pSVL-3 (AAUAAA) and pSVL-6 (AAGAAA). These plasmids contain the SV40 late (SVL) poly(A) signals, with the former containing the wild-type polyadenylation signal and the latter carrying a point mutation that eliminates cleavage and polyadenylation (Wilusz and Shenk,

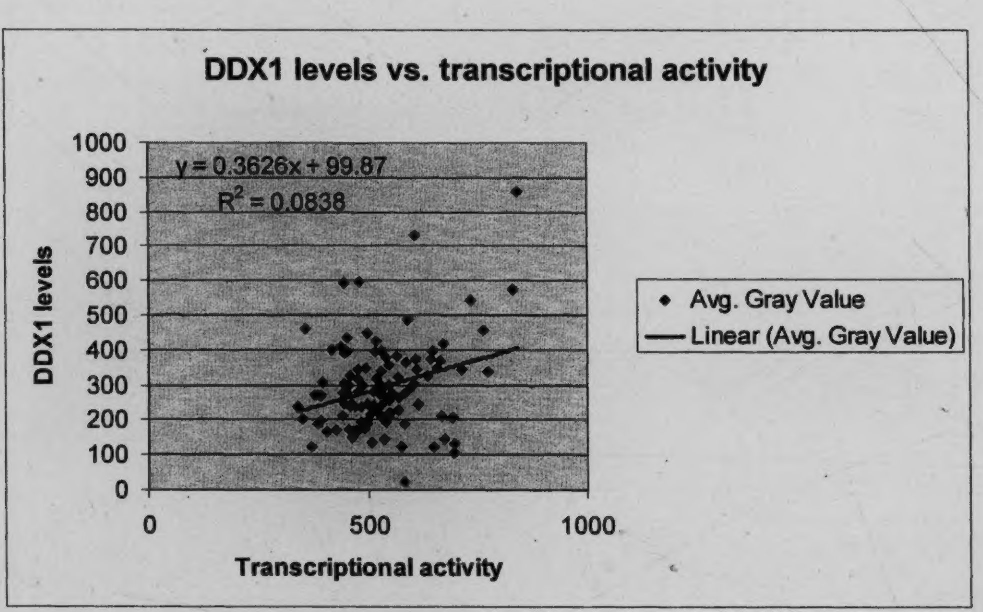

Fig. 4.11 Nuclear DDX1 protein levels positively correlate with transcription.

HeLa cells were incubated in FU for 15 min. following which, cells were fixed and double-labeled with anti-DDX1 and anti-BrdU antibodies. The cells were imaged using a Zeiss-Axioplan II microscope with a cooled charge-coupled device (CCD) camera. Transcription occurring in the nucleus, excluding the nucleoli, was quantified using Metamorph analysis software. This same region was also quantified for the channel representing DDX1 signal. The results are depicted on the scatter plot together with the corresponding linear regression trendline. Linear regression calculations indicated p=0.002.

1988). Both plasmids were sequenced following their purification to ensure that the SVL sequence was as reported.

Based on a recommendation by Dr. Jeffery Wilusz, we began testing our nuclear extracts with the *in vitro* polyadenylation reaction rather than the *in vitro* cleavage reaction, as the products are more readily visible. There are several published variations to the original *in vitro* polyadenylation reaction (Moore and Sharp, 1985); the protocol that we chose for our analysis was obtained from Dr. Jeffery Wilusz. Briefly, a modified Dignam nuclear extract (Dignam *et al.*, 1983) was prepared using fresh adherent HeLa cells (see Materials and Methods). The RNA was prepared by *in vitro* transcription of the pSVL-3 and pSVL-6 vectors using ^{32}P-UTP and gel purified on an 8M urea 8% polyacrylamide gel. The polyadenylation reaction was performed at 30°C for 60 min and the products were subsequently separated on an 8 M urea 4.5% polyacrylamide gel. Although we made numerous attempts to prepare an active Dignam nuclear extract using our adherent HeLa cells we were unsuccessful in achieving polyadenylation. Therefore, we obtained some extracts from Dr. Jeffery Wilusz. These nuclear extracts were prepared by Dr. Carol Lutz using HeLa cells adapted for culture in spinner flasks and were known to be competent for *in vitro* polyadenylation. These extracts proved to be competent in our polyadenylation reactions as we observed the characteristic smear above our RNA in the pSVL-3 lane (AAUAAA) but not in the pSVL-6 lane (AAGAAA) (Fig. 4.12 lane 3 vs. lane 4).

To determine whether DDX1 protein would influence the polyadenylation process, we cloned DDX1 into the pGEX-2T vector and bacterially expressed it

Fig. 4.12 Purified recombinant DDX1 decreases pre-mRNA polyadenylation. The effect of purified recombinant DDX1 on the pre-mRNA polyadenylation process was tested using two *in vitro* transcribed RNA substrates: pSVL-3, which contains the wild-type SV40 late polyadenylation sequence and pSVL-6, which contains a point mutation converting AAUAAA to AAGAAA. Lanes 1 and 2 represent the input RNA while lanes 3 and 4 contain the RNA + HeLa nuclear extract. Proper RNA processing results in a smear of polyadenylated RNA above the input RNA (lane 3). Lanes 5 and 6 contain pSVL-3 RNA, HeLa nuclear extract and 1 μg purified recombinant DDX1 or 1 μg purified recombinant DDX1 + purified anti-DDX1 antibody, respectively.

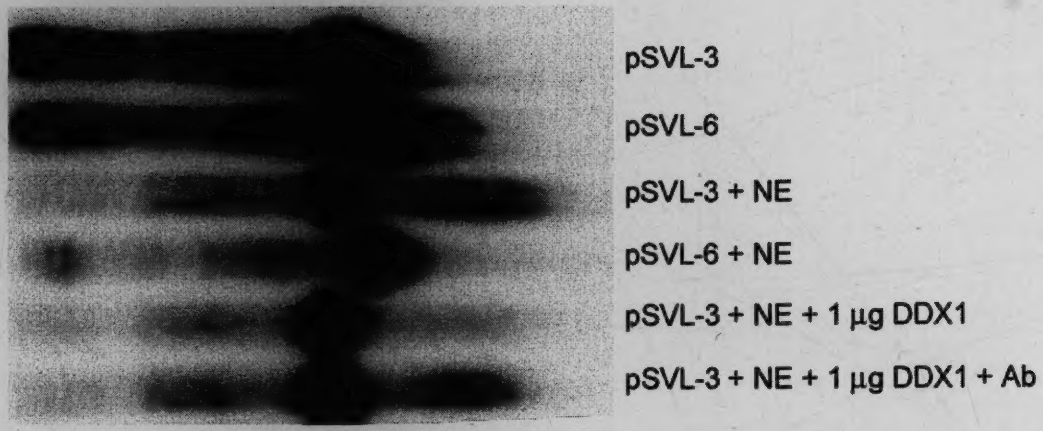
pSVL-3
pSVL-6
pSVL-3 + NE
pSVL-6 + NE
pSVL-3 + NE + 1 µg DDX1
pSVL-3 + NE + 1 µg DDX1 + Ab

as a GST-fusion protein. The protein was purified using glutathione-sepharose beads and DDX1 was cleaved from the GST moiety using thrombin. Coomassie blue staining of an SDS-polyacrylamide gel containing purified DDX1 revealed very little protein degradation (data not shown). The bacterially-expressed DDX1 was further purified using HPLC to remove contaminating ribonuclease activity seen with the non-purified protein. The addition of 1 μg of purified DDX1 to the polyadenylation reaction decreased the amount of polyadenylated RNA (Fig. 4.12 lane 5). Furthermore, the addition of approximately 0.4 μg of purified anti-DDX1 antibody to this reaction partly restored polyadenylation activity (Fig. 4.12 lane 6). This suggests that the DDX1-mediated repression of polyadenylation is specific and not due to a contaminating co-purified protein. It is important to note that these experiments have only been attempted once using the nuclear extracts prepared by Dr. Lutz. It will be critical to reproduce these experiments once we have successfully prepared our own active HeLa nuclear extracts. However, these results suggest that DDX1 may play a role in the polyadenylation process.

4.11 Summary: DDX1 frequently co-localizes with CstF-64 in nuclear cleavage bodies and DDX1 may play a role in 3'-end pre-mRNA processing

Lower eukaryotic DEAD box proteins function in many aspects of RNA metabolism including translation initiation, ribosome biogenesis and pre-mRNA splicing. As these functions occur in discrete areas of the cell, subcellular localization of higher eukaryote DEAD box proteins could lead to the identification of putative roles for these proteins. Based on this premise, we used confocal microscopy to examine the subcellular distribution of the DEAD box protein, DDX1, in a variety of cell lines. We established that the majority of DDX1 is distributed in a widespread punctate nucleoplasmic pattern, with lower levels in the cytoplasm. Interestingly, DDX1 was also found in discrete foci within the nucleus. There was an average of 5 DDX1 foci in HeLa cells with diameters of ~0.5 μm. DDX1 protein was found in every cell line examined, with discrete DDX1 foci observed in 10 out of 15 cell lines, including a variety of transformed cells as well as normal human fibroblasts. Taken together, these results support a primary role for DDX1 in nuclear, rather than cytoplasmic, RNA metabolism and suggest that many cell types have a nuclear domain that contains elevated concentrations of DDX1.

The eukaryotic nucleus is comprised of many distinct subdomains, each of which contains specific proteins believed to contribute to a functionally organized nucleus. Using a panel of antibodies previously shown to recognize specific nuclear subdomains, we found that DDX1 foci do not associate with SC-35 speckles or SNBs, but frequently reside adjacent to PML and CBs. Most importantly, we discovered that in HeLa, 65% of DDX1 foci colocalize with CstF-64-labeled cleavage bodies. Colocalization of DDX1 foci and cleavage bodies was also observed in three other cell lines tested: COS-7, SKN, and GM38 cells. Although the majority of DDX1 foci that did not colocalize with a cleavage body did contain some CstF-64 and vice versa, a few foci appeared devoid of converse protein. This observation suggests that although both of the proteins frequently associate within the same nuclear structure, DDX1 foci may represent a distinct nuclear structure. Electron microscopy and electron spectroscopic imaging of each structure will aid in defining their molecular compositions thereby determining whether they truly represent distinct nuclear bodies.

DDX1 foci rarely colocalize with CBs suggesting that either DDX1 shuttles very transiently through CBs or that DDX1 only enters CBs during specific cellular conditions. Within all three cell lines examined (HeLa, SKN, and COS-7 cells), a portion of DDX1 foci were observed to localize adjacent to CBs. Two explanations could account for the adjacent localization of DDX1 foci; DDX1 foci could be delivering CstF-64 or another protein to CBs, or alternatively the different DDX1 foci could serve different functions. For example, it might be interesting to determine whether the CBs that localize adjacent to DDX1 foci represent the same fraction of CBs that resides adjacent to histone gene clusters. This might indicate that DDX1 foci adjacent to CBs could be contributing to the transcription or processing of histone mRNA, while DDX1 foci not adjacent to CBs could be involved in the processing of other transcripts.

The frequent adjacent localization of cleavage bodies and DDX1 foci with CBs and PML bodies suggests a functional relationship. The fact that only a certain percentage of each nuclear body displays adjacent localization with another nuclear body lends sustenance to a theory of functional heterogeneity within the nuclear body population. This theory has been suggested many times (ie: Brasch and Ochs, 1992; Platani *et al.*, 2000), but remains widely unrecognized in the nuclear structure field. In support of heterogeneity within the CB population, Alliegro and Alliegro (1998) reported that CBs do not always contain fibrillarin or the bovine protein pigpen, a previously reported constituent of CBs (Alliegro and Alliegro, 1997). Similarly, sphere organelles within oocyte germinal vesicles, which are equivalent to CBs, do not contain the nucleolar components fibrillarin, nucleolin, U3 and U8 snoRNA (Wu *et al.*, 1994; Gall *et al.*, 1995). Furthermore, coilin depleted *Xenopus* egg extracts do not contain Sm snRNPs yet do contain the nucleolar components (Bauer and Gall, 1997). CBs also exhibit heterogeneity when localizing with specific gene loci such as histone gene clusters or snRNA; only a small proportion of CBs in some cells exist next to these loci – the rest exist 'free' in the nucleoplasm (Frey and Matera, 1995; Handwerger *et al.*, 2002). Further support of CB heterogeneity comes from *in vivo* observations of HeLa cells expressing GFP-p80 coilin and YFP-fibrillarin (Platani *et al.*, 2000). Platani *et al.* (2000) have observed two distinct populations of CBs, which they term CBs and mini-CBs. In addition to a size difference, it was noted that CBs and mini-CBs have different constituents (fibrillarin is not present in all CBs) and different mobilities within the nucleoplasm. It would be interesting to determine whether these subpopulations of CBs differentially associate with other nuclear bodies or with the nucleolus.

Similar to CBs, heterogeneity has been noted within the PML population. The ALT-associated PML bodies present in telomerase-negative cell lines represent only a subset of PML bodies (Yeager *et al.*, 1999). Interestingly, fusion of these cells with telomerase-positive cells results in the disappearance of the

ALT-PML bodies only (Perrem *et al.*, 2001). It has also been noted that only a subset of PML bodies contains p53 in irradiated U2OS cells (Guo *et al.*, 2000) or in mouse embryo fibroblast cells transfected with an activated *ras* (Pearson *et al.*, 2000). These results, which support the view that PML bodies are non-uniform, are further endorsed by confocal microscopy experiments on baby hamster kidney cells expressing PML body constituent, YFP-Sp100, that show at least three classes of PML bodies based on differing mobilities (Muratani *et al.*, 2002). Similar to the localization of CBs to specific gene loci, the association of PML bodies with the MHC gene cluster does not involve all PML bodies within a cell (Shiels *et al.*, 2001). Interesting conjectures can be also drawn from the observations of von Mikecz *et al.* (2000) who report that a subset of PML bodies contains CBP/p300 and that this subset of PML bodies also partially overlapped domains containing RNA polymerase II. These domains have not been further defined; however, they could represent CBs as Schul *et al.* (1998b) have previously reported the localization of RNA polymerase II to CBs. This would imply that a subset of PML bodies reside adjacent to CBs.

This heterogeneity of nuclear bodies is likely reflective of a functional divergence within one population of nuclear structures. Therefore, CBs that localize adjacent to the nucleolus could have a different function than CBs located adjacent to cleavage bodies. Likewise, PML bodies located adjacent to cleavage bodies likely function in a different manner than other PML body subsets. This theory could explain the large repertoire of proteins residing within each nuclear subdomain. Therefore, defining a specific process for each nuclear body may prove difficult. CBs localized adjacent to cleavage bodies and DDX1 foci are likely involved in some aspect of RNA polymerase II transcription and processing. It would be interesting to determine whether CBs adjacent to DDX1 foci lack components of rRNA transcription and processing such as fibrillarin, and whether these CBs represent one subset with a specific motility (i.e. mini-CBs). This functional heterogeneity may also explain the localization of DDX1 to cleavage bodies, and as well DDX1 foci adjacent to PML bodies. It is possible that the different subsets of DDX1 foci may serve different biochemical functions or they may perform the same biochemical function on different classes of transcripts.

Analysis of the distribution pattern of DDX1 foci and cleavage bodies during the cell cycle indicates distinct patterns of disappearance and reappearance. DDX1 foci were visible until metaphase, while cleavage bodies disappeared during late prophase. Furthermore, only DDX1 foci were detected in the early G1 phase of the cell cycle. Unlike DDX1 protein levels, which remained constant throughout mitosis, CstF-64 levels decreased during prophase through to telophase, as previously reported (Schul *et al.*, 1996). The disappearance of these nuclear bodies during mitosis resembles observations made with other nuclear bodies such as CBs (Andrade *et al.*, 1993; Ferreira *et al.*, 1994), SNBs (Chen *et al.*, 1999), and PNCs (Huang *et al.*, 1997), which all disintegrate during prophase. This confirms that DDX1 foci, perhaps like all nuclear bodies, are dynamic structures.

In order to further establish whether DDX1 might be involved in some aspect of the transcription process, we infected HeLa cells with HSV-1. Most cells exhibited neither exclusion nor inclusion of DDX1 protein. Additionally, DDX1 foci numbers decreased in most cells. Those cells that did retain foci appeared to localize them on the periphery of viral compartments suggesting the foci are either aiding in viral transcription or they are undergoing virus-mediated destruction. The lower numbers of foci within infected cells might suggest the latter hypothesis but the observation that DDX1 protein is not excluded from viral compartments would suggest the former. It is possible that only a subset of DDX1 foci is required for viral transcription (i.e. those which contain CstF-64) and therefore the other DDX1 foci do not remain intact. Triple labeling infected cells with anti-CstF-64 (or antibodies to PML or CBs), anti-DDX1 and anti-ICP4 antibodies would define whether any specific subset of DDX1 foci localizes adjacent to viral compartments.

Separate experiments using HeLa cells that had incorporated FU into nascent RNA demonstrated that DDX1 levels correlate with transcriptional activity of RNA polymerases II and III. As RNA polymerase III only accounts for 10% of the total transcription within the nucleus and we did not measure FU incorporation into nucleoli, the increase in DDX1 levels likely reflects an increase in RNA polymerase II activity. Although we did not achieve statistical significance upon examination of DDX1 foci, we did note that DDX1 foci appeared to be more numerous and larger in cells with increased transcription. This observation correlates with that of CBs, which have also been observed to be larger and more numerous in cells with high transcriptional activity (Brasch and Ochs, 1992; Alliegro and Alliegro, 1998). It is conceivable that we did not achieve statistical significance because a decrease in transcription could result in larger DDX1 foci disseminating to smaller foci thereby increasing their apparent number for a short period of time.

Because of the limits of resolution of the confocal microscope, proteins that appear to colocalize could be as far apart as 0.25 μm. We therefore used FRET, a technique based on the transfer of energy between molecules located within 10 nm of each other, to further study the proximity of DDX1 and CstF-64. Our method used proteins that were labeled with both primary and secondary antibodies, effectively increasing the Förster radius to greater than 10 nm. This technique indicated that labeled DDX1 is within 10 nm of labeled CstF-64 in both cleavage bodies and within the nucleoplasm. Furthermore, co-immunoprecipitation experiments demonstrate that a proportion of CstF-64 is found within the same complex as DDX1. It remains possible that the interaction of CstF-64 with DDX1 is not direct and could be mediated by RNA as immunoprecipitation experiments with the addition of a ribonuclease were inconclusive. Nevertheless, taken together, the FRET and immunoprecipitation results further endorse a spatial as well as possibly a functional relationship between these two proteins.

Within the nucleoplasm, CstF-64 is known to function as part of a heterotrimeric complex (CstF) in 3'-end pre-mRNA cleavage by binding a GU-rich element downstream of the AAUAAA consensus sequence (Wahle and

Ruegsegger, 1999). The role of CstF-64 within cleavage bodies remains to be elucidated. Schul *et al.* (1999b) have observed that in T24 bladder carcinoma cells undergoing DNA synthesis, cleavage bodies mainly exist independent of Cajal bodies and colocalize with replication-dependent histone gene clusters. These cleavage bodies were previously reported to contain newly transcribed RNA as measured by BrUTP microinjection (Schul *et al.*, 1996). Therefore, Schul *et al.* (1999b) have hypothesized that cleavage bodies may play a role in histone mRNA synthesis. As mammalian histone transcripts do not undergo typical 3' end polyadenylation and cleavage (Dominski and Marzluff, 1999), the role of cleavage bodies in histone mRNA synthesis is not immediately obvious. While our data do not refute the possibility that cleavage bodies may play a role in histone mRNA synthesis, three-dimensional analysis of 25 FU-labeled HeLa cells indicates that DDX1 foci lack nascent RNA and, consequently, do not represent sites of active transcription. Although we did not triple-label cells with anti-CstF-64, it is likely that in the 25 cells examined DDX1 did colocalize with cleavage bodies. We therefore propose that cleavage bodies and DDX1 foci may function in facilitating the formation or regeneration of transcriptional complexes, as previously suggested for Cajal bodies (Gall, 2000). In support of this, we and others have observed that the two structures frequently localize adjacent to Cajal bodies which are known to contain a number of transcriptional and splicing/polyadenylation proteins (Gall *et al.*, 1999). Additionally the localization of DDX1 foci and cleavage bodies adjacent to PML bodies (Schul *et al.*, 1996) further supports a role for these structures in the transcription process as PML bodies have been implicated in various aspects of transcription (see section 1.3.3 of the Introduction). This juxtaposition suggests coordinate roles for these structures in RNA metabolism. Taking into consideration all observations with cleavage bodies to date, we believe that these structures play a general role in the transcription and processing of pre-mRNAs. As histone gene transcription is particularly active during S phase, Schul *et al.*'s observation that histone gene clusters are associated with cleavage bodies would be consistent with a local requirement for elevated levels of factors involved in transcription and processing of histone genes (Schul *et al.*, 1999b).

The close proximity and possible interaction of DDX1 with CstF-64 suggests a role for DDX1 in 3'-end pre-mRNA cleavage and/or polyadenylation. Initial results with the *in vitro* polyadenylation assay suggested that purified recombinant DDX1 decreased polyadenylation, and the addition of purified anti-DDX1 antibodies eliminated this effect. The decrease in polyadenylation could reflect a role for DDX1 in promoting the dissociation of cleavage and polyadenylation factors from the RNA so that it can be exported from the nucleus. Further verification of this result is needed using both the SV40 RNA substrate and other RNA substrates, and using additional controls such as non-related recombinant proteins purified in a similar manner. An alternative explanation for Fig. 4.12 is that recombinant DDX1 may not be active and as such behaves in our assay as a dominant negative. Therefore, endogenous DDX1 may in fact be promoting polyadenylation, and the addition of recombinant DDX1 could irreversibly bind to pre-mRNA effectively preventing the molecule from undergoing 3'-end processing. We have noted, however, that our recombinant DDX1 (not purified by HPLC) is active in both ATPase and RNA helicase assays (data not shown). The addition of anti-DDX1 antibody to nuclear extracts not containing recombinant DDX1, in this scenario, may cause a decrease in polyadenylation due to its potential ability to affect endogenous DDX1 activity. The addition of anti-DDX1 antibody to nuclear extract in the case of the former hypothesis would likely permit substrate processing; however the mature mRNA might be confined to the nucleus pending the release of cleavage and polyadenylation factors from the transcript.

Whether DDX1 acts at the cleavage or polyadenylation step will need to be analyzed using the *in vitro* cleavage assay. Depending on the step affected, the addition of purified recombinant DDX1 could be tested using UV cross-linking of various factors to RNA. For example, if DDX1 was found to affect the cleavage step then we might examine the effect of DDX1 on CstF-64 binding to RNA. The addition of DDX1 protein to nuclear extracts may cause a decrease or increase in the amount of CstF-64 that could be UV cross-linked to substrate RNA. This role for DDX1 is plausible as the CstF complex has been found to preferentially bind short RNA molecules, suggesting that RNA structure is important for binding (Takagaki and Manley, 1997). Therefore, we could test the hypothesis that the decrease in polyadenylation could be due to DDX1-induced alterations to the RNA structure that cause the CstF complex to dissociate. Although this is only one of many possibilities, a technique such as UV cross-linking could shed light on the consequences of DDX1 binding to RNA.

Chapter 5. Co-localization of DDX1 foci with Gems

While examining the interaction of DDX1 foci with cleavage bodies, we obtained antibody to SMN, which at that time, had been reported to localize to structures called gems (Liu and Dreyfuss, 1996). Gems frequently resided adjacent to CBs, similar to our observations for DDX1 foci. We therefore wished to investigate the possibility that DDX1 foci, and subsequently cleavage bodies colocalized with gems.

Our specific objectives for this project were to:

a) investigate the relationship between DDX1 foci and gems as labeled by anti-SMN antibodies. These experiments were done using confocal microscopy.

b) investigate whether there is an association between DDX1 and SMN. These experiments involved immunoprecipitations and Western blot analysis.

c) investigate the relationship between gems and cleavage bodies. These experiments used confocal microscopy to visualize cells labeled for each nuclear structure.

d) investigate the relationship between gems, cleavage bodies, DDX1 foci and CBs using triple-labeled cells. These cells were visualized using confocal microscopy and then three-dimensionally reconstructed to reveal the location of each nuclear body with respect to the others.

5.1 Co-localization of DDX1 foci with gems

As SMN was reported to localize within gems in a HeLa cell line, we obtained HeLa cells from a neighbouring laboratory (HeLaLE) to examine for DDX1 foci and gems. The cells were fixed, permeabilized and then labeled with anti-DDX1 antibody 2923 and anti-SMN antibody. These HeLa cells had ~4.3 SMN-labeled gems and ~3.2 DDX1 foci per nucleus (Table 5.1). Three-dimensional reconstruction of the cells revealed that 59.4% of DDX1 foci colocalized with gems, and 44.2% of gems colocalized with DDX1 foci (Fig. 5.1; Table 5.1). These experiments were repeated on 3 different occasions with this HeLa cell line.

Shortly after these experiments, a report came out suggesting that SMN-containing gems usually colocalize with CBs (Carvalho *et al.*, 1999). The only known exception was the HeLa cell line used by the Dreyfuss laboratory, HeLaPV. To ensure that our HeLa cell line was similar to the one used by the Dreyfuss laboratory, containing gems which were distinct from CBs, we labeled our HeLa cells with anti-p80 coilin antibody (to detect CBs) as well as anti-SMN antibody. Interestingly, although the majority of cells displayed adjacent localization of gems with CBs, we did observe some cells that had partial colocalization and full colocalization with CBs (Fig. 5.2A-C). Thus, these observations show that SMN is a dynamic protein that can localize to different nuclear structures or exist independently.

Table 5.1 Nuclear localization of DDX1 foci with respect to SMN-containing gems in HeLa cells.

Nuclear Body (NB)	avg. # of NBs per cell	% Coloc.	% Partial coloc.	% adjacent
DDX1 foci[a]	3.2	59.4	0.0	3.0
Gems[a]	4.3	44.2	0.0	2.3
DDX1 foci[b]	5.3	34.8	23.9	17.4
Gems[b]	5.3	35.3	24.2	17.6
DDX1 foci[c]	4.8	10.9	17.8	27.9
Gems[c]	4.3	12.3	19.4	31.3

[a] Represents data from first staining set (10 cells analysed).

[b] Represents data from second staining set (29 cells analysed).

[c] Represents data from third staining set (38 cells analysed).

DDX1
SMN
Merge

Fig. 5.1 Colocalization of DDX1 foci and SMN-containing gems.

HeLa cells were labeled with anti-DDX1 and anti-SMN antibodies. Visualization using a confocal microscope revealed that DDX1 foci can colocalize with SMN-labeled gems. The bar represents 0.5 µm.

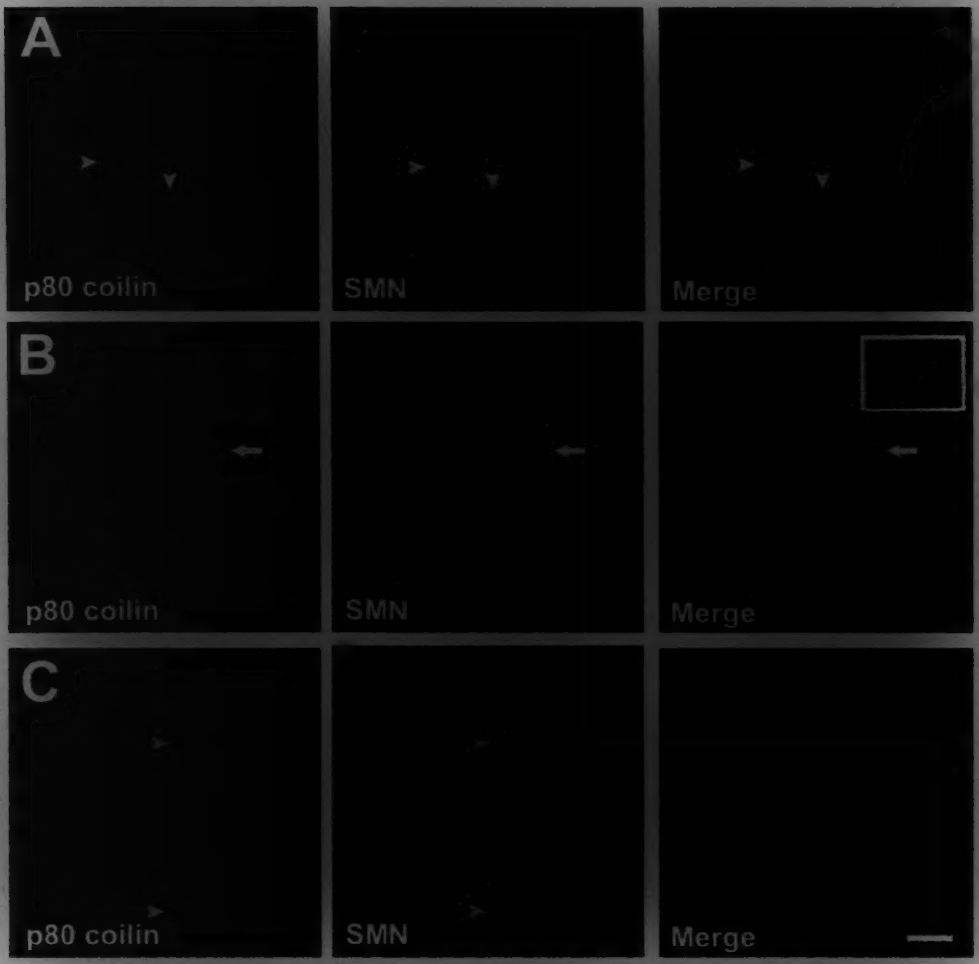
A
B
C
p80 coilin
SMN
Merge
p80 coilin
SMN
Merge
p80 coilin
SMN
Merge

Fig. 5.2 Relationship between gems and CBs in HeLa cells. HeLa cells were immunostained with anti-SMN and anti-p80 coilin antibodies. **A.** Adjacent localization of gems and CBs (arrowhead). **B.** Partial colocalization of a gem and CB (arrow). The enlarged foci (inset) was derived from a rotated three-dimensional reconstruction of the cell. **C.** Colocalization of gems and CBs. The bar represents 5 µm.

A number of months later, we repeated the above experiments co-labeling HeLa cells thawed from our stocks (HeLaST) for DDX1 and SMN; however, we obtained slightly different results. The average number of gems and DDX1 foci per nucleus was 5.3, and ~35% of each nuclear body colocalized with the other (Fig. 5.3A; Table 5.1). Approximately 24% of the structures displayed partial overlap, while ~17% of gems and DDX1 foci were adjacent (Fig. 5.3A,B). This experiment was repeated several times over the course of a month using our HeLa cell line and HeLa cell lines obtained from different laboratories. The cell lines from different laboratories displayed variable organization of nuclear bodies: some displayed good colocalization while others displayed little colocalization. In some cases this was due to a decrease in the overall number of SMN or DDX1 foci.

5.2 Immunoprecipitation of DDX1 and SMN

To determine whether DDX1 was a part of the SMN complex, DDX1 was immunoprecipitated from HeLaST cells with anti-DDX1 antibody 2910. Fig. 5.4A demonstrates that approximately 2.5%-5% of DDX1 was immunoprecipitated. Western blot analysis using anti-SMN antibody revealed that SMN co-immunoprecipitated with anti-DDX1 antibody. This experiment was repeated several times with the same result each time. Interestingly, when we attempted to immunoprecipitate SMN, we could not detect DDX1 by Western blot analysis (data not shown). Therefore, to verify that our DDX1 immunoprecipitation was not due to a nonspecific interaction, we prepared cell extracts in the presence of

Fig. 5.3 The location of DDX1 foci with respect to SMN-containing gems. HeLa cells were labeled with anti-DDX1 and anti-SMN antibodies. In addition to colocalizing with gems, DDX1 foci were found to (**A**) partially overlap gems and (**B**) localize adjacent to gems. Each inset represents a magnification of the associated foci. The bar represents 5 μm.

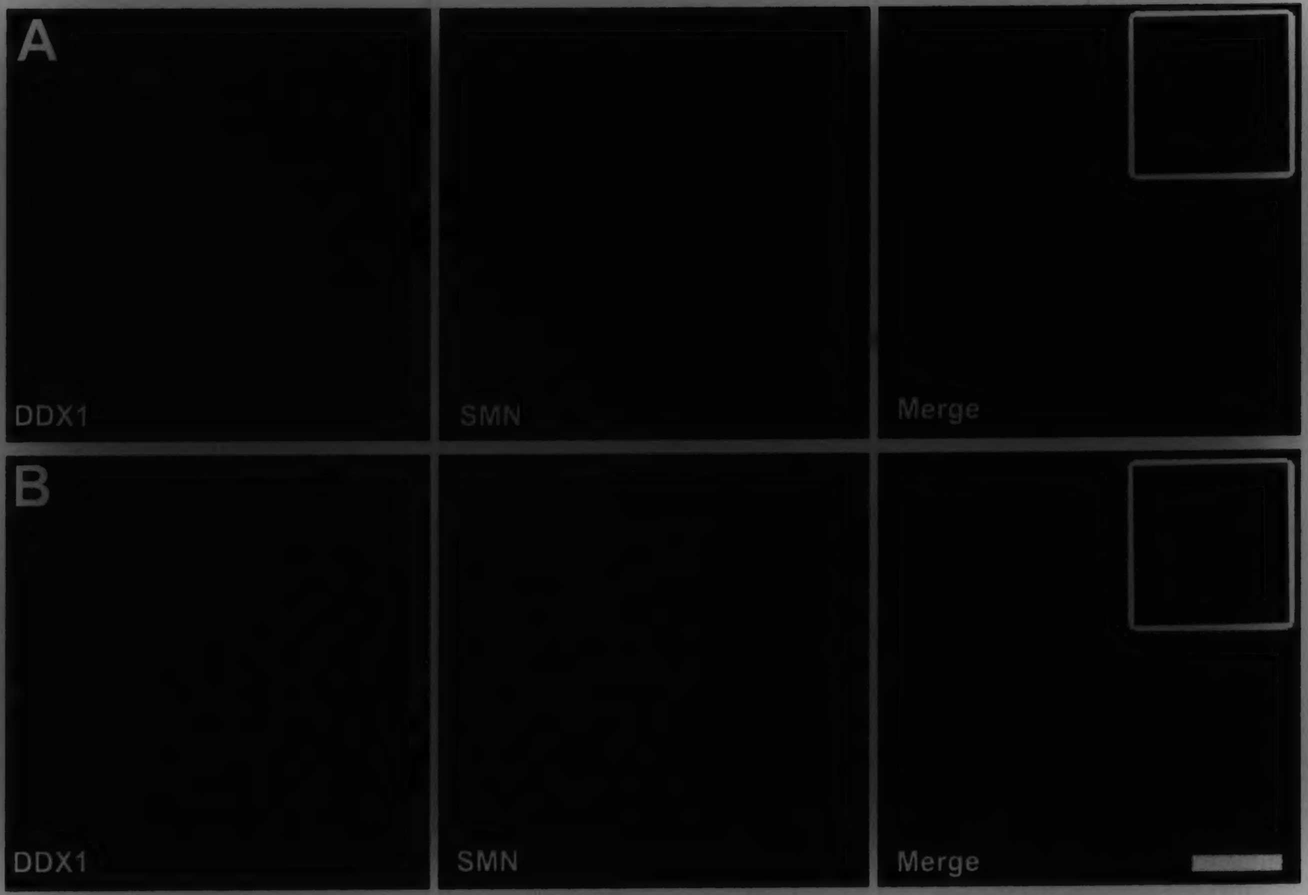
A
DDX1
SMN
Merge
B
DDX1
SMN
Merge

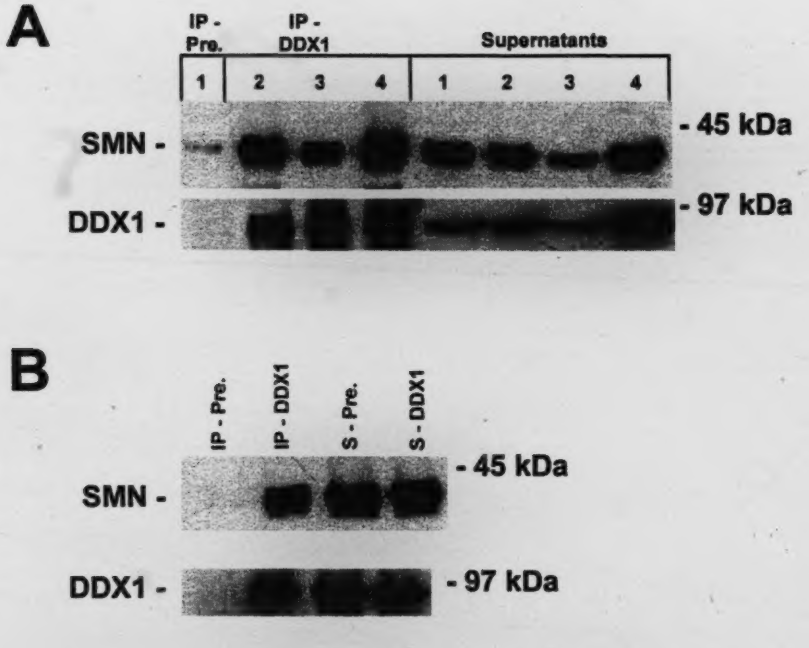
A
IP - Pre.
IP - DDX1
Supernatants
1
2
3
4
1
2
3
4
SMN -
DDX1 -
- 45 kDa
- 97 kDa
B
IP - Pre.
IP - DDX1
S - Pre.
S - DDX1
SMN -
DDX1 -
- 45 kDa
- 97 kDa

Fig. 5.4 Co-immunoprecipitation of DDX1 and SMN.

Nuclear extracts from HeLa cells were precleared and incubated with 3 µl of either preimmune serum (Pre.) or anti-DDX1 antibody 2910. Complexes were precipitated with protein A-agarose beads and electrophoresed on a 10% SDS-polyacrylamide gel. Proteins were transferred to nitrocellulose and detected with anti-SMN (top panels) and anti-DDX1 (bottom panels) antibody. For comparison, we have loaded 2.5% of the supernatant (S) from each IP in the right side of each gel. **A.** HeLa extracts were either prepared as whole cell (lanes 1 & 2) or cytoplasmic (lane 3) and nuclear (lane 4) fractions. **B.** HeLa whole cell extracts were prepared in the presence of 1% NP-40 and 0.5% sodium deoxycholate detergents.

1% NP-40 and 0.5% sodium deoxycholate. Fig. 5.4B demonstrates that even in the presence of a modest amount of detergent, anti-DDX1 antibody still immunoprecipitates SMN protein, making it likely that we are observing a valid association.

5.3 The relationship between gems and cleavage bodies

In their initial discovery of gems, Liu and Dreyfuss (1996) failed to examine the possibility that SMN localized to structures previously identified as cleavage bodies by Schul *et al.* (1996). Following our discovery that DDX1 foci colocalized to cleavage bodies, we decided to investigate the relationship between cleavage bodies and gems. As DDX1 foci resided in cleavage bodies and gems with similar frequencies in our earlier experiments, we hypothesized that the structures reported as gems were in fact the previously identified cleavage bodies. Upon co-staining our HeLaST cells with anti-CstF-64 antibody and anti-SMN antibody we were surprised to find that the majority of structures did not appear to be colocalizing (Fig 5.5A,B; Table 5.2). Subsequent labeling of these HeLa cells with anti-DDX1 antibody and anti-SMN antibody revealed a similar result: few DDX1 foci colocalized with gems (~11%); however, a large proportion of the nuclear structures were adjacent to gems (~28%) (Fig. 5.3C; Table 5.1). It appeared that the growth conditions of the cells had somehow been altered such that gems now appeared mostly within CBs. Carvalho *et al.* (1999), who examined their own HeLa cell line, made a similar observation: SMN exists mainly within CBs. However, despite the fact that SMN now frequently

Fig. 5.5 The nuclear configurations of CstF-64-containing cleavage bodies with respect to SMN-containing gems.

HeLa (**A-C**) or 293 human kidney (**D**) cells were labeled with anti-CstF-64 and anti-SMN antibodies. Panels **A-D** demonstrate: (**A**) no colocalization between the cleavage bodies and gems, (**B**) adjacent localization of cleavage bodies and gems (arrow and arrowhead). (**C**,**D**) colocalization of cleavage bodies and gems (arrow and arrowheads in **C**). The enlarged insets in **B** and **C** represent the foci depicted by the arrows. The bars represent 5 μm.

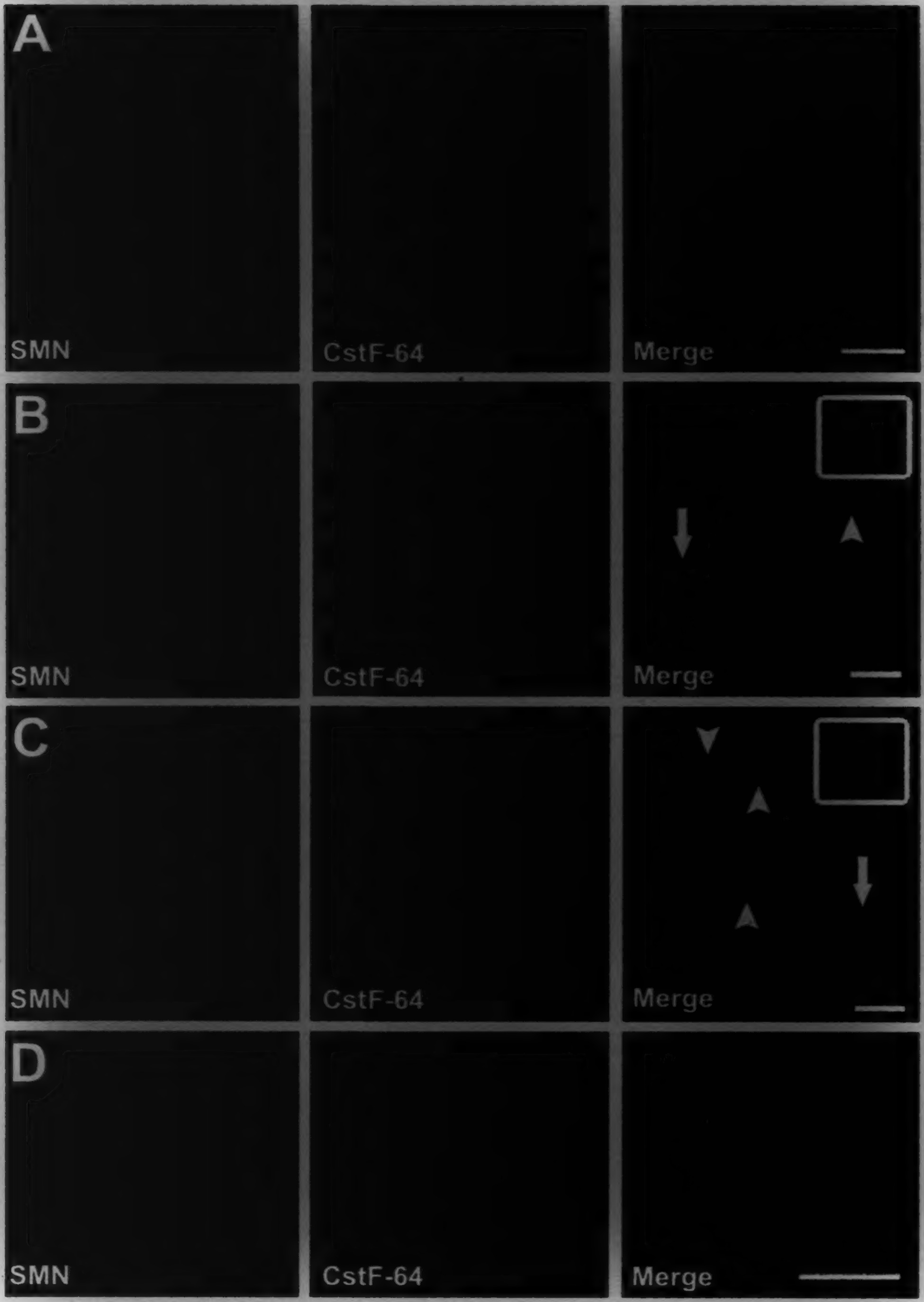
A
SMN
CstF-64
Merge
B
SMN
CstF-64
Merge
C
SMN
CstF-64
Merge
D
SMN
CstF-64
Merge

Table 5.2 Nuclear localization of CstF-64 containing cleavage bodies with respect to SMN-containing gems in HeLa cells.

Nuclear Body (NB)	avg. # of NBs per cell	% Coloc.	% Partial coloc.	% adjacent
Cleavage Bodies[a]	3.3	14.7	1.1	13.4
Gems[a]	4.7	10.4	2.2	18.9

[a] A total of 65 cells were three-dimensionally reconstructed and analysed.

resided within CBs, we did observe some colocalization of gems with cleavage bodies (Fig. 5.5C; Table 5.2). SMN colocalization with cleavage bodies was also observed in the two other cell lines we examined: 293 human kidney cells (Fig. 5.5D) and T24 bladder carcinoma cells (data not shown).

The fact that SMN has been reported to associate with RNA polymerase II, and that it occasionally colocalized with cleavage bodies led us to propose that SMN may play a role in 3'-end processing. To investigate this possibility we cloned SMN into pGEX-4T2 in order to produce purified recombinant protein. This protein would be used in our *in vitro* polyadenylation assay to discern any effects of SMN protein. Unfortunately, although SMN was in frame according to sequencing data, *E.coli* produced only very small amounts of the protein. We tried a different strain of *E. coli*, as well as different methods of protein induction; however, we were unsuccessful in obtaining adequate amounts of SMN protein. We attempted to further define whether SMN was involved in 3'-end processing by immunoprecipitating SMN and detecting for CstF-64 protein. Initial results with this experiment have shown that SMN does not co-immunoprecipitate CstF-64. We have not tried the reverse experiment as we do not have enough anti-CstF-64 antibody.

5.4 Gems, CBs, cleavage bodies and DDX1 foci: the dynamic nature of nuclear structures

To investigate the nature of the relationship between gems, cleavage bodies, CBs and DDX1 foci, we performed triple labeling of fixed HeLa cells. We three dimensionally reconstructed each multi-labeled nuclei and visualized the spatial relationship between each foci. At least 20 nuclei were examined for each set of triple-labeled cells. Labeling with anti-DDX1, anti-SMN and anti-CstF-64 antibodies resulted in a multitude of arrangements (Table 5.3) with the most frequent arrangement consisting of all three foci colocalized (6 cells out of 20 had foci that colocalized; Fig 5.6A). Five cells out of 20 had DDX1 foci that colocalized with cleavage bodies, which were in turn adjacent to a gem (Fig5.6B). Colocalization of all 3 foci was also observed in the other cell line examined, 293 human kidney cells (data not shown). It is important to note that for these analyses we defined foci as structures that were brighter than background nucleoplasmic levels. Frequently, a structure was not devoid of another protein, but we did not label it as an independent body as the level of staining was similar to nucleoplasmic levels. Based on our results, gems, cleavage bodies and DDX1 foci are likely to be dynamic structures, which can exist independently or localize with another structure.

Triple labeling of cleavage bodies, CBs, and gems also revealed numerous patterns (Table 5.4). The most frequent arrangement involving all three foci was colocalization of gems and CBs, which in turn were adjacent to cleavage bodies (7 cells out of 26 contained foci with this arrangement; Fig 5.7A). We also observed that in 5 cells out of 26, all three foci colocalized (Fig. 5.7B). In one nucleus, we observed the adjacent localization of all three foci (Fig. 5.7C). These results suggest that gems are indeed distinct structures from CBs and cleavage bodies, and that the three structures affiliate in many HeLa cell nuclei.

Table 5.3 Configurations of DDX1 foci, cleavage bodies (ClvgBds) and gems in triple-labeled HeLa cells.

Nuclear Body (NB)	avg. # of NBs per cell[a]	% Gems coloc. with ClvgBds & adj. to DDX1	% DDX1 coloc. with ClvgBds & adj. to Gems	% Gems coloc. with DDX1	% DDX1 coloc. with ClvgBds	% DDX1 adj. to Gems	% DDX1 adj. to ClvgBds	% All 3 coloc.	% All 3 Adj.
DDX1 foci	5.5	0.9	7.3	17.3	10.9	10.9	0.9	14.5	1.8
Cleavage Bodies	4.3	1.2	9.4	N/A	14.1	N/A	1.2	18.8	2.4
Gems	4.8	1	8.3	19.8	N/A	12.5	N/A	16.7	2.1

[a] A total of 20 cells were three-dimensionally reconstructed and analysed.

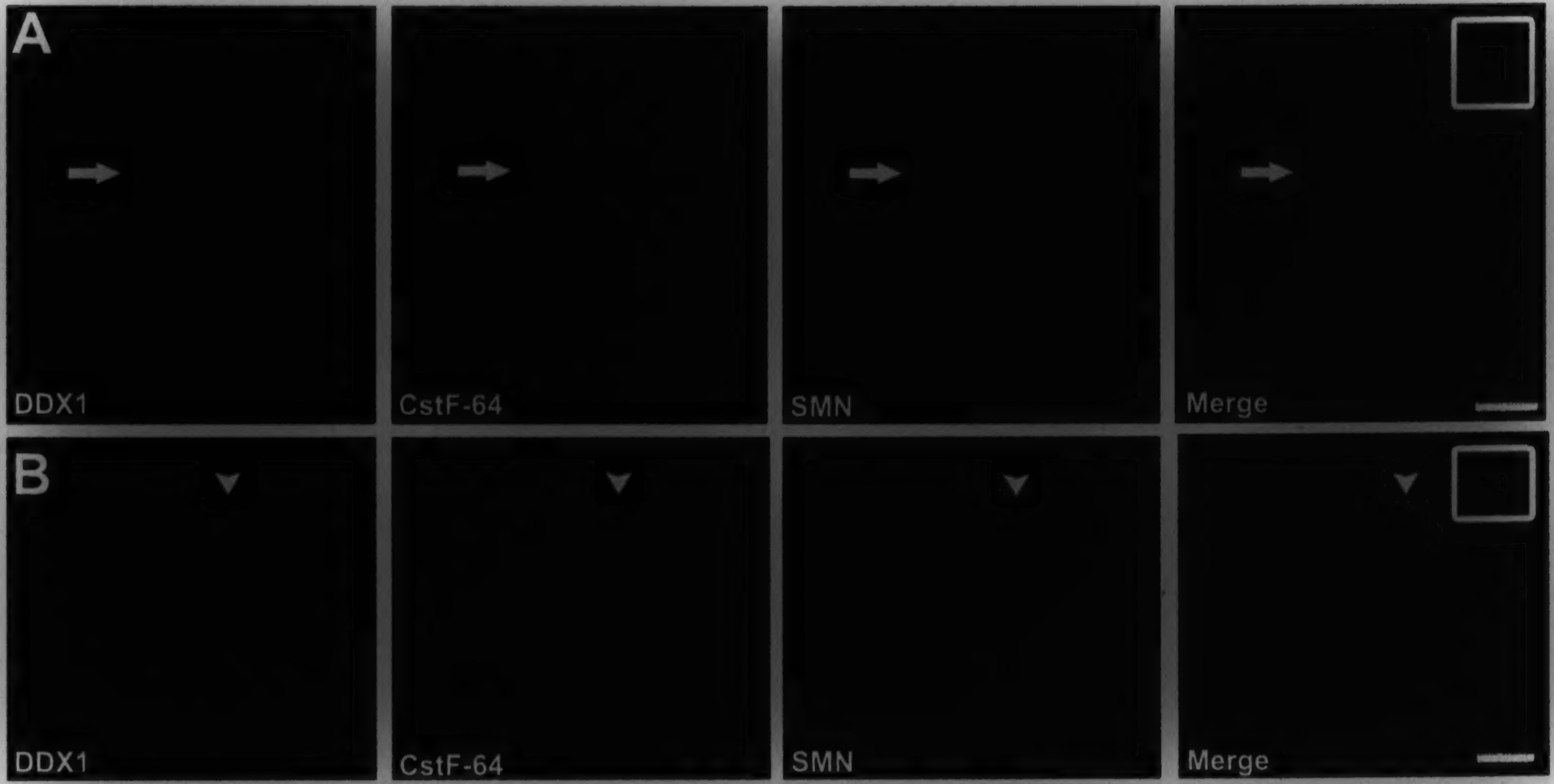
A
DDX1
CstF-64
SMN
Merge
B
DDX1
CstF-64
SMN
Merge

Fig. 5.6 Triple labeling of DDX1 foci, cleavage bodies, and gems in HeLa cells.

A. The most frequent association between DDX1 foci, cleavage bodies and gems was the colocalization of all three foci. **B.** Many of the cells also displayed the colocalization of DDX1 foci and cleavage bodies which were adjacent to gems. The foci depicted by the arrow (**A**) and arrowhead (**B**) are enlarged in the insets. The bar represents 5 µm.

Table 5.4 Configurations of cleavage bodies (ClvgBds), gems, and Cajal bodies (CBs) in triple-labeled HeLa cells.

Nuclear Body (NB)	avg. # of NBs per cell[a]	% Gems coloc. with ClvgBds	% Gems coloc. with ClvgBds & adj. to CBs	% Gems coloc. with CBs	% Gems coloc. with CBs & adj. to ClvgBds	% ClvgBds coloc. with CBs	% ClvgBds adj. to CBs	% All 3 coloc.	% All 3 Adj.
Cleavage Bodies	5.5	9.4	4.7	N/A	12.9	4.7	10.6	8.2	1.2
Gems	4.3	6.5	3.3	55.3	8.9	N/A	N/A	5.7	0.8
CBs	4.8	N/A	2.8	48.2	7.8	2.8	6.4	5.0	0.7

[a] A total of 26 cells were three-dimensionally reconstructed and analysed.

Fig. 5.7 Triple labeling of cleavage bodies, gems, and CBs in HeLa cells. HeLa cells were labeled using anti-CstF-64 (cleavage bodies), anti-SMN (gems), and anti-p80 coilin (CBs) antibodies. **A.** The most frequent relationship between all three foci was gems and CBs colocalizing adjacent to cleavage bodies (arrowhead). **B.** The next most common association between all three foci was complete colocalization (arrow). **C.** In one nucleus (out of 26) we observed all three foci located adjacent to one another (yellow arrowhead). This was best visualized upon three-dimensional reconstruction and rotation of the cell. The inset represents the enlarged foci from the three-dimensionally reconstructed cell that has been rotated on the X-axis. The bar represents 5 μm.

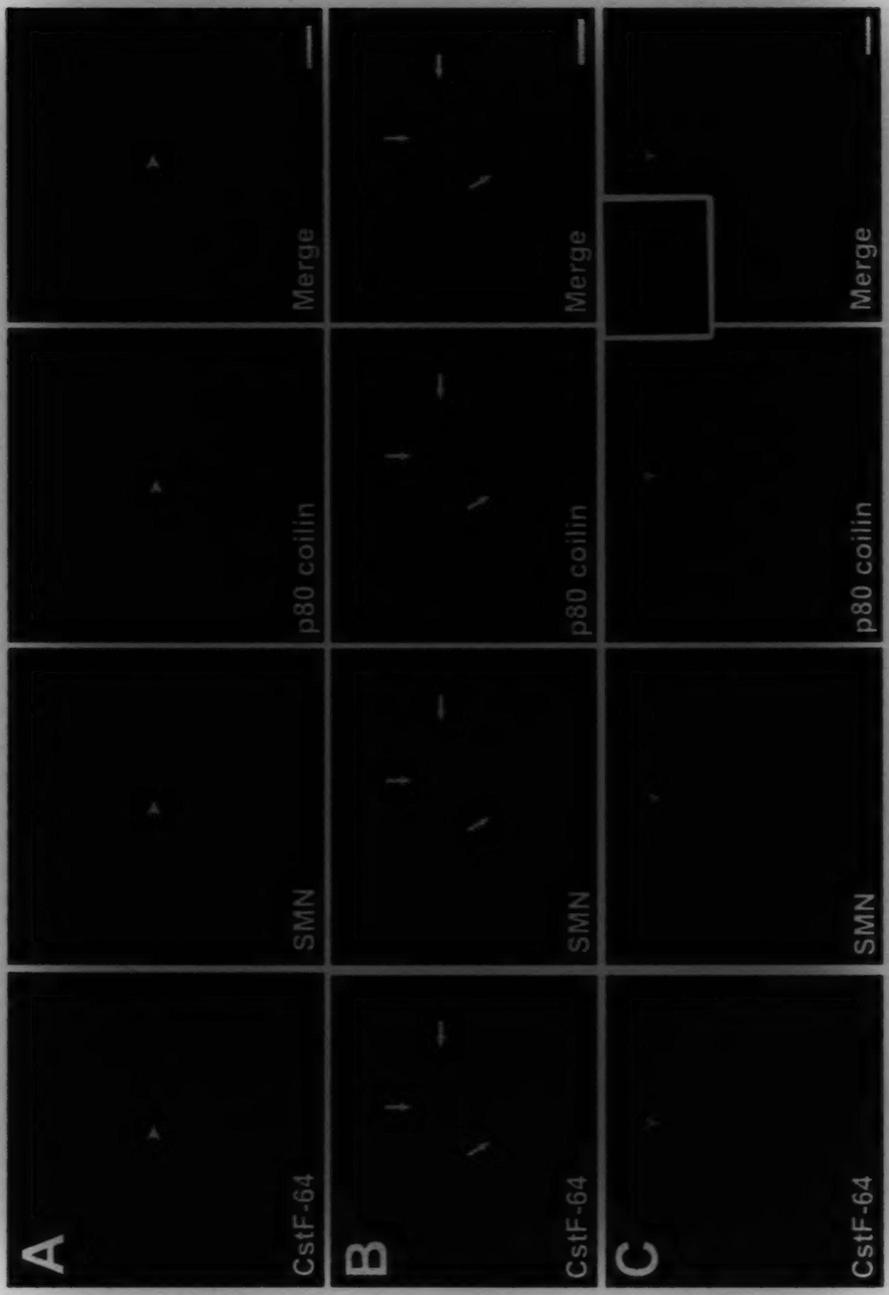
A
CstF-64
SMN
p80 coilin
Merge
B
CstF-64
SMN
p80 coilin
Merge
C
CstF-64
SMN
p80 coilin
Merge

5.5 Relationship between DDX1 foci, cleavage bodies and gems in HeLaPV

It has been noted by many that HeLaPV, which was the cell line originally used to characterize gems (Liu and Dreyfuss, 1996), is substantially different from other HeLa cell lines. In this cell line, gems frequently reside adjacent to CBs. Therefore, we obtained this cell line from Dr. Gideon Dreyfuss (University of Pennsylvania School of Medicine, Philadelphia, Pennsylvania) to examine the relationship of gems to cleavage bodies and DDX1 foci. Double labeling of HeLaPV with anti-SMN and anti-DDX1 antibodies revealed that DDX1 rarely colocalized with SMN (only one nucleus out of 19 had one colocalizing focus; this corresponds to 0.9% of DDX1 foci and 1% of gems). Additionally, there were fewer DDX1 foci localized adjacent to gems compared to previous results obtained with our HeLaST cell line (Table 5.5). Similar results were obtained with cleavage bodies where 2 nuclei out of 21 contained foci that colocalized (this corresponds to ~9% of cleavage bodies and 5% of gems) (Table 5.5). Approximately 14% of cleavage bodies localized adjacent to gems in HeLaPV compared to 19% in our HeLa cell line (Table 5.5). Therefore, although gems can merge with either DDX1 foci or cleavage bodies in HeLaPV, the event is less common than in our HeLa cell line.

Table 5.5 Nuclear localization of SMN-containing gems with respect to DDX1 foci and CstF-64 containing cleavage bodies in HeLaPV.

Nuclear Body (NB)	avg. # of NBs per cell[a]	% Coloc.	% Partial coloc.	% adjacent
DDX1 foci[c]	5.8	0.9	1.8	19.8
Gems[c]	5.2	1	2.0	22.2
Cleavage bodies[d]	1.8	8.6	0.0	14.3
Gems[e]	3	5	0.0	8.3

[a] For both data sets, a total of 20 cells were three-dimensionally reconstructed and analysed.

[b] Data from this row represent the percentage of DDX1 foci localizing with gems.

[c] Data from this row represent the percentage of gems localizing with DDX1 foci.

[d] Data from this row represent the percentage of cleavage bodies localizing with gems.

[e] Data from this row represent the percentage of gems localizing with cleavage bodies.

5.6 Summary: Gems appear to be dynamic structures with the capacity to colocalize with CBs, DDX1 foci or cleavage bodies

Gems are nuclear structures that have received extensive attention as they were reported to contain the protein responsible for spinal muscular atrophy, SMN (Liu and Dreyfuss, 1996). Gems frequently localize to CBs in most cell lines (Carvalho *et al.*, 1999); however, in HeLaPV, they exist as independent structures often adjacent to CBs. Examination of a few HeLa cell lines revealed that the localization of gems was inconsistent from cell line to cell line. Using a HeLa cell line cultured in another laboratory (HeLaLE), we observed that 59.4% of DDX1 foci colocalized with gems, yet a number of months later using another source of HeLa cells (HeLaST) we saw 35.3% of DDX1 foci colocalized with gems. Another vial of these same HeLaST cells were thawed some time later only to reveal that 10.9% of DDX1 foci merged with gems. We attempted to discern whether culture conditions could mediate these changing patterns. Of all the conditions tested: altering the serum lot, using freshly thawed cells, using a higher passage of cells, altering the confluency of the cells, altering the carbon dioxide percentage in the incubator, using media with a slightly different pH, or adding fresh L-glutamine to the media, none appeared to make any difference in terms of DDX1 foci and gem localization. It therefore is likely that there exists differences in HeLa cells from laboratory to laboratory (as was already made apparent from the observations by Carvalho *et al.*, 1999). Other variables that we did not control for were confluency of plating (cells were used over a range of confluency from 40-70%) and passage number of cells when used. It is possible that alterations in confluency and as well cell passage number contribute to nuclear body variability as we also observed up to 20% variability in associations of other nuclear bodies such as DDX1 foci and CBs or DDX1 foci and cleavage bodies. In hindsight, we did notice some variation in the growth rate of HeLaST depending on whether the cells were freshly thawed or well-established; however, at the time we did not correlate the growth properties with changes in nuclear body associations.

The colocalization of DDX1 foci and gems suggests a common function for both structures. The following two scenarios could explain the alteration in nuclear organization: i) the two nuclear bodies coexist transiently for different lengths of time depending on culture conditions, or ii) the nuclear bodies merge to perform a specific function (such as the processing of a specific transcript), and therefore the frequency of foci colocalization depends on the cellular requirement for the particular function. We attempted to distinguish between these two possibilities using GFP-tagged proteins; however, transient transfections of either GFP-SMN or GFP-DDX1 did not result in proper targeting within the nucleus. It is possible that stable transfectants of both constructs may display normal nuclear architecture.

The co-immunoprecipitation of SMN by anti-DDX1 antibody suggests that DDX1 exists within the SMN complex. The lack of DDX1 immunoprecipitation by anti-SMN antibody could result from a disruption of the protein complex following antibody binding. We used an antibody generated to the amino terminus of SMN. Therefore, it would be interesting to try the antibody to the carboxy terminus available from Santa Cruz Biotechnology. This antibody may not alter the conformation of the SMN protein thereby permitting co-immunoprecipitation of DDX1. Although SMN has been shown to be involved in splicing, *in vitro* splicing assays done in collaboration with Dr. Benoit Chabot (University of Sherbrooke, Sherbrooke, Quebec) have not implicated DDX1 in the splicing process (unpublished data). To explain the association of DDX1 with SMN, we are hypothesizing that SMN may also be involved in 3'end pre-mRNA processing, similar to the splicing factor SRm160 (McCracken *et al.*, 2002). As all transcriptional processes are emerging as integrated events, it is likely that proteins previously assigned one particular function may actually couple co-transcriptional processing.

The frequent colocalization of DDX1 foci with cleavage bodies and gems led us to investigate the relationship between gems and cleavage bodies. An unpublished observation by Gall (2000) stated that cleavage bodies and gems were not identical in HeLaPV. Nonetheless, we wished to determine whether our HeLaST cell line, which had gems that colocalized with DDX1 foci, contained nuclear bodies that contained both CstF-64 and SMN protein. In these experiments, our HeLaST cells displayed even fewer DDX1 foci that colocalized with gems (10.9%) than we had previously observed (59.4% in HeLaLE and 34.8% in HeLaST). Despite this lower frequency of colocalization we did find that 14.7% of cleavage bodies colocalized with gems. Attempts to immunoprecipitate CstF-64 with SMN were not successful; however, we did not attempt the reverse immunoprecipitation. Additionally, it is quite possible that if SMN is involved in 3'-

end processing, it could interact with other components of the 3'-end processing machinery, such as CPSF or PAP. A precedent for splicing factors interacting with 3'-end processing components is the splicing factor SRm160, which was found to interact with CPSF (McCracken *et al.*, 2002). This interaction likely explains the stimulatory effect of SRm160 on 3'-end cleavage.

Triple labeling our HeLa cells with anti-CstF-64, anti-DDX1 and anti-SMN antibodies revealed a multitude of arrangements further supporting the hypothesis that these nuclear bodies are dynamic structures with the capacity to alter their nuclear location. The plethora of associations could represent functional heterogeneity between subsets of nuclear bodies, or, the distinct patterns of associations could represent the processing of specific transcripts or classes of RNA. It appears from our data that not all gems contain CstF-64 or DDX1 and vice versa. This variable protein content could indicate that the foci are serving different functions at various times. In order to study this hypothesis we could examine the flux of protein in and out of these structures using GFP-expression constructs. It might be expected that a nuclear structure not actively involved in a nuclear process would contain proteins that are fairly static, while nuclear bodies active in a nuclear process would maintain a constant flux of proteins. Comparing the kinetics of a protein in a nuclear body that exists independently vs. the kinetics of that same protein in a nuclear body affiliated with other nuclear bodies using FRAP (fluorescence recovery after photobleaching) or FLIP (fluorescence loss in photobleaching) may reveal differences indicative of a functional diversity in this nuclear body subset.

Regardless, the data above support the existence of gems, cleavage bodies, DDX1 foci and CBs as distinct nuclear bodies. The finding that a percentage of these nuclear bodies can colocalize suggests that proteins in each structure can interact and are possibly involved in similar processes.

Chapter 6. Localizing cytoplasmic DDX1

While examining the nuclear location of DDX1 we noticed that DDX1 was also present in the cytoplasm in a pattern that was slightly filamentous. It is known that fixation with organic solvents washes away soluble molecules thereby exposing the underlying cellular architecture; in contrast fixation with formaldehydes cross-links free amino groups creating an intact and localized molecular network (Harlow and Lane, 1998). To examine the nature of DDX1 with respect to the cellular architecture we altered our fixation method from paraformaldehyde to methanol:acetone. The filamentous nature of DDX1 became even more apparent under such conditions. Therefore, in an attempt to examine the cytoplasmic location of DDX1 we began examining structures that were filamentous in nature and part of the cellular architecture within the cytoplasm.

Of primary interest were components of the cytoskeleton, a structural network extending from the nuclear lamina to the plasma membrane. The cytoskeleton is composed of at least three types of filaments including microtubules, microfilaments, and intermediate filaments. Microtubules, composed of α/β-tubulin heterodimers, are filaments that affect cell shape, cell transport of organelles/RNA/proteins, cell polarity, cell motility, and cell division (reviewed in Valiron *et al.*, 2001). Actin polymers make up the microfilaments and these are involved in many cellular processes such as assisting in protein and RNA transport, affecting ion transporters, and regulating cell shape and volume. Finally, intermediate filaments fall into six classes based on the composition of their chains. Each type of chain is expressed in specific cell types such as the type Ib and IIb cytokeratins, which are found in epithelia, or the type III vimentin which is found in mesenchymal cells (reviewed in Parry and Steinert, 1999). The primary role for intermediate filaments is to provide mechanical integrity to cells and tissues, although many intermediate filaments perform cell-type specific functions as well.

With respect to mRNA, the cytoskeleton is speculated to provide 'tracks' for proper mRNA subcellular localization. Theoretically, since a transcript can be used for many rounds of translation, it would be energy efficient for a cell to transport the mRNA to the site of protein requirement rather than transport the proteins themselves. This rationale has been proven valid: mRNA is targeted to its appropriate site of translation, with some transcripts enduring translational repression while enroute (reviewed in: Hovland *et al.*, 1996; Lipshitz and Smibert, 2000; Palacios and Johnston, 2001). Therefore, the strong association between the cytoskeleton and mRNA led us to hypothesize that DDX1 may colocalize to some cytoskeletal components.

To test this hypothesis we attempted to localize DDX1 to the above cytoskeletal components and subsequently, began investigating the possibility of DDX1 localizing to specific cytoplasmic organelles. Therefore the objectives of this project were:

a) to examine the location of cytoplasmic DDX1 with respect to microtubules, microfilaments, and intermediate filaments. These experiments made use of cells double-labeled with antibodies directed against proteins to the above filaments as well as anti-DDX1 antibody. The cells were visualized by confocal microscopy.

b) to examine for DDX1 localization with mitochondria. These experiments involved labeling mitochondria with either anti-cytochrome *c* oxidase subunit I antibody or MitoTracker red and labeling DDX1 protein with anti-DDX1 antibody. The cells were visualized by confocal microscopy.

c) to examine the nature of cytoplasmic GFP-DDX1 localization. These experiments involved cloning DDX1 cDNA into a GFP plasmid and transfecting the GFP-DDX1 plasmid into HeLa cells. To identify mitochondria, cells were incubated with MitoTracker red.

d) to determine whether DDX1 is found in or in close proximity to mitochondria. These experiments involved cell fractionation to purify mitochondria. Identification of DDX1 in the mitochondrial fraction was achieved by Western blot analysis. To define whether DDX1 is in close proximity to mitochondria *in vivo*, fluorescence lifetime imaging microscopy (FLIM) was performed using fixed cells labeled for DDX1 and mitochondria.

e) to examine the cytoplasmic DDX1 pattern in relation to ribosomal location. These experiments involved labeling cells for DDX1, using anti-DDX1 antibody, and ribosomes, using an antibody directed against a ribosome-specific kinase.

6.1 Frequent colocalization of DDX1 with microtubules

The cytoplasmic distribution of DDX1 was examined using anti-DDX1 antiserum (2923) on HeLa cells fixed in -20°C methanol:acetone. Fig. 6.1 demonstrates that DDX1 forms a filamentous pattern in the cytoplasm with little signal found in the nucleus. To investigate the nature of this filamentous pattern cells were double-labeled with DDX1 antibody and antibodies to various components of the cytoskeleton. Fig. 6.1A,B demonstrates that by confocal microscopy DDX1 rarely colocalizes with either cytokeratin or vimentin. Labeling cells with anti-actin antibodies revealed that DDX1 sometimes colocalized with actin (arrows, Fig. 6.1C); however, the pattern most similar to DDX1 was observed using antibodies to α-tubulin (Fig. 6.1D). Although there were areas in which colocalization was observed (arrows), DDX1 appeared to generally follow alongside microtubule tracks.

6.2. Localization of DDX1 to mitochondria

The nature of DDX1 staining observed in combination with microtubule staining was reminiscent of a mitochondrial arrangement. Furthermore, a number of organelles have previously been shown to follow along microtubules. Therefore, we used both anti-cytochrome *c* oxidase subunit I antibody and MitoTracker red to label HeLa mitochondria. Double-labeling of cytochrome *c* oxidase subunit I and DDX1 revealed nearly complete colocalization (Fig. 6.2A). These results were confirmed by analysing cells that had been incubated in MitoTracker red prior to fixation and labeling with anti-DDX1 antibody (Fig. 6.2B).

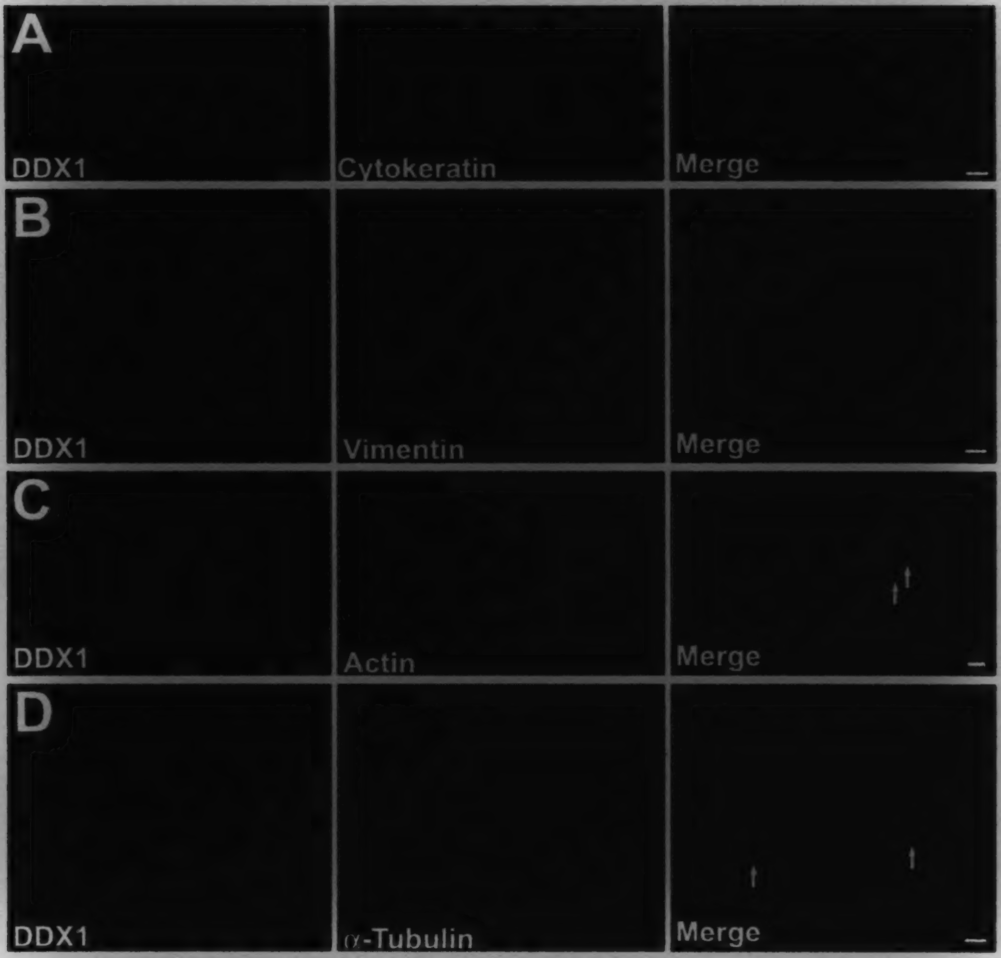
A
DDX1
Cytokeratin
Merge
B
DDX1
Vimentin
Merge
C
DDX1
Actin
Merge
D
DDX1
α-Tubulin
Merge

Fig. 6.1 Localization of DDX1 in relation to cytoskeletal components. HeLa cells were fixed in -20°C methanol:acetone followed by labeling using anti-DDX1 antibody and either **A** anti-cytokeratin, **B** anti-vimentin, **C** anti-actin, or **D** anti-α-tubulin antibodies. The cells were viewed by confocal microscopy and the above pictures represent a 0.2 µm section. The arrows indicate examples of colocalized areas. The bars represent 5 µm.

A
DDX1
Cytochrome C Oxidase
Merge
B
DDX1
MitoTracker
Merge

Fig. 6.2 Localization of DDX1 to mitochondrial regions.

A. HeLa cells were fixed in -20°C methanol:acetone and labeled using anti-DDX1 antibody and anti-cytochrome *c* oxidase subunit I antibody. **B.** HeLa cells were incubated in 250 nM MitoTracker red for 30 min prior to fixing (as above) and labeling with anti-DDX1 antibody. The bars represents 5 µm.

6.3 GFP-DDX1 expression coincides with mitochondria

In order to examine the location of DDX1 in living cells, we cloned DDX1 cDNA downstream of GFP using the pEGFP-C1 vector. This construct places GFP on the amino terminal end of DDX1. HeLa cells were then transfected with the GFP-DDX1 construct and 24 hrs later the cells examined by confocal microscopy. Fig. 6.3A demonstrates that some HeLa cells expressing GFP-DDX1 have a filamentous pattern similar to the pattern observed with cells that have been fixed and labeled with anti-DDX1 antibody. Although GFP-tagged proteins tend to be overexpressed and often do not correctly localize, the observation that both organically fixed cells which have been labeled with DDX1 antibody and cells transiently transfected with GFP-DDX1 localize to mitochondrial areas suggests that the GFP-DDX1 protein is localizing properly in the cytoplasm. It will be necessary to repeat such experiments with stably transfected constructs. Transient transfection of GFP alone did not produce a filamentous pattern (Fig. 6.3B). To ensure that GFP-DDX1 was properly expressed, we fractionated HeLa cells into cytoplasmic and nuclear fractions and subjected samples to Western blot analysis. Fig. 6.3C demonstrates that at 12, 24 and 48 hrs after transfection DDX1 antibody detected endogenous DDX1 at ~90 kDa and GFP-DDX1 at ~120 kDa. To determine whether the GFP-DDX1 signal coincided with mitochondria, we added MitoTracker red to HeLa cells that had been transfected 24 hrs prior with GFP-DDX1. Examination of the cells 30 min after exposure to MitoTracker red revealed that GFP-DDX1 colocalized with mitochondria (Fig. 6.4A). Treatment of these cells with 10 μM nocodazole

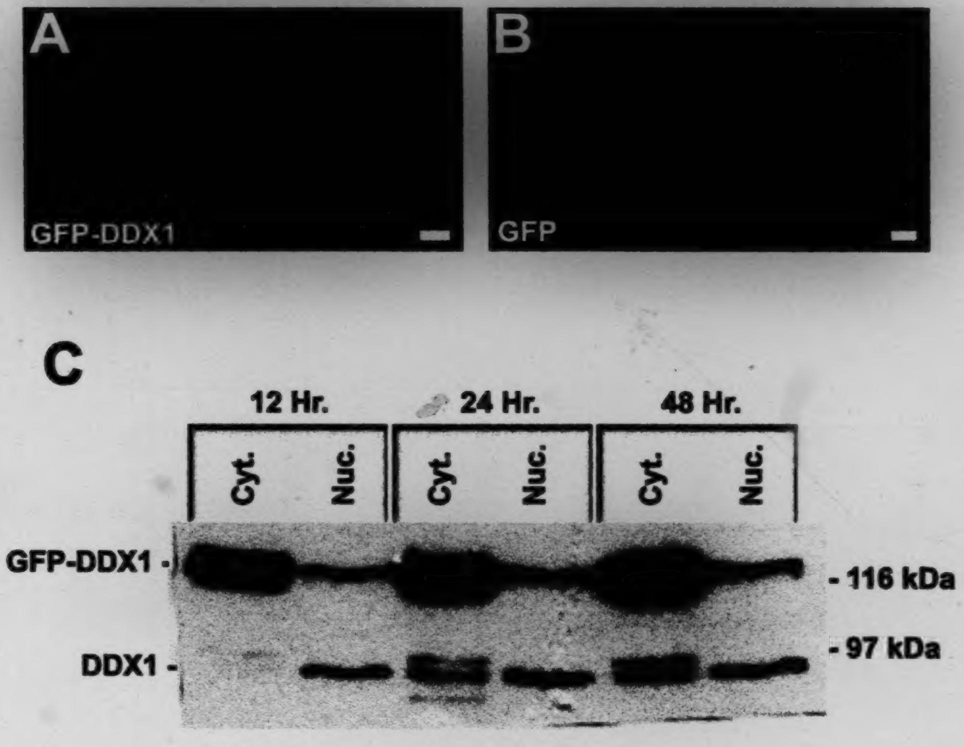
A
GFP-DDX1
B
GFP
C
12 Hr.
24 Hr.
48 Hr.
Cyt.
Nuc.
Cyt.
Nuc.
Cyt.
Nuc.
GFP-DDX1 -
DDX1 -
- 116 kDa
- 97 kDa

Fig.6.3 Filamentous pattern of GFP-DDX1.

A. HeLa cells transfected with GFP-DDX1 demonstrate a filamentous pattern. **B.** HeLa cells transfected with GFP lack an organized pattern. **C.** Western blot analysis of GFP-DDX1 at 12 hr, 24 hr, and 48 hr after transfection demonstrates endogenous DDX1 at ~90 kDa and GFP-DDX1 at ~120 kDa. The images were collected by confocal microscopy, and the bars in **A** and **B** represent 5 µm.

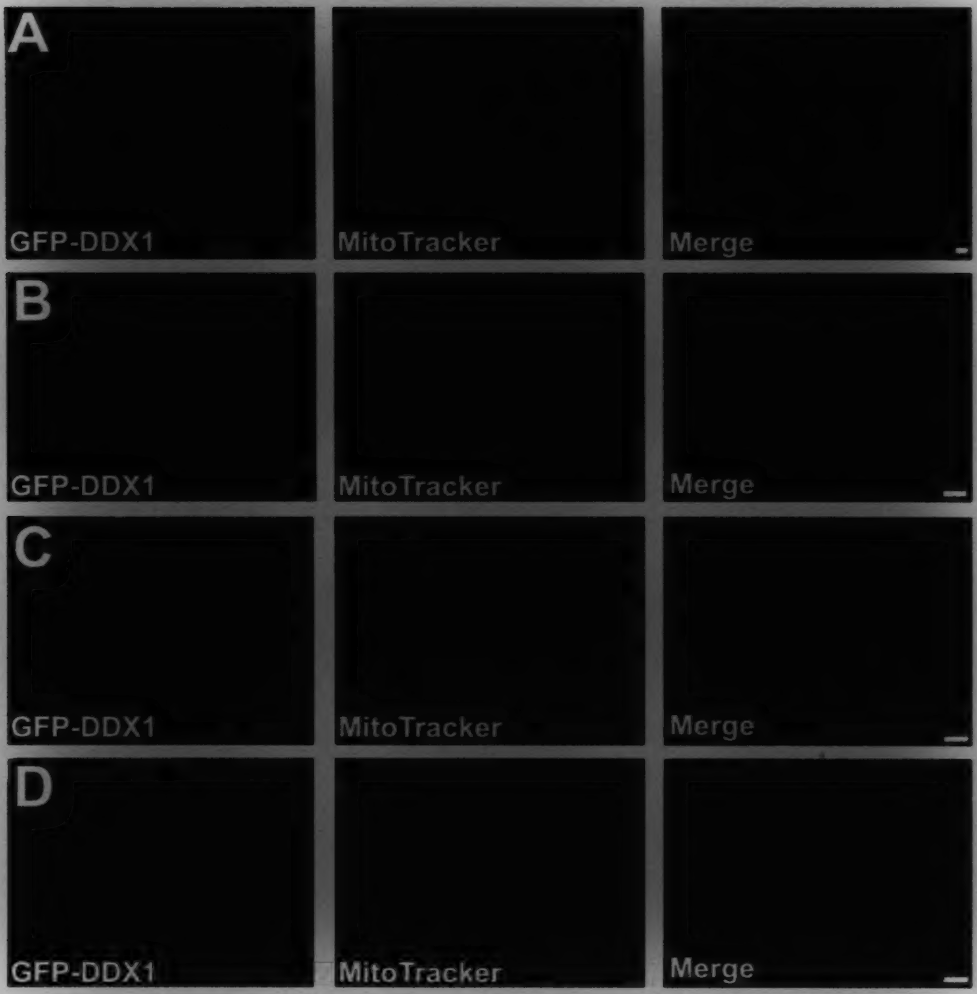
A
GFP-DDX1
MitoTracker
Merge
B
GFP-DDX1
MitoTracker
Merge
C
GFP-DDX1
MitoTracker
Merge
D
GFP-DDX1
MitoTracker
Merge

Fig. 6.4 Localization of GFP-DDX1 to mitochondrial regions.

HeLa cells expressing GFP-DDX1 were incubated in 250 nM MitoTracker red for 30 min. prior to visualization. **A.** GFP-DDX1 colocalizes with MitoTracker red. **B-D**. Ten µm nocodazole was added to HeLa cells and images were collected after 0 min. (**B**), 3 min. (**C**), and 6 min. (**D**). The bars represent 5 µm.

caused the mitochondria and DDX1 to compact within minutes of drug addition (Fig. 6.4B-D); however, it should be noted that since nocodazole is a microtubule destablizer, localization of DDX1 to either mitochondria or microtubules would produce a change in structure.

6.4 DDX1 localizes to the vicinity of the mitochondria

Analysis of DDX1 protein sequence by MitoProt, a program that searches amino-terminal protein sequence for a positively charged mitochondrial targeting peptide (Claros and Vincens, 1996), revealed that the probability of DDX1 localizing to the mitochondria was 0.20. Nonetheless, although there was no sequence support for the localization of DDX1 to mitochondria, the confocal microscopy images were persuasive. Therefore to exclude the localization of DDX1 to the mitochondria, we purified mitochondria from HeLa cells using sucrose density gradient centrifugation. Fig. 6.5 demonstrates that DDX1 is not detected in purified mitochondria (bottom sucrose fraction). The fraction containing purified mitochondria did contain cytochrome *c* oxidase subunit I (Fig. 6.5, top sucrose fraction). Interestingly, DDX1 was found in the same fraction as ribosomes (Fig. 6.5, middle sucrose fraction).

As cytochrome *c* oxidase subunit I is found in the inner membrane of the mitochondria, it is still conceivable that DDX1 could be located in the outer mitochondrial membrane (which could have been removed during our fractionation procedure). Alternatively, it is possible that DDX1 associates with proteins in the outer mitochondrial membrane and therefore is located in close

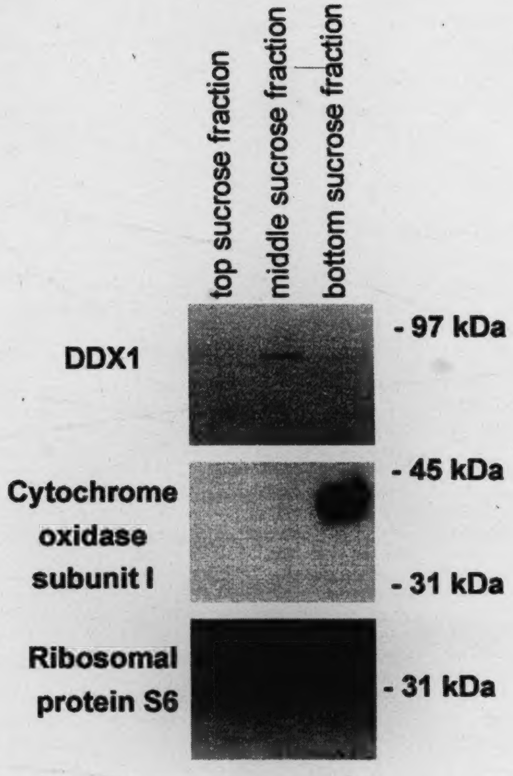
top sucrose fraction
middle sucrose fraction
bottom sucrose fraction
DDX1
- 97 kDa
Cytochrome oxidase subunit I
- 45 kDa
- 31 kDa
Ribosomal protein S6
- 31 kDa

Fig. 6.5 DDX1 is not found within purified mitochondria. Mitochondria were purified over a sucrose cushion (found in bottom sucrose fraction). Western blot analysis of all three sucrose fractions indicate that DDX1 resides in the middle sucrose fraction (top panel), which is the same fraction that contains ribosomal protein S6 (bottom panel). Detection of cytochrome *c* oxidase subunit I verifies that mitochondria are present only in the bottom sucrose fraction (middle panel). The molecular weight markers are indicated on the right.

proximity to mitochondria. To provide evidence for such associations, we performed FRET analysis using fluorescence lifetime imaging microscopy (FLIM). This technique detects FRET (which occurs when two molecules exist within the Förster 10 nm distance) by evaluating the donor fluorescent lifetime. A donor which exhibits FRET will have a shorter fluorescent lifetime than does a donor which does not exhibit FRET. This decrease in fluorescent lifetime is due to the transfer of energy to a nearby acceptor molecule. The use of secondary antibodies in these experiments does increase the FRET distance beyond 10 nm; however, even with such labeling the occurrence of FRET still represents a considerable improvement in resolution when compared to the resolution of light microscopy alone.

These experiments were performed on a Zeiss 510 laser scanning confocal microscope equipped with a time-correlated single photon counting system. Briefly, using a femtosecond pulsing laser this module detects the number of photons emitted from the fluorescent molecule and times their arrival. Using this information, the computer builds a decay curve consisting of the number of photons vs. their time of arrival. The software then applies an algorithm to the information from the decay curve to calculate the average fluorescent lifetime of the molecule for each pixel. Using this technique, we compared the fluorescent lifetime of Alexa 488-labeled cytochrome *c* oxidase subunit I to the lifetime of Alexa 488-labeled cytochrome *c* oxidase subunit I in the presence of DDX1 labeled with Cy3 (Fig. 6.6A). Calculations done with 4 images of cells labeled with cytochrome *c* oxidase subunit I antibody resulted in

Fig. 6.6 DDX1 and cytochrome oxidase subunit 1 undergo FRET in HeLa cells.

A. HeLa cells were indirectly labeled with anti-cytochrome *c* oxidase subunit I antibody plus secondary antibody conjugated to Alexa 488 or anti-cytochrome *c* oxidase subunit I antibody (plus Alexa 488 secondary antibody) in the presence of anti-DDX1 antibody plus secondary antibody conjugated to Cy3. The average fluorescent lifetime of Alexa 488 was calculated by the computer based on a decay curve, which consists of the number of photons detected vs. their time of arrival. **B.** An example of a decay curve. The average fluorescent lifetime of the Alexa 488 molecules shifted from 2.91 ns to 2.76 ns in the presence of Cy3 labeled DDX1. **C.** A colour overlay representative of the average fluorescent lifetimes of all the pixels in a cell double-labeled for cytochrome *c* oxidase subunit I and DDX1. The red pixels represent fluorescent lifetimes <1.2 ns while the blue pixels represent fluorescent lifetimes of >5.0 ns (as depicted in inset).

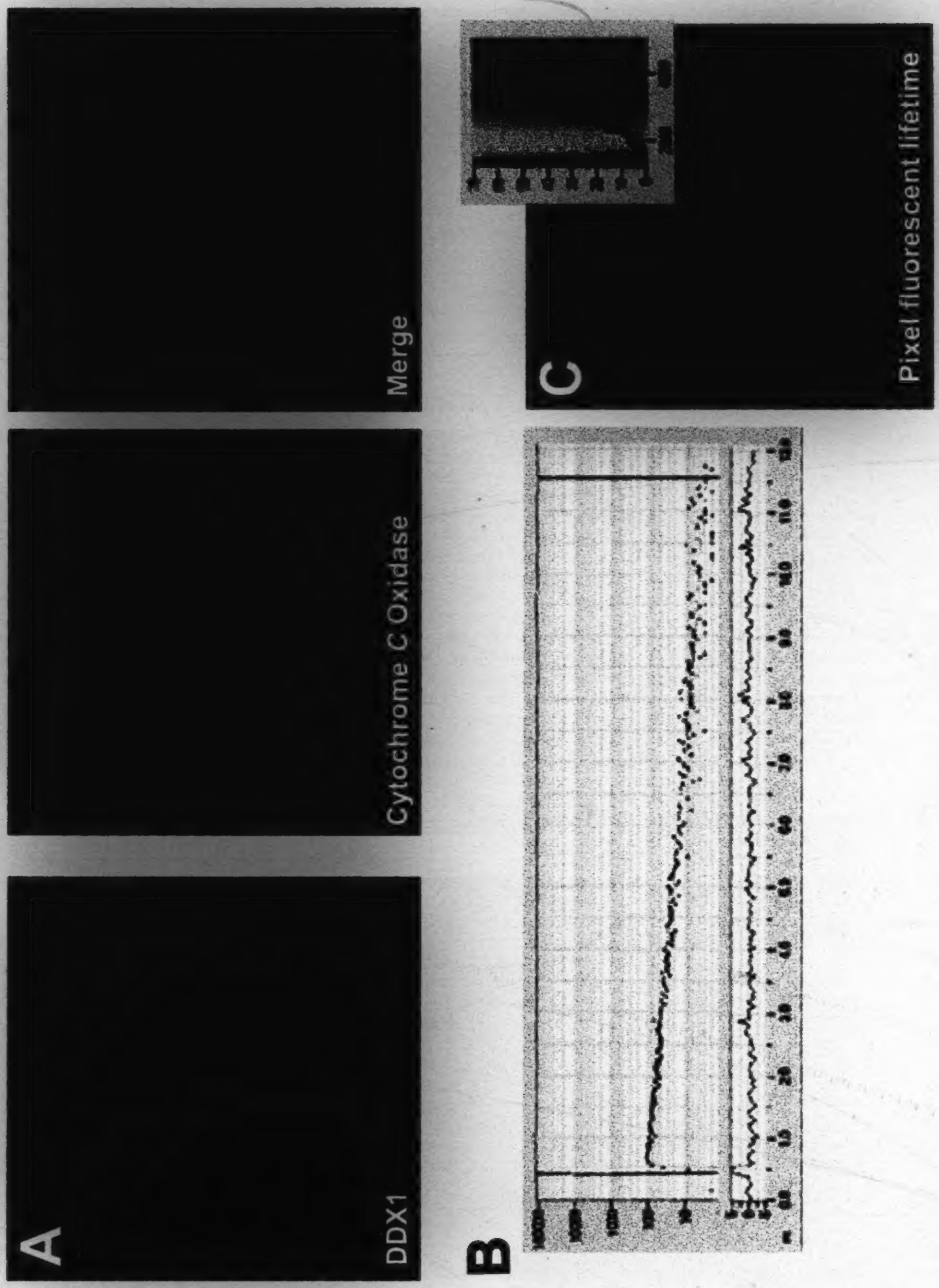
A
DDX1
Cytochrome C Oxidase
Merge
B
C
Pixel fluorescent lifetime

an Alexa 488 average fluorescent lifetime of 2.91 ns. In the presence of Cy3-labeled DDX1, the fluorescent lifetime of Alexa 488 was shortened by 0.15 ns, averaging 2.76 ns. The numbers from the analysis of the 8 cells (4 single-labeled cells and 4 double-labeled cells) were subjected to a paired student's t test. The p value was 0.002 indicating that we obtained a significant difference between the two populations. These results are preliminary and require verification; however, it is not unexpected that the shift in the fluorescent lifetime of Alexa 488 is minimal as Alexa 488 is a stable fluorophore which, consequently, exists in the excited state for short periods of time (as compared to FITC, for example). Fig. 6.6B demonstrates a decay curve used to calculate the fluorescent lifetime of Alexa 488. The image in Fig. 6.6C is a colour overlay representing the fluorescent lifetimes of all the pixels in a double-labeled cell. The red colour represents shorter fluorescent lifetimes (<1.2 ns) and at the far end of the spectrum, blue represents >5.0 ns (see inset on Fig. 6.6C). Thus, the red coloured pixels depict the areas where DDX1 is most likely in close proximity to the mitochondria.

6.5 Comparing the cytoplasmic signal of DDX1 with the location of polyribosomes

Biochemically, polyribosomes can be separated into three distinct fractions: cytoskeletal-bound, membrane-bound, and free using a sequential detergent/salt extraction (reviewed in Hovland *et al.*, 1996). The localization of DDX1 to some cytoskeletal structures and association with mitochondria regions led us to explore whether DDX1 may colocalize to areas along the mitochondria enriched in polyribosomes. To do so, we double-labeled HeLa cells with antibody to ribosomal protein S6 as well as DDX1 antibody. Fig. 6.7 demonstrates that many areas within the cytoplasm contain polyribosomes that colocalize with DDX1 (arrows). This colocalization was not as extensive as was seen for the mitochondria, nonetheless, DDX1 does appear to locate to sites of translation.

6.6 Summary: DDX1 appears to localize to mitochondrial areas

Upon organic fixation, DDX1 appeared to extend in a filamentous pattern from the nuclear lamina to the cell membrane. Double-labeling of DDX1 with cytoskeletal filaments suggested that this signal appeared to closely follow and sometimes overlap with microtubules and occasionally actin. As the resolution of the confocal microscope is at best ~250 nm, proteins which appear adjacent may in fact be far apart, therefore, to make a definitive conclusion about the relationship between DDX1 and various cytoskeletal components, it is essential that the above experiments be repeated using electron microscopy. With this in mind, the potential localization of DDX1 to cytoskeletal areas could be a reflection of DDX1 translation prior to nuclear import as transcripts encoding nuclear proteins are translated on the cytoskeleton (Hovland *et al.*, 1996). Alternatively, DDX1 could be involved in escorting mRNA transcripts to their sites of translation. In support of this latter hypothesis, treatment of HeLa cells with 100 μg/ml cycloheximide did not produce any discernible effects with regards to

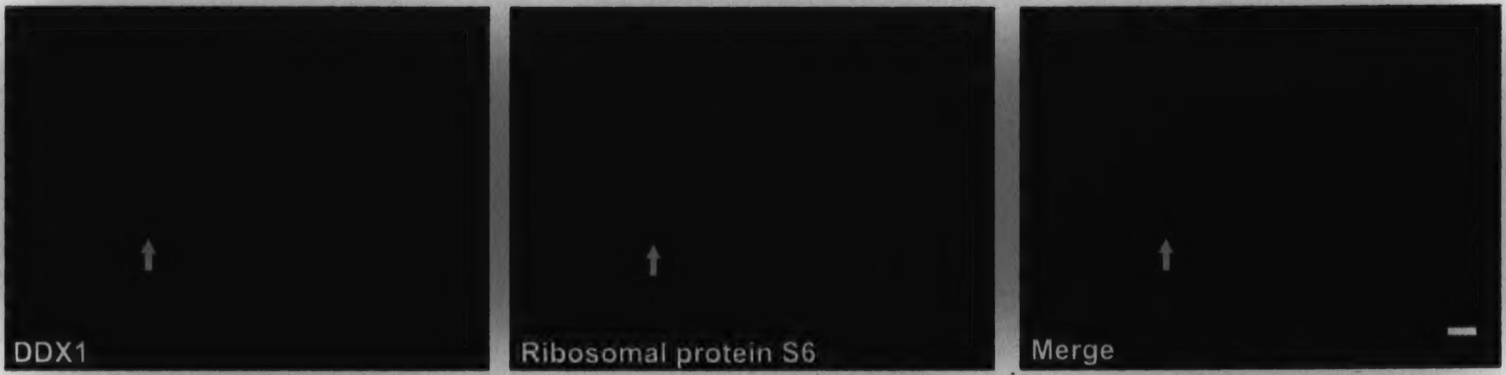

Fig. 6.7 Localization of DDX1 to areas that contain ribosomes.

HeLa cells were fixed in -20°C methanol:acetone and were then double-labeled with antibodies against DDX1 and ribosomal protein S6. The areas of colocalization are indicated by the yellow pixels in the merged image. The arrow is an example of one area demonstrating colocalization. The bar represents 5 µm.

DDX1 cytoplasmic signal (data not shown). This finding alone, however, is difficult to interpret, as we do not know the half-life of DDX1 protein. To prove that DDX1 mRNA is translated on cytoskeletal-bound polyribosomes, it is possible to extract this specific fraction of polyribosomes and then subject this fraction to poly(A) mRNA purification subsequent to Northern blot analysis. It is highly likely that *DDX1* mRNA will be detected in this fraction, as thus far, all mRNAs examined that encode nuclear proteins have been associated as such (reviewed in Hovland *et al.*, 1996). Hovland *et al.* (1996) have hypothesized that translation of nuclear proteins occurs along the cytoskeleton as it provides a track on which finished proteins can travel to the nucleus. This finding, nevertheless, would not exclude the possibility that DDX1 could still function in the nuclear export of mRNA. The discovery that *DDX1* mRNA accumulates in a fraction other than cytoskeletal-bound would likely mean that DDX1 accumulates on these structures as a result of its export from the nucleus. It would also be possible to verify these biochemical results using *in situ* hybridization and confocal microscopy. Identifying the location of *DDX1* mRNA would reveal those areas that contain newly translated protein. Direct examination of DDX1 export would involve microinjection of labeled protein (ie. GFP-DDX1) or fluorochrome labeled anti-DDX1 antibodies into the nucleus. Detection of the fluorophore in the cytoplasm would confirm nuclear export. Alternatively, we could establish pGFP-DDX1 stable transfectants in attempts to properly localize DDX1 within the nucleus (as placing the GFP at the carboxy-terminal end of DDX1 does not produce a different pattern of localization – data not shown). Photodestruction of the cytoplasmic signal would then help to discern whether GFP-DDX1 is transported out of the nucleus.

The discovery that DDX1 colocalizes remarkably well with mitochondria is unexpected. We have not found any evidence for a mitochondrial import signal in DDX1 and purified mitochondria did not contain any DDX1 protein. Preliminary analysis by FLIM suggests that DDX1 does exist in close proximity to the mitochondria. Although this technique made use of antibodies against subunits of cytochrome *c* oxidase, an inner mitochondrial membrane protein, it remains entirely possible that FRET can be achieved with a protein that resides outside of the mitochondria (and therefore exceeds the 10 nm Förster distance). The mitochondrial membranes span a distance of 22 nm (Perkins *et al.*, 1997); however, immunoglobulins span a distance of 8-10 nm (Lutter *et al.*, 2001). Therefore, double-labeling each protein would extend our FRET capacity to a minimum of 42 nm.

As well, double-labeling HeLa cells using antibodies to DDX1 and ribosomal protein suggests that DDX1 frequently colocalizes with ribosomes; a finding that is further supported by the evidence that in a sucrose density gradient, DDX1 is found in the same fraction as ribosomes. Our only explanation for the mitochondrial association would involve DDX1 delivering nuclear encoded mRNAs whose products are destined for the mitochondria. Nearly all mitochondrial proteins are transcribed in the nucleus and consequently must undergo translation in the cytoplasm and insertion through the mitochondrial membrane (reviewed in Paschen and Neupert, 2001). The mechanism for correct mRNA targeting to the mitochondria is currently unknown; however, it has been discovered that one mRNA, *ATM1*, contains a targeting signal in its coding sequence that localizes it to the mitochondria (Corral-Debrinski *et al.*, 2000). It is thought that all mRNAs contain a targeting sequence/structure that, once recognized by the appropriate mRNA binding protein, will direct its proper localization. In order to examine for the possibility that DDX1 is escorting mRNA to the mitochondria we could immunoprecipitate DDX1, amplify the bound RNA, and then subject the cDNA products to Southern blot analysis. Probing with mitochondria-specific transcripts would determine if DDX1 was associating with these specific mRNA transcripts. Alternatively the yeast three-hybrid screening technique examines for protein-RNA interactions and would be useful in discerning DDX1 transcript preferences. Verification that DDX1 does transport nuclear encoded mitochondrial transcripts would distinguish it as the first of the proposed mRNA escort proteins.

Alternatively, it is possible that because DDX1 is an ATPase it localizes to the vicinity of the mitochondria to bind ATP. This localization may occur prior to nuclear entry after translation or upon nuclear export should DDX1 be exported from the nucleus. The attraction to pools of ATP could be passive (ie. ATP becomes a DDX1 sink) or alternatively, DDX1 may actively migrate to mitochondrial areas in order to replenish its ATP supply. Experiments which may help to distinguish the reason for DDX1 localization to mitochondrial areas include treating cells with agents such as 2,4-dinitrophenol (DNP) or CCCP, which uncouple the proton motive force causing no ATP generation. If DDX1 is associating with specific mitochondrial transcripts during nuclear export, the treatment of cells with the uncoupling agents might have no effect on this process early after drug treatment, and consequently, DDX1 would be expected to continue localizing to mitochondrial areas.

Although direct evidence for DDX1 functioning in the cytoplasm is lacking, we do predict that DDX1 will have a cytoplasmic role. We do not observe significant amounts of other nuclear proteins in the cytoplasm such as Sam68, p80 coilin, PML, CstF-64 etc., making it unlikely that DDX1 exists in the cytoplasm simply due to translation. In addition, the over-expression of DDX1 protein in retinoblastoma and neuroblastoma cell lines causes excessive cytoplasmic accumulations. The abundance of DDX1 in the cytoplasm together with its localization to mitochondrial areas points to an active role for DDX1 in the cytoplasm rather than just subsisting due to translation.

Chapter 7. Discussion

7.1 A germline heterozygous mouse has yet to be achieved for *DDX1*

Thus far we have been unsuccessful in generating a germline *DDX1+/-* mouse. With only one chimeric male mouse that produced two litters, we need to carry out additional blastocyst injections. It is possible that our R1 embryonic cells have not retained pluripotency and may not be capable of contributing to the germline. Therefore, it might be beneficial to retarget the *DDX1* allele in a different embryonic stem cell line, such as the 129/J line, which we could obtain from Dr. Nancy Dower (University of Alberta, Edmonton, Alberta). We could also consider purchasing a *DDX1+/-* R1 cell line generated by the German Genetrap Consortium (clone A003G03). These cell lines have been generated by randomly targeting a reporter/selector construct into the genome. This construct has its own splice site and therefore, regardless of the integration site, will produce a fusion transcript with the endogenous gene.

It remains possible that *DDX1-/-* mice will not be viable. In this case, we may wish to create a tissue-specific knockout using the Cre/*loxP* recombinase system (reviewed in Nagy, 2000). This system places Cre recombinase under the control of a tissue-specific promoter. The expression of Cre in the tissue of interest would then cause recombination between *loxP* sites, which would be designed to flank the targeting area within the *DDX1* gene. We would initially use a vector created by Furuta *et al.* (2000) who placed the Cre recombinase under the control of the *Six3* homeobox gene promoter. This construct is specifically expressed in a retinal and ventral forebrain-specific manner. It is hoped that with such a limited expression, potentially lethal effects by a ubiquitous *DDX1* knockout would be avoided.

The targeting of DExD/H box genes in *S. cerevisiae* has resulted in mostly lethal phenotypes (32/34) (http://www.expasy.ch/linder/RNA_helicases. html). There have been very few reports of targeted deletions in higher organisms. Knockout cell lines of two *Trypanosoma brucei* DEAD box genes, HEL64 (Missel *et al.*, 1999) and mHEL61 (Missel *et al.*, 1997), have been created in *T. brucei* cell lines. HEL64, whose function is unknown, is likely an essential gene in insect-stage trypanosomes as Missel *et al.* (1999) were unsuccessful in generating a double-allele knockout cell line. Double-allele knockout trypanosome cells involving the mHEL61 gene resulted in a reduced growth rate, and the cells displayed reduced amounts of RNA editing. RNA editing is a process occurring in some protozoa that involves the removal and insertion of uridylates to complete the mRNA. Further to these knockouts, a fortuitous double allele knockout of *DDX1* in *Drosophilia* also resulted in lethality (Zinsmaier *et al.*, 1994). Therefore, considering the role for DEAD box proteins in all aspects of RNA metabolism it would not be unexpected that these genes will prove essential in many instances. It is our hope that even if *DDX1* knockout mice are lethal, we will be able to recover embryos at early stages of development to assess the consequences of inactivating this gene.

7.2 Nuclear bodies – storage or function?

One controversial aspect of nuclear bodies involves defining their role in the cell. Whereas many investigators search for a ‘nuclear body function’, others believe that they are merely storage depots for protein accumulation. We feel that the disassembly of nuclear structures during mitosis provides evidence that these structures are required during specific phases of cell growth. If the nuclear structures represented storage facilities, then structures such as DDX1 foci would be expected to possibly increase during mitosis, as DDX1 protein levels remain constant throughout the cell cycle, yet transcription ceases. Therefore, nuclear structures such as DDX1 foci are likely not random protein accumulations, but exist as processing centers for some aspect of gene transcription. Whether nuclear bodies serve an active biochemical function such as assembly of transcriptional complexes or whether they function as storage sites for proteins involved in nuclear processes, we would still define nuclear bodies as essential components of the cell nucleus.

7.3 Individual nuclear bodies are spatially heterogeneous

There is currently accumulating evidence to support the notion that nuclear bodies may exist as a heterogeneous population (see Chapter 4 Summary). It is conceivable that the various nuclear arrangements we observed for cleavage bodies, gems, CBs, PML bodies and DDX1 foci (such as a portion of DDX1 foci localizing adjacent to CBs and PML bodies, or DDX1 foci frequently colocalizing with cleavage bodies) represent a spatial heterogeneity as well as a functional heterogeneity. The specific associations, which vary from cell-to-cell and cell type-to-cell type, may reflect requirements for particular transcripts or alternatively, the requirement for particular processes. As such, DDX1 may co-operate with CstF-64 to perform one function and these may localize adjacent to CBs to perform another function or process a different subset of transcripts, such as histone transcripts.

Although the pattern of nuclear body association appears heterogeneous, it is possible that PML bodies, CBs, cleavage bodies and DDX1 foci localize adjacent to one another nearly all the time but this remains undetectable by immunofluorescence microscopy due to the limited signal produced by a small number of proteins. Therefore, the PML protein may consistently localize adjacent to CBs and cleavage bodies; however, if present in small enough amounts, would be essentially undetectable by standard immunofluorescence microscopy.

Another aspect of nuclear body heterogeneity involves mobility. It has already been shown that different populations of CBs and PML bodies exist within the nucleus based on mobilities. Platani *et al.* (2000) observed that HeLa cells transfected with GFP-p80 coilin displayed CBs as well as a smaller, slower moving population they called mini-CBs. Similarly, baby hamster kidney cells transfected with YFP-Sp100, a component of PML bodies, contained at least 3 classes of PML bodies based on differing mobilities (Muratani *et al.*, 2002). It would be interesting to extend these observations with both cleavage bodies and DDX1 foci. Taking this a step further, we would like to analyse combinations of nuclear bodies using YFP and CFP constructs. It is possible that one subpopulation of CBs or PML bodies would localize adjacent to cleavage bodies and DDX1 foci and vice-versa.

Once the various subpopulations are characterized, we would further assess the content of these subpopulations. It has been previously shown that mini-CBs do not contain fibrillarin or the Sm snRNPs (Platani *et al.*, 2000), but they do contain SMN. Interestingly, the only time we observed CstF-64 colocalization with p80 coilin was when the p80 coilin foci were small and weakly stained (resembling the mini-CBs). In addition, CBs were only identified by Sm staining when we performed double-labeling with DDX1 as we did not have access to an anti-p80 coilin antibody generated in a species other than rabbit. As Platani *et al.* (2000) have reported that mini-CBs do not contain the Sm antigen, we may have missed a significant interaction between DDX1 foci and a subset of p80 coilin-containing CBs. We will further examine the possibility that CstF-64 and DDX1 do not associate with fibrillarin-containing CBs.

As cleavage bodies have been reported to contain the transcription factors TFIIH, TFIIF and TFIIE (Schul *et al.*, 1998; Gall, 2000), we will also need to study the association between DDX1 foci and the localization of these transcription factors. We do not know if these transcription factors are present in all CstF-64 labeled cleavage bodies, and therefore, it is possible that DDX1 may only interact with a subset of cleavage bodies.

Consequently, further examination of nuclear bodies is required to fully appreciate their possible heterogeneities. These differences may assist in deciphering nuclear body function and as well, biochemical roles for various protein components.

7.4 The cellular function for DDX1

The overall objective of my project was to determine a biological and biochemical role for DDX1. Although we have yet to resolve the biological role, we are many steps closer to determining a biochemical function (Fig. 7.1). The spatial and physical association with CstF-64 led us to propose an involvement in 3'-end processing. Preliminary polyadenylation experiments vindicate this hypothesis: purified recombinant DDX1 decreased the polyadenylation of an SV40 RNA substrate, while the addition of anti-DDX1 antibody restored the polyadenylation to near wild-type levels. The binding of DDX1 to the mRNA may alter its conformation effectively destabilizing RNA binding by the cleavage and polyadenylation machinery. Therefore, the decrease in pre-mRNA polyadenylation may reflect the ability of DDX1 to 'commit' a transcript to completion of 3'-end processing. Alternatively, if recombinant DDX1 behaves as a dominant negative protein, DDX1 may actually increase 3'-end processing. In this instance DDX1 could bind to the pre-mRNA substrate again changing its conformation but now to permit the binding of other cleavage and polyadenylation factors.

Following polyadenylation, transcripts are exported from the nucleus to the cytoplasm. We hypothesize that DDX1 remains bound to the mRNA through export to the cytoplasm. A role for DExH/D box proteins in RNA export is not

Fig. 7.1 Putative biochemical function for DDX1.

DDX1 accumulates in nuclear DDX1 foci, which often colocalize with CstF-64-containing cleavage bodies. These nuclear bodies frequently localize adjacent to PML bodies or CBs, both of which likely function in transcription (ie. formation of 'transcriptosome" complexes). Preliminary evidence indicates that DDX1 is involved in transcript polyadenylation. We hypothesize that following mRNA processing, DDX1 remains bound to the mRNA through nuclear export. Upon entry into the cytoplasm DDX1 may localize nuclear-encoded mitochondrial transcripts to translational complexes surrounding the mitochondria. Whether DDX1 processes only nuclear-encoded mitochondrial transcripts, or functions as a general 3'-end pre-mRNA processing factor, remains to be seen.

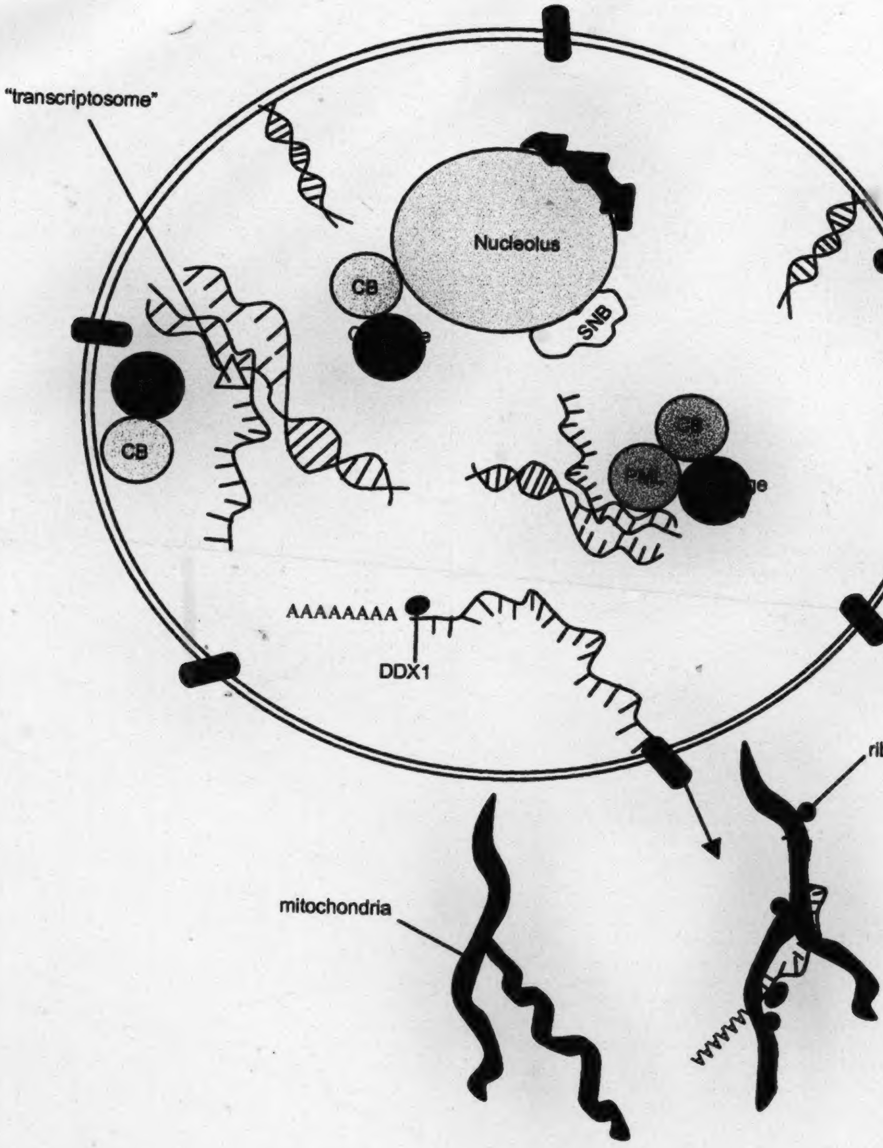
"transcriptosome"
Nucleolus
CB
SNB
CB
CB
PML
AAAAAAAA
DDX1
ribosome
mitochondria
AAAAAA

unique; the splicing factor UAP56 has been demonstrated to transport both intronless and intron-containing mRNAs from the nucleus (reviewed in Linder and Stutz, 2001), and Ddp5 has also been shown to export mRNA-protein complexes (Snay-Hodge *et al.*, 1998; Zhao *et al.*, 2002). Attempts to demonstrate export using GFP-DDX1 fluorescent loss in photobleaching experiments (FLIP) have thus far been unsuccessful, as GFP-DDX1 appears to primarily localize to the cytoplasm (Fig. 6.3). Nevertheless, the localization of DDX1 to mitochondrial areas (Figs. 6.2 and 6.3) suggests that DDX1 does function within the cytoplasm. We are hypothesizing that once past the nuclear pore, DDX1 escorts mRNA transcripts to their site of translation. The concentration of DDX1 around the mitochondria (Figs. 6.2 and 6.3), suggests that DDX1 may specifically localize nuclear-encoded mitochondrial transcripts to the area for translation. The observation that cytoplasmic DDX1 also co-localizes with a fraction of ribosomes (Fig. 6.7) further supports this theory as it is known that some ribosomes do localize in mitochondrial areas (Crowley and Payne, 1998).

The cytoplasmic localization of DDX1 to the mitochondria does not necessarily restrict DDX1 to the 3'-end processing of nuclear-encoded mitochondrial transcripts. It is possible that DDX1 assists in the final stages of 3'-end processing of many pre-mRNAs, yet it is only required for the correct cytoplasmic localization of nuclear-encoded mitochondrial transcripts.

Nonetheless, it is intriguing that DDX1 foci only associate with a fraction of CBs. If the hypothesis that CBs exist as 'transcriptosome' assembly sites is valid, the subset of DDX1 foci that associate with CBs might represent those that contribute to the transcription of nuclear-encoded mitochondrial genes. CBs have been previously reported to localize adjacent to histone gene clusters. As histone genes represent areas of high transcription during S phase, it would be logical for transcriptosome assembly facilities (ie. CBs) to locate near high demand areas. Likewise, nuclear-encoded mitochondrial genes represent up to 20% of polyadenylated transcripts (Welle *et al.*, 1999). Areas, which are gene-rich for nuclear-encoded mitochondrial transcripts, may also attract CB localization. If DDX1 is required for the proper processing and export of nuclear-encoded mitochondrial genes, then DDX1 foci may localize with CBs to form mitochondrial-specific transcriptosomes. The localization of DDX1 foci adjacent to nuclear-encoded mitochondrial genes could be shown using *in situ* hybridization in combination with immunofluorescent labeling in fixed cells as done for CBs (Frey and Matera, 1995).

Further support that DDX1 plays a role in the export of RNA polymerase II transcripts comes from observations with HeLa cells treated with leptomycin B. Leptomycin B is a drug that is known to inhibit the Crm1 karyopherin involved in nuclear export of RNA. Until recently, Crm1 was thought to be responsible for the export of all RNA species. Evidence is now accumulating that Ran-dependent karyopherins, such as Crm1, do not mediate the export of mRNA and that this responsibility lies with an export factor called Tap (reviewed in Reed and Hurt, 2002). Treatment of our HeLa cells with leptomycin B did not result in any noticeable changes to the cytoplasmic filamentous pattern of DDX1 nor did it appear to affect overall cytoplasmic DDX1 levels (data not shown). Although initially puzzling, these results concur with DDX1 assisting in the nuclear export of mRNA.

7.5 DDX1 and SMN

SMN has been found to associate with the outer mitochondrial membrane in rat spinal cord cells (Pagliardini *et al.*, 2000). Although the function of SMN at this location is unknown, SMN has been found to interact and enhance the anti-apoptotic effect of human Bcl-2, a protein that is located in the outer mitochondrial membrane (Iwahashi *et al.*, 1997; Sato *et al.*, 2000). The localization of DDX1 and SMN to mitochondrial regions, the frequent association of DDX1 foci and gems, and the immunoprecipitation of SMN with anti-DDX1 antibody suggest that DDX1 and SMN may be involved in a similar cellular process. It is possible that DDX1 functions with SMN in transcribing mitochondrial genes and then both remain bound during nuclear export until the transcript is localized to the vicinity of the mitochondria. We have not yet examined the cytoplasmic localization of SMN using methanol:acetone fixed cells. We will need to confirm that SMN does colocalize with mitochondria in HeLa cells as previously observed for rat spinal cord cells. It will also be interesting to probe our Western blots of DDX1 immunoprecipitations to determine whether Bcl-2 is found in the same complex as DDX1 and SMN. Further support for a role in the transcription of nuclear-encoded mitochondrial genes would come from *in situ* hybridization experiments whereby the *Bcl-2* gene (or another nuclear-encoded mitochondrial gene) is labeled in combination with gems and DDX1 foci. We would process these data in collaboration with Dr. Paul Freemont and Dr. Denise Sheer who have contributed to the design of software that analyses data from three-dimensionally reconstructed cells for specific associations (ie. this software rules out the possibility that two points are randomly spaced). This program has proven successful in determining that PML bodies specifically associate with the MHC gene cluster in interphase cells (Shiels *et al.*, 2001). Association of gems and DDX1 foci with nuclear-encoded mitochondrial genes would assist in defining not only possible biochemical roles for SMN and DDX1, but also in establishing cellular functions for the associated nuclear structures.

7.5 DDX1 and hnRNP K

While preparing this discussion an article was e-published that describes the interaction of DDX1 with heterogeneous ribonucleoprotein K (hnRNP K) (Chen *et al.*, 2002). The interaction was detected in K562 cells by GST-hnRNP K affinity chromatography and was confirmed by *in vitro* binding experiments using *in vitro* translated DDX1 and co-immunoprecipitation experiments using cell lines engineered to overexpress one or both proteins. The function of hnRNP K is currently unknown; however, it is known to interact with proteins involved in signal transduction (Hobert *et al.*, 1994; Schullery *et al.*, 1999; Ostrowski *et al.*, 2000), chromatin remodeling (Denisenko and Bomsztyk, 1997; 2002), transcription (Michelotti *et al.*, 1996; Du *et al.*, 1998; Miau *et al.*, 1998), RNA processing (Shnyreva *et al.*, 2000), and translation (Ostareck, 2001; Ostareck-

Lederer *et al.*, 2002). HnRNP K has been shown to bind DNA as well as RNA substrates. Of interest, hnRNP K has also been found to bind hnRNP U by yeast two-hybrid analyses (Shnyreva *et al.*, 2000). Whether the site mediating this interaction on hnRNP U is the one shared by DDX1 was not stated.

Coincidentally, hnRNP K has been recently found to associate with mitochondrial transcripts by a three-hybrid screen. Furthermore, subcellular fractionation of hnRNP K demonstrates that it localizes within purified mitochondria (Ostrowski *et al.*, 2002). Although the exact function of hnRNP K within the mitochondria is unknown, Ostrowski *et al.* (2002) hypothesize a role in apoptosis as hnRNP K has been previously shown to be modified in apoptotic Jurkat T cells (Thiede *et al.*, 2001), and it is known to be phosphorylated by PKCδ (Schullery *et al.*, 1999), a protein triggered during apoptosis.

The association of DDX1 with hnRNP K led Chen *et al.* (2002) to investigate the biochemical properties of DDX1. *In vitro* ATPase assays demonstrated that DDX1 is capable of hydrolyzing ATP and this activity is enhanced by the addition of either poly(A), poly(U), or poly(C). RNA binding assays demonstrated that DDX1 binds most strongly to poly(A) beads compared to binding with poly(C) beads. This finding is most intriguing in light of our preliminary results that DDX1 decreases the polyadenylation of SV40 substrate RNA. Chen *et al.* (2002) also tested RNA unwinding by DDX1. Using an RNA substrate that formed a double-stranded species with single-stranded ends, they saw no RNA unwinding with recombinant DDX1; however, co-immunoprecipitated DDX1 was able to unwind this substrate in the presence of

ATP. It is entirely possible that the ability to unwind RNA is partially dependent on both substrate make-up (ie. the presence of a poly(A) tail) and the presence of other co-factors.

7.6 DDX1 and cancer

The overexpression of DDX1 in retinoblastoma and neuroblastoma cell lines causes DDX1 to predominate in the cytoplasm. Whether DDX1 is associated with the mitochondria in these cell lines has yet to be determined. The localization of DDX1 to mitochondrial areas in the cytoplasm of non-amplified cell lines such as HeLa suggest that DDX1 may be required for some aspect of mitochondrial function, such as proper transcript localization. Interestingly, nuclear encoded mitochondrial transcripts that are up-regulated during tumourigenesis include anti-apoptotic inhibitors from the Bcl-2 family of proteins. This protein family is composed of anti- and pro-apoptotic members which all function to regulate the permeability of the outer mitochondrial membrane (reviewed in Tsujimoto, 1998; Martinou and Green, 2001; Igney and Krammer, 2002). Although the pro-apoptotic members of this family localize within the cytosol, the anti-apoptotic members localize to membranes belonging to the mitochondria, endoplasmic reticulum and nucleus. Within the mitochondria, the anti-apoptotic proteins function to oppose the actions of the pro-apoptotic proteins, who once activated try to disrupt mitochondrial integrity by forming pores. The overexpression of DDX1 in the cytoplasm of some tumour cell lines combined with its localization to regions surrounding the mitochondria could be linked to a role in escorting upregulated mRNAs such as the anti-apoptotic family members of Bcl-2. Accordingly, Southern blots consisting of cDNAs amplified from RNA that immunoprecipitated with DDX1 could be initially probed for these Bcl-2 transcripts. It would also be interesting to confirm whether these transcripts are up-regulated in the same cell lines that have *DDX1* amplification.

Another class of genes that exert anti-apoptotic effects include the inhibitor of apoptosis protein (IAPs). These proteins bind to active caspases and effectively inactivate them (reviewed in Verhagen *et al.*, 2001). Interestingly, one member, survivin, is only expressed in tumours and not in normal tissue (Reed, 2001). Expression of survivin in neuroblastoma correlates with advanced disease stage and is an indicator of poor prognosis (Adida *et al.*, 1998). These transcripts represent another class of genes that could be analysed by the Southern blots of DDX1 immunoprecipitations (as above). Likewise, it would be interesting to note whether *DDX1* is amplified in the same neuroblastoma tumours that express survivin.

The possibility that DDX1 is involved in 3'-end transcript processing and proper mRNA localization potentially justifies a role in tumour progression. Although tumour cells frequently overcome the apoptotic pathway, the upregulation of anti-apoptotic factors represents only one mechanism. The cells can achieve the same effect by inactivating pro-apoptotic genes (reviewed in Igney and Krammer, 2002). Consequently, the discovery that DDX1 is overexpressed in only a portion of retinoblastoma and neuroblastoma cell lines and tumours may be explained by other genetic alterations. It is also interesting that the IAP family members can demonstrate tissue-specific expression (reviewed in Verhagen *et al.*, 2001). Therefore if DDX1 were to mediate the localization of a transcript primarily involved in neuronal cells, this would account for its specificity for neuronal tumours such as neuroblastoma and retinoblastoma.

References

Adida, C., Berrebi, D., Peuchmaur, M., Reyes-Mugica, M., and Altieri, D.C. (1998). Anti-apoptosis gene, survivin, and prognosis of neuroblastoma. Lancet *351*, 882-883.

Akao, Y., Marukawa, O., Morikawa, I.L., Nakao, K., Kamei, M., Hachiya, T., and Tsujimoto, Y. (1995). The rck/p54 candidate proto-oncogene is expressed in human and mouse tissues. Cancer Res. *55*, 3444-3449.

Akao, Y., Mizoguchi, H., Ohishi, N., and Yagi, K. (1998). Growth inhibition by overexpression of human DEAD box protein rck/p54 in cells of a guinea pig cell line. FEBS Lett. *429*, 278-283.

Akao, Y., Seto, M., Takahashi, T., Kubonishi, I., Miyoshi, I., Nakazawa, S., Tsujimoto, Y., Croce, C.M., and Ueda, R. (1991). Molecular cloning of the chromosomal breakpoint of a B-cell lymphoma with the t(11;14)(q23;q32) chromosomal translocation. Cancer Res. *51*, 1574-1576.

Akao, Y., Seto, M., Yamamoto, K., Iida, S., Nakazawa, S., Inazawa, J., Abe, T., Takahashi, T., and Ueda, R. (1992). The *RCK* gene associated with t(11;14) translocation is distinct from the *MLL/ALL-1* gene with t(4;11) and t(11;19) translocations. Cancer Res. *52*, 6083-6087.

Alcalay, M., Tomassoni, L., Colombo, E., Stoldt, S., Grignani, F., Fagioli, M., Szekely, L., Helin, K., and Pelicci, P.G. (1998). The promyelocytic leukemia gene product (PML) forms stable complexes with the retinoblastoma protein. Mol. Cell. Biol. *18*, 1084-1093.

Alliegro, M.C., and Alliegro, M.A. (1997). Identification of a new coiled body component. Exp. Cell Res. *231*, 386-390.

Alliegro, M.C., and Alliegro, M.A. (1998). Protein heterogeneity in the coiled body compartment. Exp. Cell Res. *239*, 60-68.

Almeida, F., Saffrich, R., Ansorge, W., and Carmo-Fonseca, M. (1998). Microinjection of anti-coilin antibodies affects the structure of coiled bodies. J. Cell Biol. *142*, 899-912.

Amler, L.C., Schürmann, J., and Schwab, M. (1996). The *DDX1* gene maps within 400 dbp 5' to *MYCN* and is frequently coamplified in human neuroblastoma. Genes Chromosomes Cancer *15*, 134-137.

Andrade, L.E., Chan, E.K.L., Raška, I., Peebles, C.L., Roos, G., and Tan, E.M. (1991). Human autoantibody to a novel protein of the nuclear coiled body. Immunological characterization and cDNA cloning of p80-coilin. J. Exp. Med. *173*, 1407-1419.

Andrade, L.E., Tan, E.M., and Chan, E.K. (1993). Immunocytochemical analysis of the coiled body in the cell cycle and during cell proliferation. Proc. Natl. Acad. Sci. USA *90*, 1947-1951.

Anton, L.C., Schubert, U., Bacik, I., Princiotta, M.F., Wearsch, P.A., Gibbs, J., Day, P.M., Realini, C., Rechsteiner, M.C., Bennink, J.R., and Yewdell, J.W. (1999). Intracellular localization of proteasomal degradation of a viral antigen. J. Cell Biol. *146*, 113-124.

Arai, Y., Hosoda, F., Kobayashi, H., Arai, K., Hayashi, Y., Kamada, N., Kaneko, Y., and Ohki, M. (1997). The inv(11)(p15q22) chromosome translocation of de novo and therapy-related myeloid malignancies results in fusion of the nucleoporin gene, *NUP98*, with the putative RNA helicase gene, *DDX10*. Blood *89*, 3936-3944.

Aratani, S., Fujii, R., Oishi, T., Fujita, H., Amano, T., Ohshima, T., Hagiwara, M., Fukamizu, A., and Nakajima, T. (2001). Dual roles of RNA helicase A in CREB-dependent transcription. Mol. Cell. Biol. 21, 4460-4469.

Bachellerie, J.P., Puvion, E., and Zalta, J.P. (1975). Ultrastructural organization and biochemical characterization of chromatin RNA protein complexes isolated from mammalian cell nuclei. Eur. J. Biochem. *58*, 327-337.

Barlat, I., Maurier, F., Duchesne, M., Guitard, E., Tocque, B., and Schweighoffer, F. (1997). A role for Sam68 in cell cycle progression antagonized by a spliced variant within the KH domain. J. Biol. Chem. *272*, 3129-3132.

Bauer, D.W., and Gall, J.G. (1997). Coiled bodies without coilin. Mol. Biol. Cell *8*, 73-82.

Bauer D.W., Murphy, C., Wu, Z., Wu, C.-H.H., and Gall, J.G. (1994). *In vitro* assembly of coiled bodies in *Xenopus* egg extract. Mol. Biol. Cell *5*, 633-644.

Beaudouin, J., Gerlich, D., Daigle, N., Eils, R., and Ellenberg, J. (2002). Nuclear envelope breakdown proceeds by microtubule-induced tearing of the lamina. Cell *108*, 83-96.

Bell, P., Dabauvalle, M.-C., and Scheer, U. (1992). *In vitro* assembly of prenucleolar bodies in *Xenopus* egg extract. J. Cell Biol. *118*, 1297-1304.

Benowitz, L.I., and Routtenberg, A. (1997). GAP-43: an intrinsic determinant of neuronal development and plasticity. Trends Neurosci. *20*, 84-91.

Bienroth, S., Keller, W., and Wahle, E. (1993). Assembly of a processive messenger RNA polyadenylation complex. EMBO J. *12*, 585-594.

Bilger, A., Fox, C.A., Wahle, E., and Wickens, M. (1994). Nuclear polyadenylation factors recognize cytoplasmic polyadenylation elements. Genes Dev. *8*, 1106-1116.

Birse, C.E., Lee, B.A., Hansen, K. and Proudfoot, N.J. (1997). Transcriptional termination signals for RNA polymerase II in fission yeast. EMBO J., *16*, 3633–3643.

Birse, C.E., Minvielle-Sebastia, L., Lee, B.A., Keller, W., and Proudfoot, N.J. (1998). Coupling termination of transcription to messenger RNA maturation in yeast. Science *280*, 298-301.

Boisvert, F.M., Hendzel, M.J., and Bazett-Jones, D.P. (2000). Promyelocytic leukemia (PML) nuclear bodies are protein structures that do not accumulate RNA. J. Cell Biol. *148*, 283-292.

Bown, N. (2001). Neuroblastoma tumour genetics: clinical and biological aspects. J. Clin. Path. *54*, 897-910.

Bléoo, S., Sun, X., Hendzel, M.J., Rowe, J.M., Packer, M., and Godbout, R. (2002). Association of human DEAD box protein DDX1 with a cleavage stimulation factor involved in 3'-end processing of pre-MRNA. Mol. Biol. Cell 12,3046-3059.

Bradford, M.M. (1976). A rapid and sensitive method for the quantitation of microgram quantities of protein utilizing the principle of protein-dye binding. Anal. Biochem. *72*, 248-254.

Bradley, A., Evans, M., Kaufmann, M.H., and Robertson, E. (1984). Formation of germ-line chimaeras from embryo-derived teratocarcinoma cell lines. Nature *309*, 255-256.

Brasch, K., and Ochs, R.L. (1992). Nuclear bodies (NBs): a newly "rediscovered" organelle. Exp. Cell Res. *202*, 211-223.

Bregman, D.B., Du, L. van der Zee, S., and Warren, S.L. (1995). Transcription-dependent redistribution of the large subunit of RNA polymerase II to discrete nuclear domains. J. Cell Biol. *129*, 287-298.

Brehm, A., Miska, E.A., McCance, D.J., Reid, J.L., Bannister, A.J., and Kouzarides, T. (1998). Retinoblastoma protein recruits histone deacetylase to repress transcription. Nature *391*, 597-601.

Brodeur, G.M., Seeger, R.C., Schwab, M., Varmus, H.E., and Bishop, J.M. (1984). Amplification of *N-myc* in untreated human neuroblastomas correlates with advanced disease stage. Science *224*, 1121-1124.

Brodsky, A.S., and Silver, P.A. (2000). Pre-mRNA processing factors are required for nuclear export. RNA *6*, 1737-1749.

Bucci, S., Giani, L., Mancino, G., Pellegrino, M., and Ragghianti, M. (2001). TAFII70 protein in Cajal bodies of the amphibian germinal vesicle. Genome *44*, 1100-1103.

Cajal, S.R.y. (1903). Un sencillo metodo de coloracion selectiva del reticulo protoplasmico y sus efectos en los diversos organos nerviosos de vertebrados y invertebrados. Trab. Lab. Invest. Biol. (Madrid) *2*, 129-221.

Calvo, O., and Manley, J.L. (2001). Evolutionarily conserved interaction between CstF-64 and PC4 links transcription, polyadenylation, and termination. Mol. Cell *7*, 1013-1023.

Callan, H.G., Gall, J.G., Murphy, C. (1991). Histone genes are located at the sphere loci of *Xenopus* lampbrush chromosomes. Chromosoma *101*, 245-251.

Campbell, L., Hunter, K.M.D., Mohaghegh, P., Tinsley, J.M., Brasch, M.A., and Davies, K.E. (2000). Direct interaction of Smn with dp103, a putative RNA helicase: a role for Smn in transcription regulation? Hum. Mol. Genet. *9*, 1093-1100.

Carmo-Fonseca, M. (2002). The contribution of nuclear compartmentalization to gene regulation. Cell *108*, 513-521.

Carmo-Fonseca, M., Pepperkok, R., Carvalho, M.T., and Lamond, A.I. (1992). Transcription-dependent colocalization of the U1, U2, U4/U6, and U5 snRNPs in coiled bodies. J. Cell Biol. *117*, 1-14.

Carmo-Fonseca, M., Tollervey, D., Pepperkok, R., Barabino, S.M., Merdes, A., Brunner, C., Zamore, P.D., Green, M.R., Hurt, E., and Lamond, A.I. (1991). Mammalian nuclei contain foci which are highly enriched in components of the pre-mRNA splicing machinery. EMBO J. *10*, 195-206.

Caruthers, J.M., Johnson, E.R., and McKay, D.B. (2000). Crystal structure of yeast initiation factor 4A, a DEAD-box RNA helicase. Proc. Natl. Acad. Sci. USA *97*, 13080-13085.

Carvalho, T., Almeida, F., Calapez, A., Lafarga, M., Berciano, M.T., Carmo-Fonseca, M. (1999). The spinal muscular atrophy disease gene product, SMN: a link between snRNP biogenesis and the Cajal (coiled) body. J. Cell Biol. *17*, 715-727.

Causevic, M., Hislop, R.G., Kernohan, N.M., Carey, F.A., Kay, R.A., Steele, R.J.C., and Fuller-Pace, F.V. (2001). Overexpression and poly-ubiquitylation of the DEAD-box RNA helicase p68 in colorectal tumours. Oncogene *20*, 7734-7743.

Cerone, M.A., Londono-Vallejo, J.A., and Bacchetti, S. (2001). Telomere maintenance by telomerase and by recombination can coexist in human cells. Hum. Mol. Genet. *10*, 1945-1952.

Chakravarti, D., LaMorte, V.J., Nelson, M.C., Nakajima, T., Schulman, I.G., Juguilon, H., Montminy, M., and Evans, R.M. (1996). Role of CBP/P300 in nuclear receptor signalling. Nature *383*, 99-103.

Chakrabarti, S.R., Sood, R., Nandi, S., and Nucifora, G. (2000). Posttranslational modification of TEL and TEL/AML1 by SUMO-1 and cell-cycle-dependent assembly into nuclear bodies. Proc. Natl. Acad. Sci. USA *97*, 13281-13285.

Charroux, B., Pellizzoni, L., Perkinson, R.A., Shevchenko, A., Mann, M., and Dreyfuss, G. (1999). Gemin 3: A novel DEAD box protein that interacts with SMN, the spinal muscular atrophy gene product, and is a component of gems. J. Cell Biol. *147*, 1181-1193.

Charroux, B., Pellizzoni, L., Perkinson, R.A., Yong, J., Shevchenko, A., Mann, M., and Dreyfuss, G. (2000). Gemin 4: A novel component of the SMN complex that is found in both gems and nucleoli. J. Cell Biol. *148*, 1177-1186.

Chen, H.C., Lin, W.C., Tsay, Y.G., Lee, S.C., and Chang, C.J. (2002). An RNA helicase, DDX1, interacting with poly (A) RNA and heterogeneous nuclear ribonucleoprotein K (hnRNP K). J. Biol. Chem. (in press).

Chen, J.Y.-F., Stands, L., Staley, J.P., Jackups, R.R., Jr., Latus, L.J., and Chang, T.-H. (2001). Specific alterations of U1-C protein or U1 small nuclear RNA can eliminate the requirement of Prp28p, an essential DEAD box splicing factor. Mol. Cell *7*, 227-232.

Chen, P.-L., Riley, D.J., Chen, Y., and Lee, W.-H. (1996). Retinoblastoma protein positively regulates terminal adipocyte differentiation through direct interaction with C/EBPs. Genes Dev. *10*, 2794-2804.

Chen, P.-L., Ueng, Y.-C., Durfee, T., Chen, K.-C., Yang-Feng, T., and Lee, W.-H. (1995). Identification of a human homologue of yeast nuc2 which interacts with the retinoblastoma protein in a specific manner. Cell Growth Differ. *6*, 199-210.

Chen, T., Boisvert, F.M., Bazett-Jones, D.P., and Richard, S. (1999). A role for the GSG domain in localizing Sam68 to novel nuclear structures in cancer cell lines. Mol. Biol. Cell *10*, 3015-3033.

Cho., B., Lim, Y., Lee, D.Y., Park, S.Y., Lee, H., Kim, W.H., Yang, H., Bang, Y.J., and Jeoung, D.I. (2002). Identification and characterization of a novel cancer/testis antigen gene CAGE. Biochem. Biophys. Res. Commun. *292*, 715-726.

Clark, A.R., Maandag, E.R., van Roon, M., van der Lugt, N.M.T., van der Valk, M., Hooper, M.L., Berns, A., and te Riele, H. (1992). Requirement for a functional *Rb-1* gene in murine development. Nature *359*, 328-330.

M.G. Claros, and P. Vincens. (1996). Computational method to predict mitochondrially imported proteins and their targeting sequences. Eur. J. Biochem. *241*, 770-786.

Cmarko, D., Verschure, P.J., Martin, T.E., Dahmus, M.E., Krause, S., Fu, X.-D., van Driel, R., and Fakan, S. (1999). Ultrastructural analysis of transcription and splicing in the cell nucleus after bromo-UTP microinjection. Mol. Biol. Cell. *10*, 211-223.

Colgin, L.M., and Reddel, R.R. (1999). Telomere maintenance mechanisms and cellular immortalization. Curr. Opin. Genet. Dev. *9*, 97-103.

Corral-Debrinski, M., Blugeon, C., and Jacq, C. (2000). In yeast, the 3' untranslated region or the presequence of ATM1 is required for the exclusive localization of its mRNA to the vicinity of mitochondria. Mol. Cell. Biol. *20*, 7881-7892.

Crowley, K.S., and Payne, R.M. (1998). Ribosome binding to mitochondria is regulated by GTP and the transit peptide. J. Biol. Chem. 273, 17278-17285.

Dahmus, M.E. (1996). Reversible phosphorylation of the C-terminal domain of RNA polymerase II. J. Biol. Chem. *271*, 19009-19012.

Dantonel, J.C., Murthy, K.G., Manley, J.L., and Tora, L. (1997). Transcription factor TFIID recruits factor CPSF for formation of 3' end of mRNA. Nature *389*, 399-402.

Darley-Usmar, V.M., Rickwood, D., and Wilson, M.T. eds (1987). Mitochondria: a practical approach. IRL Press Ltd., Eynsham, Oxford, England p.6.

de la Cruz, J., Kressler, D., and Linder, P. (1999). Unwinding RNA in *Saccharomyces cerevisiae*: DEAD-box proteins and related families. Trends Biochem. Sci. *24*, 192-198.

Denegri, M., Chiodi, I., Corioni, M., Cobianchi, F., Riva, S., and Biamonti, G. (2001). Stress-induced nuclear bodies are sites of accumulation of pre-mRNA processing factors. Mol. Biol. Cell *12*, 3502-3514.

Denisenko, O., and Bomsztyk, K. (1997). The product of the murine homolog of the Drosophila extra sex combs gene displays transcriptional repressor activity. Mol. Cell. Biol. *17*, 4707-4717.

Denisenko, O., and Bomsztyk, K. (2002). Yeast hnRNP K-like genes are involved in regulation of the telomeric position effect and telomere length. Mol. Cell. Biol. *22*, 286-297.

De Preter, K., Speleman, F., Combaret, V., Lunec, J., Laureys, G., Eussen, B.H.J., Francotte, N., Board, J., Pearson, A.D.J., De Paepe, A., Van Roy, N., and Vandesompele, J. (2002). Quantification of MYCN, DDX1, and NAG gene copy number in neuroblastoma using real-time quantitative PCR assay. Mod. Pathol. *15*, 159-166.

Desbois, C., Rousset, R., Bantignies, F., and Jalinot, P. (1996). Exclusion of Int-6 from PML nuclear bodies by binding to the HTLV-I Tax oncoprotein. Science *273*, 951-953.

Desterro, J.M., Rodriguez, M.S., and Hay, R.T. (1998). SUMO-1 modification of IkappaBalpha inhibits NF-kappaB activation. Mol. Cell *2*, 233-239.

de Vries, H., Rüegsegger, U., Hubner, W., Friedlein, A., Langen, H., and Keller, W. (2000). Human pre-mRNA cleavage factor II(m) contains homologs of yeast proteins and bridges two other cleavage factors. EMBO J. *19*, 5895-5904.

Di Fruscio, M., Chen, T., and Richard, S. (1999). Two novel Sam68-like mammalian proteins SLM-1 and SLM-2: SLM-1 is a Src substrate during mitosis. Proc. Natl. Acad. Sci. USA *96*, 2710-2715.

Dignam, J.D., Lebovitz, R.M., and Roeder, R.G. (1983). Accurate transcription initiation by RNA polymerase II in a soluble extract from isolated mammalian nuclei. Nucleic Acids Res. *11*, 1475-1489.

Di Leonardo, A., Khan, S.H., Linke, S.P., Greco, V., Seidita, G., and Wahl, G.M. (1997). DNA rereplication in the presence of mitotic spindle inhibitors in human and mouse fibroblasts lacking either p53 or pRb function. Cancer Res. 57, 1013-1019.

Dirks, R.W., de Pauw, E.S., and Raap, A.K. (1997). Splicing factors associate with nuclear HCMV-IE transcripts after transcriptional activation of the gene, but dissociate upon transcription inhibition: Evidence for a dynamic organization of splicing factors. J. Cell Sci. *110*, 515-522.

Dominski, Z., and Marzluff, W.F. (1999). Formation of the 3' end of histone mRNA. Gene *239*. 1-14.

D'Orazi, G., Cecchinelli, B., Bruno, T., Manni, I., Higashimoto, Y., Saito, S., Gostissa, M., Coen, S., Marchetti, A., Del Sal, G., Piaggio, G., Fanciulli, M., Apella, E., and Soddu, S. (2002). Homeodomain-interacting protein kinase-3 phosphorylates p53 at Ser 46 and mediates apoptosis. Nat. Cell Biol. *4*, 11-19.

Doucas, V.,and Evans, R.M. (1999). Human T-cell leukemia retrovirus-Tax protein is a repressor of nuclear receptor signaling. Proc. Natl. Acad. Sci. USA *96*, 2633-2638.

Doucas, V., Tini, M., Egan, D.A., Evans, R.M. (1999). Modulation of CREB binding protein function by the promyelocytic (PML) oncoprotein suggests a role for nuclear bodies in hormone signaling. Proc. Natl. Acad. Sci. USA *96*, 2627-2632.

Dower, N.A., Stang, S.L., Bottorff, D.A., Ebinu, J.O., Dickie, P., Ostergaard, H.L., and Stone, J.C. (2000). RasGRP is essential for mouse thymocyte differentiation and TCR signaling. Nat. Immunol. *1*, 317-321.

Du, Q., Melnikova, I.N., and Gardner, P.D. (1998). Differential effects of heterogeneous nuclear ribonucleoprotein K on Sp1- and Sp3-mediated transcriptional activation of a neuronal nicotinic acetylcholine receptor promoter. J. Biol. Chem. *273*, 19877-19883.

Dubey, P., Hendrickson, R.C., Meredith, S.C., Siegel, C.T., Shabanowitz, J., Skipper, J.C.A., Engelhard, V.H., Hunt, D.F., and Schreiber, H. (1997). The immunodominant antigen of an ultraviolet-induced regressor tumor is generated by a somatic point mutation in the DEAD box helicase p68. J. Exp. Med. *185*, 695-705.

Dunaief, J.L., Strober, B.E., Guha, S., Khavari, P.A., Alin, K., Luban, J., Begemann, M., Crabtree, G.R., and Goff, S.P. (1994). The retinoblastoma protein and BRG1 form a complex and cooperate to induce cell cycle arrest. Cell *79*, 119-130.

Duncan, R., Bazar, L, Michelotti, G., Tomonaga, T., Krutzsch, H., Avigan, M., and Levens, D. (1994). A sequence-specific, single-strand binding protein activates the far upstream element of c-myc and defines a new DNA-binding motif. Genes Dev. *8*, 465-480.

Dyck, J.A., Maul, G.G., Miller, W.H. Jr., Chen, J.D., Kakizuka, A., and Evans, R.M. (1994). A novel macromolecular structure is a target of the promyelocyte-retinoic acid receptor oncoprotein. Cell *76*, 333-343.

Dye, M.J., and Proudfoot, N.J. (1999). Terminal exon definition occurs cotranscriptionally and promotes termination of RNA polymerase II. Mol. Cell *3*, 371-378.

Dye, M.J., and Proudfoot, N.J. (2001). Multiple transcript cleavage precedes polymerase release in termination by RNA polymerase II. Cell *105*, 669-681.

Dyson, N. (1998). The regulation of E2F by pRB-family proteins. Genes Dev. 12, 2245-2262.

Eckner, R., Ellmeier, W., and Birnstiel, M.L. (1991). Mature mRNA 3' end formation stimulates RNA export from the nucleus. EMBO J. *10*, 3513-3522.

Edwalds-Gilbert, G., Prescott, J. and Falck-Pedersen, E. (1993). 3' RNA processing efficiency plays a primary role in generating termination competent RNA polymerase II elongation complexes. Mol. Cell. Biol., *13*, 3472–3480.

Eliceiri, G.L., and Ryerse, J.S. (1984). Detection of intranuclear clusters of Sm antigens with monoclonal anti-Sm antibodies by immunoelectron microscopy. J. Cell. Physiol. *121*, 449-451.

Elsden, J., Kenyon, R.M., George, R.E., Godbout, R., Pearson, A.D.J., and Lunec, J. (2001). The oncogenic properties of DDX1 and its expression in neuroblastoma. Proc. Am. Assoc. Cancer Res. *42*, 191.

Endoh, H., Maruyama, K., Masuhiro, Y., Kobayashi, Y., Goto, M., Tai, H., Yanagisawa, J., Metzger, D., Hashimoto, S., and Kato, S. (1999). Purificiation and identification of p68 RNA helicase acting as a transcriptional coactivator specific for the activation function 1 of human estrogen receptor α. Mol. Cell. Biol. *19*, 5363-5372.

Fakan, S. (1994). Perichromatin fibrils are in situ forms of nascent transcripts. Trends Cell Biol. *4*, 86-90.

Fakan, S., and Bernhard, W., (1971). Localisation of rapidly and slowly labelled nuclear RNA as visualized by high resolution autoradiography. Exp. Cell Res. *67*, 129-141.

Fakan, S., and Bernhard, W. (1973). Nuclear labelling after prolonged ^{3}H-uridine incorporation as visualized by high resolution autoradiography. Exp. Cell Res. *79*, 431-444.

Fakan, S., Leser, G., and Martin, T.E. (1984). Ultrastructural distribution of nuclear ribonucleoproteins as visualized by immunocytochemistry on thin sections. J. Cell Biol. *98*, 358-363.

Fakan, S., and Nobis, P. (1978). Ultrastructural localization of transcription sites and of RNA distribution during the cell cycle of synchronized CHO cells. Exp. Cell Res. *113*, 327-337.

Fakan, S., Puvioin, E., and Spohr, G. (1976). Localization and characterization of newly synthesized nuclear RNA in isolated rat hepatocytes. Exp. Cell Res. *99*, 155-164.

Ferbeyre, G., de Stanchina, E., Querido, E, Baptiste, N., Prives, C, and Lowe, S.W. (2000). PML is induced by oncogenic ras and promotes premature senescence. Genes Dev. *14*, 2015-2027.

Ferreira, J.A., Carmo-Fonseca, M., and Lamond, A.I. (1994). Differential interaction of splicing snRNPs with coiled bodies and interchromatin granules during mitosis and assembly of daughter cell nuclei. J. Cell Biol. *126*, 11-23.

Fischer, U., Liu, Q., and Dreyfuss G. (1997). The SMN-SIP1 complex has an essential role in spliceosomal snRNP biogenesis. Cell *90*, 1023-1029.

Flaherty, S.M., Fortes, P., Izaurralde, E., Mattaj, I.W., and Gilmartin, G.M. (1997). Participation of the nuclear cap binding complex in pre-mRNA 3' processing. Proc. Natl. Acad. Sci. USA *94*, 11893-11898.

Flemington, E.K., Speck, S.H., and Kaelin, W.G., Jr. (1993). E2F-1-mediated transactivation is inhibited by complex formation with the retinoblastoma susceptibility gene product. Proc. Natl. Acad. Sci. *90*, 6914-6918.

Fogal, V., Gostissa, M., Sandy, P., Zacchi, P., Sternsdorf, T., Jensen, K., Pandolfi, P.P., Will, H., Schneider, C., and Del Sal, G. (2000). Regulation of p53 activity in nuclear bodies by a specific PML isoform. EMBO J. *19*, 6185-6195.

Fox, A.H., Lam, Y.W., Leung, A.K.L., Lyon, C.E., Anderson, J., Mann, M., and Lamond, A.I. (2002). Paraspeckles: a novel nuclear domain. Curr. Biol. *12*, 13-25.

Frey, M.R., Bailey, A.D., Weiner, A.M., and Matera, A.G. (1999). Association of snRNA genes with coiled bodies is mediated by nascent snRNA transcripts. Curr. Biol. *9*, 126-135.

Frey, M.R., and Matera, A.G. (1995). Coiled bodies contain U7 small nuclear RNA and associate with specific DNA sequences in interphase human cells. Proc. Natl. Acad. Sci. USA *92*, 5915-5919.

Friend, S.H., Bernards, R., Rogelj, S., Weinberg, R.A., Rapaport, J.M., Albert, D.M., and Dryja, T.P. (1986). A human DNA segment with properties of the gene that predisposes to retinoblastoma and osteosarcoma. Nature *323*, 643-646.

Fu, X.D., and Maniatis, T. (1990). Factor required for mammalian spliceosome assembly is localized to discrete regions in the nucleus. Nature *343*, 437-441.

Fuks, F., Burgers, W.A., Brehm, A., Hughes-Davies, L., and Kouzarides, T. (2000). DNA methyltransferase Dnmt1 associates with histone deacetylase activity. Nat. Genet. *24*, 88-91.

Furuta, Y., Lagutin, O., Hogan, B.L., and Oliver, G.C. (2000). Retina- and ventral forebrain-specific Cre recombinase activity in transgenic mice. Genesis *26*, 130-132.

Gall, J.G. (2000). Cajal bodies: The first 100 years. Annu. Rev. Cell Dev. Biol. *16*, 273-300.

Gall, J.G., Bellini, M., Wu, Z., and Murphy, C. (1999). Assembly of the nuclear transcription and processing machinery: Cajal bodies (coiled bodies) and transcriptosomes. Mol. Biol. Cell *10*, 4385-4402.

Gall, J.G., and Murphy, C. (1998). Assemblly of lampbrush chromosomes from sperm chromatin. Mol. Biol. Cell *9*, 733-747.

Gall, J.G., Stephenson, E.C., Erba, H.P., Diaz, M.O., and Barsacchi-Pilone, G. (1981). Histone genes are located at the sphere loci of newt lampbrush chromosomes. Chromosoma *84*, 159-171.

Gall, J.G., Tsvetkov, A., Wu, Z., and Murphy C. (1995). Is the sphere organelle/coiled body a universal nuclear component? Dev. Genet. *16*, 25-35.

Gangwani, L., Mikrut, M., Theroux, S., Sharma, M., and Davis, R.J. (2001). Spinal muscular atrophy disrupts the interaction of ZPR1 with the SMN protein. Nat. Cell Biol. *3*. 376-383.

Gao, L., Frey, M.R., and Matera, A.G. (1997). Human genes encoding U3 snRNA associate with coiled bodies in interphase cells and are clustered on chromosome 17p11.2 in a complex inverted repeat structure. Nucleic Acids Res. *25*, 4740-4747.

George, R.E., Kenyon, R., McGuckin, A.G., Kohl, N., Kogner, P., Christiansen, H., Pearson, A.D., and Lunec, J. (1997). Analysis of candidate gene co-amplification with *MYCN* in neuroblastoma. Eur. J. Cancer *33*, 2037-2042.

George, R.E., Thomas, H., McGuckin, A.G., Angus, B., Newell, D.R., Pearson, A.D.J., and Lunec, J. (1998). The *DDX1* gene which is frequently co-amplified with *MYCN* in primary neuroblastoma is itself tumorigenic. Proc. Am. Assoc. Cancer Res. *39*, 471.

Ghetti, A., Pin ol-Roma, S., Michael, W.M., Morandi, C., and Dreyfuss, G. (1992). hnRNP I, the polypyrimidine tract-binding protein: Distinct nuclear localization and association with hnRNAs. Nucleic Acids Res. *20*, 3671-3678.

Gilmartin, G.M., and Nevins, J.R. (1989). An ordered pathway of assembly of components required for polyadenylation site recognition and processing. Genes Dev. *3*, 2180-2189.

Godbout, R., Hale, M., and Bisgrove, D. (1994). A human DEAD box protein with partial homology to heterogenous nuclear ribonucleoprotein U. Gene *138*, 243-245.

Godbout, R., Packer, M., and Bie, W. (1998). Overexpression of a DEAD box protein (DDX1) in neuroblastoma and retinoblastoma cell lines. J. Biol. Chem. *273*, 21161-21168.

Godbout, R., Packer, M., Katyal, S., and Bléoo, S. (2002). Cloning and expression analysis of the chicken DEAD box gene *DDX1*. Biochim. Biophys. Acta. *1574*, 63-71.

Godbout, R., and Squire, J. (1993). Amplification of a DEAD box protein in retinoblastoma cell lines. Proc. Natl. Acad. Sci. USA *90*, 7578-7582.

Gorbalenya, A.E., and Koonin, E.V. (1993). Helicases: amino acid sequence comparisons and structure-function relationships. Curr. Opin. Struct. Biol. *3*, 419-429.

Gordan, G.W., Berry, G., Liang, X.H., Levine, B., and Herman, B. (1998). Quantitative fluorescence resonance energy transfer measurements using fluorescence microscopy. Biophys. J. *74*, 2702-2713.

Grady-Leopardi, E.F., Schwab, M., Ablin, A.R.,and Rosenau, W. (1986). Detection of *N-myc* oncogene expression in human neuroblastoma by in situ hybridization and blot analysis: relationship to clinical outcome. Cancer Res. *46*, 3196-3199.

Grande, M.A., van der Kraan, I., de Jong, L., van Driel, R. (1997). Nuclear distribution of transcription factors in relation to sites of transcription and RNA polymerase II. J. Cell Sci. *110*, 1781-1791.

Grande, M.A., van der Kraan, I., van Steensel, B., Schul, W., de The, H., van der Voort, H.T., de Jong, L., and van Driel, R. (1996). PML-containing nuclear bodies: their spatial distribution in relation to other nuclear components. J. Cell. Biochem. *63*, 280-291.

Grandori, C., Mac, J., Siëbelt, F., Ayer, D.E., and Eisenman, R.N. (1996). Myc-Max heterodimers activate a DEAD box gene and interact with multiple E box-related sites *in vivo*. EMBO J. *15*, 4344-4357.

Grisolano, J.L., Wesselschmidt, R.L., Pelicci, P.G., and Ley, T.J. (1997). Altered myeloid development and acute leukemia in transgenic mice expressing PML-RAR alpha under control of cathepsin G regulatory sequences. Blood *89*, 376-387.

Grobelny, J.V., Kulp-McEliece, M., and Broccoli, D. (2001). Effects of reconstitution of telomerase activity on telomere maintenance by the alternative lengthening of telomeres (ALT) pathway. Hum. Mol. Genet. *10*, 1953-1961.

Gross, C.H., and Shuman, S. (1998). The nucleoside triphosphatase and helicase activities of vaccina virus NPH-II are essential for virus replication. J. Virol. *72*, 4729-4736.

Grotzinger, T., Sternsdorf, T., Jensen, K., and Will, H. (1996). Interferon-modulated expression of genes encoding the nuclear-dot-associated proteins Sp100 and promyelocytic leukemia protein (PML). Eur. J. Biochem. *238*, 554-560.

Gubitz, A.K., Mourelatos, Z., Abel, L., Rappsilber, J., Mann, M., and Dreyfuss, G. (2002). Gemin 5, a novel WD repeat protein component of the SMN complex that binds Sm proteins. J. Biol. Chem. *277*, 5631-5636.

Guo, A., Salomoni, P., Luo, J., Shih, A., Zhong, S., Gu, W., and Pandolfi, P.P. (2000). The function of PML in p53-dependent apoptosis. Nat. Cell Biol. *10*, 730-736.

Handwerger, K.E., Wu. Z., Murphy, C., and Gall, J.G. (2002). Heat shock induces mini-Cajal bodies in the *Xenopus* germinal vesicle. J. Cell Sci. *115*, 2011-2020.

Hannus, S., Bühler, D., Romano, M., Seraphin, B., and Fischer, U. (2000). The *Schizosaccaromyces pombe* protein Yab8p and a novel factor, Yip1p, share structural and functional similarity with the spinal muscular atrophy-associated proteins SMN and SIP1. Hum. Mol. Genet. *9*, 663-674.

Harbour, J.W., and Dean D.C. (2000). The Rb/E2F pathway: expanding roles and emerging paradigms. Genes Dev. *14*, 2393-2409.

Harlow, E. and Lane, D. (1998). Using antibodies: a laboratory manual. Cold Spring Harbor Laboratory Press, Cold Spring Harbor, New York. pp 103-124.

Hashimoto, K., Nakagawa, Y., Morikawa, H., Niki, M., Egashira, Y., Hirata, I., Katsu, K., and Akao, Y. (2001). Co-overexpression of DEAD box protein rck/p54 and c-myc protein in human colorectal adenomas and the relevance of their expression in cultured cell lines. Carcinogenesis *22*, 1965-1970.

Hasty, P., and Bradley, A. (1993). Gene targeting vectors for mammalian cells. In Gene targeting: A practical approach (ed. A.L. Joyner). IRL Press at Oxford University Press, England. pp 1-31.

Havas, K., Whitehouse, I., and Owen-Hughes, T. (2001). ATP-dependent chromatin remodelling activities. Cell. Mol. Life Sci. *58*, 673-682.

Hebert, M.D., Szymczyk, P.W., Shpargel, K.B., and Matera, A.G. (2001). Coilin forms the bridge between Cajal bodies and SMN, the spinal muscular atrophy protein. Genes Dev. *15*, 2720-2729.

Hector, R.E., Nykamp, K.R., Dheur, S., Anderson, J.T., Non, P.J., Urbinati, C.R., Wilson, S.M., Minvielle-Sebastia, L., and Swanson, M.S. (2002). Dual requirement for yeast hnRNP Nab2p in mRNA poly(A) tail length control and nuclear export. EMBO J. *21*, 1800-1810.

Helin, K., Harlow, E., and Fattaey, A. (1993). Inhibition of E2F-1 transactivation by direct binding of the retinoblastoma protein. Mol. Cell. Biol. *13*, 6501-6508.

He, L.Z., Tribioli, C., Rivi, R., Peruzzi, D., Pelicci, P.G., Soares, V., Cattoretti, G., and Pandolfi, P.P. (1997). Acute leukemia with promyelocytic features in PML/RARalpha transgenic mice. Proc. Natl. Acad. Sci. USA *94*, 5302-5307.

Henn, A., Medalia, O., Shi, S.-P., Steinberg, M., Fraceschi, F., and Sagi, I. (2001). Visualization of unwinding activity of duplex RNA by DbpA, a DEAD box helicase, at single-molecule resolution by atomic force microscopy. Proc. Natl. Acad. Sci. USA *98*, 5007-5012.

Henson, J.D., Neumann, A.A., Yeager, T.R., and Reddel, R.R. (2002). Alternative lengthening of telomeres in mammalian cells. Oncogene *21*, 598-610.

Hilleren, P., McCarthy, .T., Rosbash, M., Parker, R., and Jensen, T.H. (2001). Quality control of mRNA 3'-end processing is linked to the nuclear exosome. Nature *413*, 538-542.

Hirose, Y., and Manley, J.L. (1998). RNA polymerase II is an essential mRNA polyadenylation factor. Nature *395*, 93-96.

Hobert, O., Jallal, B., Schlessinger, J., and Ullrich, A. (1994). Novel signaling pathway suggested by SH3 domain-mediated p95vav/heterogeneous ribonucleoprotein K interaction. J. Biol. Chem. *269*, 20225-20228.

Hofmann, T.G., Möller, A., Sirma, H., Zentgraf, H., Taya, Y., Dröge, W., Will, H. and Schmitz, M.L. (2002). Regulation of p53 activity by its interaction with homeodomain-interacting protein. Nat. Cell Biol. *4*, 1-10.

Hogan, B., Beddington, R., Costantini, F., and Lacy, E. (1994). Manipulating the Mouse Embryo: a laboratory manual. 2nd ed. Cold Spring Harbor Laboratory Press, New York.

Horowitz, J.M., Park, S.-H., Bogenmann, E., Cheng, J.-C., Yandell, D.W., Kaye, F.J., Minna, J.D., Dryja, T.P., and Weinberg, R.A. (1990). Frequent inactivation of the retinoblastoma antioncogene is restricted to a subset of human tumor cells. Proc. Natl. Acad. Sci. USA *87*, 2775–2779.

Hovland, R., Hesketh, J.E., and Pryme, I.R. (1996). The compartmentalization of protein synthesis: importance of cytosketeton and role in mRNA targeting. Int. J. Biochem. Cell Biol. *28*, 1089-1105.

Hsieh, J.-K., Fredersdorf, S., Kouzarides, T., Martin, K., and Lu, X. (1997). E2F-1- induced apoptosis requires DNA binding but not transactivation and is inhibited by the retinoblastoma protein through direct interaction. Genes Dev. *11*, 1840-1852.

Huang, S. (2000). Review: Perinuclolar Structures. J. Struct. Biol. *129*, 233-240.

Huang, S., Deernick, T., Ellisman, M.H., and Spector, D.L. (1997). The dynamic organization of the perinucleolar compartment in the mammalian cell nucleus. J. Cell Biol. *137*, 965-974.

Huang, S., Deernick, T., Ellisman, M.H., and Spector, D.L. (1998). The perinucleolar compartment and transcription. J. Cell Biol. *143*, 35-47.

Huang, Y., and Lui, Z.-R. (2002). The ATPase, RNA unwinding, and RNA binding activities of recombinant p68 RNA helicase. J. Biol. Chem. *277*, 12810-12815.

Huang, S., and Spector, D.L. (1991). Nascent pre-mRNA transcripts are associated with nuclear regions enriched in splicing factors. Genes Dev. *5*, 2288-2302.

Huang, S. and Spector, D.L. (1992). U1 and U2 small nuclear RNAs are present in nuclear speckles. Proc. Natl. Acad. Sci. USA *89*, 305-308.

Huang, S., and Spector, D.L. (1996). Intron-dependent recruitment of pre-mRNA splicing factors to sites of transcription. J. Cell Biol. *133*, 719-732.

Iavarone, A., Garg, P., Lasorella, A., Hsu, J., and Israel, M.A. (1994). The helix-loop-helix protein Id-2 enhances cell proliferation and binds to the retinoblastoma protein. Genes Dev. *8*, 1270-1284.

Igney, F.H., and Krammer, P.H. (2002). Death and anti-death: tumour resistance to apoptosis. Nat. Rev. Cancer 2, 277-288

Ikeda, T., Ikeda, K., Sasaki, K., Kawakami, K., and Takahara, J. (1999). The inv(11)(p15q22) chromosome translocation of therapy-related myelodysplasia with NUP98-DDX10 and DDX10-NUP98 fusion transcripts. Int. J. Hematol. *69*, 160-164.

Irwin, N., Baekelandt, V., Goritchenko, L., and Benowitz, L.I. (1997). Identification of two proteins that bind to a pyrimidine-rich sequence in the 3'-untranslated region of GAP-43 mRNA. Nucleic Acids Res. *25*, 1281-1288.

Ishov, A.M., Sotnikov, A.G., Negorev, D., Vladimirova, O.V., Neff, N., Kamitani, T., Yeh, E.T., Strauss, J.F., and Maul, G.G. (1999). PML is critical for ND10 formation and recruits the PML-interacting protein Daxx to this nuclear structure when modified by SUMO-1. J. Cell Biol. *147*, 221-234.

Ishov, A.M., Stenberg, R.M., and Maul, G.G. (1997). Human cytomegalovirus immediate early interaction with host nuclear structures: definition of an immediate transcript environment. J. Cell Biol. *138*, 5-16.

Iwahashi, H., Eguchi, Y., Yasuhara, N., Hanafusa, T., Matsuzawa, Y., and Tsujimoto, Y. (1997). Synergistic anti-apoptotic activity between Bcl-2 and SMN implicated in spinal muscular atrophy. Nature *390*, 413-417.

Jablonka, S., Rossoll, W., Schrank, B., and Sendtner, M. (2000). The role of SMN in spinal muscular atrophy. J. Neurol. *247* (Suppl 1), i37-i42.

Jackson, D.A., Hassan, A.B., Errington, R.J., and Cook, P.R. (1993). Visualization of focal sites of transcription within human nuclei. EMBO J. *12*, 1059-1065.

Jacks, T., Fazeli, A., Schmitt, E.M., Bronson, R.T., Goodell, M.A., and Weinberg, R.A. (1992). Effects of an *Rb* mutation in the mouse. Nature 359, 295-300.

Jacobs, E.Y., Frey, M.R., Wu, W., Ingledue, T.C., Gebuhr, T.C., Gao, L., Marzluff, W.F., and Matera, A.G. (1999). Coiled bodies preferentially associate with U4, U11, U12 small nuclear RNA genes in interphase HeLa cells but not with U6 and U7 genes. Mol. Biol. Cell *10*, 1653-1663.

Jankowsky, E., Gross, C.H., Shuman, S., and Pyle, A.M. (2000). The DExH protein NPH-II is a processive and directional motor for unwinding RNA. Nature *403*, 447-451.

Jankowsky, E., Gross, C.H., Shuman, S., and Pyle, A.M (2001). Active disruption of an RNA-protein interaction by a DexH/D RNA helicase. Science *291*, 121-125.

Jensen, K., Shiels, C., and Freemont, P.S. (2001). PML protein isoforms and the RBCC/TRIM motif. Oncogene *20*, 7223-7233.

Jiménez-Garcia, L.F., Segura-Valdez, M.L., Ochs, R.L., Rothblum, L.I., Hannan, R., Spector, D.L. (1994). Nucleologenesis: U3 snRNA-containing prenucleolar bodies move to sites of active pre-rRNA transcription after mitosis. Mol. Biol. Cell *5*, 955-966.

Jiménez-Garcia, L.F., and Spector, D.L. (1993). *In vivo* evidence that transcription and splicing are cooridinated by a recuiting mechanism. Cell *73*, 47-59.

Johnson, D.G., Cress, W.D., Jakoi, L., and Nevins, J.R. (1994). Oncogenic capacity of the E2F1 gene. Proc. Natl. Acad. Sci. USA *91*, 12823-12827.

Johnson, D.G., Schwarz, J.K., Cress, W.D., and Nevins, J.R. (1993). Expression of transcription factor E2F1 induces quiescent cells to enter S phase. Nature *23*, 349-352.

Jones, K.W., Gorzynski, K., Hales, C.M., Fischer, U., Badbanchi, F., Terns, R.M., and Terns, M.P. (2001). Direct interaction of the spinal muscular atrophy disease protein SMN with the small nucleolar RNA-associated protein fibrillarin. J. Biol. Chem. *276*, 38645-38651.

Jordan, P., Cunha, C., and Carmo-Fonseca, M. (1997). The cdk-cyclin H-MAT1 complex associated with TFIIH is localized in coiled bodies. Mol. Biol. Cell *8*, 1207-1217.

Kaelin, W.G., Jr. (1999). Functions of the retinoblastoma protein. Bioessays *21*, 950-958.

Kamei, Y., Xu, L., Heinzel, T., Torchia, J., Kurokawa, R., Gloss, B., Lin, S.C., Heyman, R.A., Rose, D.W., Glass, C.K., and Rosenfeld, M.G. (1996). A CBP integrator complex mediates transcriptional activation and AP-1 inhibition by nuclear receptors. Cell *85*, 403-414.

Kamitani, T., Nguyen, H.P., Kito, k., Fukuda-Kamitani, T., and Yeh, E.T. (1998). Covalent modification of PML by the sentrin family of ubiquitin-like proteins. J. Biol. Chem. *273*, 3117-3120.

Kang, D.-c., Gopalkrishnan, R.V., Wu, Q., Jankowsky, E., Pyle, A.M., and Fisher, P.B. (2002). mda-5: An interferon-inducible putative RNA helicase with double-stranded RNA-dependent ATPase activity and melanoma growth-suppressive properties. Proc. Natl. Acad. Sci. USA *99*, 637-642.

Karlsson, A., Helou, K., Walentinsson, A., Hedrich, H.J., Szpirer, C., and Levan, G. (2001). Amplification of *Mycn*, *Rrm2*, and *Odc1* in rat uterine endometrial carcinomas. Genes Chromosomes Cancer *31*, 345-356.

Kaser, A., Bogengruber, E., Hallegger, M., Doppler, E., Lepperdinger, G., Jantsch, M., Breitenbach, M., and Kreil, G. (2001). Brix from *Xenopus laevis* and brx1p from yeast define a new family of proteins involved in the biogenesis of large ribosomal subunits. Biol. Chem. *382*, 1637-1647.

Kelly, C., Van Driel, R., and Wilkinson, G.W. (1995). Disruption of PML-associated nuclear bodies during human cytomegalovirus infection. J. Gen. Virol. *76*, 2887-2893.

Kessler, M.M., Henry, M.F., Shen, E., Zhao, J., Gross, S., Silver, P.A, and Moore, C.L. (1997). Hrp1, a sequence-specific RNA-binding protein that shuttles between the nucleus and the cytoplasm, is required for mRNA 3'-end formation in yeast. Genes Dev. *11*, 2545-2456.

Khan, M.M., Nomura, T., Kim, H., Kaul, S.C., Wadhwa, R., Zhong, S., Pandolfi, P.P., and Ishii, S. (2001a). PML-RARalpha alleviates the transcriptional repression mediated by tumor suppressor Rb. J. Biol. Chem. *276*, 43491-43494.

Khan, M.M., Nomura, T., Kim, H., Kaul, S.C., Wadhwa, R., Shinagawa, T., Ichikawa-Iwata, E., Zhong, S., Pandolfi, P.P., and Ishii, S. (2001b). Role of PML and PML-RARalpha in Mad-mediated transcriptional repression. Mol. Cell *6*, 1233-1243.

Khan, S.H., and Wahl, G.M. (1998). p53 and pRb prevent rereplication in response to microtubule inhibitiors by mediating a reversible G1 arrest. Cancer Res. *58*, 396-401.

Kim, Y.H., Choi, C.Y., and Kim, Y. (1999). Covalent modification of the homeodomain-interacting protein kinase 2 (HIPK2) by the ubiquitin-like protein SUMO-1. Proc. Natl. Acad. Sci. USA *96*, 12350-12355.

Kim, H., and Lee, Y. (2001). Interaction of poly(A) polymerase with the 25-kDa subunit of cleavage factor I. Biochem. Biophys. Res. Commun. *289*, 513-518.

Kim, M.K., and Nikodem, V.M. (1999). HnRNP U inhibits carboxy-terminal domain phosphorylation by TFIIH and represses RNA polymerase II elongation. Mol. Cell. Biol. *10*, 6833-6844.

Kistler, A.L., and Guthrie, C. (2001). Deletion of MUD2, the yeast homolog of U2AF65 can bypass the requirement for Sub2, an essential spliceosomal ATPase. Genes Dev. *15*, 42-49.

Kleiman, F.E., and Manley, J.L. (1999). Functional interaction of BRCA1-associated BARD1 with polyadenylation factor CstF-50. Science *285*, 1576-1579.

Kleiman, F.E., and Manley, J.L. (2001). The BARD1-CstF-50 interaction links mRNA 3' end formation to DNA damage and tumor suppression. Cell *104*, 743-753.

Knudson AG Jr. (1971). Mutation and cancer: statistical study of retinoblastoma. Proc. Natl. Acad. Sci. USA *68*, 820-823.

Koken, M.H., Linares-Cruz, G., Quignon, F., Viron, A., Chelbi-Alix, M.K., Sobczak-Thepot, J., Juhlin, L., Degos, L., Calvo, F., and de The, H. (1995). The PML growth-suppressor has an altered expression in human oncogenesis. Oncogene *10*, 1315-1324.

Koken, M.H., Puvion-Dutilleul, F., Guillemin, M.C., Viron, A., Linares-Cruz, G., Stuurman, N., de Jong, L., Szostecki, C., Calvo, F., Chomienne, C., et al. (1994). The t(15;17) translocation alters a nuclear body in a retinoic acid-reversible fashion. EMBO J. *13*, 1073-1083.

Krause, S., Fakan, S., Weis, K., and Wahle, E. (1994). Immunodetection of poly(A) binding protein II in the cell nucleus. Exp. Cell Res. *214*, 75-82.

Kuroda, H., White, P.S., Sulman, E.P., Manohar, C.F., Reiter, J.L., Cohn, S.L., and Brodeur, G.M. (1996). Physical mapping of the *DDX1* gene to 340 kb 5' of *MYCN*. Oncogene *13*, 1561-1565.

La Bella, V., Kallenbach, S., and Pettmann, B. (2000). Expression and subcellular localization of two isoforms of the survival motor neuron protein in different cell types. J. Neurosci. Res. *62*, 346-356.

Lafontaine, D.L.J., and Tollervey, D. (1998). Birth of the snoRNPs: the evolution of the modification-guide snoRNAs. Trends Biochem. Sci. *23*, 383-388.

Lai, A., Lee, J.M., Yang, W.M., DeCaprio, J.A., Kaelin, W.G., Jr., Seto, E., and Branton, P.E. (1999). RBP1 recruits both histone deacetylase-dependent and –independent repression activities to retinoblastoma family proteins. Mol. Cell. Biol. 19, 6632-6641.

Lamond, A.I., and Carmo-Fonseca, M. (1993). The coiled body. Trends Cell Biol. *3*, 198-204.

Lamond, A.I., and Earnshaw, W.C. (1998). Structure and function in the nucleus. Science *280*, 547-553.

LaMorte, V.J,, Dyck, J.A., Ochs, R.L., and Evans, R.M. (1998). Localization of nascent RNA and CREB binding protein with the PML-containing nuclear body. Proc. Natl. Acad. Sci. USA *95*, 4991-4996.

Langley, E., Pearson, M., Faretta, M., Bauer, U.-M., Frye, R.A., Minucci, S., Pelicci, P.G., and Kouzarides, T. (2002). Human SIR2 deacetylates p53 and antagonizes PML/p53-induced cellular senescence. EMBO J. *21*, 2383-2396.

Lasorella, A., Noseda, M., Beyna, M., and Iavarone, A. (2000). Id2 is a retinoblastoma protein target and mediates signalling by Myc oncoproteins. Nature *407*, 592-598.

Lavau, C., Marchio, A., Fagioli, M., Jansen, J., Falini, B., Lebon, P., Grosveld, F., Pandolfi, P.P., Pelicci, P.G., and Dejean, A. (1995). The acute promyelocytic leukaemia-associated PML gene is induced by interferon. Oncogene *11*, 871-876.

Leary, D.J., and Huang, S. (2001). Regulation of ribosome biogenesis within the nucleolus. FEBS Lett. *509*, 145-150.

Lee, E.Y.-H.P., Chang, C.-Y., Hu, N., Wang, Y.-C.J., Lai, C.-C., Herrup, K., Lee, W.-H., and Bradley, A. (1992). Mice deficient for Rb are nonviable and show defects in neurogenesis and haematopoiesis. Nature *359*, 288-294.

Lerner, E.A., Lerner, M.R., Janeway, C.A., Jr., and Steitz, J.A. (1981). Monoclonal antibodies to nucleic acid-containing cellular constituents: Probes for molecular biology and autoimmune disease. Proc. Natl. Acad. Sci. USA *78*, 2737-2741.

Li, H., Leo, C., Zhu, J., Wu, X., O'Neil, J., Park, E.J., and Chen, J.D. (2000). Sequestration and inhibition of Daxx-mediated transcriptional repression by PML. Mol. Cell. Biol. *20*, 1784-1796.

Linder, P., and Stutz, F. (2001). mRNA export: travelling with DEAD box proteins. Curr. Biol. *11*, R961-R963.

Linder, P., Tanner, K., and Banroques, J. (2001). From RNA helicases to RNPases. Trends Biochem. Sci. *26*, 339-341.

Lipshitz, H.D., and Smibert, C.A. (2000). Mechanisms of RNA localization and translational regulation. Curr. Opin. Genet. Dev. *10*, 476-488.

Liu, Q., and Dreyfuss, G. (1996). A novel nuclear structure containing the survival of motor neurons protein. EMBO J. *15*, 3555-3565.

Liu, Q., Fischer, U., Wang, F., and Dreyfuss, G. (1997). The spinal muscular atrophy disease gene product SMN, and its associated protein SIP1 are in a complex with spliceosomal snRNP proteins. Cell *90*, 1013-1021.

Long, R.M., Elliott, D.J., Stutz, F., Rosbash, M., and Singer, R.H. (1995). Spatial consequences of defective processing of specific yeast mRNAs revealed by fluorescent in situ hybridization. RNA *1*, 1071-1078.

Luking, A., Stahl, U., and Schmidt, U. (1998). The protein family of RNA helicases. Crit. Rev. Biochem. Mol. Biol. *33*, 259-296.

Luo, M.L., Zhou, Z., Magni, K., Christoforides, C., Rappsilber, J., Mann, M., and Reed, R. (2001). Pre-mRNA splicing and mRNA export linked by direct interactions between UAP56 and Aly. Nature *413*, 644-647.

Luo, R.X., Postigo, A.A., and Dean, D.C. (1998). Rb interacts with histone deacetylase to repress transcription. Cell *92*, 463-473.

Luscher, B. (2001). Function and regulation of the transcription factors of the Myc/Max/Mad network. Gene *277*, 1-14.

Lutter, M., Perkins, G.A., and Wang, X. (2001). The pro-apoptotic Bcl-2 family member tBid localizes to mitochondrial contact sites. BMC Cell Biol. *2*, 22.

Lutz, C.S., Murthy, K.G.K., Schek, N., O'Connor, J.P., Manley, J.L., and Alwine, J.C. (1996). Interaction between the U1 snRNP-A protein and the 160-kD subunit of cleavage-polyadenylation specificity factor increases polyadenylation efficiency *in vitro*. Genes Dev. *10*, 325-337.

Ma, T., Van Tine, B.A., Yue, W., Garrett, MM., Nelson, D., Adams, P.D., Wang, J., Qin, J., Chow, L.T., and Harper, J.W. (2000). Cell cycle-regulated phosphorylation of $p220^{NPAT}$ by cyclin E/Cdk2 in Cajal bodies promotes histone gene transcription. Genes Dev. *14*, 2298-2313.

Macleod, K.F., Hu, Y., and Jacks, T. (1996). Loss of Rb activates both p53-dependent and independent cell death pathways in the developing mouse nervous system. EMBO J. *15*, 6178-6188.

Magnaghi-Jaulin, L., Groisman, R., Naguibneva, I., Robin, P., Lorain, S., Le Villain, J.P., Troalen, F., Trouche, D., and Harel-Bellan, A. (1998). Retinoblastoma protein represses transcription by recruiting a histone deacetylase. Nature *391*, 601-605.

Mahajan, R., Delphin, C., Guan, T., Gerace, L., and Melchior, F. (1997). A small ubiquitin-related polypeptide involved in targeting RanGAP1 to nuclear pore complex protein RanBP2. Cell *88*, 97-107.

Manohar, C.F., Salwen, H.R., Brodeur, G.M., and Cohn, S.L. (1995). Co-amplification and concomitant high levels of expression of a DEAD box gene with *MYCN* in human neuroblastoma. Genes Chromosomes Cancer *14*, 196-203.

Martelange, V., De Smet, C., De Plaen, E., Lurquin, C., and Boon, T. (2000). Identification on a human sarcoma of two new genes with tumor-specific expression. Cancer Res. *60*, 3848-3855.

Martinou, J.C., and Green, D.R. (2001). Breaking the mitochondrial barrier. Nat. Rev. Mol. Cell. Biol. *2*, 63-67.

Matera, A.G., and Frey, M.R. (1998). Coiled bodies and gems: Janus or jemini? Am. J. Hum. Genet. *63*, 317-321.

Matera, A.G., Frey, M.R., Margleot, K., and Woilin, S.L. (1995). A perinucleolar compartment contains several RNA polymerase III transcripts as well as the polypyrimidine tract-binding protein, hnRNP I. J. Cell Biol. *129*, 1181-1193.

Matera, A.G., and Ward, D.C. (1993). Nucleoplasmic organization of small nuclear ribonucleoproteins in cultured human cells. J. Cell Biol. *121*, 715-727.

Mathon, N. F., and Lloyd, A. C. (2001). Cell senescence and cancer. Nature Rev Cancer *1*, 203-213.

Maul, G.G., Guldner, H.H., and Spivack, J.G. (1993). Modification of discrete nuclear domains induced by herpes simplex virus type 1 immediate early gene 1 product (ICP0). J. Gen. Virol. *74*, 2679-2690.

Maul, G.G., Jensen, D.E., Ishov, A.M., Herlyn, M., and Rauscher, F.J., III (1998). Nuclear redistribution of BRCA1 during viral infection. Cell. Growth Differ. *9*, 743-755.

Maul, G.G., Yu, E., Ishov, A.M., and Epstein, A.L. (1995). Nuclear domain 10 (ND10) associated proteins are also present in nuclear bodies and redistribute to hundreds of nuclear sites after stress. J. Cell. Biochem. *59*, 498-513.

McCracken, S.N., Fong, N., Yankulov, K., Ballantyne, S., Pan, G., Greenblatt, J., Patterson, S.D., Wickens, M., and Bentley, D.L. (1997). The C-terminal domain of RNA polymerse II couples mRNA processing to transcription. Nature *385*, 357-361.

McCracken, S.N., Lambermon, M., and Blencowe, B.J. (2002). SRm160 splicing coactivator promotes transcript 3'-end cleavage. Mol. Cell. Biol. *22*, 148-160.

Meier, U.T., Blobel, G. (1994). NAP57, a mammalian nucleolar protein with a putative homolog in yeast and bacteria. J. Cell Biol. *127*, 1505-1514.

Meister, G., Bühler, D., Laggerbauer, B., Zobawa, M., Lottspeich, F., and Fischer, U. (2000). Characterization of a nuclear 20S complex containing the survival of motor neurons (SMN) protein and a specific subset of spliceosomal Sm proteins. Hum. Mol. Genet. *9*, 1977-1986.

Meister, G., Bühler, D., Pillai, R., Lottspeich, F., and Fischer, U. (2001). A multiprotein complex mediates the ATP-dependent assembly of spliceosomal U snRNPs. Nat. Cell Biol. *3*, 945-949.

Miau, L.H., Chang, C.J., Shen, B.J., Tsai, W.H., and Lee, S.C. (1998). Identification of heterogeneous nuclear ribonucleoprotein K (hnRNP K) as a repressor of C/EBPbeta-mediated gene activation. J. Biol. Chem. *273*, 10784-10791.

Michaelson, J.S., Bader, D., Kuo, F., Kozak, C., and Leder, P. (1999). Loss of Daxx, a promiscuously interacting protein, results in extensive apoptosis in early mouse development. Genes Dev. *13*, 1918-1923.

Michelotti, G.A., Michelotti, E.F., Pullner, A., Duncan, R.C., Eick, D., and Levens, D. (1996). Multiple single-stranded *cis* elements are associated with activated chromatin of the human *c-myc gene* in vivo. Mol. Cell. Biol. *16*, 2350-2360.

Mierendorf, R.C., and Pfeffer, D. (1987). Direct sequencing of denatured plasmid DNA. Methods Enzymol. *152*, 556-562.

Miller, H. (1987) Practical aspects of preparing phage and plasmid DNA: Growth, maintenance, and storage of bacteria and bacteriophage. Methods Enzymol 152: 158-162.

Min, H., Turck, C.W., Nikolic, J.M., and Black, D.L. (1997). A new regulatory protein, KSRP, mediates exon inclusion through an intronic splicing enhancer. Genes Dev. *11*, 1023-1036.

Minshall, N., Thom, G., and Standart, N. (2001). A conserved role of a DEAD box helicase in mRNA masking. RNA *7*, 1728-1742.

Mintz, P.J., Patterson, S.D., Neuwald, A.F., Spahr, C.S., and Spector, D.L. (1999). Purification and biochemical characterization of interchromatin granule clusters. EMBO J. *18*, 4308-4320.

Mintz, P.J., and Spector, D.L. (2000). Compartmentalization of RNA processing factors within nuclear speckles. J. Struct. Biol. *129*, 241-251.

Missel, A., Lambert, L., Norskau, G., Goringer, H.U. (1999). DEAD-box protein HEL64 from Trypanosoma brucei: subcellular localization and gene knockout analysis. Parasitol. Res. *85*, 324-330.

Missel, A., Souza, A.E., Norskau, G., Goringer, H.U. (1997). Disruption of a gene encoding a novel mitochondrial DEAD-box protein in Trypanosoma brucei affects edited mRNAs. Mol. Cell. Biol. *17*, 4895-4903.

Mistelli, T. (2001). Protein dynamics: implications for nuclear architecture and gene expression. Science *291*, 843-847.

Mistelli, T., Cáceres, J.F., and Spector, D.L. (1997). The dynamics of a pre-mRNA splicing factor in living cells. Nature *387*, 523-527.

Monneron, A., and Bernhard, W. (1969). Fine structural organization of the interphase nucleus in some mammalian cells. J. Ultrastruc. Res. *27*, 266-288.

Moore, C.L., and Sharp, P.A. (1985). Accurate cleavage and polyadenylation of exogenous RNA substrate. Cell *41*, 845-855.

Moreira, A., Takagaki, Y., Brackenridge, S., Wollerton, M., Manley, J.L., and Proudfoot, N.J. (1998). The upstream sequence element of the C2 complement poly(A) signal activates mRNA 3' end formation by two distinct mechanisms. Genes Dev. *12*, 2522-2534.

Moreno Diaz de la Espina, S., Risueno, M.C., and Medina, F.J. (1982). Ultrastructural, cytochemical and autoradiographic characterization of coiled bodies in the plant cell nucleus. Biol. Cell *44*, 229-238.

Morgan, G.T., Doyle, O., Murphy, C., and Gall, J.G. (2000). RNA polymerase II holoenzymes and subcomplexes. J. Biol. Chem. *273*, 27757-27760.

Morgenbesser, S.D., Williams, B.O., Jacks, T., and DePinho, R.A. (1994). p53-dependent apoptosis produced by Rb-deficiency in the developing mouse lens. Nature *371*, 72-74.

Mortensen, R. (1993). Gene targeting by homologous recombination. In Current Protocols in Molecular Biology. 9.15.1-9.17.3.

Mourelatos, Z., Abel, L., Yong, J., Kataoka, N., and Dreyfuss, G. (2001). SMN interacts with a novel family of hnRNP and spliceosomal proteins. EMBO J. *20*, 5443-5452.

Muller, S., Matunis, M.J., and Dejean, A. (1998). Conjugation with the ubiquitin-related modifier SUMO-1 regulates the partitioning of PML within the nucleus. EMBO J. *17*, 61-70.

Muratani, M., Gerlich, D., Janicki, S.M., Gebhard, M., Eils, R., and Spector, D.L. (2002). Metabolic-energy-dependent movement of PML bodies within the mammalian cell nucleus. Nat. Cell Biol. *4*, 106-110.

Murthy, K.G.K., and Manley, J.L. (1995). The 160-kD subunit of human cleavage-polyadenylation specificity factor coordinates pre-mRNA 3'–end formation. Genes Dev. *9*, 2672-2683.

Mu, Z.M., Chin, K.V., Liu, J.H., Lozano G., and Chang, K.S. (1994). PML, a growth suppressor disrupted in acute promyelocytic leukemia. Mol. Cell. Biol. *14*, 6858-6867.

Nagy, A. (2000). Cre recombinase: the universal reagent for genome tailoring. Genesis *26*, 99-109.

Nagy, A., Gócza, E., Diaz, E.M., Prideaux, V.R., Iványi, E., Markkula, M., and Rossant, J. (1990). Embryonic stem cells alone are able to support fetal development in the mouse. Development *110*, 815-821.

Nagy, A., Rossant, J., Nagy, R., Abramow-Newerly, W., and Roder, J.C. (1993). Derivation of completely cell culture-derived mice from early-passage embryonic stem cells. Proc. Natl. Acad. Sci. USA *90*, 8424-8428.

Nakamura, A., Amikura, R., Hanyu, K., and Kobayashi, S. (2001). Me31B silences translation of oocyte-localizing RNAs through the formation of cytoplasmic RNP complex during *Drosophila* oogenesis. Development *128*, 3233-3242.

Nakagawa, Y., Morikawa, H., Hirata, I., Shiozaki, M., Matsumoto, A., Maemura, K., Nishikawa, T., Niki, M., Tanigawa, N., Ikegami, M., Katsu, K., and Akao, Y. (1999). Overexpression of rck/p54, a DEAD box protein, in human colorectal tumours. Br. J. Cancer *80*, 914-917.

Nakao, K., Nishino, M., Takeuchi, K., Iwata, M., Kawano, A., Arai, Y., and Ohki, M. (2000). Fusion of the nucleoporin gene, NUP98, and the putative RNA helicase gene, DDX10, by inversion 11 (p15q22) chromosome translocation in a patient with etoposide-related myelodysplastic syndrome. Intern. Med. *39*, 412-415.

Narayanan, A., Speckmann, W., Terns, R., and Terns, M.P. (1999). Role of the box C/D motif in localization of small nucleolar RNAs to coiled bodies and nucleoli. Mol. Biol. Cell *10*, 2131-2147.

Naylor, O., Hartmann, A.M., and Stamm, S. (2000). The ER repeat protein YT521-B localizes to a novel subnuclear compartment. J. Cell Biol. *150*, 949-961.

Negorev, D., and Maul, G.G. (2001). Cellular proteins localized at and interacting within ND10/PML nuclear bodies/PODs suggest functions of a nuclear depot. Oncogene *20*, 7234-7242.

Neisen, P.D., Waber, P.G., Rich, M.A., Pierce, S., Garvin, J.R., Jr., Gilbert, F., and Lanzkowsky, P. (1988). *N-myc* oncogene RNA expression in neuroblastoma. J. Natl. Cancer Inst. *80*, 1633-1637.

Nervi, C., Ferrara, F.F., Fanelli, M., Rippo, M.R., Tomassini, B., Ferrucci, P.F., Ruthardt, M., Gelmetti, V., Gambacorti-Passerini, C., Diverio, D., Grignani, F., Pelicci, P.G., and Testi, R. (1998). Caspases mediate retinoic acid-induced degradation of the acute promyelocytic leukemia PML/RARalpha fusion protein. Blood *92*, 2244-2251.

Neubauer, G., King, A., Rappsilber, J., Calvio, C., Watson, M., Ajuh, P., Sleeman, J., Lamond, A.,and Mann, M. (1998). Mass spectrometry and EST-database searching allows characterization of the multi-protein spliceosome complex. Nat. Genet. *20*, 46-50.

Nishiyama, M., Arai, Y., Tsunematsu, Y., Kobayashi, H., Asami, K., Yabe, M., Kato, S., Oda, M., Eguchi, H., Ohki, M., and Kaneko, Y. (1999). 11p15 translocations involving the *NUP98* gene in childhood therapy-related acute myeloid leukemia/myelodysplastic syndrome. Genes Chromosomes Cancer *26*, 215-220.

Niwa, M., MacDonald, C.C., and Berget, S.M. (1992). Are vertebrate exons scanned during splice-site selection? Nature *360,* 277-280.

Noguchi, T., Akiyama, K., Yokoyama, M., Kanda, N., Matsunaga, T., and Nishi, Y. (1996). Amplification of a DEAD box gene (*DDX1*) with the *MYCN* gene in neuroblastomas as a result of cosegregation of sequences flanking the *MYCN* locus. Genes Chromosomes Cancer *15*, 129-133.

Ostareck, D.H., Ostareck-Lederer, A., Wilm, M., Thiele, B.J., and Mann, M., Hentze, M.W. (2001). mRNA silencing in erythroid differentiation: hnRNP K and hnRNP E1 regulate 15-lipoxygenase translation from the 3' end. Cell. *89*, 597-606.

Ostareck-Lederer, A., Ostareck, D.H., Cans, C., Neubauer, G., Bomsztyk, K., Superti-Furga, G., and Hentze, M.W. (2002). c-Src-mediated phosphorylation of hnRNP K drives translational activation of specifically silenced mRNAs. Mol. Cell. Biol. *22*, 4535-4543.

Ostrowski, J., Schullery, D.S., Denisenko, O.N., Higaki, Y., Watts, J., Aebersold, R., Stempka, L., Gschwendt, M., and Bomsztyk, K. (2000). Role of tyrosine phosphorylation in the regulation of the interaction of heterogenous nuclear ribonucleoprotein K protein with its protein and RNA partners. J. Biol. Chem. 275, 3619-3628.

Ostrowski, J., Wyrwicz, L., Rychlewski, L., and Bomsztyk, K. (2002). Heterogeneous nuclear ribonucleoprotein K protein associates with multiple mitochondrial transcripts within the organelle. J. Biol. Chem. *277*, 6303-6310.

Otero, L.J., Ashe, M.P., and Sachs, A.B. (1999). The yeast poly(A)-binding protein Pab1p stimulates *in vitro* poly(A)-dependent and cap-dependent translation by distinct mechanisms. EMBO J. *18*, 3153-3163.

Page, A.M., and Hieter, P. (1999). The anaphase-promoting complex: New subunits and regulators. Annu. Rev. Biochem. *68*,583-609.

Pagliardini, S., Giavazzi, A., Setola, V., Lizier, C., Di Luca, M., DeBiasi, S., and Battaglia, G. (2000). Subcellular localization and axonal transport of the survival motor neuron (SMN) protein in the developing rat spinal cord. Hum. Mol. Genet. *9*, 47-56.

Palacios, I.M., and Johnston, D.S. (2001). Getting the message across: the intracellular localization of mRNAs in higher eukaryotes. Annu. Rev. Cell Dev. Biol. *17*, 569-614.

Pandita, A., Godbout, R., Zielenska, M., Thorner, P., Bayani, J., and Squire, J.A. (1997). Relational mapping of *MYCN* and *DDX1* in band 2p24 and analysis of amplicon arrays in double minute chromosomes and homogeneously staining regions by use of free chromatin FISH. Genes Chromosomes Cancer *20*, 243-252.

Pandita, A., Zielenska, M., Thorner, P., Bayani, Godbout, R., Greenberg, M., and Squire, J.A. (1999). Application of comparative genomic hybridizaion, spectral karyotyping, and microarray analysis in the identification of subtype-specific patterns of genomic changes in rhabdomyosarcoma. Neoplasia *1*, 262-275.

Parry, D.A.D., and Steinert, P.M. (1999). Intermediate filaments: molecular architecture, assembly, dynamics and polymorphism. Q. Rev. Biophys. *32*, 99-187.

Pause, A., Méthot, N., and Sonenberg, N. (1993). The HRIGRXXR region of the DEAD box RNA helicase eukaryotic translation initiation factor 4A is required for RNA binding and ATP hydrolysis. Mol. Cell. Biol. *13*, 6789-6798.

Pause, A., and Sonenberg, N. (1992). Mutational anaylsis of a DEAD box RNA helicase: the mammalian translation initiation factor eIF-4A. EMBO J. *11*, 2643-2654.

Pearson, M., Carbone, R,, Sebastiani, C., Cioce, M., Fagioli, M., Saito, S., Higashimoto, Y., Appella, E,. Minucci, S., Pandolfi, P.P., and Pelicci, P.G. (2000). PML regulates p53 acetylation and premature senescence induced by oncogenic Ras. Nature *406*, 207-210.

Pease, S., Braghetta, P., Gearing, D., Grail, D., and Williams, R.L. (1990). Isolation of embryonic stem (ES) cells in media supplemented with recombinant leukemia inhibitory factor (LIF). Dev. Biol. *141*, 344-352.

Pederson, T. (1998). The plurifunctional nucleolus. Nucleic Acids Res. *26*, 3871-3876.

Pellizzoni, L., Baccon, J., Charroux, B., and Dreyfuss, G. (2001a). The survival of motor neurons (SMN) protein interacts with the snoRNP proteins fibrillarin and GAR1. Curr. Biol. *11*, 1079-1088.

Pellizzoni, L., Baccon, J., Rappsilber, J., Mann, M., and Dreyfuss, G. (2002). Purification of native survival motor neurons complexes and identification of gemin6 as a novel component. J. Biol. Chem. *277*, 7540-7545.

Pellizzoni, L., Charroux, B., Rappsilber, J., Mann, M., and Dreyfuss, G. (2001b). A functional interaction between the survival of motor neuron complex and RNA polymerase II. J. Cell Biol. *152*, 75-86.

Pellizzoni, L., Kataoka, N., Charroux, B., and Dreyfuss, G. (1998). A novel function for SMN, the spinal muscular atrophy gene product, in pre-mRNA splicing. Cell *95*, 615-624.

Perkins, G., Renken, C., Martone, M.E., Young, S.J., Ellisman, M., and Frey, T. (1997). Electron tomography of neuronal mitochondria: three-dimensional structure and organization of cristae and membrane contacts. J. Struct. Biol. *119*, 260-272.

Perrem, K., Colgin, L.M., Neumann, A.A., Yeager, T.R., and Reddel, R.R. (2001). Coexistence of alternative lengthening of telomeres and telomerase in hTERT-transformed GM847 cells. Mol. Cell. Biol. *21*, 3862-3875.

Pestova, T.V., and Hellen, C.U.T. (2000). The structure and function of initiation factors in eukaryotic protein synthesis. Cell. Mol. Life Sci. *57*, 651-674.

Pettersson, I., Hinterberger, M., Mimori, T., Gottlieb, E., and Steitz, J.A. (1984). The structure of mammalian small nuclear ribonucleoproteins. Identification of multiple protein components reactive with anti-(U1)ribonucleoprotein and anti-Sm autoantibodies. J. Biol. Chem. *259*, 5907-5914.

Phillips, A.C., Bates, S., Ryan, K.M., Helin, K., and Vousden, K.H. (1997). Induction of DNA synthesis and apoptosis are separable functions of E2F-1. Genes Dev. *11*, 1853-1863.

Phillips, A.C., Ernst, M.K., Bates, S., Rice, N.R., and Vousden, K.H. (1999). E2F-1 potentiates cell death by blocking antiapoptotic signalling pathways. Mol. Cell *4*, 771-781.

Pinol-Roma, S., Swanson, M.S., Gall, J.G., and Dreyfuss, G. (1989). A novel heterogeneous nuclear RNP protein with a unique distribution on nascent transcripts. J. Cell Biol. *109*, 2575-2587.

Platani, M., Goldberg, I., Swedlow, J.R., and Lamond, A.I. (2000). *In vivo* analysis of Cajal body movement, separation, and joining in live human cells. J. Cell Biol. *151*, 1561-1574.

Pombo, A., Cuello, P., Schul, W., Yoon, J.B., Roeder, R.G., Cook, P.R., and Murphy, S. (1988). Regional and temporal specialization in the nucleus: a transcriptionally-active nuclear domain rich in PTF, Oct1, and PIKA antigens associates with specific chromosomes early in the cell cycle. EMBO J. *17*, 1768-1778.

Pomerantz, J., Schreiber-Agus, N., Liegeois, N.J., Silverman, A., Alland, L., Chin, L., Potes, J., Chen, K., Orlow, I., Lee, H.W., Cordon-Cardo, C., and DePinho, R.A. (1998). The Ink4a tumor suppressor gene product, p19Arf, interacts with Mdm2 and neutralizes Mdm2's inhibition of p53. Cell *92*, 713-723.

Ponting, C., Schultz, J., and Bork, P. (1997). SPRY domains in ryanodine receptors (Ca^{+2}-release channels). Trends Biochem. Sci. *22*, 193-194.

Pradhan, S., and Kim, G.-D. (2002). The retinoblastoma gene product interacts with maintenance human DNA (cytosine-5) methyltransferase and modulates its activity. EMBO J. *21*, 779-788.

Proudfoot, J. (1996). Ending the message is not so simple. Cell *87*, 779-781.

Proudfoot N.J., Furger, A., and Dye, M.J. (2002). Integrating mRNA processing with transcription. Cell *108*, 501-512.

Puvion-Dutilleul, F., Chelbi-Alix, M.K., Koken, M., Quignon, F., Puvion, E., and de The, H. (1995). Adenovirus infection induces rearrangements in the intranuclear distribution of the nuclear body-associated PML protein. Exp. Cell Res. *218*, 9-16.

Quignon, F., De Bels, F., Koken, M. Feunteun, J., Ameisen, J.C., and de The, H. (1998). PML induces a novel caspase-independent death process. Nat. Genet. *20*, 259-265.

Ramakrishnan, V. (2002). Ribosome Structure and the Mechanism of Translation. Cell *108*, 557-572.

Raška, I. (1995). Nuclear ultrastructures associated with the RNA synthesis and processing. J. Cell. Biochem. *59*, 11-26.

Raška, I., Andrade, L.E.C., Ochs, R.L., Chan, E.K.L., Chang, C.-M., Roos, G., and Tan, E.M. (1991). Immunological and ultrastructural studies of the nuclear coiled body with autoimmune antibodies. Exp. Cell Res. *195*, 27-37.

Raška, I., Ochs, R.L., Andrade, L.E.C., Chan, E.K.L., Burlingame, R., Peebles, C., Gruol, D., and Tan, E.M. (1990). Association between the nucleolus and the coiled body. J. Struct. Biol. *104*, 120-127.

Rafti, F., Scarvelis, D., and Lasko, P.F. (1996). A Drosophila melanogaster homologue of the human DEAD-box gene *DDX1*. Gene *171*, 225-229.

Reddy, T.R., Xu, W., Mau, J.K., Goodwin, C.D., Suhasini, M., Tang, H., Frimpong, K., Rose, D.W., and Wong-Staal, F. (1999). Inhibition of HIV replication by dominant negative mutants of Sam68, a functional homolog of HIV-1. Rev. Nat. Med. *5*, 635-642.

Reed, J.C. (2001). The Survivin saga goes *in vivo*. J. Clin. Invest. *108*, 965-969.

Reed, R., and Hurt, E. (2002). A conserved mRNA export machinery coupled to pre-mRNA splicing. Cell *108*, 523-531.

Rego, E.M., Wang, Z.G., Peruzzi, D., He, L.Z., Cordon-Cardo, C., and Pandolfi, P.P. (2001). Role of promyelocytic leukemia (PML) protein in tumor suppression. J. Exp. Med. *193*, 521-529.

Reiter, J.L., and Brodeur, G.M. (1996). High-resolution mapping of a 130-kb core region of the MYCN amplicon in neuroblastomas. Genomics *15*, 97-103.

Richard, S., Yu, D., Blumer, K.J., Hausladen, D., Olszowy, M.W., Connelly, P.A., and Shaw, A.S. (1995). Association of p62, a multifunctional SH2- and SH3-binding protein, with src-family tyrosine kinases, Grb2, and phospholiapse Cγ-1. Mol. Cell. Biol. *15*, 186-197.

Robertson, K.D., Ait-Si-Ali, S., Yokochi, T., Wade, P.A., Jones, P.L. and Wollfe, A.P. (2000). DNMT1 forms a complex with Rb, E2F1, HDAC1 and represses transcription from E2F-responsive promoters. Nat. Genet. *25*, 338-342.

Rogers, G.W., Richter, N.J., Lima, W.F., and Merrick, W.C. (2001). Modulation of the helicase activity of eIF4A by eIF4B, eIF4H, and eIF4F. J. Biol. Chem. *276*, 30914-30922.

Rogers, G.W., Richter, N.J., and Merrick, W.C. (1999). Biochemical and kinetic characterization of the RNA helicase activity of eukaryotic initiation factor 4A. J. Biol. Chem. *274*, 12236-12244.

Ross, J.F., Liu, X., and Dynlacht, B.D. (1999). Mechanism of transcriptional repression of E2F by the retinoblastoma tumor suppressor protein. Mol. Cell *3*, 195-205.

Rossler, O.G., Hloch, P., Schutz, N., Weitzennegger, T., and Stahl, H. (2000). Structure and expression of the human p68 RNA helicase gene. Nucleic Acids Res. *28*, 932-939.

Rossoll, W., Kröning, A.-K., Ohndorf, U.-M., Steegborn, C., Jablonka, S., and Sendtner, M. (2002). Specific interaction of Smn, the spinal muscular atrophy determining gene product, with hnRNP-R and gry-rbp/hnRNP-Q: a role for Smn in RNA processing in motor axons? Hum. Mol. Genet. *11*, 93-105.

Rozen, F., Pelletier, J., Trachsel, H., and Sonenberg, N. (1989). A lysine substitution in the ATP-binding site of eucaryotic initiation factor 4A abrogates nucleotide-binding activity. Mol. Cell. Biol. *9*, 4061-4963.

Rüegsegger, U., Blank, D., and Keller, W. (1998). Human pre-mRNA cleavage factor Im is related to spliceosomal SR proteins and can be reconstituted *in vitro* from recombinant subunits. Mol. Cell *1*, 243-253.

Ruggero, D., Wang, Z.-G., and Pandolfi, P.P. (2000). The puzzling multiple lives of PML and its role in the genesis of cancer. Bioessays *22*, 827-835.

Sato, K., Eguchi, Y., Kodama, T.S., and Tsujimoto, Y. (2000). Regions essential for the interaction between Bcl-2 and SMN, the spinal muscular atrophy disease gene product. Cell Death Differ. *7*, 374-383.

Savitsky, K., Ziv, Y., Bar-Shira, A., Gilad, S., Tagle, D.A., Smith, S., Uziel, T., Sfez, S., Nahmias, J., Sartiel, A., Eddy, R.L., Shows, T.B., Collins, F.S., Shiloh, Y., and Rotman, G. (1996). A human gene (*DDX10*) encoding a putative DEAD-box RNA helicase at 11q22-23. Genomics *33*, 199-206.

Schmid, J.A., Scholze, P., Kudlacek, O., Freissmuth, M., Singer, E.A., and Sitte, H.H. (2001). Oligomerization of the human serotonin transporter and of the rat GABA transporter 1 visualized by fluorescence resonance energy transfer microscopy in living cells. J. Biol. Chem. *276*, 3805-3810.

Schneider, S.S., Hiemstra, J.L., Zehnbauer, B.A., Taillon-Miller, P., Le Paslier, D.L., Vogelstein, B., and Brodeur, G.M. (1992). Isolation and structural analysis of a 1.2-megabase *N-myc* amplicon from a human neuroblastoma. Mol. Cell. Biol. *12*, 5563-5570.

Schul, W., Adelaar, B., van Driel, R., and de Jong, L. (1999a). Coiled bodies are predisposed to a spatial association with genes that contain snoRNA sequences in their introns. J. Cell. Biochem. *75*, 393-403.

Schul, W., de Jong, L., and van Driel, R. (1998a). Nuclear neighbours: the spatial and functional organization of genes and nuclear domains. J. Cell. Biochem. *70*, 159-171.

Schul, W., Groenhout, B., Koberna, K., Takagaki, Y., Jenny, A., Manders, E.M.M., Raška, I., van Driel, R., and de Jong, L. (1996). The RNA 3' cleavage factors CstF 64 kDa and CPSF 100 kDa are concentrated in nuclear domains closely associated with coiled bodies and newly synthesized RNA. EMBO J. *15*, 2883-2892.

Schul, W., van der Kraan, I., Matera, G.A., van Driel, and de Jong, L. (1999b). Nuclear domains enriched in RNA 3'-processing factors associate with coiled bodies and histone genes in a cell-cycle dependent manner. Mol. Biol. Cell *10*, 3815-3824.

Schul, W., van Driel, R, de Jong L. (1998b). Coiled bodies and U2 snRNA genes adjacent to coiled bodies are enriched in factors required for snRNA transcription. Mol. Biol. Cell *9*, 1025-1036.

Schullery, D.S., Ostrowski, J., Denisenko, O.N., Stempka, L., Shnyreva, M., Suzuki, H., Gschwendt, M., and Bomsztyk, K. (1999). Regulated interaction of protein kinase Cδ with the heterogeneous nuclear ribonucleoprotein K protein. J. Biol. Chem. *274*, 15101-15109.

Schwab M, Alitalo K, Klempnauer KH, Varmus HE, Bishop JM, Gilbert F, Brodeur G, Goldstein M, and Trent J. (1983). Amplified DNA with limited homology to *myc* cellular oncogene is shared by human neuroblastoma cell lines and a neuroblastoma tumour. Nature *305*, 245-248.

Schwab, M., and Amler, L. (1990). Amplification of cellular oncogenes: a predictor of clinical outcome in human cancer. Genes Chromosomes Cancer *1*, 181-193.

Schwab, M., Ellison, J., Busch, M., Rosenau, W., Varmus, H.E., and Bishop, J.M. (1984). Enhanced expression of the human gene *N-myc* consequent to amplification of DNA may contribute to malignant progression of neuroblastoma. Proc. Natl. Acad. Sci. USA *81*, 4940-4944.

Schwer, B. (2001). A new twist on RNA helicases: DExH/D box proteins as RNPases. Nat. Struct. Biol. 8, 113-116.

Seeger, R.C., Brodeur, G.M., Sather, H., Dalton, A., Siegel, S.E., Wong, K.Y., and Hammond, D. (1985). Association of multiple copies of the *N-myc* oncogene with rapid progression of neuroblastomas. N. Engl. J. Med. *313*, 1111-1116.

Seeler, J.S, and Dejean, A. (1999). The PML nuclear bodies: actors or extras? Curr. Opin. Genet. Dev. *3*, 362-367.

Segref, A., Sharma, K., Doye, V., Hellwig, A., Huber, J., Luhrmann, R., and Hurt, E. (1997). Mex67p, a novel factor for nuclear mRNA export, binds to both poly(A)$^+$ RNA and nuclear pores. EMBO J. *16*, 3256-3271.

Seufert, D.W., Kos, R., Erickson, C.A., and Swalla, B.J. (2000). *p68*, a DEAD-box RNA helicase, is expressed in chordate embryo neural and mesodermal tissues. J. Exp. Zool. *28*, 193-204.

Shiels, C., Islam, S.A., Vatcheva, R., Sasieni, P., Sternberg, M.J.E., Freemont, P.S., and Sheer, D. (2001). PML bodies associate specifically with the MHC gene cluster in interphase nuclei. J. Cell Sci. *114*, 3705-3716.

Shnyreva, M., Schullery, D.S., Suzuki, H., Higaki, Y., and Bomsztyk, K. (2000). Interaction of two multifunctional proteins. Heterogeneous nuclear ribonucleoprotein K and Y-box-binding protein. J. Biol. Chem. *275*, 15498-15503.

Singh, P., Wong, S.H., and Hong, W. (1994). Overexpression of E2F-1 in rat embryo fibroblasts leads to neoplastic transformation. EMBO J. *13*, 3329-3338.

Slavc, I., Ellenbogen, R., Jung, W.H., Vawter, G.F., Kretschmar, C., Grier, H., and Korf, B.R. (1990). *myc* gene amplification and expression in primary human neuroblastoma. Cancer Res. *50*, 1459-1463.

Sleeman, J.E., and Lamond, E.G. (1999). Newly assembled snRNPs associate with coiled bodies before speckles, suggesting a nuclear snRNP maturation pathway. Curr. Biol. *9*, 1065-1074.

Smith, A.G., Heath, J.K., Donaldson, D.D., Wong, G.G., Moreau, J., Stahl, M., and Rogers, D. (1988). Inhibition of pluripotential embryonic stem cell differentiation by purified polypeptides. Nature *336*, 688-670.

Smith, C.W., and Valcarcel, J. (2000). Alternative pre-mRNA splicing: the logic of combinatorial control. Trends Biochem. Sci. *25*, 381-388.

Smith, K.P., Carter, K.C., Johnson, C.V., Lawrence, J.B. (1995). U2 and U1 snRNA gene loci associate with coiled bodies. J. Cell. Biochem. *59*, 473-485.

Smith, K.P., Moen, P.T., Wydner, K.L., Coleman, J.R., and Lawrence, J.B. (1999). Processing of endogenous pre-mRNAs in association with SC-35 domains is gene specific. J. Cell Biol. 144, 617-629.

Snay-Hodge, C.A., Colot, H.V., Goldstein, A.L., and Cole, C.N. (1998). Dbp5p/Rat8p is a yeast nuclear pore-associated DEAD-box protein essential for RNA export. EMBO J. *17*, 2663-2676.

Speckman, W., Narayanan, A., Terns, R., and Terns, M. (1999). Nuclear retention elements of U3 small nucleolar RNA. Mol. Cell. Biol. *19*, 8412-8421.

Spector, D.L. (2001). Nuclear domains. J. Cell Sci. *114*, 2891-2893.

Spector, D.L., Fu, X.D., and Maniatis, T. (1991). Associations between distinct pre-mRNA splicing components and the cell nucleus. EMBO J. *10*, 3467-3481.

Spector, D.L., Lark, G., and Huang, S. (1992). Differences in snRNP localization between transformed and nontransformed cells. Mol. Biol. Cell *3*, 555-569.

Squire, J., Gallie, B.L., and Phillips, R.A. (1985). A detailed analysis of chromosomal changes in heritable and non-heritable retinoblastoma. Hum. Genet. *70*, 291-301.

Squire, J.A., Thorner, P.S., Weitzman, S., Maggi, J.D., Dirks, P., Doyle, J., Hale, M., and Godbout, R. (1995). Co-amplification of *MYCN* and a DEAD box gene (*DDX1*) in primary neuroblastoma. Oncogene *10*, 1417-1422.

Stadler, M., Chelbi-Alix, M.K., Koken, M.H., Venturini, L., Lee, C., Saib, A., Quignon, F., Pelicano, L., Guillemin, M.C., Schindler, C., and de The, H. (1995). Transcriptional induction of the PML growth suppressor gene by interferons is mediated through an ISRE and a GAS element. Oncogene *11*, 2565-2573.

Sternsdorf, T., Jensen, K., and Will, H. (1997). Evidence for covalent modification of the nuclear dot-associated proteins PML and Sp100 by PIC1/SUMO-1. J. Cell Biol. *139*, 1621-1634.

Stevenson, R.J., Hamilton, S.J., MacCallum, D.E., Hall, P., and Fulller-Pace, F.V. (1998). Expression of the 'dead box' RNA helicase p68 is developmentally and growth regulated and correlates with organ differentiation/maturation in the fetus. J. Pathol. *184*, 351-359.

Stoss, O., Olbrich, M., Hartmann, A.M., Konig, H., Memmott, J., Andreadis, A., and Stamm, S. (2001). The STAR/GSG family protein rSLM-2 regulates the selection of alternative splice sites. J. Biol. Chem. *276*, 8665-8673.

Strasser, K, and Hurt, E. (2000). Yra1p, a conserved nuclear RNA-binding protein, interacts directly with Mex67p and is required for mRNA export. EMBO J. *19*, 410-420.

Strasser, K, and Hurt, E. (2001). Splicing factor Sub2p is required for nuclear mRNA export through its interaction with Yra1p. Nature *413*, 648-652.

Strasser, K., Masuda, S., Mason, P., Pfannstiel, J., Oppizzi, M., Rodriguez-Navarro, S., Rondon, A.G., Aguilera, A., Struhl, K., Reed, R., and Hurt, E. (2002). TREX is a conserved complex coupling transcription with messenger RNA export. Nature *417*, 304-308.

Strasswimmer, J., Lorson, C.L., Breiding, D.E., Chen, J.J., Le, T., Burghes, A.H.M., and Androphy, E.J. (1999). Identification of survival motor neuron as a transcriptional activator-binding protein. Hum. Mol. Genet. *8*, 1219-1226.

Strober, B.E., Dunaief, J.L., Guha, S., and Goff, S.P. (1996). Functional interactions between the hBRM/hBRG1 transcriptional activators and the pRB family of proteins. Mol. Cell. Biol. *16*, 1576-1583.

Stuurman, N., de Graaf, A., Floore, A., Josso, A., Humbel, B., de Jong, L., and van Driel, R. (1992). A monoclonal antibody recognizing nuclear matrix-associated nuclear bodies. J.Cell Sci. *101*, 773-784.

Svitkin, Y.V., Pause, A., Haghighat, A., Pyronnet, S., Witherell, G., Belsham, G.J., and Sonenberg, N. (2001). The requirement for eukaryotic initiation factor 4A (eIF4A) in translation is in direct proportion to the degree of mRNA 5' secondary structure. RNA *7*, 382-394.

Takagaki, Y., and Manley, J.L. (1994). A polyadenylation factor subunit is the human homologue of the *Drosophila* suppressor of forked protein. Nature *372*, 471-474.

Takagaki, Y., and Manley, J.L. (1997). RNA recognition by the human polyadenylation factor CstF. Mol. Cell. Biol. *17*, 3907-3914.

Takagaki, Y., and Manley, J.L. (1998). Levels of polyadenylation factor CstF-64 control IgM heavy chain mRNA accumulation and other events associated with B cell differentiation. Mol. Cell *2*, 761-771.

Takagaki, Y., MacDonald, C.C., Shenk, T., and Manley, J.L. (1992). The human 64-kDa polyadenylylation factor contains a ribonucleoprotein-type RNA binding domain and unusual auxiliary motifs. Proc. Natl. Acad. Sci. USA *89*, 1403-1407.

Takagaki, Y., Manley, J.L., MacDonald, C.C., Wilusz, J., and Shenk, T. (1990). A multisubunit factor, CstF, is required for polyadenylation of mammalian pre-mRNAs. Genes Dev. *4*, 2112-2120.

Takagaki, Y., Ryner, L.C., and Manley, J.L. (1989). Four factors are required for 3'-end cleavage of pre-mRNAs. Genes Dev. *3*, 1711-1724.

Takagaki, Y., Seipelt, R.L., Peterson, M.L., and Manley, J.L. (1996). The polyadenylation factor CstF-64 regulates alternative processing of IgM heavy chain pre-mRNA during B cell differentiation. Cell *87*, 941-952.

Takahashi, N., Sasagawa, N., Usuki, F., Kino, Y., Kawahara, H., Sorimachi, H., Maeda, T., Suzuki, K., and Ishiura, S. (2001). Coexpression of the CUG-binding protein reduces DM protein kinase expression in COS cells. J. Biochem. (Tokyo) *130*, 581-587.

Talbot, K. (1999). Spinal muscular atrophy. J. Inherit. Metab. Dis. *22*, 545-554.

Tanner, N.K., and Linder, P. (2001). DExD/H box RNA helicases: from generic motors to specific dissociation functions. Mol. Cell *8*, 251-262.

Taylor, S.J., Anafi, M., Pawson, T., and Slalloway, D. (1995). Functional interaction between c-src and its mitotic target, Sam68. J. Biol. Chem. *270*, 10120-10124.

Terns, M.P., and Terns, R.M. (2001). Macromolecular complexes: SMN – the master assembler. Curr. Biol. *11*, R862-R864.

Terris, B., Baldin, V., Dubois, S., Degott, C., Flejou, J.F., Henin, D., and Dejean, A. (1995). PML nuclear bodies are general targets for inflammation and cell proliferation. Cancer Res. *55*, 1590-1597.

Thiede, B., Dimmler, C., Siejak, F., and Rudel, T. (2001). Predominant identification of RNA-binding proteins in Fas-induced apoptosis by proteome analysis. J. Biol. Chem. *276*, 26044-26050.

Thiry, M. (1994). Cytochemical and immunocytochemical study of coiled bodies in different cultured cell lines. Chromosoma *103*, 268-276.

Timchenko, L.T., Miller, J.W., Timchenko, N.A., DeVore, D.R., Datar, K.V., Lin, L., Roberts, R., Caskey, C.T., and Swanson, M.S. (1996). Identification of a $(CUG)_n$ triplet repeat RNA-binding protein and its expression in myotonic dystrophy. Nucleic Acids Res. *24*, 4407-4414.

Torii, S., Egan, D.A., Evans, R.A., and Reed, J.C. (1999). Human Daxx regulates Fas-induced apoptosis from nuclear PML oncogenic domains (PODs). EMBO J. *18*, 6037-6049.

Trent, J.M., Kaneko, Y., and Mittelman, F. (1991). Report of the committee on structural chromosome changes in neoplasia. Cytogenet. Cell Genet. *51*, 1053-1079.

Trouche, D., Le Chalony, C., Muchardt, C., Yaniv, M., and Kouzarides, T. (1997). RB and hBRM cooperate to repress the activation function of E2F1. Proc. Natl. Acad. Sci. USA *94*, 11268-11273.

Tsai, K.Y., MacPherson, D., Rubinson, D.A., Crowley, D., and Jacks, T. (2002). *ARF* is not required for apoptosis in *Rb* mutant mouse embryos. Curr. Biol. *12*, 159-163.

Tsai, K.Y., Yanwen, H., Macleod, K.F., Crowley, D., Yamasaki, L., and Jacks, T. (1998). Mutation of *E2f-1* suppresses apoptosis and inappropriate S phase entry and extends survival of *Rb*-defcient mouse embryos. Mol. Cell *2*, 293-304.

Tsujimoto Y. (1998). Role of Bcl-2 family proteins in apoptosis: apoptosomes or mitochondria? Genes Cells *3*, 697-707.

Vagner, S., Vagner, C., and Mattaj, I.W. (2000). The carboxyl terminus of vertebrate poly(A) polymerase interacts with U2AF 65 to couple 3'-end processing and splicing. Genes Dev *14*, 403-413.

Valcarcel, J., and Gebauer, F. (1997). Post-transcriptional regulation: the dawn of PTB. Curr. Biol. *7*, R705-R708.

Valiron, O., Caudron, N., and Job, D. (2001). Microtubule dynamics. Cell. Mol. Life Sci. *58*, 2069-2084.

Vallian, S., Chin, K.V., and Chang, K.S. (1998). The promyelocytic leukemia protein interacts with Sp1 and inhibits its transactivation of the epidermal growth factor receptor promoter. Mol. Cell. Biol. *18*, 7147-7156.

Vallian, S., Gaken, J.A., Trayner, I.D., Gingold, E.B., Kouzarides, T., Chang, K.S., and Farzaneh, F. (1997). Transcriptional repression by the promyelocytic leukemia protein, PML. Exp. Cell Res. *237*, 371-382.

Verhagen, A.M., Coulson, E.J., and Vaux, D.L. (2001). Inhibitor of apoptosis proteins and their relatives: IAPs and other BIRPs. Genome Biol. *2*, 3009.

Vindeløvm, L.L. Christensen, I.J., and Nissen, N.I. (1983). A detergent-trypsin method for the preparation of nuclei for flow cytometric DNA analysis. Cytometry *3*, 323-327.

von Mikecz, A., Zhang, S., Montminy, M., Tan, E.M., and Hemmerich, P. (2000). CREB-binding protein (CBP)/p300 and RNA polymerase II colocalize in transcriptionally active domains in the nucleus. J. Cell Biol. *150*, 265-273.

Wagner, E.J., and Garcia-Blanco, M.A. (2001). Polypyrimidine tract binding protein antagonizes exon definition. Mol. Cell. Biol. *21*, 3281-3288.

Wahle, E. (1995). Poly(A) tail length control is caused by termination of processive synthesis. J. Biol. Chem. *270*, 2800-2808.

Wahle, E., and Rüegsegger, U. (1999). 3'-End processing of pre-mRNA in eukaryotes. FEMS Microbiol. Rev. *23*, 277-295.

Wang, Z.G., Ruggero, D., Ronchetti, S., Zhong, S., Gaboli, M., Rivi, R, Pandolfi, P.P. (1998). PML is essential for multiple apoptotic pathways. Nat. Genet. *20*, 266-272.

Wansink, D.G., Schul, W., van der Kraan, I., van Steensel, B., van Driel, R., and de Jong, L. (1993). Fluorescent labelling of nascent RNA reveals transcription by RNA polymerase II in domains scattered throughout the nucleus. J. Cell Biol. *122*, 283-293.

Weis, K., Rambaud, S., Lavau, C., Jansen, J., Carvalho, T., Carmo-Fonseca, M., Lamond, A., and Dejean, A. (1994). Retinoic acid regulates aberrant nuclear localization of PML-RAR alpha in acute promyelocytic leukemia cells. Cell *76*, 345-356.

Welle, S., Bhatt, K., and Thornton, C.A. (1999). Inventory of high-abundance mRNAs in skeletal muscle of normal men. Genome Res. *9*, 506-513.

Westermarck, J., Weiss, C., Saffrich, R., Kast, J., Musti, A.-M., Wessely, M., Ansorge, W., Séraphin, B., Wilm, M., Valdez, B.C., and Bohmann, D. (2002). The DEXD/H-box RNA helicase RHII/Gu is a co-factor for c-Jun-activated transcription. EMBO J. *21*, 451-460.

Whitelaw, E. and Proudfoot, N. (1986). α-Thalassaemia caused by a poly(A) site mutation reveals that transcriptional termination is linked to 3' end processing in the human α2 globin gene. EMBO J., *5*, 2915–2922.

Wieland, I., Arden, K.C., Michels, D., Klein-Hitpass, L., Böhm, M., Viars, C.S., and Weidle, U.H. (1999). Isolation of DICE1: A gene frequently affected by LOH and downregulated in lung carcinomas. Oncogene *18*, 4530-4537.

Wieland, I., Röpke, A., Stumm, M., Sell, C., Weidle, U.H., and Wieacker, P.F. (2001). Molecular characterization of the *DICE1* (*DDX26*) tumor suppressor gene in lung carcinoma cells. Oncol. Res. *12*, 491-500.

Will, C.L., and Lührmann, R. (2001). RNP remodelling with DExH/D boxes. Science *291*, 1916-1917.

Williams, B.Y., Hamilton, S.L., and Sarkar, H.K. (2000). The survival motor neuron protein interacts with the transactivator FUSE binding protein from human fetal brain. FEBS Lett. *470*, 207-210.

Williams, R.L., Hilton, D.J., Pease, S., Willson, T.A., Stewart, C.L., Gearing, D.P., Wagner, E.F., Metcalf, D., Nicola, N.A., and Gough, N.M. (1988). Myeloid leukaemia inhibitory factor maintains the developmental potential of embryonic stem cells. Nature *336*, 684-687.

Wilusz, J., and Shenk, T. (1988). A 64 kd nuclear protein binds to RNA segments that include the AAUAAA polyadenylation motif. Cell *52*, 221-228.

Wilusz, J., Shenk, T., Takagaki, Y., and Manley, J.L. (1990). A multicomponent complex is required for the AAUAAA-dependent cross-linking of a 64-kilodalton protein to polyadenylation substrates. Mol. Cell. Biol. *10*, 1244-1248.

Wilusz, C.J., Wormington, M., and Peltz, S.W. (2001). The cap-to-tail guide to mRNA turnover. Nat. Rev. Mol. Cell. Biol. *2*, 237-246.

Wimmer, K., Zhu, X.X., Lamb, B.J., Kuick, R., Ambros, P., Kovar, H., Thoraval, D., Elkahloun, A., Meltzer, P., and Hanash, S.M. (2001). Two-dimensional DNA electrophoresis identifies novel CpG islands frequently coamplified with *MYCN* in neuroblastoma. Med. Pediatr. Oncol. *36*, 75-79.

Wimmer, K., Zhu, X.X., Lamb, B.J,, Kuick, R., Ambros, P.F., Kovar, H., Thoraval, D., Motyka, S., Alberts, J.R., and Hanash, S.M. (1999). Co-amplification of a novel gene, *NAG*, with the N-myc gene in neuroblastoma. Oncogene *7*, 233-238.

Wong, G., Muller, O., Clark, R., Conroy, L., Moran, M.F., Polakis, P., and McCormick, F. (1992). Molecular cloning and nucleic acid binding properties of the GAP-associated tyrosine phosphoprotein p62. Cell *69*, 551-558.

Wood, M.A., McMahon, S.B., and Cole, M.D. (2000). An ATPase/helicase complex is an essential cofactor for oncogenic transformation by c-Myc. Mol. Cell *5*, 321-330.

Wurst, W., and Joyner, A.L. (1993). Production of targeted embryonic stem cell clones. In Gene targeting: A practical approach. (ed. A.L. Joyner). IRL Press at Oxford University Press, England. pp. 33-61.

Wu, Z., Murphy, C., and Gall, J.G. (1994). Human p80-coilin is targeted to sphere organelles in the amphibian germinal vesicle. Mol. Biol. Cell *5*, 1119-1127.

Wu, W.S., Vallian, S., Seto, E., Yang, W.M., Edmondson, D., Roth, S., and Chang, K.S. (2001). The growth suppressor PML represses transcription by functionally and physically interacting with histone deacetylases. Mol. Cell. Biol. *21*, 2259-2268.

Xing, Y., Carol, V.J., Dobner, P.R., and Lawrence, J.B. (1993). Higher level organization of individual gene transcription and RNA splicing. Science *259*, 1326-1330.

Xing, Y., Johnson, C.V., Moen, P.T., McNeil, J.A., and Lawrence, J.B. (1995). Nonrandom gene organization: Structural arrangements of specific pre-mRNA transcription and splicing with SC-35 domains. J. Cell Biol. *131*, 1635-1647.

Yamasaki, L., Jacks, T., Bronson, R., Goillot, E., Harlow, E., and Dyson, N.J. (1996). Tumor induction and tissue atrophy in mice lacking *E2F-1*. Cell *85*, 537-548.

Yang, X., Khosravi-Far, R., Chang, H.Y., and Baltimore, D. (1997). Daxx, a novel Fas-binding protein that activates JNK and apoptosis. Cell *89*, 1067-1076.

Yeager, T.R., Neumann, A.A., Englezou, A., Huschtscha, L.I., Noble, J.R., and Reddel, R.R. (1999). Telomerase-negative immortalized human cells contain a novel type of promyelocytic leukemia (PML) body. Cancer Res. *59*, 4175-4179.

Yokota, Y. (2001). Id and development. Oncogene 20, 8290-8298.

Yonaha, M., and Proudfoot, N.J. (1999). Specific transcriptional pausing activates polyadenylation in a coupled *in vitro* system. Mol. Cell *3*, 593-600.

Young, P.J., Day, P.M., Zhou, J., Androphy, E.J., Morris, G.E., and Lorson, C.L. (2002). A direct interaction between the survival motor neuron protein and p53 and its relationship to spinal muscular atrophy. J. Biol. Chem. *277*, 2852-2859.

Young, P.J., Le, T.T., Dunckley, M., thi Man, N., Burghes, A.H.M., and Morris, G.E. (2001). Nuclear gems and cajal (coiled) bodies in fetal tissues: nucleolar distribution of the spinal muscular atrophy protein, SMN. Exp. Cell Res. *265*, 252-261.

Young, P.J., Le, T.T., thi Man, N., Burghes, A.H., and Morris, G.E. (2000). The relationship between SMN, the spinal muscular atrophy protein, and nuclear coiled bodies in differentiated tissues and cultured cells. Exp. Cell Res. *256*, 365-374.

Youvan, D.C., Silva, C.M., Petersen, J., Bylina, E.J., Coleman, W.J., Dilworth, M.R., and Yang, M.M. (1997). Calibration of fluorescence resonance energy transfer in microscopy using genetically engineered GFP derivatives on nickel chelating beads. Biotechnology et alia, *3*: 1-18.

Zaffran, S., Chartier, A., Gallant, P., Astier, M., Arquier, N., Doherty, D., Gratecos, D., and Sémériva, M. (1998). A *Drosophila* RNA helicase gene, *pitchoune*, is required for cell growth and proliferation and is a potential target of d-Myc. Development *125*, 3571-3584.

Zhang, G., Taneja, K.L., Singer, R.H., and Green, M.R. (1994). Localization of pre-mRNA splicing in mammalian nuclei. Nature *372*, 809-812.

Zhang, H.S., Gavin, M., Dahiya, A., Postigo, A.A., Ma, D., Luo, R.X., Harbour, J.W., and Dean, D.C. (2000). Exit from G1 and S phase of the cell cycle is regulated by repressor complexes containing HDAC-Rb-hSWI/SNF and Rb-hSWI/SNF. Cell *101*, 79-89.

Zhang, Y., Xiong, Y., and Yarbrough, W.G. (1998). ARF promotes Mdm2 degradation and stablizes p53: *ARF-INK4a* locus deletion impairs both the Rb and p53 tumor suppression pathways. Cell *92*, 725-735.

Zhao, J., Jin, S.B., Bjorkroth, B., Wieslander, L., and Daneholt, B. (2002). The mRNA export factor Dbp5 is associated with Balbiani ring mRNP from gene to cytoplasm. EMBO J. *21*, 1177-1187.

Zhao, J., Kennedy, B.K., Lawrence, B.D., Barbie, D., Matera, A.G., Fletcher, J.A., and Harlow, E. (2000). NPAT links cyclin E-Cdk2 to the regulation of replication-dependent histone gene transcription. Genes Dev. *14*, 2283-2297.

Zheng, L., Chen, Y., Riley, D.J., Chen, P.L., and Lee, W.H. (2000). Retinoblastoma protein enhances the fidelity of chromosome segregation mediated by hsHec1p. Mol. Cell. Biol. *20*, 3529-3537.

Zheng, L., and Lee, W.H. (2001). The retinoblastoma gene: a prototypic and multifunctional tumor suppressor. Exp. Cell Res. *264*, 2-18.

Zhong, S., Delva, L., Rachez, C., Cenciarelli, C., Gandini, D., Zhang, H., Kalantry, S., Freedman, L.P., and Pandolfi, P.P. (1999). A RA-dependent, tumour-growth suppressive transcription complex is the target of the PML-RARalpha and T18 oncoproteins. Nat. Genet. *23*, 287-295.

Zhong, S., Müller, S., Ronchetti, S., Freemont, P.S., Dejean, A., and Pandolfi, P.P. (2000a). Role of SUMO-1-modified PML in nuclear body formation. Blood *95*, 2748-2752.

Zhong, S., Salomoni, P., Ronchetti, S., Guo, A., Ruggero, D, and Pandolfi, P.P. (2000b). Promyelocytic leukemia protein (PML) and Daxx participate in a novel nuclear pathway for apoptosis. J. Exp. Med. *191*, 631-640.

Zhou, Z., Luo, M.J., Straesser, K., Katahira, J., Hurt, E., and Reed, R. (2000). The protein Aly links pre-messenger-RNA splicing to nuclear export in metazoans. Nature *407*, 401-405.

Zinsmaier, K.E., Eberle, K.K., Buchner, E., Walter, N., and Benzer, S. (1994). Paralysis and early death in cysteine string protein mutants of Drosophila. Science *263*, 977-980.